

50-334/412

Memorandum

To: Tim Colburn

From: Brian Sepelak

Date: 01/07/04

Re: References Requested During 12/10/03 MAAP-DBA Meeting

On December 10, 2003 a working level meeting was held with the NRC to discuss the Containment Conversion Pre-application Report submitted by Beaver Valley Power Station (BVPS) by letter L-03-188 dated November 24, 2003. During the meeting, Rich Lobel requested copies of References 10, 13 and 19 cited in Section 2.6 of the pre-application report. While these references are available in the public domain, they were readily available to BVPS and are being provided for the convenience of the staff.

Asol
1/11

AN EXPERIMENTAL AND THEORETICAL STUDY OF
SIMULTANEOUS HEAT AND MASS TRANSFER
APPLIED TO STEAM DOUSING

by

EMIN KULIĆ, Dipl.Ing., University of Sarajevo, Yugoslavia,
M.A.Sc., University of Waterloo

A thesis
presented to the University of Waterloo
in partial fulfillment of the
requirements for the degree of
Doctor of Philosophy
in
Chemical Engineering

Waterloo, Ontario, 1976

© Emin Kulić, 1976

CONTAINMENT SPRAY EXPERIMENTS FOR PRESSURE SUPPRESSION

Susumu Kitani¹

ABSTRACT

A containment spray system is one of the nuclear safety devices installed in pressurized water reactors to suppress the inner pressure and to remove iodine vapor in the containment vessel in a postulated large accident.

A subject of the Containment Spray Test is to confirm the effectiveness of pressure suppression. Cold water was injected as spray droplets into a large vessel of 700 m³ prepared in a given steam-air condition. Practically applied spray nozzles of hollow cone type were used at several heights by changing the number of nozzles.

The experimental results showed that the pressure decreased mostly with flow rate of spray injected and independently of the position of nozzle height.

NOMENCLATURE

- f = spray flux (m/hr)
- F = total flow rate (m³/hr)
- F_i = flow rate at i -th stage (m³/hr)
- h = average height of nozzle (m)
- h_i = height of nozzle at i -th stage (m)
- I = spray injection ratio (hr⁻¹)
- T_g = average temperature in vapor phase (°C)
- T_{spi} = temperature of inlet water (°C)
- T_{sp2} = temperature of water reaching bottom of containment vessel (°C)
- V = volume of containment above operating floor (m³)
- V' = volume of containment vessel (m³)
- n = heat absorption efficiency (-)

INTRODUCTION

In the safety analysis of a pressurized water reactor (PWR), an accident of the primary coolant blow-down into the containment vessel (loss-of coolant accident or LOCA) is postulated. If the postulated accident occurs, the inner pressure of the containment vessel will be built up due to the blown-down steam. Therefore, PWR's plants have the containment spray system to reduce the pressure by cooling the steam-air atmosphere. Another important role of the containment spray system is to washout airborne fission products released from any perforated fuels into the contain-

ment vessel.

For the containment spray cooling, the presence of air in the containment vessel lowers the condensation heat transfer rate. Furthermore, spray flow rate, spray drop size, and spray pattern will also affect it.

Many fundamental researches on cooling the steam atmosphere by spray have been reported. Nevertheless, the experimental investigation in a large vessel has been performed to understand the gas-space mixing and the temperature distribution in the actual reactor containment vessel.

The Marviken Full Scale Containment experiments in Sweden (1) and the simulated design basis tests of the Carolinas Virginia Tube Reactor in U.S.A. (2) evaluated the heat transfer in the spray cooling qualitatively.

Hitachi, Ltd. evaluated the heat transfer efficiency of spray-cooling as a function of the pressure with a vessel of 42 m³ (3.3 m in diameter and 6 m in height) (3).

Tokyo Shibaura Co. Ltd. made an experiment with a vessel of 3 m³ (1.2 m in diameter and 3.5 m high) and found that the theoretically calculated value agreed well with the experimental results. (4-6) In their experiments the effect of gas-space mixing under spraying was not evaluated.

In the present experiment a fairly large vessel was used for clarifying the effectiveness of PWR's containment spray cooling.

TEST FACILITY

Fig. 1 shows a schematic diagram of the containment spray test apparatus. It consists of a model

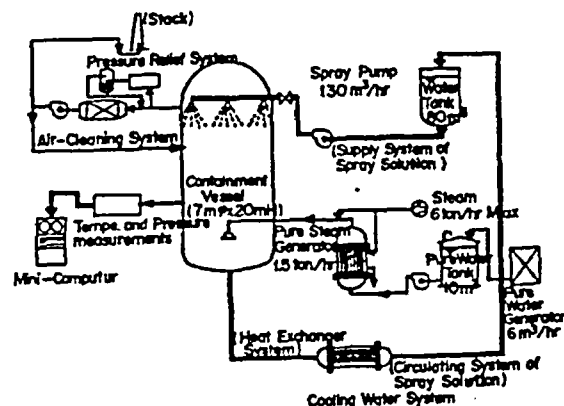


Fig.1 Block Diagram of Containment Spray Test Apparatus

¹ Japan Atomic Energy Research Institute, Tokai-mura, Ibaraki-ken, Japan

Contributed by the Fuel Society of Japan for presentation at the 1st International Conference on Liquid Atomization and Spray Systems held in Tokyo, Japan from August 27th to 31st, 1978.

containment vessel, spray systems, instruments for measuring several experimental data and an air cleaning system.

The Model Containment Vessel

The Model Containment Vessel is 20 m high, 7 m in diameter and 702 m³ in volume. It is designed for the condition of 5 kg/cm²G in pressure and 160 °C in temperature. The pressure test was carried out at 6.25 kg /cm²G and the leak was examined to be less than 0.1 l/day at 3.5 kg/cm²G.

It is made of carbon steel plate ranged in thickness from 25 mm to 28 mm.

The inside surface of the vessel is clad with 2 mm thickness stainless steel.

The wall of the containment vessel is covered with 5 cm calcium silicate boards for the thermal insulation (the density of board is 0.22 g/cm³ and the thermal conductivity 0.042 kcal/m.hr.C).

Pressurization

Steam supply into the containment vessel can be sent from a boiler directly with flow rate of 6 ton/hr. Pressure relief valves are installed in the main ventilation loop header adjacent to the containment vessel and rupture disks are also set for the same object because of potential overpressurization and vacuum.

Spray systems

The elevation, El., of spray headers is taken from the bottom of the containment vessel. Single nozzle can be set at 18 m(#0). The ring-shaped headers are located at 15 m(#1), 12 m(#2) and 15 m(#3) on which 18 nozzles can be set respectively.

A hollow cone type nozzle (the same specification with SPRACO-1713A) was used for the present work with water flow rate of 58 l/min at 2.8 kg/cm², spray angle of 65 - 67°.

Air Cleaning System

An air cleaning loop is provided to relieve the depleted air due to water vapor and supply fresh air with flow rate of 1700 m³/hr or 3400 m³/hr.

Data acquisition: A digital computer system is connected to the containment spray test apparatus for logging collected data, processing them and plotting the calculated results.

The system is to be able to file a large amount of analogue physical inputs such as temperature, pressure, flow rate of fluid, etc., less than one second continuously.

Heat transfer coefficient, kinetic viscosity, Prandtl number, thermal conductivity and absorption efficiency of sprayed water are calculated to analyze the experimental data.

Heat-Transfer-Data Measurement System: To measure heat-transfer data, following sensors are equipped in the containment spray test apparatus.

1) Temperature measurement by copper-constantan thermocouples

Steam injected	1
Steam-air atmosphere	59
Spray water	58
Spray header	6
Wall	three positions 6/position
Water flowing on wall surfaces	12
Water in sump	1
Steam inlet	1

2) Pressure

Steam duct	1
Steam-air atmosphere	3

3) Flow rate

Steam under injection	1
Spray water	4
Water flowing on wall surface	12
Water circulated from the sump	1

EXPERIMENTAL PROGRAM

The containment spray test for pressure suppression simulated to a LOCA condition of PWR was performed, where heat transfer between spray droplets and steam-air atmosphere in the containment vessel was investigated.

The heat absorption efficiency, η , is shown as follows,

$$\eta = (T_{sp2} - T_{spl}) / (T_g - T_{spl}) \quad (1)$$

where T_g is the gas temperature in the containment vessel, T_{spl} the temperature of water in the spray header and T_{sp2} the temperature of water above the bottom of the containment vessel.

The initial conditions were set at 2.5 kg/cm²G for the atmosphere of the containment vessel and 40C for the water of spray tank. The distribution of spray nozzle on the spray headers was set according to the object of runs.

The height of containment vessel of a 800 MWe class PWR's plant may be 80 m, however, the lower part of it consists of compartments for instrumentation and radiation protection upto about 30 m high. Thus, there is a large free volume above the highest floor, where the containment spray is applied.

The test condition for PWR is simulated by calculating the spray flux, f , defined by

$$f = \sum_i F_i h_i / V = F h / V \quad (2)$$

where F_i is the flow rate of solution issued from the i -th stage of spray header at the height h_i above the highest floor or operating floor of the PWR's containment vessel, and V is the free volume above the operating floor.

On the other hand, the spray injection ratio, l , is defined by

$$l = \sum_i F_i / V' = F / V' \quad (3)$$

where V' is the total volume of the containment vessel. The spray injection ratio is introduced from the consideration that the steam existing not only in the spray region but also in non-spray region of compartments will work to retain the inside pressure of containment vessel.

Table 1 shows the program of containment spray test for PWR's LOCA condition. For the model containment vessel, V and V' are taken to be same.

RESULTS

The steam-air atmosphere of 2.5 kg/cm²G was made by introducing steam at flow rate of 6 ton/hr into the model containment vessel having contained air of 1 atm at the room temperature. After arriving at 2.5 kg/cm²G the supply of steam was stopped and the

Table 1 The Containment Spray Tests for Pressure Suppression

Run No.	Number of Nozzles on Header				F (m ³ /hr)	Fh/V (m/hr)	F/V' (hr ⁻¹)	Purpose
	#0	#1	#2	#3				
PHS-1	0	6	0	0	20.9	0.447	3×10^{-2}	PWR containment spray demonstration test by transient method Simulation of PWR flux (one subsystem flux simulated)
PHS-2	0	6	0	0	20.9	0.447	3×10^{-2}	PWR containment spray demonstration test (by steady state method)
PHS-3	0	12	0	0	41.8	0.893	6×10^{-2}	PWR containment spray demonstration test by transient method (2 subsystems flux simulated)
PHS-4	a	0	0	6	20.9	0.357	3×10^{-2}	Effect of spray flux and mixing within gas phase (by transient method)
	b	0	0	6		0.268		
PHS-5	0	6	0	6	41.8	0.715	6×10^{-2}	Simulation of PWR spray flux by transient method (2 subsystems)
PHS-6	1	0	0	0	3.48	0.0892	5×10^{-3}	Characteristic experiment of single spray nozzle
PWR					795	0.506	1.1×10^{-2}	

(Temperature of Spray Solution 40°C)

vessel was left for about 20 min to decrease the temperature difference between steam-air and the structure of the vessel. Then, spraying water was ejected into the vessel.

Fig. 2 shows the experimental results for the pressure change over the time in run PHS-1 with a curve obtained in calculation of CONTEMP-LT (7), which is popular for estimating temperature-pressure behavior of light water reactor's containment vessel under the LOCA condition. In the calculation, the heat absorption efficiency is taken as 100 %. It means that the temperature of spray droplets becomes equal to that of the gas-phase in a period of falling. The code includes the term of heat transfer between the structure of the containment vessel and the vapor atmosphere. In the calculation, the heat transfer coefficient reported by Uchida et al. was used (8).

Fig. 3 shows the pressure change plotted with the computer after spray injection in all runs. In the figure, it is found that the pressure suppression curves are classified roughly into three groups determined by rate of spray, regardless of the height of spray headers or the configuration of spray nozzles on the condition tested. In other words, the pressure suppression is closely related to spray injection rate shown by F/V' in Table 1.

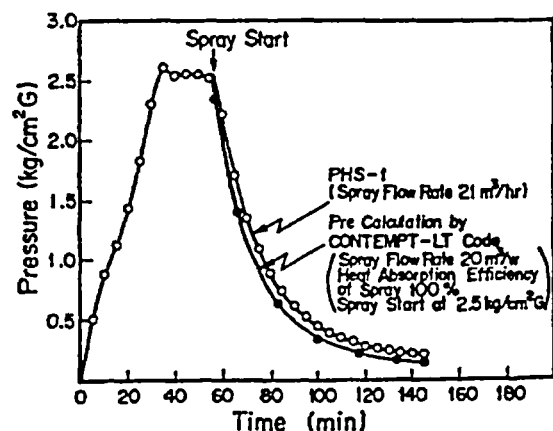


Fig.2 Pressure Change in PHS-1

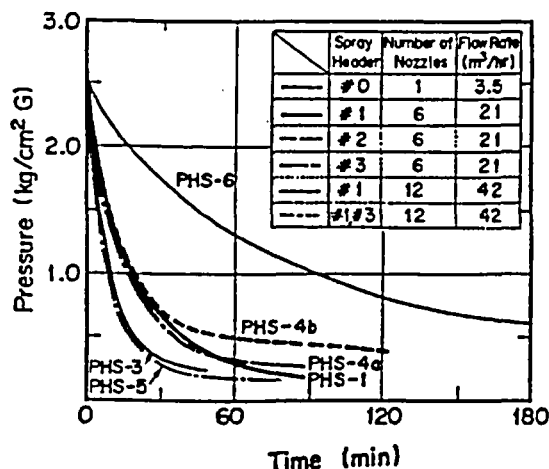


Fig. 3 Pressure Change in PHS Runs

Fig. 4 shows the average temperature-profile measured at the level in the containment vessel as a function of time after spray injection in run PHS-4b. The test was carried out with flow rate of water of 21 m³/hr from the header of #3 stage at the elevation of 9 m, located nearly half of the vessel.

It is noted that the temperature falls more speedily in lower level. The temperature at the level of 9.5 m and 11 m in non-spray region falls at the same rate as the temperature at the level of 7.5 m in spray region. However, the rate of temperature falling decreases with higher elevation. These results may be related to the heat preservation by air molecules in non-spray region. It is interesting to see after the start of spray for a while and then that is kept constant.

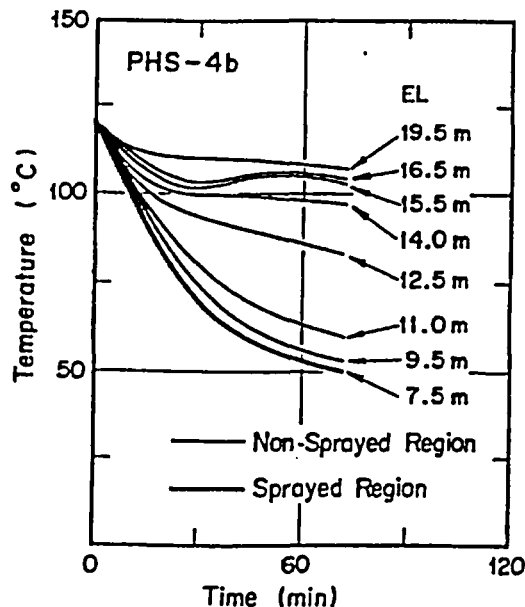


Fig. 4 Temperature in PHS-4b

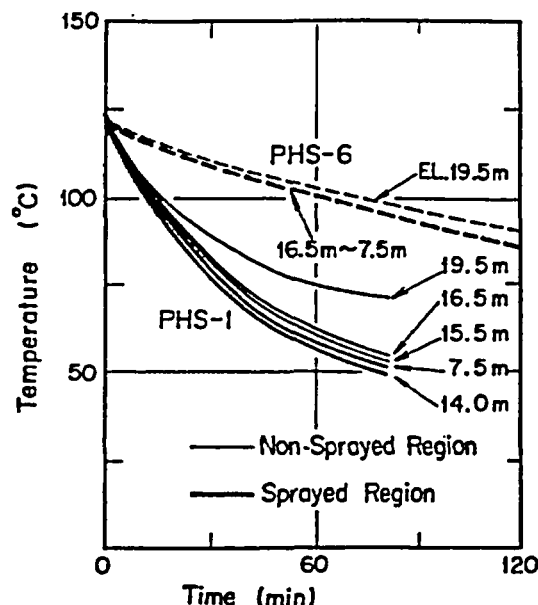


Fig. 5 Temperature change in PHS-1 and PHS-6

Fig. 5 shows the average temperature-profile in runs PHS-1 and PHS-6. In both cases, as the location of spray nozzles set at higher levels the temperature difference between spray region and non-spray region becomes smaller in comparison with the results in run PHS-4b. This smooth decrease of temperature in the vessel is considered as the effect of convection in the gas space between spray region and non-spray region by the drag forces of falling droplets. Another process considered is that the vaporization of droplets in the gas space of higher temperature may occur and the vapor move in the direction of the sprayed water on which the vapor condenses.

As mentioned above, when the steam is condensed on water droplets, the pressure in the containment vessel decreases and not only the steam but also the air existing in non-spray region move to spray region.

Considering these phenomena, fission products, especially radioiodine vapor, existing in both region of spray and non-spray in the containment vessel of PWR in the LOCA condition will have chance to be washed out.

References

- 1) Thorén, H.-G., Ericson, L., Heshöl, R., and Brandt, W.; "Full-Scale Containment Experiments Performed in the Märviken Power Plant", ANS National Topical Meeting on Water Reactor Safety, Salt Lake, Utah, March 26-28, 1973
- 2) Schmidt, R.C., Bingham, G.E. and Norberg, J.A.; "Simulated Design Basis Accident Tests of the Carolinas Virginia Tube Reactor Containment -- Final Report", IN-1403 (1970)
- 3) Sagawa, N.; "An Experimental Study of Spray Cooling in Nuclear Reactor Containers", Journal of Nuclear Science and Technology, Vol. 5, pp. 419 ~ 426 (1968)
- 4) Nagasaka, H.; 1976 Fall Meeting of the Atomic Energy Society of Japan, B72 (1976)

- 5) Kagawa, T., Nagasaka, H. and Tobimatsu, T.; 1976 Fall Meeting of the Atomic Energy Society of Japan, B73 (1976)
- 6) Nagasaka, H., Tobimatsu, T., Yanai, R. and Kagawa, T.; 1977 Annual Meeting of the Atomic Energy Society of Japan, E50 (1977)
- 7) Argonne Code Center; "CONTEMPT-LT Users Manual", (1973)
- 8) Uchida, H., Oyama, A. and Togo, Y.; "Evaluation of Post-Incident Cooling Systems of Light-Water Power Reactors", Proceeding of the Third International Conference on the Peaceful Uses of Atomic Energy Held in Geneva, 31 August-9 September 1964, Vol. 13 (1965)

DRAG FORCES IN A HYDRAULIC MODEL OF A FLUIDISED BED—PART I

By P. N. ROWE, B.Sc.(Tech.), Ph.D., A.M.C.T., D.I.C. (ASSOCIATE MEMBER)* and G. A. HENWOOD*

SUMMARY

This paper describes experiments that were made to measure the drag on a sphere in a water stream and how this drag varied with the presence of neighbouring spheres. The spheres were $\frac{1}{4}$ in. and $\frac{1}{2}$ in. in diameter and the flow conditions gave Reynolds numbers in the range 10 to 1000.

Increases of drag coefficient of almost two orders of magnitude are obtained when the sphere forms part of a regular packed array. Very large changes are associated with the surfaces of particle assemblies. Repulsive forces between particles have been found and also conditions that lead to a reduction in drag.

The results are used to explain some of the features of fluidised beds. They indicate the need to know more of the gas flow patterns before these results can be applied to bubble formation in gas fluidised beds.

Introduction

When fluid is passed upwards through a bed of particles, the bed is said to be fluidised when the drag force equals the effective weight of the particles and they are supported by the stream. The drag on an individual particle will depend, amongst other things, on the closeness and geometrical arrangement of neighbouring particles for this will determine the local flow pattern. The object of this research was to examine a model consisting of regular spheres and to see how the drag forces varied as fluid was passed through different geometrical arrangements.

Apparatus

A hydraulic system was used to measure drag forces as this simplifies much of the experimentation. It is well known that the drag on a body can be correlated with the product of its frontal area and the dynamic pressure by a coefficient (the coefficient of drag) which is a function of Reynolds number. Hence this investigation which is concerned with the geometrical arrangement of neighbouring bodies can be made independent of the nature of the fluid and of absolute size. There is no reason to suppose that the Reynolds number is a critical parameter in a fluidised bed. Systems spanning several orders of magnitude of this group behave in a broadly similar manner and both liquid and gas supported beds may have the same Reynolds number. $\frac{1}{4}$ in. spheres were used for convenience and drag forces could be measured at Reynolds numbers 25 to 100. This is roughly equivalent to 16 B.S.S. particles gently fluidised by air. In some different but related experiments observations were made on $\frac{1}{2}$ in. spheres at Reynolds numbers around 400.

The principal apparatus is shown in the photograph of Fig. 1. Distilled water was circulated through an open-topped Perspex tank 3 ft long with a flow cross section 6 in. \times 6 in. The superficial velocity could be varied from 0.5 to 1.5 ft/min. This corresponds to Reynolds numbers from 32 to 96 with respect to a $\frac{1}{4}$ in. sphere in the stream. Calming sections at the two ends of the tank were arranged to give a substantially uniform velocity over the centre two-thirds of

the flow section. The local water velocity was measured by introducing a fine stream of dye (about 0.016 in. diam.) from a drawn-out glass tube bent at right angles near its end to discharge horizontally downstream. When the tank was tapped sharply a small kink appeared in the dye stream and the progress of this was timed between scribe marks on the tank walls.

The spheres were made of polythene, $\frac{1}{4}$ in. diameter, obtained as cast sheets of several attached spheres. The surface finish was generally good except at the four points of attachment to other spheres. These rough points were removed by polishing. A small hole was drilled in the sphere and this was plugged with solder to make the overall density just greater than that of water. The sphere was supported by a 4 in. length of 0.007 in. Nichrome wire which was pushed into it.

For some experiments the sphere hung by its wire as a pendulum as shown in Fig. 2(a). The wire was bent at its top end and hooked over a tiny wire stirrup. Most of the wire was shrouded by a water-filled glass tube. The fluid

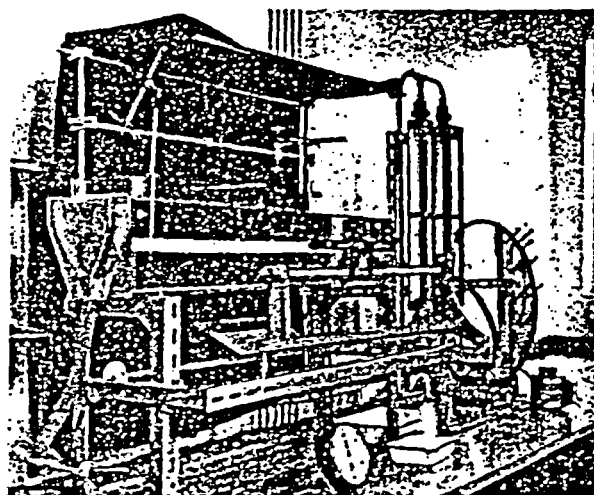


Fig. 1.—Photograph of apparatus—water tank

* Chemical Engineering Division, A.E.R.E., Harwell.

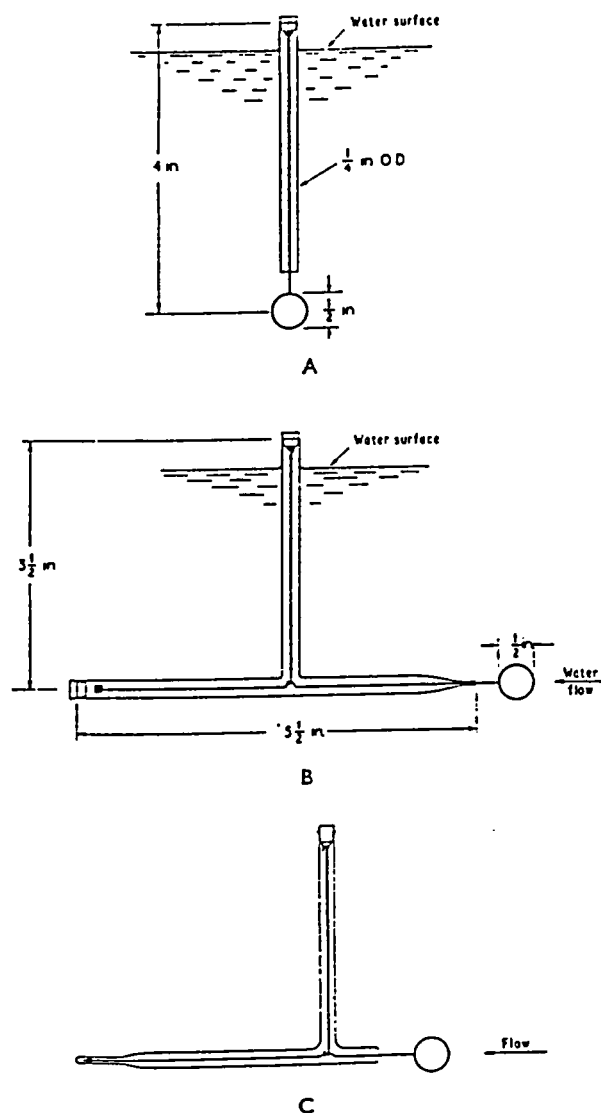


Fig. 2.—Sketch of apparatus—force balances

stream caused deflection which was measured by sighting a cathetometer on one edge. At small angles the deflection is proportional to drag and an absolute value can be calculated from the measured submerged weight of sphere and wire, the length of suspension, and the observed deflection. Typical values are, deflection = 0.05 cm, suspension length = 10 cm, submerged weight = 0.08 g, and resulting drag force = 4×10^{-4} g wt. The sensitivity of this method was about 5×10^{-6} g wt. The fluctuations in water temperature that were observed did not affect this sensitivity. An alternative method of suspension is shown in Fig. 2(b). This was particularly convenient when it was required to insert the sphere into some array of other spheres. It has the advantage of a support which is entirely downstream but it is heavier and hence its sensitivity is less. The horizontal support is counter-weighted at its downstream end and is supported at its centre of gravity in water by a hooked wire as previously. The wires are shrouded in a water-filled glass T drawn out where the wire protrudes about $\frac{1}{2}$ in. downstream from the sphere. The moving parts were weighed under water before assembly

in the glass shield and the drag force estimated from the deflection, weight, and length as before.

A further modification is shown in Fig. 2(c). This is for measuring drag and lift forces simultaneously. It is similar to the force balance of Fig. 2(b) but the upstream-facing limb of the glass T is left open and the opposite end is drawn down to a narrow diameter and closed. The horizontal wire-support can pass freely through the restriction to allow measurement of drag forces as previously. When lift forces act perpendicularly to the plane of the sketch, the horizontal beam hinges about its downstream restriction. By viewing a mirror below the transparent tank, the two deflections at right angles can be measured and the simultaneous drag and lift forces can be estimated.

Observations were initially made on a solitary sphere in the tank and these were compared with the correlation of other data in the same range of Reynolds number.¹ After making allowance for the drag on the short length of exposed wire, it was found that the drag using a downstream support was some 10% higher than previously reported.² This seems most probably to be a wall effect³ but was considered small enough to be of no consequence when measuring the effect on drag of neighbouring particles. There was some variation from sphere to sphere (about a dozen in all were examined) but a given one gave reproducible drag values.

All results are quoted as a ratio of the observed drag force to that when the same sphere was alone in the water tank (*i.e.* at infinite separation from any interfering sphere). Thus, any variation in the drag characteristics from sphere to sphere was effectively eliminated.

The other apparatus used was extremely simple and consisted of a Perspex tank $5\frac{1}{2}$ in. \times $5\frac{1}{2}$ in. \times 3 ft deep. This was filled with water and 5 in. \times 5 in. sheets of attached polythene spheres were allowed to rise through it whilst their velocity was measured.

In all the experimental work observations were made in random order except for the selection of water velocity which was not easy to set to a required value and was always tedious to measure. Once adjusted, observations were made over a range of sphere configurations with frequent checks of the velocity. In almost all cases these observations were repeated at least once with a fresh adjustment to the same water velocity. Where appropriate, the pattern of observations formed a simple factorial experiment.

Experimental Results—Part I

These results were all obtained with $\frac{1}{2}$ in. diameter spheres in the tank with horizontally flowing water just described. They are presented as a drag ratio, $\alpha = F_x/F_\infty$, varying with a separation ratio, $\delta = x/d$. The particle diameter, d , was not varied as this was not practicable and the Reynolds number was varied by a factor of three simply by changing the water velocity. In this narrow range the results were found to be independent of Reynolds number and it is believed that this is true over a wide range. McNown and Newlin⁴ have shown that this is at least approximately true for spheres within cylindrical boundaries.

Inspection of all the data suggests that the drag ratio varies inversely as the separation ratio for all the configurations examined. At infinite separation the drag coefficient is unity by definition so that the simplest equation that can be written is,

$$\alpha = \frac{K}{\delta} + 1.00 \quad (1)$$

where K depends only on geometry. This equation does not meet the terminal condition when $\delta = 0$ so that it can only apply above a certain minimum spacing.

The coefficient in equation (1) was found by averaging, i.e.

$$K = \frac{1}{n} \sum \delta(\alpha - 1)$$

and the resulting equation, where appropriate, has been drawn on the graph showing the results and is referred to as the "best hyperbola".

Consideration of purely viscous and purely turbulent flow suggests that the relationship between α and δ is more complex than equation (1) in the flow regime that is of interest in fluidisation. Nevertheless it will be seen that a simple hyperbola fits the data reasonably well and provides a simple form to include in any mathematical treatment of the consequences of particle interactions in a fluid stream.

Two spheres in line

The drag on a sphere was observed whilst it remained stationary in the water stream and another sphere was placed in line at different distances upstream and downstream. The results are shown in Fig. 3.

When the interfering sphere is upstream of that observed, the best hyperbola is,

$$\alpha = 1.00 - \frac{0.85}{\delta} \quad (2)$$

and when the interfering sphere is downstream,

$$\alpha = 1.00 + \frac{0.15}{\delta} \quad (3)$$

with the convention that downstream distances are negative. The error of a single observation about these curves is roughly $\pm 0.6/\delta$ so that it is high when δ is small. A practical limit to the drag ratio for near touching spheres appears to be 0.4 when the interfering particles is upstream and 0.8 when it is downstream. Thus, equation (2) and (3) are not valid with δ less than 2. The effect of an interfering sphere in line is not large unless the separation is only a few sphere diameters. Nevertheless, it appears that a drag reduction could be detected over 100 diameters away upstream but only about 30 diameters away downstream. As would be expected, an upstream obstruction has a greater effect on drag than a downstream one.

At very low Reynolds numbers when two spheres of equal diameter are in line in a fluid stream, the drag on each is equal.⁵ At the Reynolds numbers relevant to fluidisation, the leading sphere develops a wake which affects the drag on a following one. The average drag obtained from equations (2) and (3) agrees within a few per cent with the drag calculated for each of a pair in purely streamline flow.

Two spheres misaligned

The sphere was next observed whilst it remained stationary in the water stream and another, at a fixed radial distance was placed around it in a horizontal plane. The results are shown in Fig. 4 where the drag ratio is plotted against angular position. Curves have been drawn by hand to indicate the form of the variation but no attempt has been made to derive an equation which would obviously be fairly complex.

As the previous experiments showed, the effect dies away rapidly with increasing separation. Comparing areas bounded by the curve and the horizontal line $\alpha = 1.0$, it is seen that the general effect of a single near neighbour is to reduce the

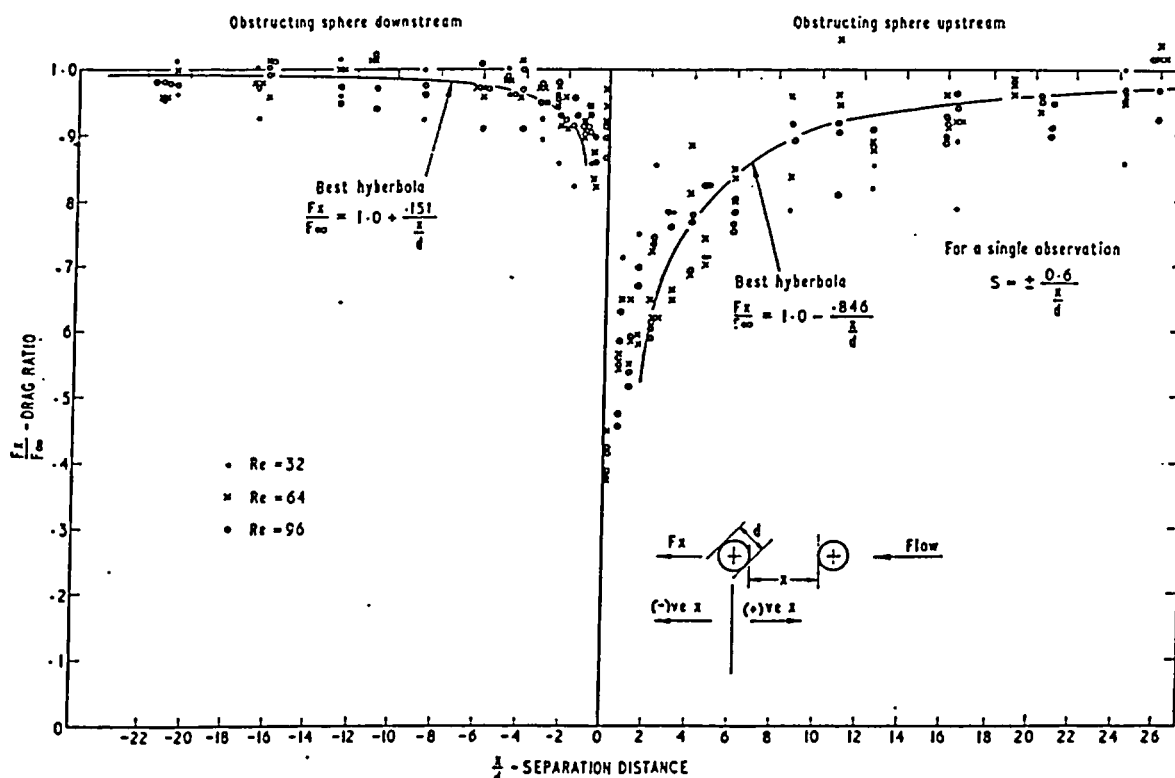


Fig. 3.—Graph of drag variation—two spheres in line

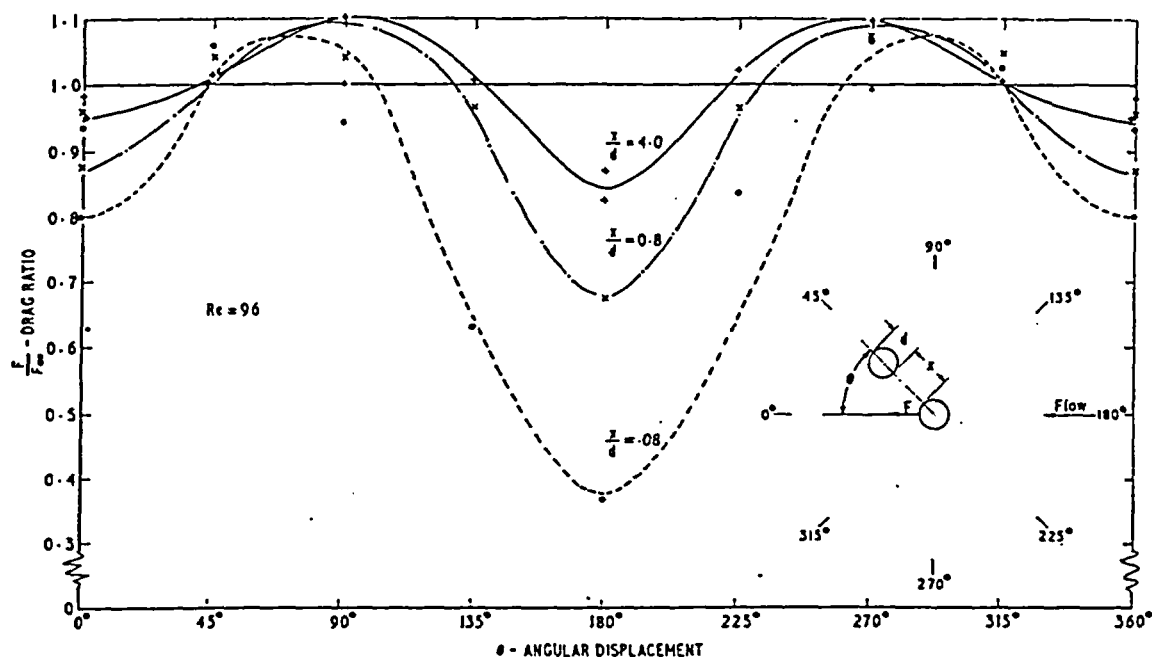


Fig. 4.—Graph of drag variation—two spheres misaligned

drag on a sphere. There is, however, a region adjacent to, but a little downstream of, the sphere where a drag increase occurs. The curve is, of course, symmetrical about the line of flow.

The lift and drag on adjacent spheres

A sphere was supported in the water stream in the manner shown in Fig. 2(a) and its deflection normal to the line of flow observed as well as the usual parallel deflection. This was done by viewing in a mirror set below the transparent tank. Observations were made as a second sphere was placed adjacent to the first at various separation distances. The results are shown in Fig. 5. By convention, lift and drag act at right angles. As the spheres approach, the drag increases by a maximum of about 15%. The lift increases sharply with approach and can be described approximately by the equation,

$$L_x/F_\infty = 0.15/\delta \quad (4)$$

This equation is unreliable at separations less than $\frac{1}{2}$ of a sphere diameter and the maximum lift observed was about 0.6 of the drag on an isolated sphere. Although only large at separations of less than one diameter, lift was detectable with the interfering sphere almost 10 diameters away. This is evidence in support of the already suspected slight wall effect in this apparatus.

This lift force is a special case of the lateral dispersive forces arising from fluid viscosity and described by Bagnold.⁶

The drag on a sphere near an assembly

The polythene spheres were cast as sheets of several attached spheres arranged in square packing. The sheets were square and two opposite edges finished in complete spheres whilst the other two edges were formed from half spheres as shown in Fig. 6. When several sheets are set one on top of the other with alternate ones turned through 90°, they form an assembly of spheres in rhombohedral packing, the closest possible.

Four sheets packed in this way were placed in the water tank so that they completely filled the cross section and all the fluid had to pass through the assembly. The drag on a single sphere at rest in the water stream was observed as this assembly was approached from the downstream and upstream directions. In a second experiment one sphere was removed from the centre of the sheet facing the solitary sphere which was moved up until it fitted into the vacant site.

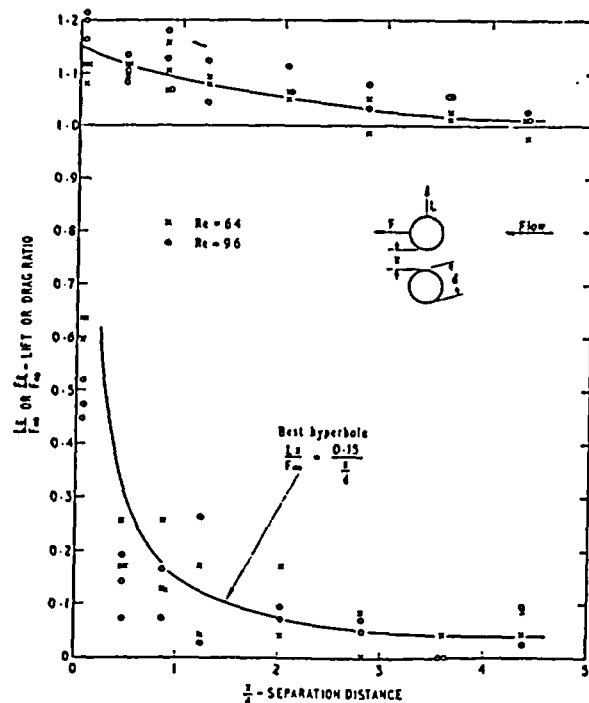


Fig. 5.—Graph of drag variation—lift and drag on adjacent spheres

The results for approach to a complete assembly are shown in Fig. 7. A hyperbola fits the data reasonably well at separations greater than six sphere-diameters but closer than this the slope of the curve reverses. An upstream obstruction causes quite a large increase in drag which falls off as the lone sphere gains the shelter of one in the assembly. A downstream obstruction has little effect but reduces the drag.

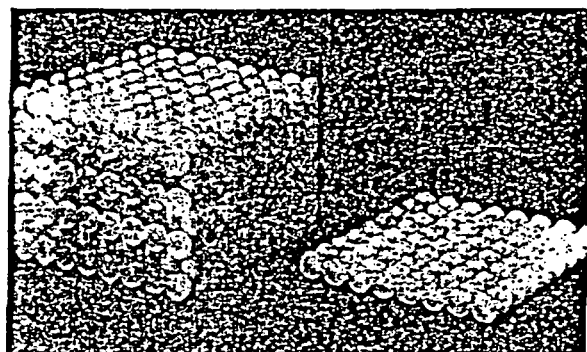


Fig. 6.—Photograph of sheet of spheres and of a stack

When there is a vacant site in the assembly the drag becomes very large indeed as the sphere approaches the hole, and forces approaching one hundred times the drag of an isolated sphere appear to be possible. Again the data can be represented by a hyperbola and the constants are shown in Fig. 8. With an upstream obstruction the same curve fits the data at separations more than six diameters but when the obstruction is downstream the forces are very different depending on whether there is a vacant site or not. From the equations which are based on all the data, the drag with an upstream obstruction is always greater than when it is downstream. It may therefore be inferred that the terminal value is greater and this is particularly relevant to the behaviour of fluidised

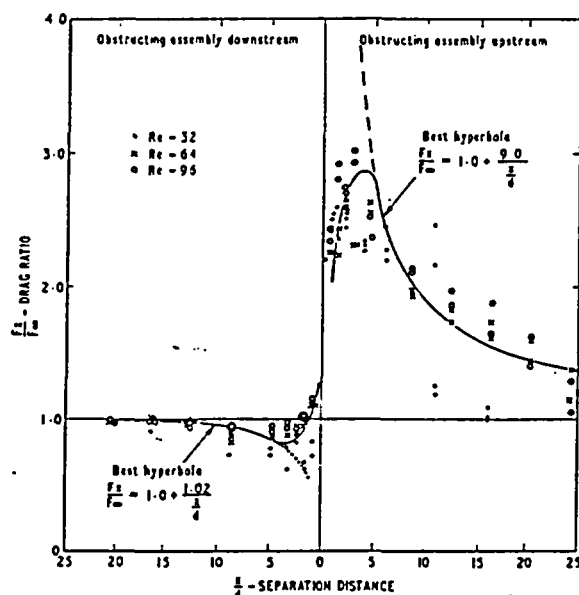
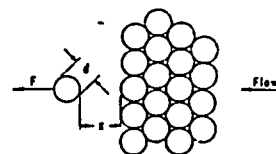


Fig. 7.—Graph of drag variation—single sphere near an assembly

particles and will be discussed later. Experimental observations with the sphere almost filling the vacant site are rather unreliable because the sphere tends to foul its neighbours and precise measurement of position is difficult.

Some of the above observations were repeated with the thickness of the assembly increased from four up to twenty-four layers without any detectable difference in drag forces.

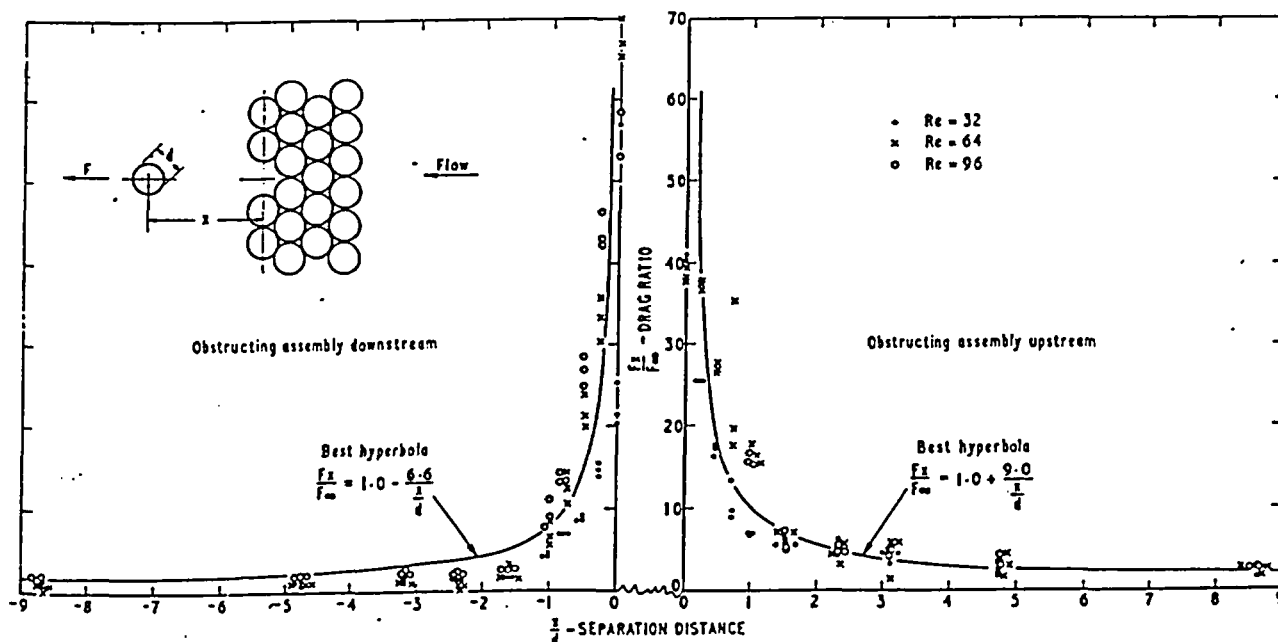


Fig. 8.—Graph of drag variation—single sphere near a defect in an assembly

It is concluded from this that the effect is independent of the thickness of the obstructing assembly once it is greater than about four particle diameters.

The greatly reduced drag as a sphere leaves an assembly for the open stream arises from the change in local fluid velocity. In this investigation it is more meaningful to regard the change as a geometrical effect which in turn controls the fluid velocity.

The drag on a sphere in an assembly and near a defect

The previous experiment was repeated in a modified form so that the drag forces on a sphere adjacent to a vacant site were measured as another sphere was brought up to the unoccupied place. Two adjacent spheres were removed from the centre of one face of an assembly and one was replaced by a sphere supported as in Fig. 2(c). By viewing in two directions at right angles the deflections due to lift and drag could be measured. Observations were made as a second sphere was moved into the remaining vacant site. Only the case of an upstream obstruction was examined.

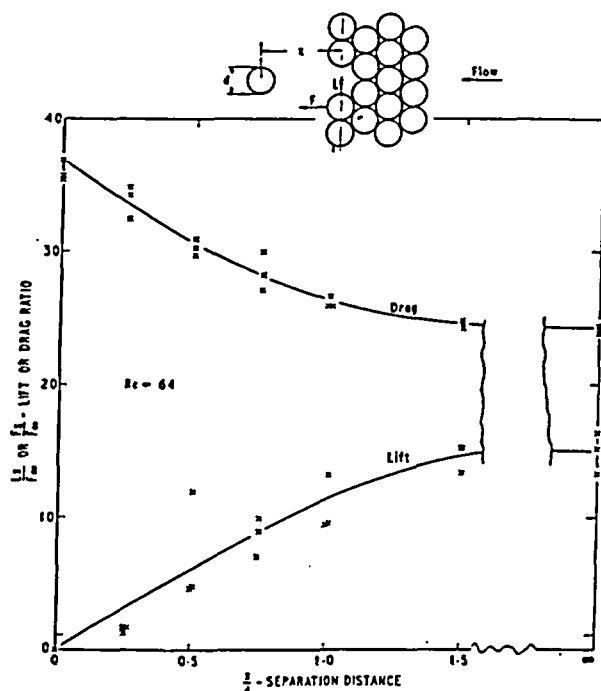


Fig. 9.—Graph of drag variation—sphere in an assembly near a defect

The results are shown in Fig. 9 where lift and drag ratios are plotted against separation distance of the second sphere. The drag ratio for a sphere in the assembly falls as its neighbour leaves from an initial value of about 40 to a terminal value of about 25, which is reached when the neighbour is little more than one diameter away. As has already been stated, these limiting values are not necessarily very accurate because of the difficulty of positioning a sphere in the assembly whilst leaving it free to deflect in order to measure the drag. Nonetheless, the form of the variation is shown in Fig. 9. The lift increases as a neighbour departs up to a terminal value of 15 times that of the drag on an isolated sphere and this is achieved when the departing sphere is one-and-a-half diameters away. Its sense is such that neighbours tend to move towards the path of the departing sphere.

Experimental Results—Part II

The results described in this part were all obtained by allowing assemblies of polythene spheres to rise through a stationary tank of distilled water. The assemblies were made from cast sheets of $\frac{1}{8}$ in. diameter spheres, each sheet 5 in. square ($8 \times 8 = 64$ spheres per sheet) arranged in square packing. Two opposite edges were formed by complete spheres and the other two by half spheres as shown in Fig. 6. The Perspex water tank was 3 ft deep and of $5\frac{1}{2}$ in. square in section. The clearance around the sheets of spheres was therefore such that a hydraulic diameter for interstices at the edge was similar to one near the centre. It was intended that flow through a complete sheet as it rose piston-like through the tank would be essentially parallel and could be regarded as typical of an infinite sheet.*

The drag on spheres in a plane array from which spheres are missing

A single complete sheet of spheres was timed as it rose over the centre 12 in. section of the tank. Some spheres were then removed from the sheet and the experiment repeated. Spheres were always removed in a symmetrical pattern to ensure that the sheet remained horizontal in the tank and they were taken either from the centre or from the sides.

The observed average coefficient of drag per sphere was calculated from the known drag (the buoyancy force), the frontal area of a sphere, the fluid density, and the observed terminal velocity.

$$\bar{C}_D = \frac{gF}{A \cdot \frac{1}{2}\rho u^2} \quad (5)$$

$$= K \cdot t^2 \quad (6)$$

where t is the time to rise past the measured marks. A Reynolds number based on the diameter of a single sphere was also calculated, and this used to calculate the drag coefficient for a single sphere moving at the same velocity from Schiller and Naumann's correlation,¹

$$C'_D = \frac{24}{Re} (1 + 0.15 Re^{0.687}) \quad (7)$$

which applies to the range of Reynolds number observed during these experiments ($Re \sim 300$). The ratio of these two drag coefficients, \bar{C}_D/C'_D is a measure of the drag increase caused by packing the spheres together. It is an average drag ratio, $\bar{\alpha}$.

The results for a single sheet are shown in Fig. 10 where the ratio of drag coefficients is plotted against the number of spheres removed from a sheet. The average drag per sphere does not appear to depend upon which spheres are removed but only on the number removed. This confirms the expectation of parallel flow and the equivalence of edge and centre spheres. The drag ratio for a complete sheet is 36.7 and this is based on 30 independent measurements. The standard deviation of a single observation is ± 0.6 but this error increases with the rate of rise until, with a single sphere, it is impossible to obtain a satisfactory drag value because the terminal velocity is not achieved until the sphere has risen through about half the depth of the tank. For all but a single sphere this limitation was not reached.

* The drag force on a sphere in an array can be related to the pressure drop through the assembly and this compared with accepted equations for flow through packed beds. The authors hope to publish a note on this topic in the near future.

As a further check on the absence of wall effect, a single observation was made in a 12 in. square tank in which a large sheet built up from the standard 5 in. sheets was allowed to rise. This gave a similar drag ratio. Thus, for a complete and regular array, the drag appears to be equally shared by all members.

As spheres are removed, the average drag per sphere falls rapidly. The removal of 12 spheres (less than 20%) halves the drag ratio. Since the majority of spheres are still surrounded by neighbours as in a complete sheet, it follows that the reduced drag per sphere is not so much a changed local drag coefficient as a change in overall flow pattern and channelling through the hole. The drag is halved by a reduction in velocity of $1/\sqrt{2}$ and this would little more than double the velocity of flow through a 20% hole. This is not a very great distortion of normal parallel streamlines and illustrates the point that small deviations from uniform flow may have large effects on the distribution of drag forces.

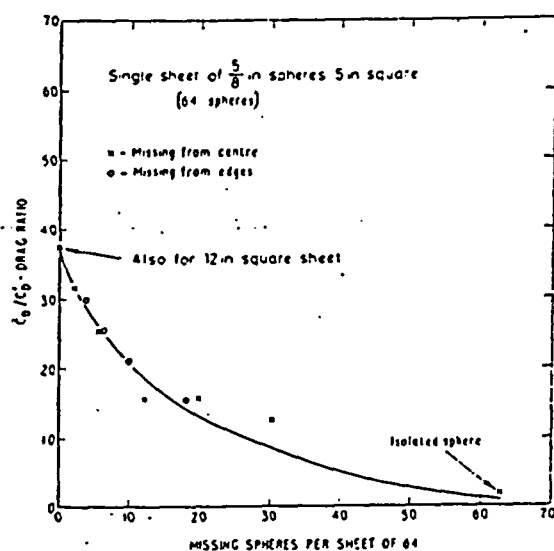


Fig. 10.—Graph of drag variation—plane array of spheres with members missing

The drag on spheres in multi-layered assemblies

Several complete sheets of spheres were stacked, tied together with fine wire, and allowed to rise through the tank. The sheets were stacked in either rhombohedral or cubic packing and in the latter case small pins were necessary to hold the sheets in position. A stack of 10 layers was the maximum that could be accommodated without excessive binding against the walls.

The results are shown in Fig. 11 where the drag ratio is plotted against number of layers for the two kinds of packing. It is seen that close rhombohedral packing results in a drag coefficient almost four times that for open cubic packing. With open packing, the average drag per sphere diminishes as additional spheres shield one another. This effect, however, is not felt above about 4 layers. With close packing the partial closing of interstices in one layer by spheres in the next immediately increases the average drag which continues to increase with a stack up to about 4 layers thick. Further layers reduce the drag a little. A stack of 10 layers was turned on its side when it almost filled the cross section of the tank and gave a drag ratio some 25% greater than previously.

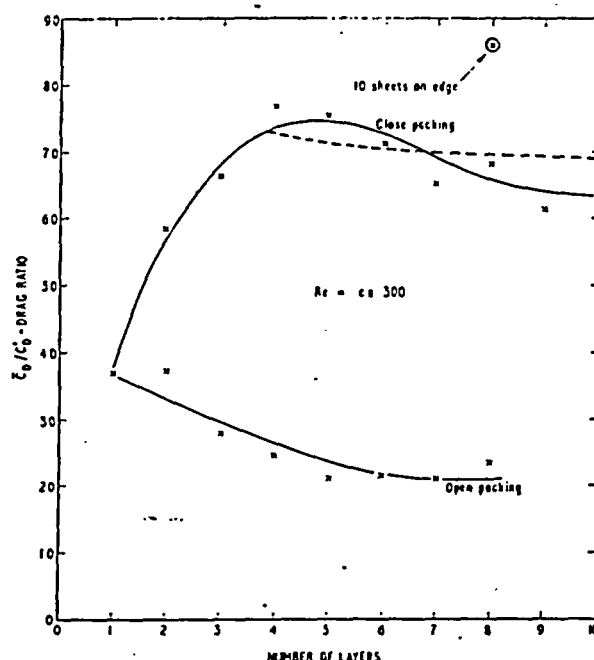


Fig. 11.—Graph-effect of layer thickness and packing on drag increase

This suggests a packing orientation effect⁷ although it must be remembered that the stack now includes many half spheres in its upper and lower face.

The experimental work reported in the previous section measured the drag on an individual sphere in the downstream and upstream facing layers of a close-packed assembly. As explained, the actual terminal value is difficult to measure and it might be argued that this is an arbitrary concept anyway. As two spheres approach in a fluid stream, the repulsion caused by flow will eventually be replaced by a repulsion resulting from physical contact. In a case such as that represented by Fig. 8, the change from one form of repulsion to another might appear to be continuous as a first approximation over a short range. In this way the best hyperbolas of Fig. 8 can be regarded as applying when the spheres are lightly in contact and a terminal drag value can be defined by an appropriate selection of separation distance. Arbitrarily, let this terminal separation ratio, δ_0 , be 0.01, which was about the limit of possible measurement. This gives a "terminal" drag ratio of 91 for a sphere in a downstream facing surface and 67 for one in an upstream facing surface. At small value of δ the ratio of these two numbers is virtually independent of this arbitrarily chosen critical distance.

Refer again to Fig. 11 and in particular to the drag ratio obtained for a four-layer stack in close packing which is analogous to the situation examined in Fig. 8. The value obtained is about 74 which is intermediate between the two suggested values for drag on the spheres in the upper and lower surfaces. This indicates that a sphere in the upstream-facing surface is typical of the interior whilst one in the downstream facing surface is in a plane of high drag. The distribution of drag forces thus appears to be as shown in Fig. 12 giving a predicted average drag ratio of 73. This indicates that the arbitrarily chosen critical separation distance is a fair estimate of contact conditions.

As the thickness of a stack grows, the average drag ratio will tend to that of a typical interior sphere which appears to

be about 67. Thus the curve of Fig. 11 shows a maximum before falling off asymptotically. A curve based on this and the distribution indicated by Fig. 12 is shown dotted in Fig. 11. The data suggests that the difference between the drag on the upper and lower layers is greater than the previous estimate but the absolute values are not greatly in error. Because of the greater drag on the downstream facing layer, it tends to separate from the stack unless they are all tied together. This is another fact of importance in interpreting fluidisation phenomena.

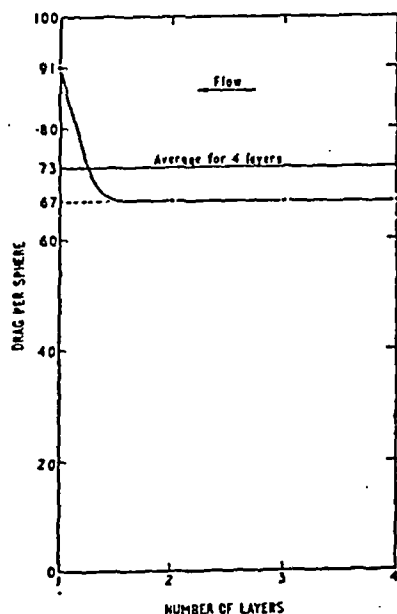


Fig. 12.—Distribution of drag forces amongst layers

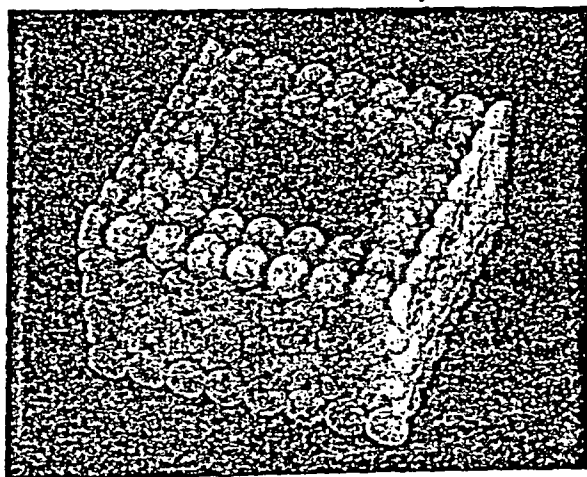


Fig. 13.—Photograph of sheet of spheres with members removed

The drag on spheres in multi-layered assemblies containing cavities

The previous experiment was repeated with layers in close packing only and with spheres removed from some of the sheets. Spheres were removed symmetrically as shown in Fig. 13 and stacks were built in such a way that the void was roughly spherical and in the centre of the assembly. A few

cases were included with spheres missing from the edges. Stacks of 3, 5, 7, and 9 layers were examined.

The results are shown in Fig. 14 where the drag ratio is plotted against the missing spheres expressed as a fraction of the total. They fall into two classes depending upon whether the hole extends right through the stack or not. Although the

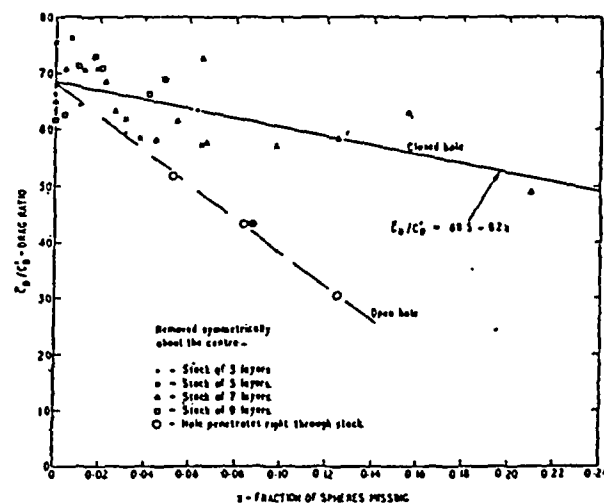


Fig. 14.—Graph-effect of cavity size on average drag per sphere

scatter is high [standard deviation of a single observation of drag ratio is $\pm 5 (28 d/F)$], there is a uniform trend for closed holes which can be described by,

$$\bar{a} = 68.5 - 82x \quad (8)$$

where x is the fraction of spheres missing. This applies to closed roughly spherical holes.

In a few cases an open hole was formed. That is to say, spheres were missing from the top and bottom. This arrangement produced a much more rapid reduction in drag because of the streaming that can occur through the centre.

Equation (8) has a necessary end condition. When $x = \pi/6$ or 0.5, the spherical hole will just break the surface of a containing cube and an open hole is formed so that the drag ratio will fall considerably. The results for assemblies with spheres removed from the edges are shown in Fig. 15

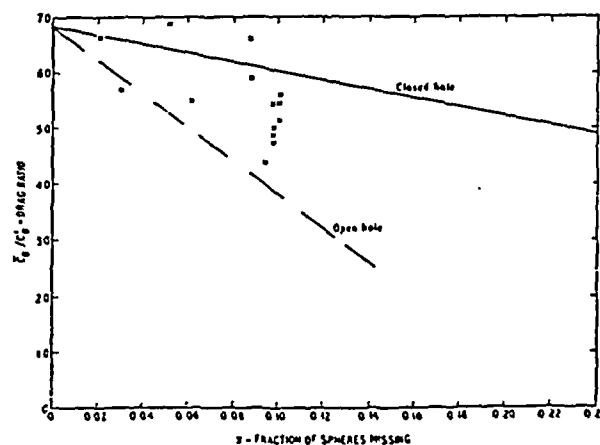


Fig. 15.—Graph-effect of edge cavities

and in general they lie in between the curves for open and closed holes. When the pattern of spaces was such that channels were formed, the drag ratio more nearly approached that for an open hole.

The drag on linear chains of spheres

The last experiment in this series was made with a chain of 6 attached spheres cut from one of the sheets. A sphere at one end was weighted with a plug of metal, and the assembly allowed to rise through the water tank whilst its velocity was measured. An unweighted sphere was removed from the top end and the experiment repeated with 5 spheres. This procedure was repeated for 4 and 3 spheres, the minimum number that would rise vertically without oscillation. At each stage the drag force was measured by weighing the prepared chain under water.

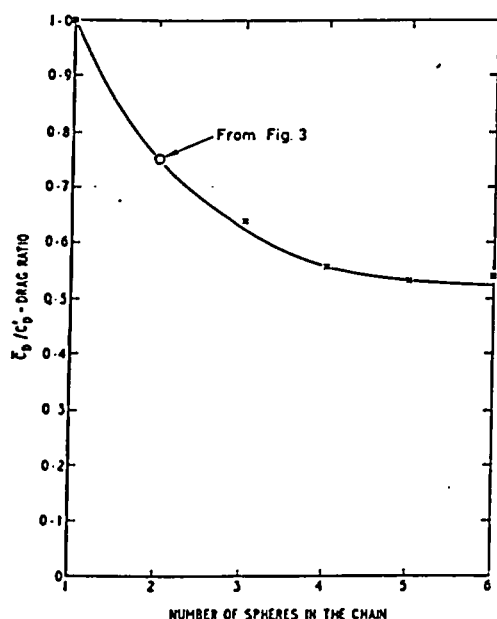


Fig. 16.—Graph-effect of chain length on average drag per sphere

The results are shown in Fig. 16 where the drag ratio is plotted against the length of chain. The Reynolds number based on a single sphere diameter was higher than previously and averaged about 3000. The average drag per sphere is seen to reach a limiting value of about half that of a solitary sphere and this is reached once the sphere is 4 members long or more. Again it is seen that assemblies more than 3 or 4 diameters thick approximate to infinite systems. Included in Fig. 16 is a value for a two-member chain obtained by averaging the limiting values previously observed and shown in Fig. 3. This shows good agreement with the present results and, since it was obtained at a Reynolds number two orders of magnitude less than the others, supports the view that there is no Reynolds number effect.

Discussion

From all the foregoing evidence, the following facts appear to have an immediate bearing on fluidisation phenomena:

1. Spheres in line or approximately so shield one another so that the drag of each is reduced. This is quite a long-range effect persisting for tens of sphere diameters.

2. In a close assembly, the drag on a sphere is increased by an order of magnitude. How many spheres constitute an assembly has not been determined but it is probably quite a small number.

3. Adjacent spheres repel one another. (If fluidised particles achieve a degree of random motion, Bagnolds' dispersive forces originating from grain inertia will arise.)

4. Upstream-facing surfaces strongly attract particles to any defect.

5. Downstream-facing surfaces strongly expel particles but this is a force that falls off very rapidly with distance.

6. A sphere in a downstream-facing surface is subjected to a higher drag than any other in a uniform packed array.

7. The loss of a sphere from a downstream-facing surface is accompanied by a reduction in drag on the remaining neighbours.

8. Small departures from parallel flow will have a large effect on drag distribution within any array of particles.

9. The drag on a sphere in an array varies fairly considerably with the packing arrangement.

10. The drag on spheres in an array seems to be insensitive to the size of any void in the assembly.

11. The drag ratio is insensitive to changes in Reynolds number if not independent of it.

The liquid-like properties of a fluidised bed can be explained in general terms by these conclusions. Lateral repulsive forces will cause the bed to spread and fill its container whilst the greatly reduced drag experienced by a particle which leaves the top will cause it to fall back and so maintain a stable and definite upper surface.

Stability of upper surface

The stability of this surface can be considered in more detail. When the fluid velocity is just sufficient to support a particle in the interior of the bed, one on the surface will tend to be expelled since the drag here is higher than elsewhere. If expelled, the particle will soon fall back as the drag falls off rapidly with distance from the surface but its departure will reduce the drag on those remaining which will tend to close the vacated site. Thus there is activity on the surface of a bed at the point of incipient fluidisation with numerous individual particles leaping a few diameters free of the surface and falling back again. This can be seen quite clearly especially when uniform spherical particles are fluidised by gas or liquid.

Even if the fluid velocity is so great that occasional particles do escape, there is still a fair chance that they will be recaptured. This is because of the long-range shielding effect of particles in line. Whenever particles align in a stream just sufficient to support them, they will fall and "condense" back to the surface from which they had previously escaped. Thus, the surface has very great stability and a property somewhat analogous to surface tension. It is interesting to note that this surface stability stems from a repulsion between particles and therefore it may be misleading to pursue too far this analogy with surface tension in liquids.

It is only when spheres are in line that they reduce one another's drag, but this must be an unstable arrangement because of the lateral repulsive forces that exist. The extreme case of open packing must be very rare and an approximation to close packing will be more usual. The repulsive forces will keep the particles separated and physical contacts between them will be limited so that the bulk of the bed has liquid-like properties.

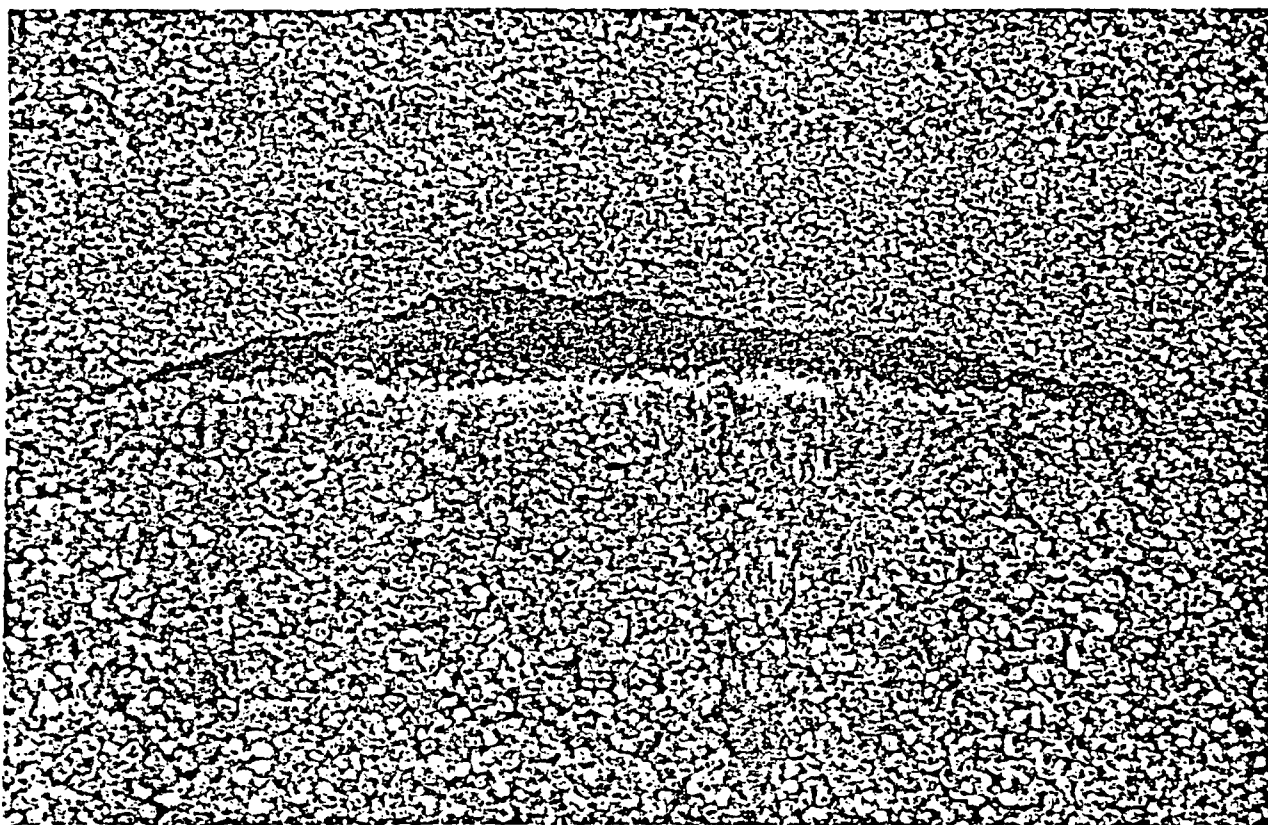


Fig. 17.—Photograph of stationary lens-shaped void in a fluidised bed

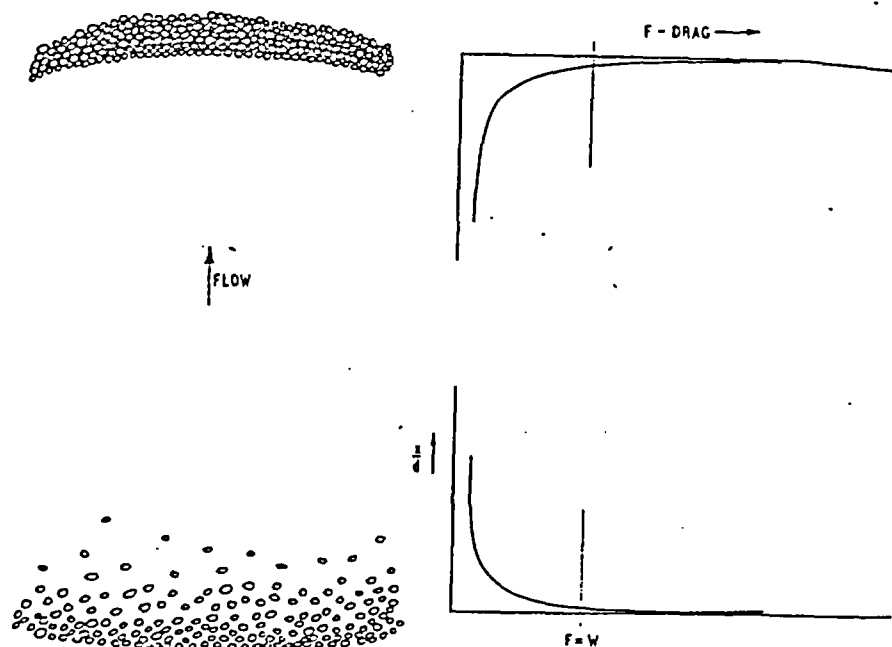


Fig. 18.—Distribution of drag forces through a stationary void

Before the minimum fluidisation velocity is reached, the topmost layer of particles will be subjected to the greatest drag. They will therefore be the first to lift and under conditions of uniform flow, fluidisation will start from the top and develop downwards as each layer lifts and allows the one below it to follow suit. This would not occur with square packing where the leading sphere of each line carries the greatest drag.

The uniform fluidisation "from the top downwards" described above is a common feature of liquid fluidised systems but is rarely seen with a gas-supported bed. The reason for this is difficult to see but is probably associated with non-uniform gas distribution. It has been shown that the drag distribution is sensitive to departures from parallel flow. Drag is also sensitive to changes in packing arrangement so that an initial small disturbance might grow and the characteristically heterogeneous gas fluidised bed will develop. Because of the greater inertia of the fluid, liquid-supported systems will be less prone to channel formation and the maldistribution of drag forces that follows.

Formation of voids

The formation of gas pockets, voids or "bubbles" in gas fluidised systems is a puzzling feature that has so far defied any logical explanation. The foregoing assists in understanding the stability of such voids once formed. For example, it has shown that the forces associated with a surface lead to a form of surface tension and so maintain the stability of a downstream facing surface. An upstream-facing surface is similarly stable for the drag forces increase enormously as a particle approaches it. The surface is supported and maintained by a flow of fluid through it at a rate far less than that needed to support an isolated particle.

This can be illustrated by a simple experiment. Uniform spherical particles of 0.75 mm diameter were fluidised by both gas and liquid in a long tube the top of which was closed by a porous plate. The fluid velocity was increased until particles were transported and the material built up as cake against the upper closure. The under-surface of this cake was smooth and regular and the fluid velocity could now be reduced and the cake was still firmly supported.

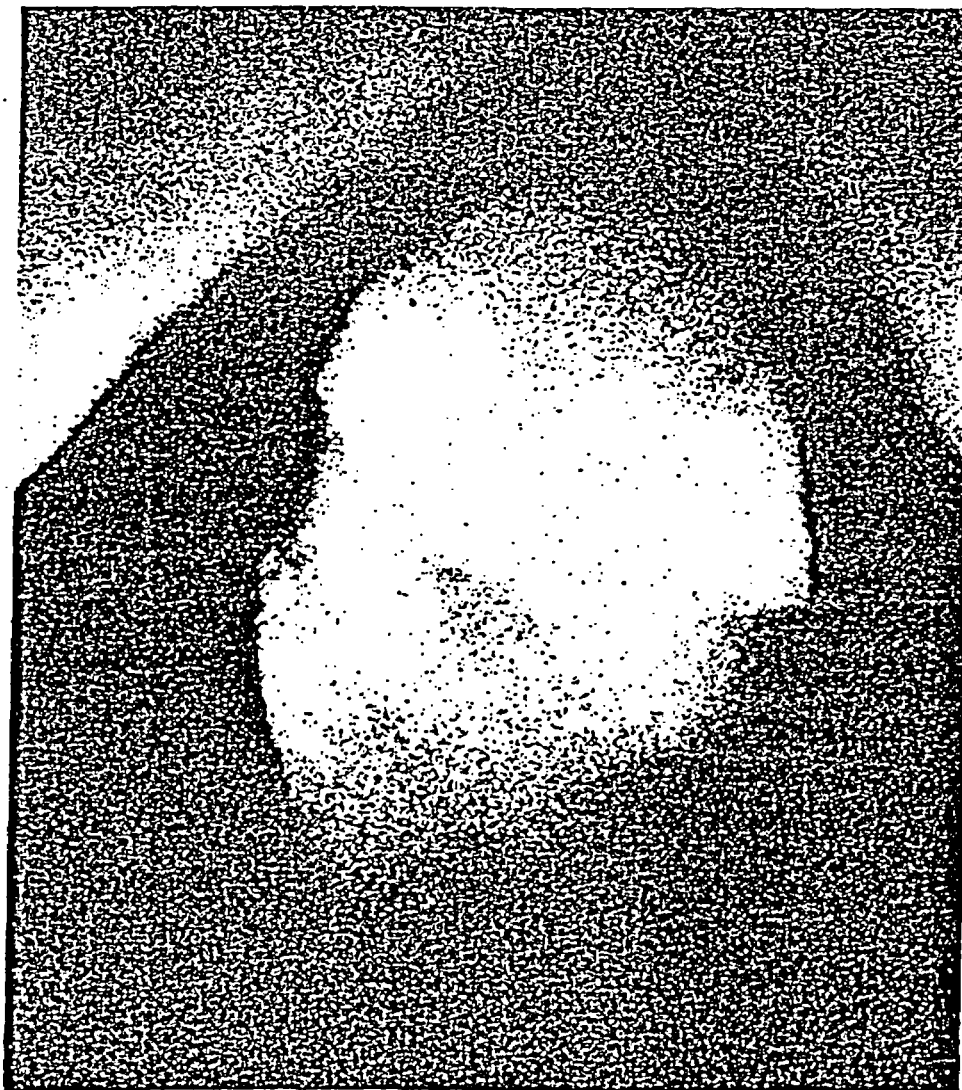


Fig. 19.—Photograph of "bubble" breaking the surface of a gas fluidised bed

Particles were not locked for the tube could be shaken but eventually, at a rate roughly twice the minimum fluidisation velocity, they rained down in a uniform manner. The minimum supporting velocity was quite clearly defined. The drag on a sphere at the bottom of the cake was thus a little less than on one in the fluidised bed and the drag was fairly uniformly distributed so that the particles eventually rained down and did not fall as a cake. This dynamic consolidation is in accord with the drag forces that have been reported.

The stability of the lens-shaped stationary voids that occasionally occur in fluidised beds is thus explained. Fig. 17 is a photograph of a stationary void against the transparent wall of a bed of sand fluidised by air. A deliberately-long exposure shows that particles in the roof are more or less at rest whilst those in the floor are in a state of motion. (a few particles are apparently stationary in the void but they are attached to the wall by static charges.) In the centre of the void the drag is insufficient to support particles so that they fall. The lower surface is stable but maintained in a state of agitation and the upper surface is dynamically consolidated as a clear and definite interface. Fig. 18 illustrates the distribution of drag forces. Although its stability can be explained, the means by which such voids are initially formed is not clear.

Fig. 19 is a photograph of a free "bubble" just breaking the surface of a bed of sand fluidised by air. The bed, 12 in. wide but only 1 in. from back to front, is effectively two-dimensional. The void is seen to be fairly free of particles and those that can be seen are mainly falling close to the wall where the gas velocity is low. The edges of the void are definite and suggestive of the high drag force situations that arise at the surfaces of particle assemblies. The arched bubble-roof implies dynamic consolidation and a horizontal component of gas velocity. It does not break as a bubble in liquid does but falls back as a coherent mass as the gas from the void passes through it. Drag measurements give some clues as to the nature of bubbles in fluidised beds but little progress can be made until the gas flow associated with them is known.

The findings described by Fig. 14 are a little surprising. They show that the drag on spheres in an array is insensitive to the presence of a void in the assembly. This conflicts with the conclusions to be drawn from Fig. 10 which indicates channelling towards the hole in a single sheet. Bubbles in a gas fluidised bed almost certainly disturb the gas flow in adjacent material. Perhaps the important criterion of void-size in this context is the ratio of diameter to particle diameter and by this standard the experimental voids were very small.

Conclusions

The drag on a sphere can vary widely depending on the arrangement of neighbours. In a packed assembly, the drag is increased by one or two orders of magnitude over that on a sphere at the same nominal velocity but in isolation. Adjacent particles repel one another and it is generally only

when spheres are in line that they reduce the drag on each other. Commonly drag forces vary inversely with separation distance. Large increases in drag are observed as a particle approaches the surface of an assembly.

Some features of fluidised beds can be explained in terms of the prevailing drag forces acting on its constituent particles. Surfaces formed by particle assemblies normal to the direction of flow are shown to be stable and to possess a property loosely analogous to surface tension. Little light has been thrown on the problem of bubble formation in gas fluidised beds but the investigation has pointed to the need to know something of the gas flow patterns that are associated with bubbles.

Acknowledgment

The authors are much indebted to Mr. J. B. Lewis for helpful discussion and suggestions throughout the research.

Symbols Used

- A = frontal area of sphere.
- \bar{C}_D = measured average drag coefficient.
- C'_D = calculated drag coefficient for an isolated sphere.
- d = sphere diameter.
- F_x = drag force with spheres separated by distance x (in weight units).
- F_∞ = drag force at infinite separation (in weight units).
- g = gravitational acceleration.
- K = a constant.
- L = lift force (in weight units).
- Re = Reynolds number.
- U = sphere velocity or nominal fluid velocity.
- x = separation distance or fraction of spheres missing.
- α = drag ratio = F_x/F_∞ or \bar{C}_D/C'_D .
- δ = separation ratio = x/d .
- ρ = fluid density.

The above quantities may be expressed in any set of consistent units in which force and mass are not defined independently.

References

- ¹ Schiller, L. and Naumann, A. *Z. Ver. deutsch. Ing.*, 1935, 77, 318.
- ² Henwood, G. A. and Rowe, P. N. *The Drag on a Half Inch Sphere in Water at $Re = 25$ to 100*, U.K.A.E.A. Memo. A.E.R.E., M.633, February, 1960.
- ³ McNown, J. S., Lee, H. M., McPherson, M. B., and Engez, S. M. *Influence of Boundary Proximity on the Drag of Spheres in Proceedings of the 7th International Congress for Applied Mechanics*, London, 1948. (London: The Institution of Mechanical Engineers.)
- ⁴ McNown, J. S. and Newlin, J. I. *Drag Spheres within Cylindrical Boundaries*, in *Proceedings of the 1st National Congress of Applied Mechanics*, 1951. (New York: American Society of Mechanical Engineers.)
- ⁵ Stimson, M. and Jeffery, G. B. *Proc. roy. Soc.*, 1926, A.111, 110.
- ⁶ Bagnold, R. A. *Proc. roy. Soc.*, 1954, A.225, 49.
- ⁷ Graton, L. C. and Fraser, H. J. *J. Geol.*, 1935, 43, 77.

The manuscript of this paper was received on 5 April, 1960.

DRAG FORCES IN A HYDRAULIC MODEL OF A FLUIDISED BED—PART II

By P. N. ROWE, B.Sc., Ph.D., A.M.C.T., D.I.C. (ASSOCIATE MEMBER)*

SUMMARY

A regular array of $\frac{1}{4}$ inch spherical particles was constructed and placed in a water stream. The drag on a sphere was measured as a function of the spacing between particles and expressed as a ratio of that on a sphere at a given spacing to one in isolation at the same superficial fluid velocity. This drag ratio was found to vary inversely as the separation distance.

The results are applied to fluidised beds and it is concluded that small local changes in particle concentration are unstable as they would require a very large re-distribution of fluid velocity. The only exception to this is when the particles are separated by tens of sphere diameters. On the other hand, the displacement of one sphere from its lattice position makes very little difference to the drag forces.

The results are also used to predict the minimum fluidisation velocity and this agrees quite well with experimental observations.

Introduction

The particles in a fluidised bed are supported by the drag forces produced by the relative flow of fluid upwards through the bed. The drag force can be correlated with the product of dynamic pressure and the projected area of the particle by a coefficient, the coefficient of drag, which is a function of Reynolds number, the particle shape, and the geometrical arrangement and closeness or concentration of the particles. This paper describes an experimental determination of the effect of concentration on the drag acting on spheres arranged in a regular geometrical pattern in a fluid stream. The results are used to discuss the stability of fluidised beds and to predict the minimum fluidisation velocity.

Experimentation

The apparatus has been described by Rowe and Henwood¹ and consisted of an open-topped Perspex tank 3 ft long and of 6 in. \times 6 in. cross section. Water was circulated through the tank at a velocity of about 1 ft/min. so that the flow was streamline and the velocity was uniform over the centre section of the tank. A $\frac{1}{4}$ in. diameter polythene sphere was suspended in the stream. The sphere was supported on a horizontal wire which hung at its centre of gravity from a vertical wire hooked at its upper and lower ends. The wire was shrouded by an inverted glass T and a drag force on the sphere deflected the sphere and wire as a pendulum, the displacement being measured by a cathetometer. The submerged weight of the sphere and wire was about 0.1 g and a deflection of about 0.02 cm occurred at a velocity of 1 ft/min. This corresponds to a drag force of about 2×10^{-4} gram weight at a Reynolds number of 64.

A number of other $\frac{1}{4}$ in. polythene spheres was drilled across a diameter and threaded on to 0.022 in. diameter Nichrome wire on which they were a tight sliding fit. Several of these strings of beads were mounted parallel to one another in a rectangular frame, the wire being kept taut by tension springs. The beads in this "abacus" were arranged in a rectangular net with a constant distance, x , between adjacent spheres. Three of these frames were made and held

together as three layers with the same particle spacing, x , between them and the pitch of the centre layer displaced by half a unit. The whole assembly was placed in the water tank with the plane of the layers inclined at 60° to the direction of flow. In this way the spheres lay in an hexagonal pattern in planes parallel to the direction of flow. The assembly just filled the cross-section of the water tank and is shown in Fig. 1.

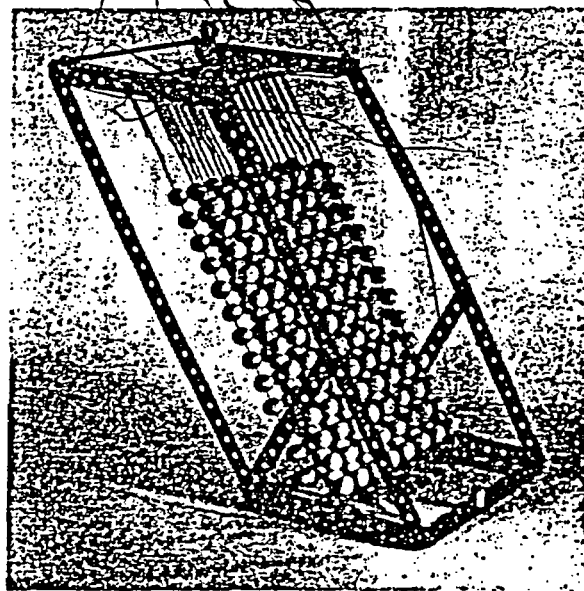


Fig. 1.—Photograph of sphere assembly

It was made so that the separation distance, x , could be varied.

The centre sphere of the middle layer was omitted and its position occupied by the sphere mounted in the inverted glass T referred to above. In this way the drag on a sphere was measured as it was surrounded by a regular array of other spheres at a constant and known separation distance. Pre-

* Chemical Engineering Division, A.E.R.E., Harwell.

vious work¹ has shown that the drag on three layers of close-packed spheres approximates to the conditions obtaining in larger assemblies and so this arrangement gives a fair indication of the forces that will act on a sphere in a uniform large cloud of spheres in a fluid stream.

Procedure

The experimental procedure was as follows. The water velocity was set to a given value and measured by timing the progress of an interrupted dye-stream through the working section and the drag on the sphere alone was measured. The sphere assembly, previously built to a chosen spacing, was lowered into the tank, placed around the drag-measuring sphere, and the drag measured again. The water velocity was changed and a further observation made after which the assembly was removed and the drag on the sphere alone measured at the new velocity. The assembly was replaced and the measurement repeated. In all, the measurements were replicated three times at each of the water velocities, 0.5, 1.0, 1.5 ft/min. The velocity was varied in random order as was the setting of sphere spacing but once a given spacing had been built all measurements were made with the one setting.

A supplementary experiment was also carried out. The sphere-assembly was built to a spacing $\delta = 0.35$, placed in the tank and the water velocity set to 1.5 ft/min. The drag-measuring sphere was placed in its normal position in the lattice and the drag was recorded. It was then moved along a principal lattice axis and the drag recorded at various displacement positions until it touched its neighbour. Observations were repeated with movement along another axis at right angles and also with the sphere in its central position whilst a neighbouring sphere was displaced similarly. Accurate positioning was difficult but no significant changes in drag were observed during these displacements.

Results

The results are shown in Fig. 2 where the ratio of the observed drag to that of a sphere in isolation, $\alpha = F/F_\infty$ is plotted against the separation ratio, $\delta = x/d$. From previous

work¹ it was thought that the variation might take the form of:

$$\alpha = \frac{K}{\delta} + 1.00 \quad (1)$$

and accordingly a line with the best estimate of K has been drawn which is,

$$\alpha = \frac{0.68}{\delta} + 1.00 \quad (2)$$

The standard deviation of an estimate from this equation is about $\pm 0.1/\delta$ and it is seen to be a reasonably good description of the data. This assumption of a hyperbolic relationship between α and δ is arbitrary but it does in fact fit the data well over the range examined. There is no reason to believe that equation (2) has theoretical significance and it is likely that an analytically derived equation would be much more complex.

The value of the drag ratio when $\delta = 0.01$ is given as 69 by equation (2) and this is in good agreement with the previously determined value of 68.5.¹ For reasons discussed in Ref. 1, $\delta = 0.01$ is taken to refer to the terminal condition.

Over the range examined, there is no systematic variation with Reynolds number of the relationship between drag ratio and separation distance and this agrees with previous findings. In these experiments the sphere diameter, d , has not been varied but it is believed that the results are independent of absolute size over the range of interest in fluidisation. The reason for this belief is that, with a great variety of shapes, geometrical similarity is known to be preserved with respect to drag forces.⁵ Variations in drag coefficient, boundary layer thickness, and other flow phenomena are usually functions only of Reynolds number. The application of this argument to systems of spheres has been developed in some detail by Richardson and Zaki.⁶ It will be shown later that the results appear to apply to spheres two orders of magnitude smaller than those on which drag measurements were made. This is convincing support for the hydraulic model.

The Stability of Particles in a Fluidised Bed

Consider an ideal fluidised bed of uniform spheres in which the particles are arranged in an orderly rhombohedral pattern as was built in the water tank. To be supported in the fluid

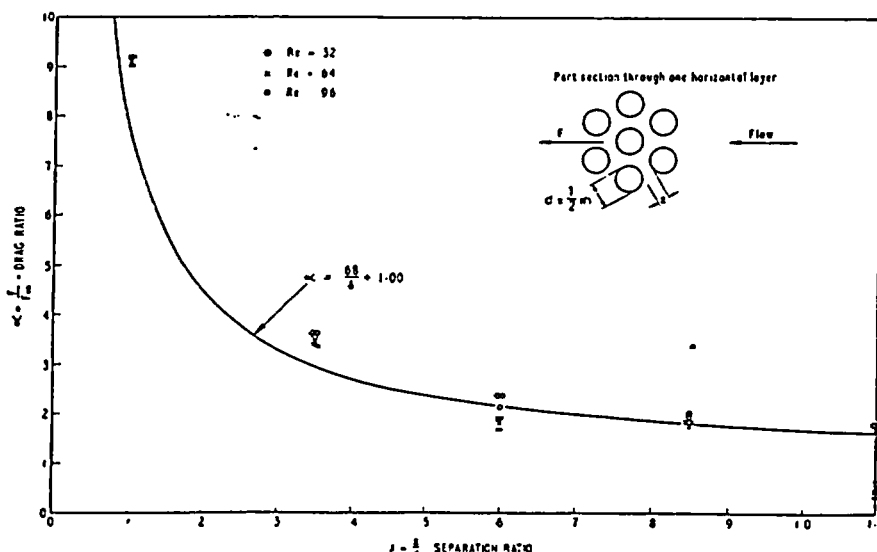


Fig. 2.—Variation of drag ratio with separation

stream the submerged weight and drag must be equal:

$$g \frac{\pi}{6} d^3 \cdot (\rho_s - \rho_f) = C_D \frac{\pi}{4} \cdot d^2 \cdot \frac{1}{2} \rho_f u^2 \quad (3)$$

Equation (3) must apply to each particle. The velocity, u , is that based on an empty cross section and C_D is the coefficient of drag for a single sphere moving with a velocity, u , in an infinite extent of fluid. Equation (3) is essentially a re-definition of α and C_D .

Consider a disturbance of this orderly array. In a small region let the particle concentration fall by a small amount. That is to say, locally, δ increases by an amount $\Delta\delta$. To accommodate this expansion, let the remaining particles in the bed close up a little. If the region of expansion is small, changes in δ elsewhere will be negligible. In the region where δ has increased, the drag ratio, α will fall and spheres will be supported only if the velocity increases to compensate. The drag coefficient varies with velocity so that for continued stability equation (3) can be re-written:

$$\alpha C_D u^2 = \frac{4}{3} d \cdot g \cdot \frac{(\rho_s - \rho_f)}{\rho_f} \quad (4)$$

In the range of Reynolds number relevant to most fluidised systems,

$$C_D = \frac{24}{Re} (1 + 0.15 Re^{0.687}) \quad (5)$$

(See Ref. 2.)

Between equations (2), (4), and (5), we can estimate the local change in velocity, Δu , that is needed to support a particle which has changed its separation from its neighbours by $\Delta\delta$. This is seen to be:

$$\Delta u = \frac{1}{18} \cdot \frac{g d^2 \cdot (\rho_s - \rho_f)}{\mu \cdot (1 + 0.25 Re^{0.687})} \cdot \frac{0.68}{(0.68 + \delta)^2} \Delta\delta \quad (6)$$

The ratio of the velocity-increment to the spacing-increment, $\Delta u/\Delta\delta$ is not very sensitive to the absolute value of the spacing. It increases by a factor of 4 as δ decreases from 1.0 to zero. The Reynolds number term is also not important. It varies between 1 and 3 for much of the range of interest in fluidisation. The ratio is sensitive to density only when that of the solid approaches that of the liquid. The most important factors are the particle diameter and the fluid viscosity. The ratio has been evaluated for glass spheres fluidised in air and in water for the initial condition where $\delta = 0$, and the results are shown in Table I. The ratios for air-supported systems are two orders of magnitude greater than for water but they are in proportion to the experimentally determined minimum fluidisation velocities. Thus, in response to a disturbance of this kind, both systems are required to increase the local fluid velocity by about the same factor if the particles are to remain supported. It is seen that a very small displacement requires an enormous relative change in velocity to keep the particle supported. A change in separation ratio, $\Delta\delta = 0.01$ requires that the velocity approximately doubles in every case. This separation corresponds to a local decrease in concentration of 3%.

TABLE I.—The Velocity Change Required by Particle Displacement

Particle diam. d (cm)	Fluidising medium	$\Delta u/\Delta\delta$ (cm/s)	Min. fluidising velocity $u_{m.f.}$ (cm/s) (see Fig. 4)
0.0114	Water	2.01	0.013
0.0650	Water	40.7	0.60
0.0114	Air	179.0	1.00
0.0650	Air	2 290.0	30.5

It follows from this that local small changes in concentration cannot persist: if they did the particles in this region would cease to fluidise. Very small local changes in concentration would require a very large redistribution of fluid velocity if they were to remain stable. Thus we might expect to find that the particles in a fluidised bed are uniformly distributed and superficially this appears to be the case for liquid fluidised beds and for the dense phase of gas-supported systems. It would be virtually impossible to detect experimentally the small spacing changes that have been considered above but at least obvious concentration variations are not observed in fluidised beds with the exception of "bubble" formation. This is not to say that concentration defects can never occur but only that they cannot persist.

Consideration of drag forces alone does not appear to explain why bubbles form in some fluidised systems and not in others, but in view of the foregoing argument it is significant that bubbles involve an abrupt and discontinuous change in particle concentration. Perhaps the reason for this phenomenon lies with the flow responses that follow a small change in particle concentration.

Referring again to Fig. 2, it is seen that at large separations the drag ratio changes very little. Therefore, once the particles are well separated, their stability will be insensitive to small changes in concentration. This corresponds to the so-called "lean phase" fluidisation observed with gas-supported systems. From visual observation of 0.065 cm diameter spheres fluidised in air at high velocities, the stable lean phase concentration was seen to develop at a separation ratio, δ , of the order of 100. At this concentration the drag on a particle will be within 1% of its terminal value.

During the model-experiments it was shown that the axial drag on a sphere or on its neighbours does not change appreciably when it is displaced from its lattice position. Previous work¹ has shown that there is a lateral repulsive force as spheres approach closely so that fluid-supported spheres in a rhombohedral lattice are in neutral or weakly stable equilibrium. This means that fluidised particles initially arranged in a regular pattern might be expected to decay slowly into a more random assembly without great changes in the drag forces occurring as long as the local particle concentration does not change. The conclusions about stability could therefore apply to a more disordered assembly of particles.

The Minimum Fluidisation Velocity

Consider a bed of uniform spheres arranged in uniform close packing through which fluid is passing upwards. Fluidisation will start when the drag on the particles is equal to their submerged weight. The drag on a particle in this situation has been shown¹ to be 68.5 times that of an isolated sphere at the same superficial velocity. Thus, the minimum fluidisation velocity can be calculated from the terminal falling velocity for an isolated sphere in the same fluid.

When a sphere is falling freely at its terminal velocity, the drag force and its submerged weight are equal. The same is true for a sphere that is fluidised so that the drag forces for the two situations can be equated:

$$C_{DT} \cdot \frac{\pi}{4} d^2 \cdot \frac{1}{2} \rho_f u_T^2 = C_{Dm.f.} \frac{\pi}{4} d^2 \cdot \frac{1}{2} \rho_f u_{m.f.}^2 \quad (7)$$

and therefore,

$$C_{Dm.f.}/C_{DT} = u_T^2/u_{m.f.}^2 \quad (8)$$

$= \alpha_0 = 68.5$ when the drag coefficients are measured at the same Reynolds numbers.

Because of the complex relationship between drag coefficient and velocity in the range of interest, the terminal velocity cannot be calculated directly from first principles but it can be shown^{3, 4} that:

$$C_{DT} \cdot Re^2_T = \frac{4}{3} \cdot \frac{d^3 \rho_F g (\rho_S - \rho_F)}{\mu^2} \quad (9)$$

Therefore the product of the drag coefficient and the square of the Reynolds number at the minimum fluidisation velocity will be $1/68.5$ of this. The relationship between drag coefficient and Reynolds number for a sphere is known from semi-empirical equations such as those of Schiller and Naumann.² Thus the term $C_D Re^2$ can be calculated and a graph of this product for spheres is shown as a function of Reynolds number in Fig. 3. With this graph and equation (9), Re_T

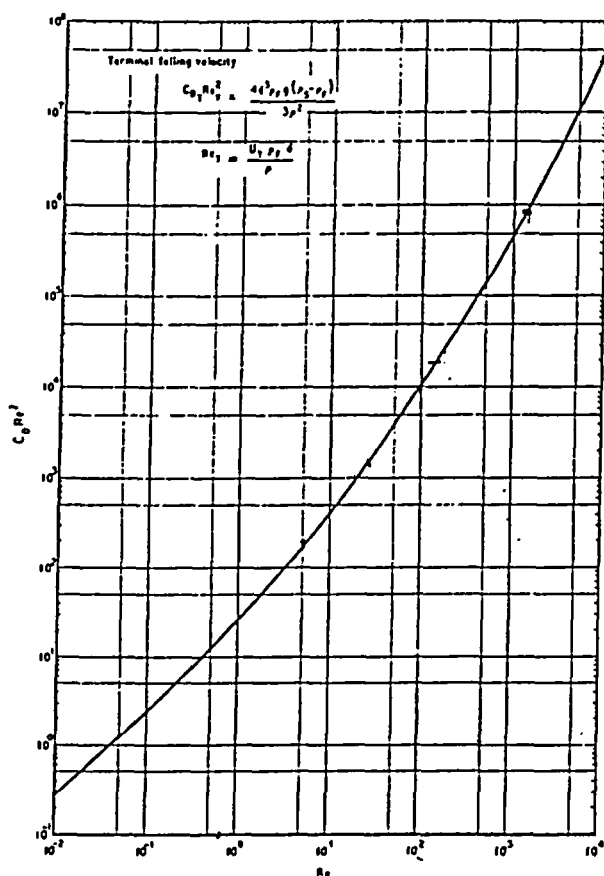


Fig. 3.—Variation of $C_D Re^2$ with Re for spheres

(and therefore the terminal velocity) can be calculated for an isolated sphere. If in equation (9) C_{DT} is replaced by

$$C_{Dm.f.} = 68.5 C_{DT}$$

and Re_T is replaced by $Re_{m.f.}$, the minimum fluidisation velocity can be calculated in a similar manner.

For example, for a spherical copper particle of 0.040 cm diameter falling in air at 0°C, the right hand side of equation (9) becomes 33,140. From Fig. 3 $Re_T = 202$ which corresponds to a terminal velocity of 666 cm/s. Substituting now the minimum fluidisation conditions, the right hand side of equation (9) becomes $33,140/68.5$ and Fig. 3 gives $Re_{m.f.} = 11.1$ corresponding to a minimum fluidisation velocity of 36.3 cm/s.

The minimum fluidisation velocity calculated in this way is shown in Table II for several systems and is also plotted in Fig. 4. Some experimental values are also included for comparison. In spite of the assumption of initially ideal packing, the agreement is quite good. It compares favourably with most published empirical correlations which is surprising in view of the premises involved in applying the hydraulic model results to real fluidised beds. Fig. 5 illustrates that the method is not sensitive to the value chosen for α_0 . The work of Pinchbeck and Popper⁷ and of van Herdens, Nobel, and van Krevelen⁸ suggests $\alpha_0 = 70$.

TABLE II.—Minimum Fluidisation Velocities

$(C_D Re_2)_{m.f.} = \frac{1}{68.5} \cdot \times$		$u_{m.f.}$ (cm/s)		
d (cm)	$\frac{4}{3} \frac{d^3 \rho_F g (\rho_S - \rho_F)}{\mu^2}$	$Re_{m.f.}$ (from graph)	Calculated	Observed
<i>Ballotini in Water</i>				
0.0114	0.546	0.023	0.0202	0.0128
0.0650	101	3.5	0.538	0.597
0.300	9 940	94	3.13	3.87
1.20	492 000	1 030	8.58	10.12
<i>Ballotini in Air</i>				
0.0083	1.44	0.061	0.961	0.823
0.0097	2.30	0.096	1.29	0.853
0.0114	3.73	0.154	1.77	1.01
0.0273	51.2	1.74	8.33	7.01
0.0388	147	4.33	14.6	14.3
0.0650	691	14.3	28.8	30.5
<i>Copper Shot in Air</i>				
0.0083	4.32	0.175	2.76	2.84
0.0114	11.2	0.44	5.05	3.84
0.0400	484	11.1	36.3	40.2
0.0650	2 076	32.5	65.4	84.7

The spherical material on which measurements of minimum fluidisation velocity were made was classified by sieving, the diameters quoted being the average mesh size of adjacent screens. From this it follows that the material is not strictly of one size and deviation from single-sized particles increases with finer material. This means that the packing of the fine material will be more dense than the ideal that was assumed and hence α_0 will be greater and the minimum fluidisation velocity will be less than that predicted. This is generally the case as Fig. 4 shows. With the large material, the sphere diameters are more nearly equal and the ideal packing becomes possible. However, as poured into the container, somewhat less dense packing will be achieved and a fluid velocity greater than that predicted will be required to fluidise the bed. Again Fig. 4 shows that this is in fact generally observed.

Conclusions

Measurement of the drag on spheres arranged in a regular array has shown that the fluid velocity required to support a particle is extremely sensitive to the separation between the spheres. This means that in a fluidised bed small local changes of particle concentration are unstable because they require a very large change in velocity distribution. This applies whether the supporting fluid is a gas or a liquid. This is not so, however, when the particles are separated by something in the region of 100 diameters. At this concentration local changes can occur with little consequent adjustment of velocity. This condition corresponds to the lean phase fluidisation observed with gas supported systems.

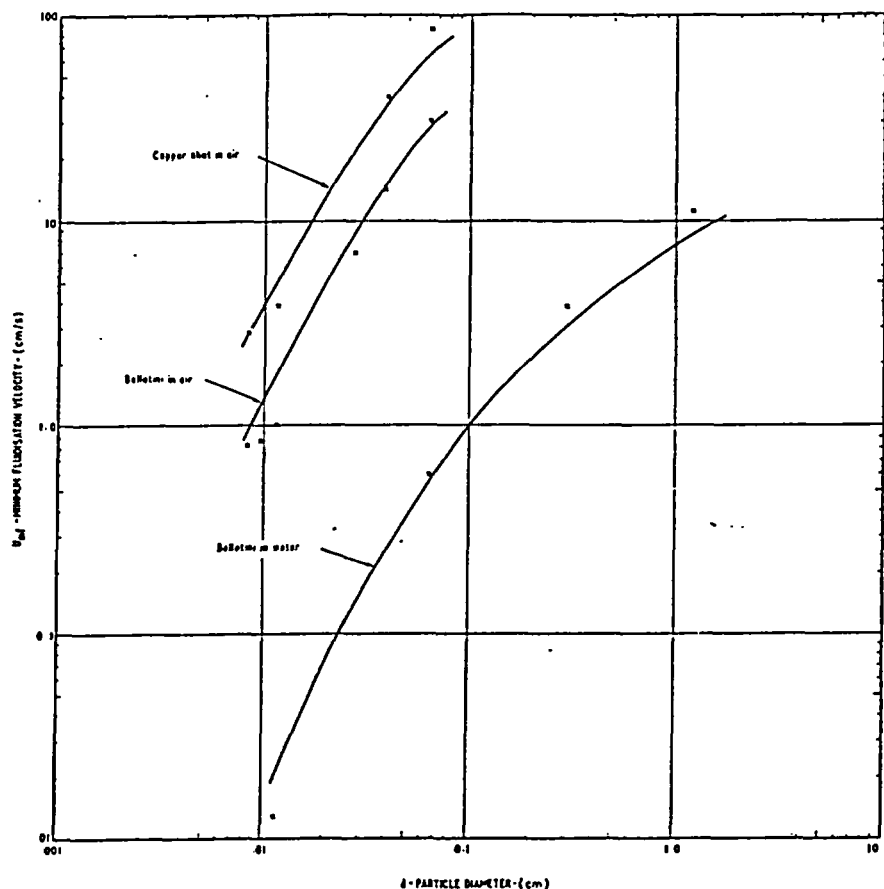


Fig. 4.—Minimum fluidisation velocity. Comparison of theory with experiment

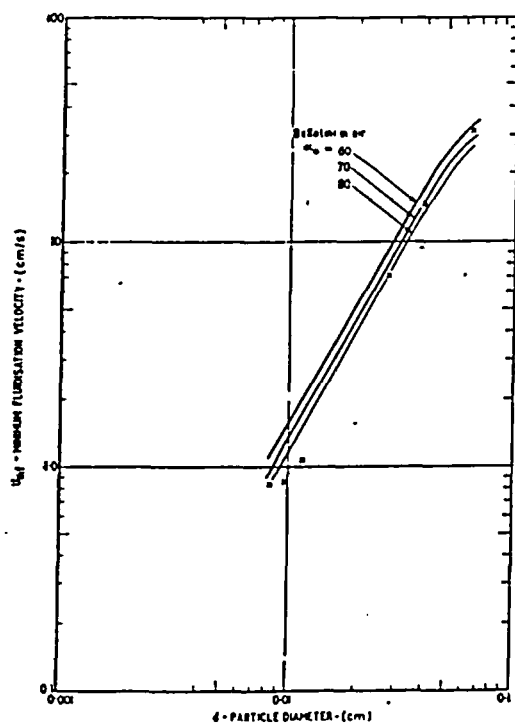


Fig. 5.—Minimum fluidisation velocity. Effect of varying α_s

By considering the drag force that acts when the spheres are close packed and touching, it was shown that the minimum fluidisation velocity could be predicted. This agrees reasonably well with experimental measurements made with close sized spherical particles. The agreement is probably as good as is possible in a system where random variations in packing are bound to affect the result. The main value of this method of prediction is that it is based on first principles and a minimum of empirical coefficients. The empirical measurements are the drag on a particle in close packing and the variation of drag coefficient with Reynolds number for an isolated sphere. The method can be applied to beds of non-spherical particles by applying similar corrections as are used when predicting the terminal falling velocities of irregularly shaped particles.

Acknowledgment

The author wishes to thank G. A. Henwood and D. L. Pyle (a vacation student of the Manchester College of Technology) who carried out the experimental work and J. B. Lewis for helpful discussion.

Symbols Used

$$C_D = \text{drag coefficient} = \frac{gF}{\frac{\pi}{4} d^2 \cdot \frac{1}{2} \rho_F u^2}$$

d = sphere diameter (cm or in.).

F = drag force (in weight units) (g wt).

- Re = Reynolds number = $\frac{u d \rho_F}{\mu}$.
 u = fluid velocity based on empty section or relative velocity of sphere and fluid (cm/s).
 x = separation distance (cm or in.).
 α = drag ratio, $F/F_\infty = C_D/C_{D\infty}$.
 α_0 = drag ratio when $x = 0$.
 δ = separation ratio = x/d .
 μ = fluid viscosity (g wt/cm s).
 ρ_F = fluid density (g wt/cm³).
 ρ_s = solids density (g wt/cm³).

Subscripts

- ∞ = at infinite separation of particles, $x = \infty$.
 $m.f.$ = at a velocity such that the bed is just fluidised.
 t = terminal falling conditions for a sphere in an infinite medium.

References

- ¹ Rowe, P. N. and Henwood, G. A. *Trans. Instn chem. Engrs*, 1961, 39, 43.
- ² Schiller, L. and Naumann, A. *Z. Ver. deutsch. Ing.*, 1935, 77, 318.
- ³ Heywood, H. *J. imp. Coll. chem. Engng Soc.*, 1948, 4, 17.
- ⁴ Coulson, J. M. and Richardson, J. F. *Chemical Engineering*, Vol. II, 1955, p. 489, (London: Pergamon Press Ltd.).
- ⁵ Hoerner, S. F. *Fluid Dynamic Drag*, 1958 (Published by the author, 148 Busteed Drive, Midland Park, N.J., U.S.A.).
- ⁶ Richardson, J. F. and Zaki, W. N. *Trans. Instn chem. Engrs*, 1954, 32, 35.
- ⁷ Pinchbeck, P. H. and Popper, F. *Chemical Engineering Science*, 1956, 1, 57.
- ⁸ van Heerden, D., Nobel, A. P. P. and van Krevelen, D. W. *Chemical Engineering Science*, 1951, 1, 63.

The manuscript of this paper was received on 3 November 1960, and the paper was presented at a symposium of the Institution in London on 7 March 1960.

ABSTRACT

The containment of decompressed heavy water steam is a problem which has to be solved in the design of nuclear generating plants. In the CANDU type of reactor, this is done in large vacuum buildings into which large quantities of water are injected in the form of a spray. The condensation process from an air-steam mixture must take place in a relatively short period of time, and the pressure in the chamber must not rise above ambient pressure.

The final objective of this project was to provide reliable and scientific design bases for nuclear power plant vacuum buildings and these have been achieved through the following:

- i) The combined heat and mass transfer to a single water droplet moving freely in an air-stream mixture has been treated theoretically and experimentally. Three distinctive models of heat transfer within the droplet were developed. The experimental results are in excellent agreement with the second model which allows for internal resistance and mixing in the droplet.
- ii) Two experimental techniques--"catch in cell" and "direct photography"--have been used to determine the droplet size distribution in a dousing chamber spray.
- iii) Findings of previous steps have been subsequently applied to predict the results of existing dousing chamber tests. For this prediction a new numerical algorithm has been developed.

The agreement between the predictions and experiments is very good over a wide range of experimental results. This result supports the further use of combined heat and mass transfer theory in the design and simulation of full scale steam dousing systems.

CONTENTS

	Page
ACKNOWLEDGEMENTS	v
ABSTRACT	vi
GENERAL INTRODUCTION	1

PART ISIMULTANEOUS MOMENTUM, HEAT AND MASS TRANSFER
APPLIED TO A SINGLE DROPLET

1. INTRODUCTION TO PART I	7
2. DROPLET MOVING FREELY (UP AND/OR DOWN) IN AN AIR- STEAM MIXTURE	9
2.1 The Solution Approach	9
2.2 Hydrodynamics of a Droplet	11
2.3 Gas Side Heat and Mass Transfer	15
2.4 Droplet Temperature Response with No Internal Resistance	24
2.5 Droplet Temperature Response with Internal Resistance and Mixing	25
2.6 Droplet Radius Change	28
2.7 Droplet Temperature Response with Internal Resistance and No Mixing	29
2.8 Thermodynamic and Transport Properties of Air, Water and Steam	34
2.9 Outline of the Numerical Algorithm, No Internal Resistance	35
2.10 Outline of the Numerical Algorithm with Internal Resistance and Mixing	36
2.11 Outline of the Numerical Algorithm with Internal Resistance and No Mixing	43

2.12 Discussion of Droplet Temperature Response Predictions	45
3. THE SURVEY OF EXISTING EXPERIMENTAL RESULTS OF HEAT TRANSFER COEFFICIENT DURING CONDENSATION FROM PURE STEAM AND AIR/STEAM MIXTURE AND THEIR COMPARISON WITH PREDICTIONS	50
4. EXPERIMENTAL APPARATUS	60
4.1 Air System	61
4.2 Steam System	61
4.3 Test Section	64
4.4 Droplet Producing Unit	64
4.5 Measurement Techniques	65
4.6 Experimental Procedure	68
4.7 Heat Conduction and Radiation Influence on the Droplet Temperature Response Measurement	70
5. EVALUATION AND DISCUSSION OF EXPERIMENTAL RESULTS	76
6. CONCLUSIONS AND RECOMMENDATIONS	88

PART II

SIMULATION OF THE SPRAY SYSTEM AND DESIGN SYNTHESIS OF A DOUSING CHAMBER

7. INTRODUCTION	92
8. EXPERIMENTAL	94
8.1 Dousing Chamber Tests	94
8.2 Droplet Size Distribution Measurements	96
9. THEORETICAL ANALYSIS	99
9.1 Problem Definition and Simplifying Assumptions	100
9.2 Basis of the Simulation	103

9.3 Droplet Size Distribution	107
9.4 Equation of Motion Solution	108
9.5 Droplets Temperature Distribution	113
9.6 Heat Losses Simulation	119
10. THE NUMERICAL ALGORITHM OUTLINE	120
11. EXPERIMENTAL RESULTS AND DISCUSSION	124
11.1 Droplet Size Distribution	124
11.2 Dousing Tests Prediction	131
12. CONCLUSIONS AND RECOMMENDATIONS	140
13. FINAL SUMMARY	142
REFERENCES	147
NOMENCLATURE	156

APPENDICES

	Page
A. Some Analytical Solutions of the Macroscopic Momentum Equation for a Sphere	162
B. Reinhart's Correlations for Droplet Drag Coefficient	168
C. Evaluation of the Droplet Temperature Response with Internal Resistance and No Internal Mixing	170
D. Thermodynamics and Transport Properties of Water, Air, Steam and Their Mixture	175
E. The Computer Program for No Internal Resistance Solution of the Single Droplet Response	189
F. The Computer Program for Internal Resistance and Mixing Model of the Single Droplet Response	200
G. The Computer Program for Internal Resistance and No Mixing Solution of the Single Droplet Response	220
H. The Air Rotameter Calibration Curve	244
I. The Humidity Calibration Curve	247
J. Feed Water Thermocouple Calibration Curve	249
K. Thermistors and Recorder Calibration Curves	251
L. Data of Experimental Runs for Single Droplets	257
M. Dimensional Analysis for the Response Time Corelation	265
N. Dousing Chamber Simulation Algorithm	268
O. Droplet Size Distribution Measurements	284

Figure 35.	Thermal Utilization Predictions Compared to Experimental Values	117
Figure 36.	Different Diameter Droplets Temperature at the Different Positions in the Chamber	118
Figure 37.	Comparison of Different Droplet Size Distributions Obtained by the Catch in Cell Technique	127
Figure 38.	Droplet Size Distribution Obtained by the Direct Photography Technique	130
Figure 39.	Dousing Tests #1, 1A and 1B	132
Figure 40.	Dousing Tests #2A, 2B, 2C and 3A with a Single Nozzle	133
Figure 41.	Dousing Tests #2D, 2E, 2F, 3D and 3E with Five Nozzles	134
Figure 42.	Effects of Different Droplet Size Distributions on the Dousing Chamber Pressure Response	138
Figure H1.	The Air Rotameter Calibration Curve	246
Figure I1.	The Humidity Calibration Curve	248
Figure J1.	Feed Water Thermocouple Calibration Curve	250
Figure K1.	Thermistor #1 Calibration Curve	253
Figure K2.	Recorder Calibration Curve for Thermistor #1	254
Figure K3.	Thermistor #2 Calibration Curve	255
Figure K4.	Recorder Calibration Curve for Thermistor #2	256
Figure O1.	Photograph of Droplets Obtained Using the Catch in Cell Technique for 30 IGPM near the Spray Centre	285
Figure O2.	Photograph of Droplets Obtained Using the Catch in Cell Technique for 30 IGPM near the Edge of the Spray	286
Figure O3.	Photograph of Droplets Obtained Using the Catch in Cell Technique for 40 IGPM near the Spray Centre	287

Figure 04.	Photograph of Droplets Obtained Using the Catch in Cell Technique for 40 IGPM near the Edge of the Spray	288
Figure 05.	Photograph of Droplets Obtained Using the Catch in Cell Technique for 50 IGPM near the Spray Centre	289
Figure 06.	Photograph of Droplets Obtained Using the Catch in Cell Technique for 50 IGPM near the Edge of the Spray	290
Figure 07.	Droplet Size Distribution for Droplets Shown in Figure 01.	291
Figure 08.	Droplet Size Distribution for Droplets Shown in Figure 02.	292
Figure 09.	Droplet Size Distribution for Droplets Shown in Figure 03.	293
Figure 010.	Droplet Size Distribution for Droplets Shown in Figure 04.	294
Figure 011.	Droplet Size Distribution for Droplets Shown in Figure 05.	295
Figure 012.	Droplet Size Distribution for Droplets Shown in Figure 06.	296
Figure 013.	Photograph of Droplets Obtained Using the Direct Photography Technique for 30 IGPM near to the Edge of the Spray	297
Figure 014.	Photograph of Droplets Obtained Using the Direct Photography Technique for 40 IGPM near to the Edge of the Spray	298
Figure 015.	Photograph of Droplets Obtained Using the Direct Photography Technique for 50 IGPM near to the Edge of the Spray	299
Figure 016.	Droplet Size Distribution for Droplets Shown in Figure 014.	300
Figure 017.	Droplet Size Distribution for Droplets Shown in Figure 015.	301

LIST OF TABLES

	Page
Table I.1 Dimensions of the Needles	68
Table II.2 Droplet Temperature Response Model Fits	115
Table II.2 Upper Limit Droplet Size Distribution Parameter Predictions for the Catch in Oil Technique	125
Table II.3 Upper Limit Droplet Size Distribution Parameters Prediction for the Direct Photography Technique	129

GENERAL INTRODUCTION

A provision for the remote possibility of released heavy water steam is a problem which has to be solved in the design of nuclear generating plants with heavy water cooled reactors. This steam could originate from the primary cycle shown in Figure 1, which illustrates a simple scheme of the primary and secondary cycles of a nuclear power generating plant. One of the ways to solve this problem is to entrap potential nuclear pollutants, contained in the steam, in vacuum buildings. Every reactor building is connected with the vacuum building by the relief duct (#17 in Figure 2) which transfers the unwanted steam to it. A pressure rise in the vacuum building actuates the water cycle to inject a huge quantity of water (from the reservoir in the top of the vacuum building) in the form of a spray. The condensation process, in the presence of air as an inert gas, must take place in a relatively short period of time (30 to 50 seconds) and the pressure in the chamber must not rise above ambient pressure. To fulfill this, it is desirable to be able to design and predict the performance of such a dousing chamber shown in Figure 3 on a firm scientific basis. Several questions relating to the steam dousing problem (an Atomic Energy of Canada--AECL--term signifying the condensation of steam in a mixture with air on a falling water spray) have previously remained unanswered. Typical unanswered questions were: (a) How fast could free falling water droplets pick up heat from an air/steam mixture in which the

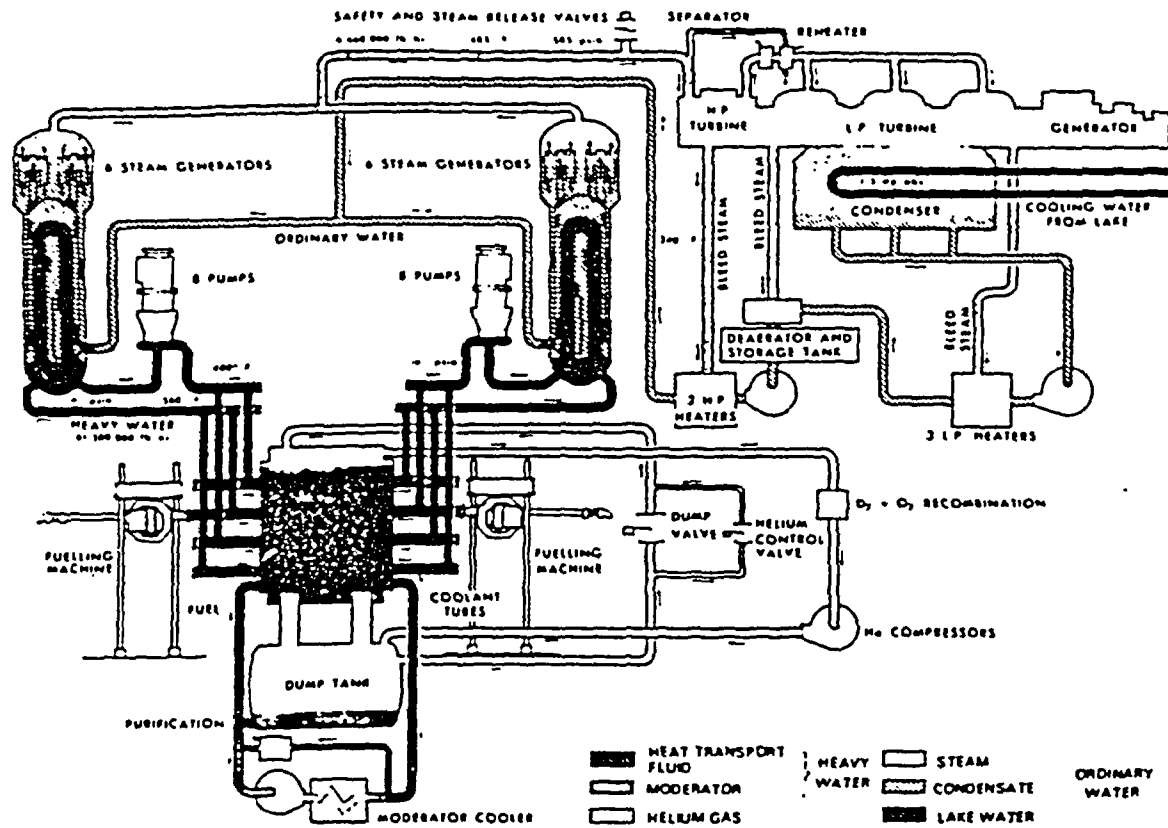


Figure 1. Primary and Secondary Cycle of a Nuclear Power Plant.

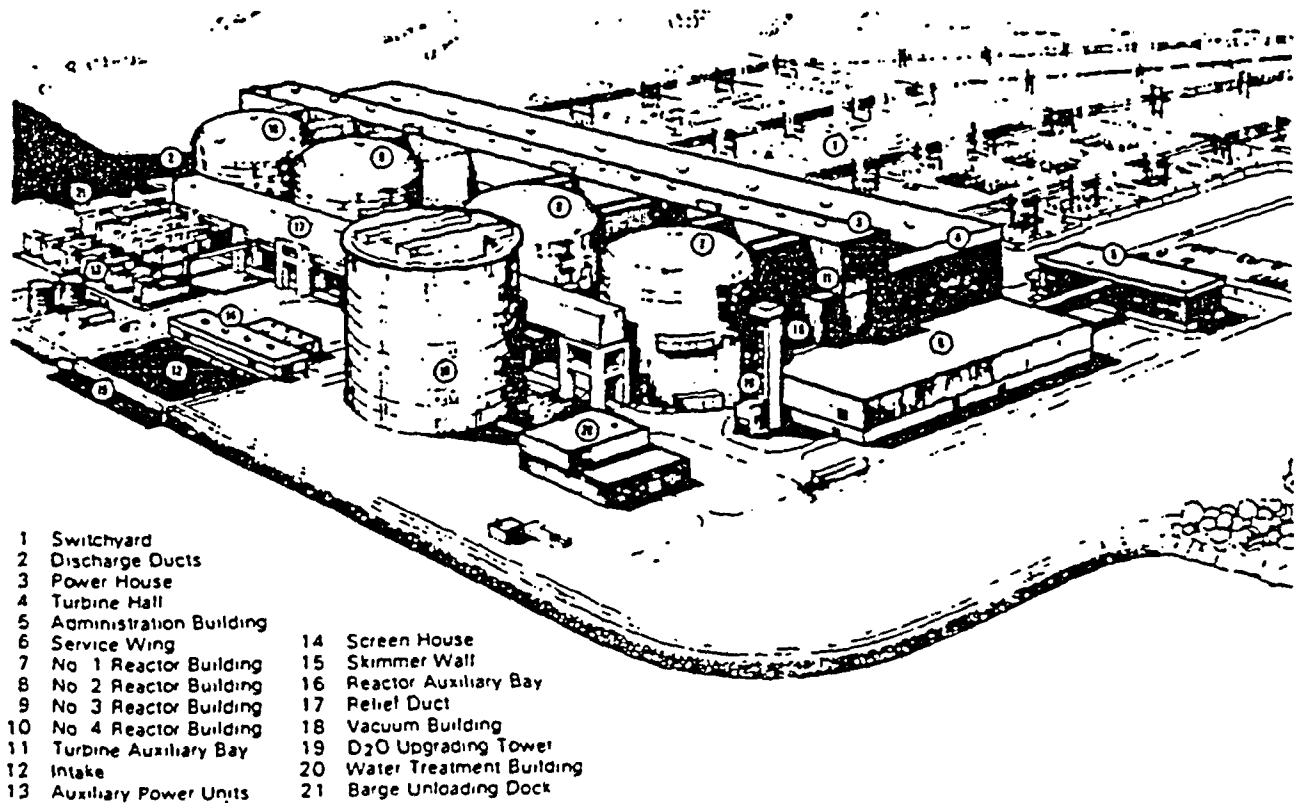
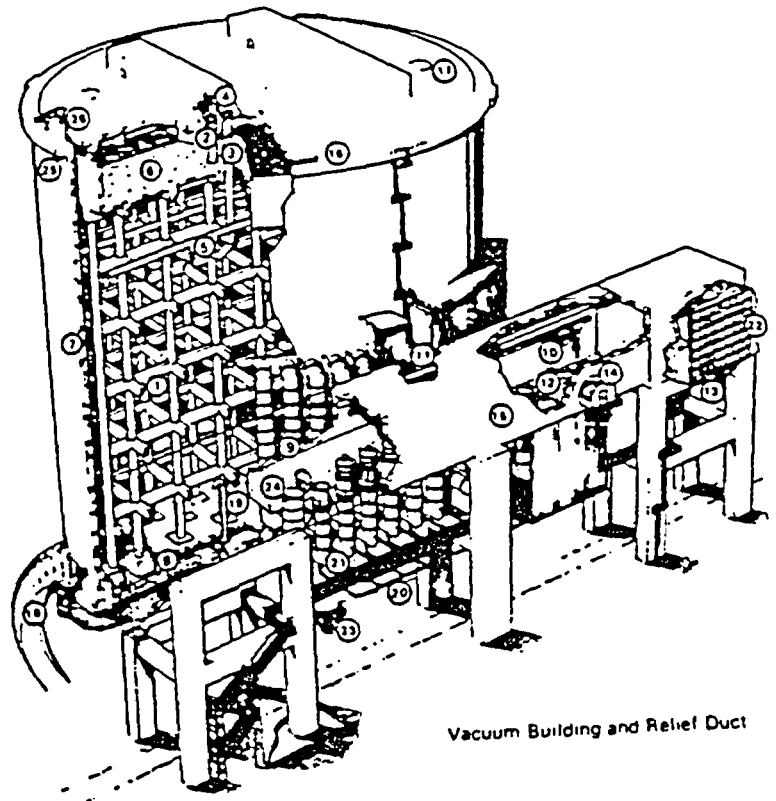


Figure 2. Elements of a Nuclear Power Plant.

- 1 Vacuum Building Internals
- 2 Pressure actuated water displacement system inlet header
- 3 Pressure actuated water displacement system outlet header
- 4 Vacuum Chamber
- 5 Distribution and Spray Header
- 6 Emergency Water Storage Tank
- 7 Perimeter Wall
- 8 Basement
- 9 Vacuum Ducts
- 10 Monorail and Hoist
- 11 Emergency Water Line
- 12 Pressure Relief Valves
- 13 Shielding Walls
- 14 Personnel Airlock
- 15 Pressure Relief Duct
- 16 Roof/Wall Seal
- 17 Water Tank Access Hatch
- 18 Basement Access Ramp
- 19 Vacuum Pump Suction Header
- 20 Vacuum Duct Drain Pipe
- 21 Vacuum Duct Fill Pipe
- 22 Reactor Building Pressure Relief Louvers
- 23 Services Tunnel
- 24 Equipment Airlock
- 25 Perimeter Wall Monorail
- 26 Jib Crane



Vacuum Building and Relief Duct

Figure 3. Vacuum Building and Relief Duct.

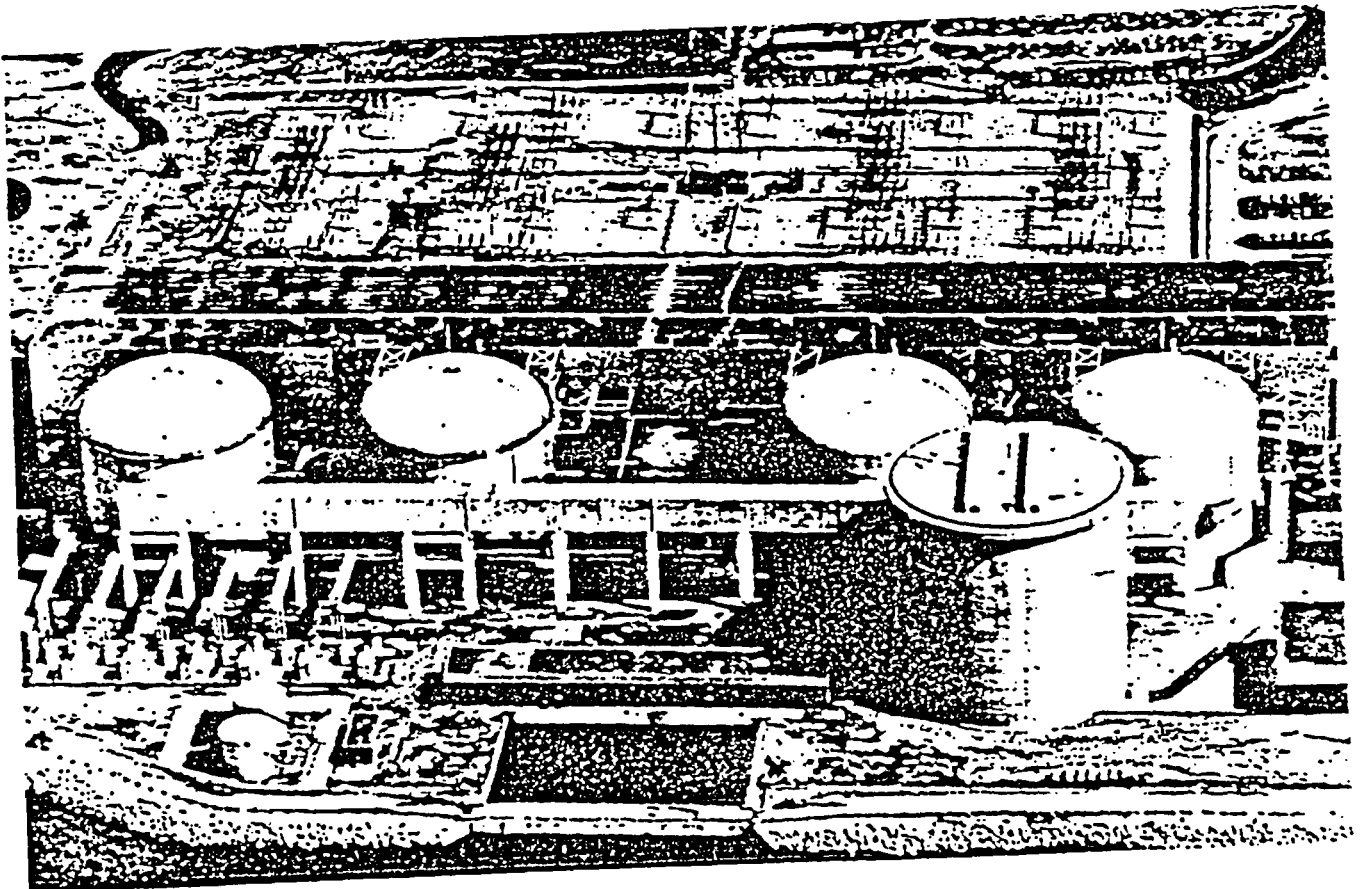


Figure 4. Airview of Pickering Nuclear Power Plant.

concentration of the steam was changing with time and in which the droplets had a range of sizes and velocities? (b) What would be the effects of the previous variables on the heat transfer coefficients to sprays? (c) Could the performance of a dousing chamber be predicted with any accuracy by use of basic theories of heat, mass and momentum transfer? It was therefore decided to study the problem in two parts, one concerning the transport processes associated with a single droplet and another one treating the spray problem as a design synthesis. Thus the thesis is presented in two parts:

- Part I. Simultaneous momentum, heat and mass transfer applied to a single droplet moving relative to an air/steam mixture;
- Part II. Simulation of a spray system and design synthesis of a dousing chamber.

The main objectives of this research were as follows:

- i) to develop and/or apply theory of combined transport phenomena in the case of a single droplet moving relative to an air/steam mixture,
- ii) to produce reliable experimental results and compare them with the existing experimental evidence on heat and mass transfer rates especially in the case of high concentrations of non-condensables 50% and over.
- iii) to use information obtained in steps i) and ii) to simulate the experimental dousing chamber situation, and to compare the simulation results with existing experimental data.

These steps will hopefully provide a sound basis for the simulation and the design of a real dousing system (Figure 4-- Air-view of Pickering nuclear generating plant). The optimal design of a full scale dousing system is not treated in this study but it is felt that a basis is now available for this to be done.

Parts of this research have been reported in:

1. E. Kulić, E. Rhodes, G. Sullivan: Heat Transfer Rates obtained in Condensation on Droplets from Air/Steam Mixtures, 24th Annual Conference of the Canadian Society for Chemical Engineering, Ottawa, Oct. 1974.
2. E. Kulić, E. Rhodes, G. Sullivan: Heat Transfer Rate Predictions in Condensation on Droplets from Air/Steam Mixtures, The Canadian Journal of Chemical Engineering, 53 (1975), pp. 252-258.
3. E. Kulić, E. Rhodes, G. Sullivan, K. McLean: Direct Contact Condensation from Air/Steam Mixtures on Falling Sprays, Heat Transfer Section Paper #.2.1, Vth-International CHISA Congress, Prague, August, 1975.

PART I

SIMULTANEOUS MOMENTUM, HEAT AND MASS TRANSFER
APPLIED TO A SINGLE DROPLET

1. INTRODUCTION TO PART I

Combined momentum, heat and mass transfer to droplets occurs in a number of technical processes such as spray drying [1], spray cooling [2], flash drying, spray crystallization, cyclone evaporation [3], combustion of liquid fuels [4], spray or void of fill cooling towers [5] and water sprays at the bottom of cooling towers [6], air conditioning units [7], direct contact condensers in thermal power generating plants [8], etc. In spite of the fact that one of these operations was used 5000 years ago (evaporative cooling [9]) and the relatively young process such as the combustion of liquid fuels is about 100 years old, and although intensive research has been undertaken for decades in the area, even the simple single droplet problem involving these three transport phenomena is far from being resolved and completely understood for the whole range of variables of practical interest. For an extensive review of the subject development and accompanying problems the reader is referred to surveys of Hedley [10] and Williams [11].

Although all these practical applications have many things in common it is necessary to investigate them separately in order to cover the range of variables of the specific application. Thus, because there are no data supported by basic theory for the condensation of steam from a dilute air/steam mixture on moving droplets, the steam dousing problem has been approached in this specific fashion. In Chapter 2 the temperature response of a single droplet

moving freely in an infinite air/steam medium is investigated.

Chapter 3 reviews existing experimental results and compares them with our predictions. The experimental apparatus and results are discussed in Chapters 4 and 5, respectively.

2. DROPLET MOVING FREELY (UP/OR DOWN) IN AN AIR/STEAM MIXTURE

2.1 The Approach to Solving the Problem

The problem can be stated as follows. It is necessary to predict the velocity, distance travelled and the temperature (as a function of time) of a droplet moving freely in an air/steam mixture of known temperature, pressure and humidity. In general, there are two approaches to solving this problem, which are:

- i) the microscopic or the "point to point" treatment,
- ii) the macrosopic balances treatment.

In the first case it is necessary to write the governing differential equations of momentum, heat and mass transfer for the surrounding gaseous phase and solve them simultaneously (analytically or numerically) with the momentum and energy equations for the droplet itself. This approach is the most rigorous one, and the solution will contain all the necessary information for every "point" of the system. Analytical solutions of this kind would be most convenient, However, there is presently no complete analytical solution available even for the momentum transfer to the droplet when the Reynolds Number exceeds 1 [10]. This lack of analytical solution is simply caused by the complexity of the problem itself. Despite the fact that numerical solutions of the basic equations have contributed immensely in many transport phenomena areas, in this particular problem there is still a lot of work to be done. Canadian workers, in particular, have made significant contributions towards solving the problem as is evident

from recent references [12 to 20]. A review of these contributions shows that they have been successful up to $N_{Re} \sim 400-500$, or to the point when shedding of vortices from the rear of a falling drop takes place. The only exception in this respect is Hoffman and Ross's [17] treatment who used Galerkin's error distribution solution [21] for the momentum equation and integral-boundary layer formulation [22] for the energy equation, to extend the solution to $N_{Re} \sim 1000$, which is the first solution (to the author's knowledge) going that far. The authors are aware of the fact that this extension presents a problem since the originators of the method [21] express their doubts about it saying: "Additional study of separated flows will be necessary before the application of the Galerkin's method in such systems can be definitely evaluated."

The Reynolds numbers in this particular research program cover a relatively wide range ($N_{Re} \sim 50$ to ~ 4000) covered only in part by the existing analytical or approximate analytical solutions. Early in the present work the author was fortunate to be introduced to the Spalding and Patankar approximate boundary layer numerical methods [23] and serious consideration was given to their applications in this study. However, it was realized that these methods were applicable only below the separation point Reynolds number. This left little doubt that the problem in question should be approached using a macroscopic balance treatment involving transport rate equations.

2.2 Hydrodynamics of a Droplet

The problem is to predict the velocity and position of a droplet injected into a moving air/steam mixture at any time of the moment of injection.

A macroscopic momentum balance applied to a single free falling liquid droplet yields the following equation (neglecting buoyancy forces).

$$m \frac{dv_D}{dt} = - \rho_M C_D \frac{\pi d^2}{8} (v_D - v_M) |v_D - v_M| + F_b \quad (1)$$

where

$$F_b = mg \quad (2)$$

The distance travelled by a droplet can be determined from

$$z = \int_0^t v_D dt \quad (3)$$

In some cases it is possible to express the drag coefficient C_D as a simple function of the Reynolds number N_{Re} and obtain an analytical solution for the velocity and the distance travelled. This has been done in Appendix A, for the case of a solid sphere. However, the drag coefficients for water droplets are somewhat different than those for solid spheres. Some of the effects influencing the drag coefficient (not in order of a respective importance) are: mass transfer, acceleration, deceleration, free stream turbulence scale and intensity, particle rotation, internal circulation, roughness,

etc., and some of them influence spheres and droplets differently, resulting in different values of the drag coefficient. The most exhaustive review of these effects is presented in the six part paper by Torobin and Gauvin [26]. The situation is complicated by the fact that some research findings on the subject contradict each other. For example, Ingebo's [27] results indicate a decrease in the drag coefficient due to acceleration rather than an increase found by most other investigators. Lunnon, Williams and others, as well as Torobin and Gauvin [24] suggest the increase in drag coefficient values due to acceleration. Some drag effects cancel each other. For example an increase in wake turbulence caused by Reynolds number increase or by surface roughening seems to decrease the effect of the acceleration on the drag. When Torobin and Gauvin published their paper they dramatically underlined the necessity of further investigations. However, at the present time there is very little new information available.

In the selection of the droplet drag coefficients to be used over the whole range of Reynolds numbers, the technique proposed by Lapple and Shepard [25] was adopted to at first. This technique essentially uses the known value of the droplet terminal velocity to determine the steady state drag coefficient from the equation of motion. The terminal velocities were determined from Best's equation:

$$v_{RT} = 943 [1 - \exp(-d/1.77)]^{1.147} \quad (4)$$

*specific diameter
numbers on
trajectory*

where:

v_{RT} - relative terminal velocity, [cm/s]

d - droplet diameter, [mm],

which was obtained to approximate the experimental results of Gunn and Kinzer [28]. Curve #11 in Figure 5 was obtained in this way, and afterwards approximated by three straight lines (#5, #6 and #7) in the same figure, as reported in [29]. The three straight lines are:

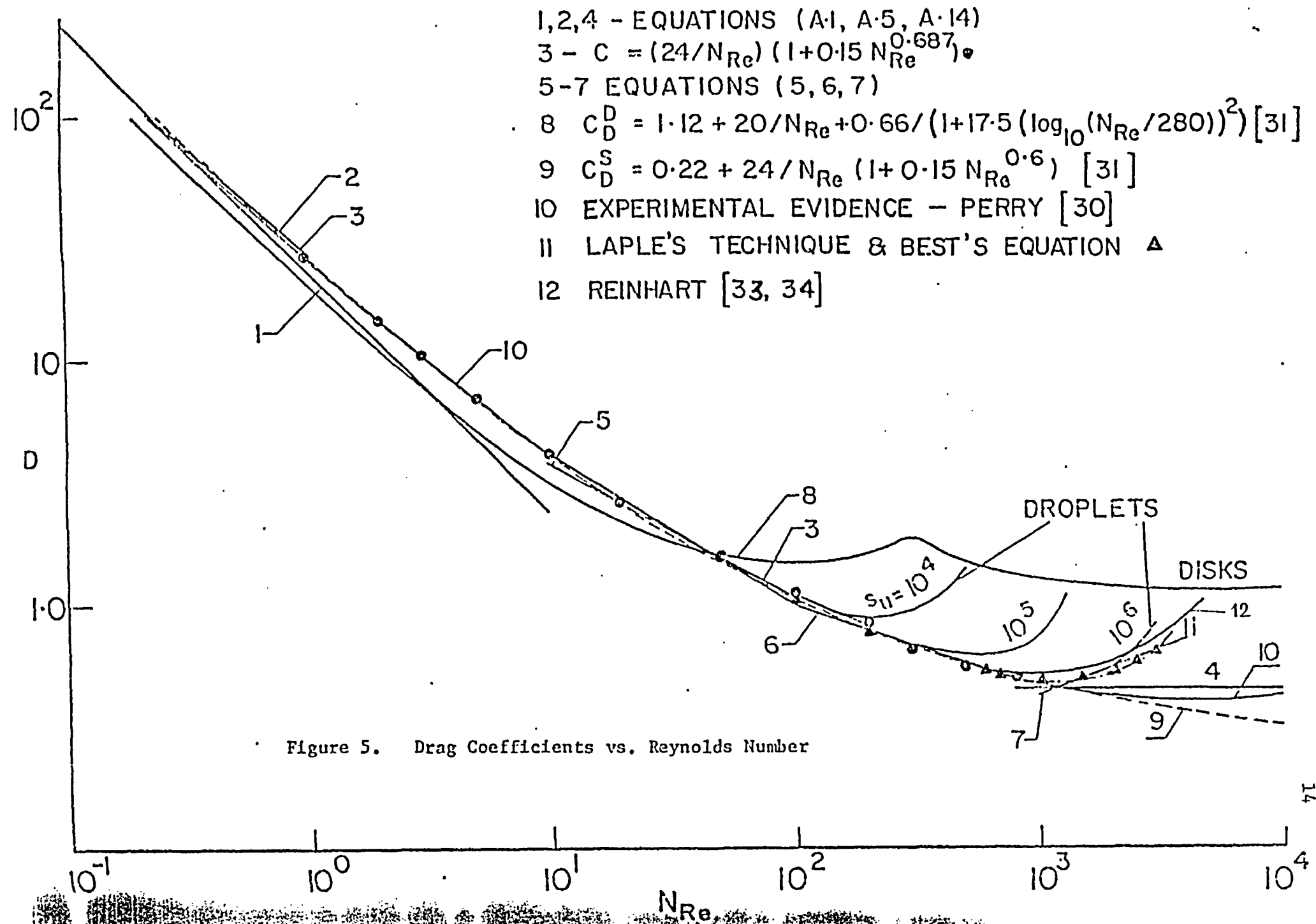
$$C_D = 14.098 N_{Re}^{-0.571}, \quad \text{for } 10 < N_{Re} < 10^2 \quad (5)$$

$$C_D = 4.61 N_{Re}^{-0.337}, \quad \text{for } 10^2 < N_{Re} < 10^3 \quad (6)$$

$$C_D = 0.0264 N_{Re}^{0.396}, \quad \text{for } N_{Re} > 10^3 \quad (7)$$

The drag coefficient values determined in this manner were then compared with Hughes and Gilliland [30] values, used by Hollands [31] and Groeneweg [32], as shown in the same figure.

The results of very thorough theoretical and experimental research by Reinhart [33,34] are summarized in Appendix B and represented by curve 12 in Figure 5. Although the agreement between equations (4) to (6) and Reinhart's results is very good over the whole range of Reynolds numbers it was later (in the dousing chamber simulation) decided to use Reinhart's correlations, because of the thoroughness of the research and because of the extent of the Reynolds number range. Clearly enough, the equation of motion could only be solved using Reinhart's correlation by numerical methods.



For that purpose two subroutines were written, one for the case of a droplet moving downwards and another one for the droplet moving upwards. Basically the equation of motion is solved for both cases using the fourth order Runge-Kutta technique, see Kuo [36]. The results of these calculations for the relative velocity and the distance travelled versus time, of a 1 mm droplet moving upwards, subjected to different initial conditions (volume fraction of steam in a mixture 5%, total pressure 1 bar) are shown in Figures 6 and 7, respectively. The solid lines represent the conditions when the air/steam mixture (moving upwards also) velocity is smaller than the relative terminal velocity and the dashed lines represent the opposite situation. In any case the droplet reaches its relative terminal velocity of about 4 m/s. This is in agreement with the data of Gunn and Kinzer [28] and Foote and DuToit [37]. From Figure 7 one can see that when $v_M < v_{RT}$ the droplet moves upwards initially then after it reaches its maximum height starts to fall down. However, when $v_M > v_{RT}$ the droplet is carried away by the air/steam mixture having higher velocity.

2.3 Gas Side Heat and Mass Transfer

The problem is to predict the rate of heat pick-up of a single free falling droplet in a mixture of steam and an inert gas (in this case air). A droplet of known diameter d , initially at uniform temperature T_i , is injected with a velocity v_{Do} into an air/steam mixture of known concentration C_M and temperature T_M . The

CURVE NO	DROPLE INITIAL VELOCITY m/s	MIXTURE VELOCITY m/s
1	10 <i>upward</i>	5 <i>upward</i>
2	5	10
3	2	5
4	11	1
5	3	2
6	2	3

Figure 6. A Relative Velocity of Upward Moving Droplets (1 mm dia. initially & finally)

$\text{---} V_M < V_{RT}$
 $\text{---} V_M \geq V_{RT}$

$p = 1 \text{ bar}$
 $X = 5\%$
(mostly air)

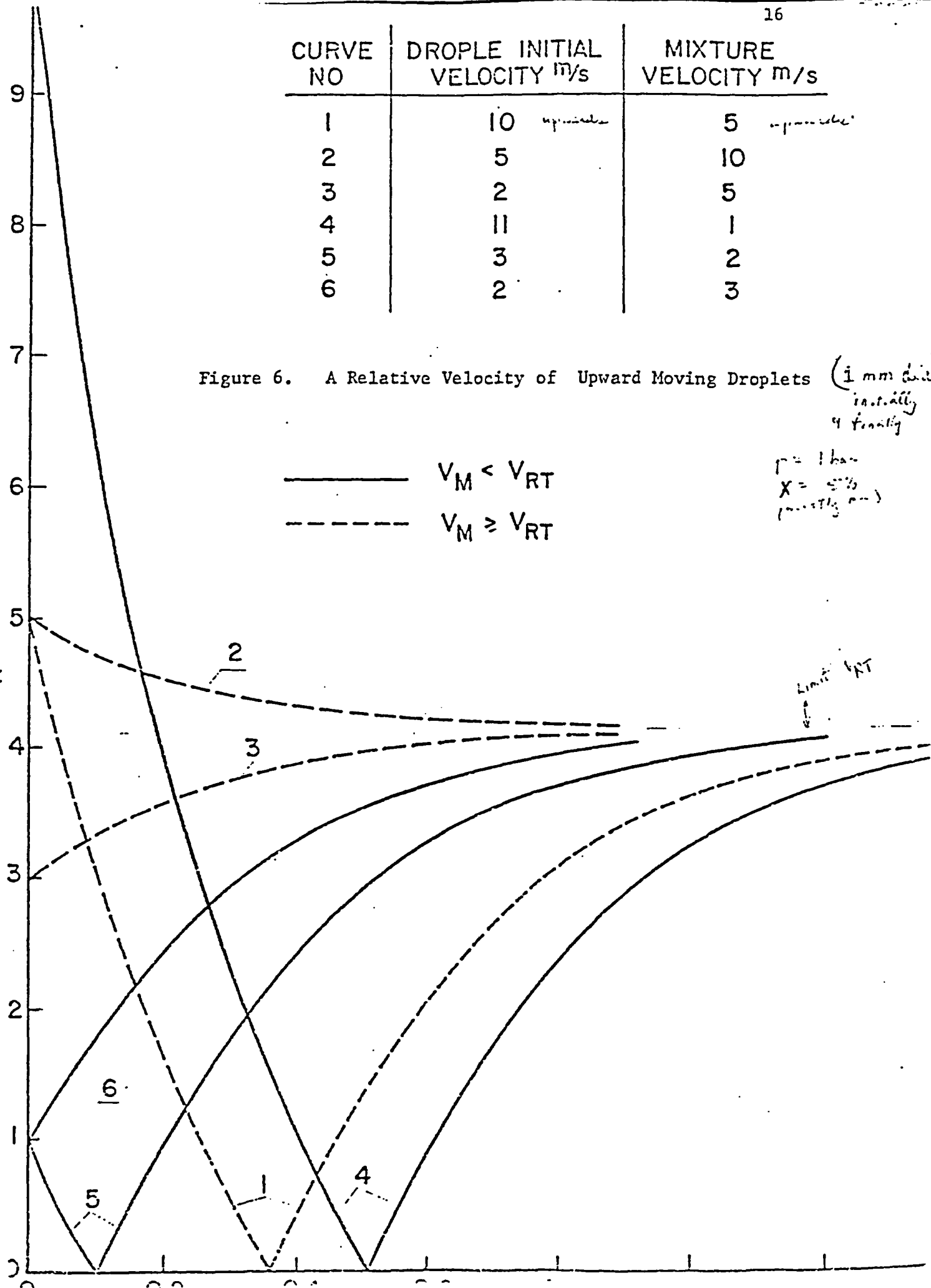
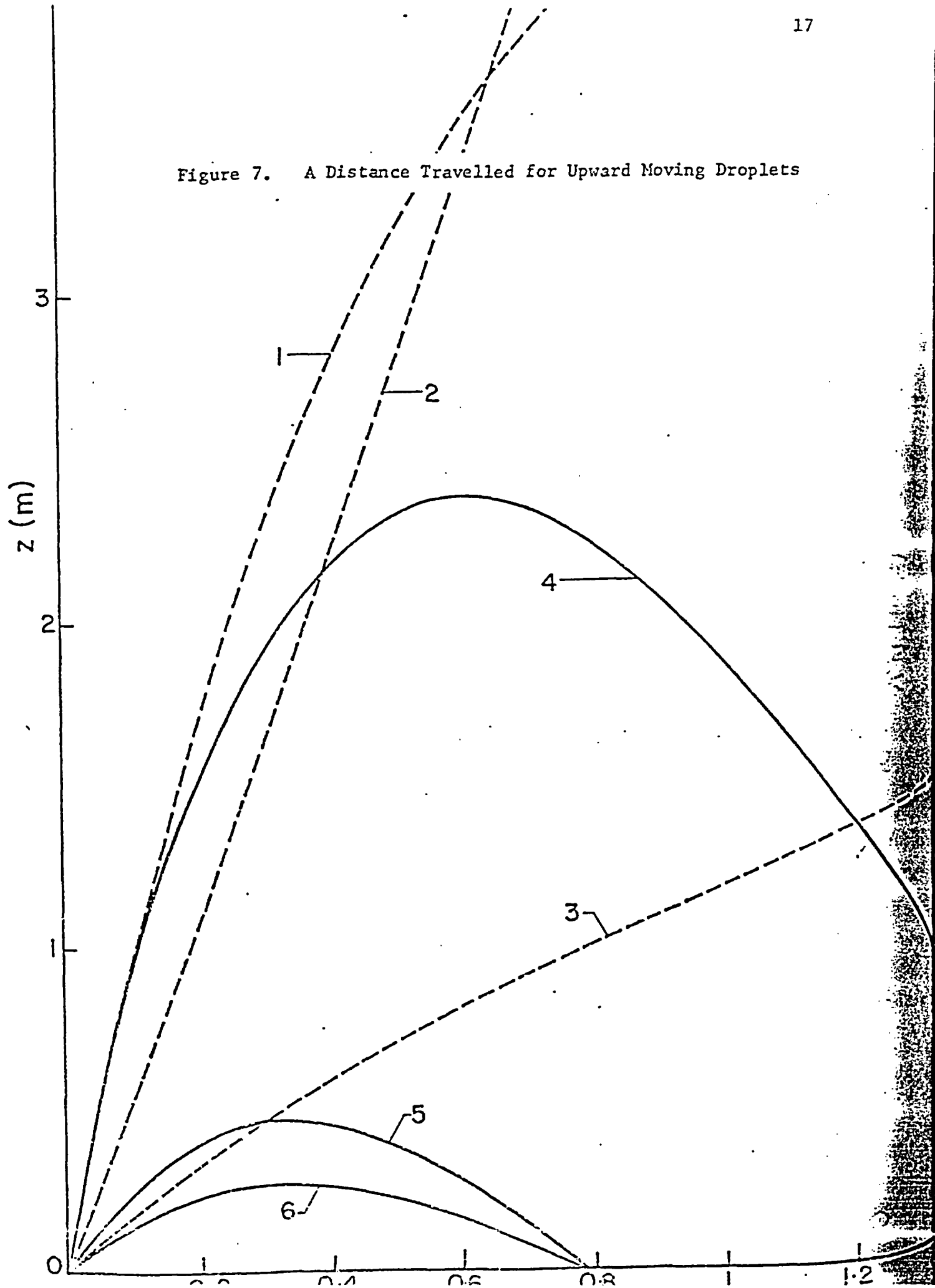


Figure 7. A Distance Travelled for Upward Moving Droplets



2
 injected droplet experiences two unidirectional heat fluxes directed towards its surface; one caused by the temperature difference acting as a driving force between the surroundings and itself and usually called the sensible heat transfer component Q_S ; the second caused by the steam concentration difference in the bulk and at the droplet surface acting as a mass transfer driving force and called the latent heat transfer component Q_L . These components comprise the total heat Q_T , which is exchanged between the surroundings and the droplet. The total heat (see Trybal [38]) can be determined from:

$$Q_T = Q_S + Q_L \quad (8)$$

The sensible heat transfer flux may be expressed as:

$$Q_S = N_{Ac} h_s (T_M - T_S) \quad (9)$$

Skelland [39] proposed the introduction of the Ackermann number N_{Ac} to honour the early contributor in this area [40,41,42]. The Ackermann number

$$N_{Ac} = \frac{a}{1 - e^{-a}} \quad (10)$$

allows for the mass transfer out of the gas phase and is the correction factor to the heat transfer coefficient h_s , obtained without mass transfer to the droplet. In the case of mass transfer from a binary mixture with one inert gas (air), the coefficient a can be represented as:

$$a = (N_A M_A C_{PA} + N_S M_S C_{PS}) / h_S$$

$$N_S = 0$$

$$= N_S M_S C_{PS} / h_S \quad (11)$$

The latent heat component can be expressed as

$$Q_L = N_S M_S \quad (12)$$

The mass flux of the steam from the mixture can be expressed as:

$$\begin{aligned} N_S &= F \ln[(1 - C_{Si}/C_M)/(1 - C_{SM}/C_M)] \\ &= F \ln[(1 - P_{Si}/P_M)/(1 - P_{SM}/P_M)] \end{aligned} \quad (13)$$

Using equations (8) to (13) the total heat transfer to a droplet Q_T can be determined if the values of the heat ^(h_s) and mass transfer ^(F) coefficients are known. Heat transfer coefficients h_S can usually be calculated for most engineering situations by use of correlations involving the Nusselt number. However, the determination of the mass transfer coefficient F is not always at hand, mainly because there are fewer available experimentally based correlations for the Sherwood number, due to the complexities of the experimental and theoretical determinations. The situation is eased considerably by the discovery of transport phenomena analogies, especially the heat and mass transfer analogy which has proved useful in many engineering applications. The validity of this concept for a dilute (rich in an inert gas) air/steam mixture was confirmed some fifty years ago by Lewis [43], and reconfirmed by many investigators, e.g. for the

evaporation of liquids inside a tube [44], for the evaporation of water in film type of cooling towers [45], evaporation of droplets in spray drying [46,47] as well as for the evaporation of solid spheres in gas streams [48]. A number of experimental results on the condensation of steam in the presence of an inert gas confirms the validity of the heat and mass transfer analogy, in the range of Reynolds numbers 20 to 2000, see Bobe and Malyshev [49], who studied the condensation of steam from air-gas mixtures on tubes. They included the experimental results of Semein [50] who studied the condensation of steam from an air/steam mixture on cooling tower packing producing liquid film flow, and of Schrodt and Gerhard [51] for the condensation of steam from a mixture with a non-condensing gas on vertical tubes in a bank. In a series of papers covering the last two decades Berman [52,53,54,55,56] (citing some of the papers) has treated the problem of combined heat and mass transfer for different industrial applications (mainly condensers and cooling towers). He proposes the introduction of additional groups to correlate with the Nusselt and Sherwood numbers. Thus he suggests:

$$N_{Nu} = f(N_{Re}, N_{Pr}, N_{Gr}, \Pi_w, C_{PS}/C_{PM}) \quad (14)$$

and

$$N_{Sh} = f(N_{Re}, N_{Sc}, N_{Gr}, \Pi_g, \epsilon_S, R_S/R_M) \quad (15)$$

where:

$$\Gamma_w = \frac{j_S \ell}{v_M \rho_M}, \quad \Gamma_g = \frac{P_{SM} - P_{Si}}{P_M}, \quad (16)$$

$$j_S = N_S M_S \quad \text{and} \quad \epsilon_S = P_{SM}/P_M \quad (17)$$

In this manner it is possible to determine directly the corrected heat transfer coefficient (i.e. $N_{Ac} \cdot h_S$) in the presence of mass transfer for many experimental situations. The same approach is used by Bobe and Solukhin [57]. The obvious limitation of this approach is the necessity of having at hand the correlation for the Nusselt and the Sherwood numbers in every particular case considered. However, in all the work reviewed above there were no reported experimental data for the case of condensation on droplets in the presence of non-condensables. The literature search was encouraging enough, however, to allow the presumption of the validity of the analogy in our calculations of mass transfer coefficients. Thus for the situation involving forced convection around a sphere or a droplet of diameter d , the Nusselt number correlation is:

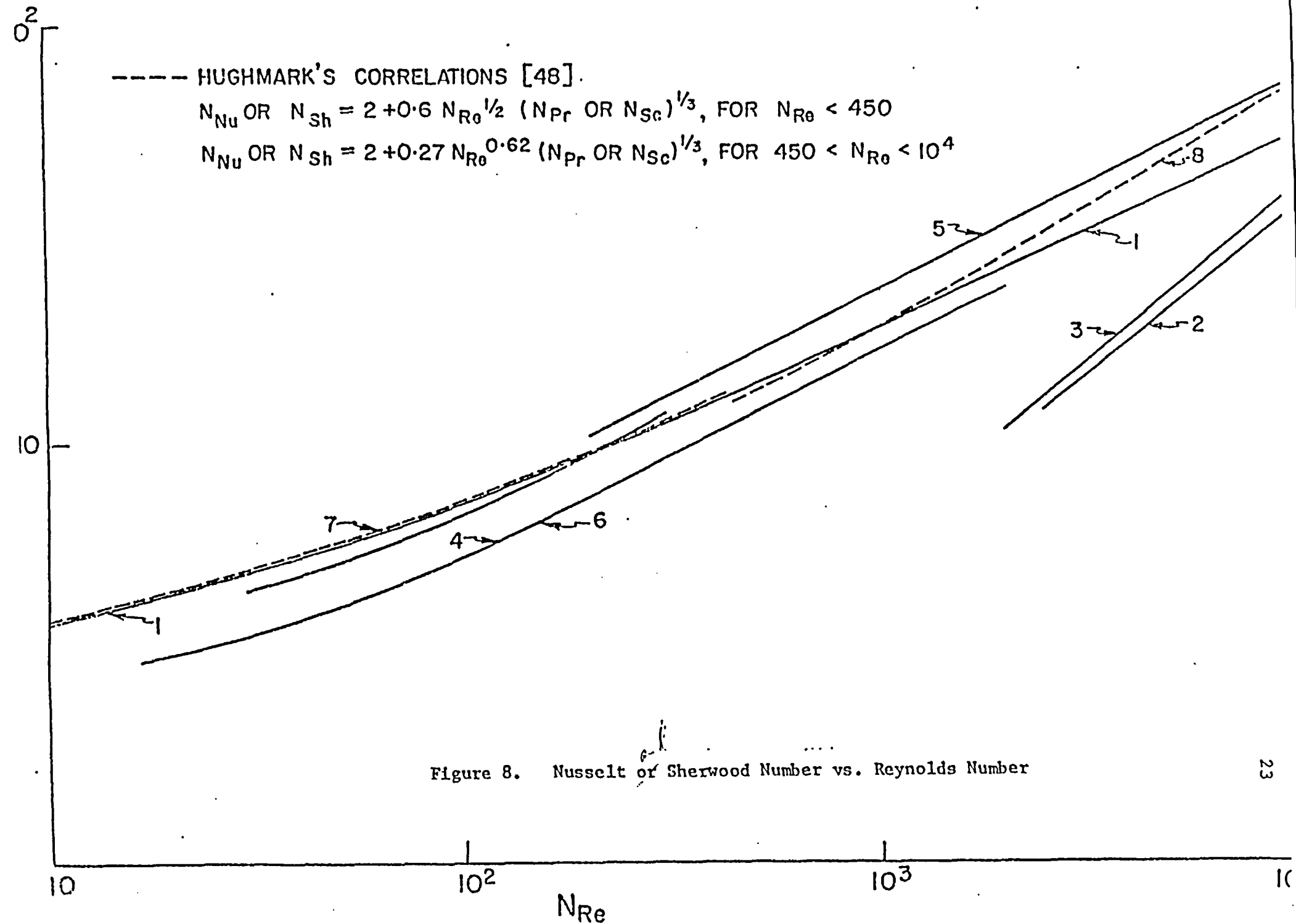
$$N_{Nu} = A + B N_{Re}^m N_{Pr}^n \quad (18)$$

and the analogous equation for mass transfer is the Sherwood number correlation:

$$N_{Sh} = A + B N_{Re}^m N_{Sc}^n \quad (19)$$

The reported values of A in equations (18) and (19) are either 0 or

2 depending on the ranges of Reynolds number over which the experiments were performed. The only exceptions to this rule are Kramer's [58] values reported from 3.2 to 5 and reviewed by Keey and Glean [59] who reported only the value 5. Since these values for A correspond to the case of liquid-liquid mass transfer, for the present consideration the value $A = 2$ has been used. Thus equations (18) and (19) are then correct in the reported limit when $N_{Re} \rightarrow 0$. The reported values of B vary from 0.085 [58] through 0.27 [48], 0.459 [60], 0.6 [48,47] to 0.98 as reported by Ward et al [61]. Theoretical considerations of Hoffman and Ross [17] and Masliyah and Epstein [19] indicate that the exponents m and n in equations (18) and (19) depend on the value of the Reynolds number itself. This was not taken into account in the present study because the reported values cover relatively narrow ranges of Reynolds numbers. In most reported (e.g. 4,31,32,62,63) applications of the correlation the values used are 1/2 and 1/3, respectively. The very thorough study of Rowe et al [64] also reaffirms the applicability of the correlation. Some of the correlations mentioned above are shown in Figure 8. Curve 1 represents the results of Ranz and Marshall [46] for the evaporation of droplets in a spray drying apparatus. Curve 2 represents Semeyin's [50] results for the case of condensation of steam from an air/steam mixture on the cooling tower packing of the film type. Curve 3 represents the results of Sherwood and Gilliland [44] for the evaporation of liquids in a tube. Hoffman and Ross's [17] results on



the evaporation of droplets are represented by curve 4. Curve 5 represents Bobe and Malyshev's [49] results on the condensation of steam from air/steam mixtures on tubes. Berman's [45] results on the droplet evaporation are represented by curve 6. Hughmark's [48] correlations on the solid spheres heat and mass transfer are represented by curves 7 and 8. All the curves for spheres and droplets are very close to each other. (within 5%)

The correlations proposed by Hughmark [48] have been used in this study, since they are based on a large number of experimental heat and mass transfer data. They satisfy the limiting value of $N_{Nu} = 2$ for a stagnant fluid, see Lightfoot [65].

2.4 Droplet Temperature Response with No Internal Resistance

Now when the heat transfer rate Q_T from the surrounding medium to the droplet is known it is possible to predict what effects this will have on the droplet temperature response.

The simplest approach to the problem of predicting the temperature response of the droplet is to assume that the internal resistance to heat transfer of the droplet is negligible compared to the external gas phase resistance. (In normal convective heat transfer problems this is a perfectly valid assumption.) This assumption implies that there is no temperature gradient within the droplet. Thus the rate of heat transfer to the droplet is equal to the rate of heat pick-up of the droplet;

$$\frac{d}{dt} (m C_P T) = Q_T A \quad (20)$$

Assuming negligible change in radius (see below for a discussion of this) and mass of the sphere, equation (20) may be rearranged to give:

$$\frac{dT}{dt} = C(T_M - T) + C_1 \lambda N_A M_A \quad (21)$$

$$C_1 = 6/\rho C_P d \quad (22)$$

$$C_2 = N_{Ac} h_S \quad (23)$$

$$C = C_1 C_2 \quad (24)$$

If only a small temperature change is assumed, then all the quantities in equation (21) can be considered to be constants, except t and T .

Hence,

$$T = T_M + \frac{\lambda N_S M_S}{C_2} - \left(T_M - T_i + \frac{\lambda N_S M_S}{C_2} \right) \exp(-Ct) \quad (25)$$

which represents the temperature-time response of a droplet over a small temperature change.

2.5 Droplet Temperature Response with Partial Internal Resistance and Mixing

Normally in convective heat transfer, the liquid side resistance in gas-liquid contacting is negligible. However, in combined heat and mass transfer, where the latent heat component is

large, the gas side resistance may be lowered enough so that the liquid side resistance becomes significant. It will be shown later that the internal resistance of the larger droplets may play a significant role in the droplet temperature response. The following theory is reviewed as a means of taking this into account.

Both sensible and latent heat transfer contributions combine to provide an apparent vapour phase heat transfer coefficient h_{app} defined as:

$$h_{app} = Q_T / (T_M - T_S) \quad (26)$$

which thus includes the effects of sensible and latent heat transfer components (see equation (8)).

This definition of an apparent heat transfer coefficient makes it possible to treat the droplet as a sphere suddenly exposed to convective heating or cooling [66,67]. The temperature field inside such a sphere is described by the following differential equation.

$$\frac{\partial T}{\partial t} = \alpha \left(\frac{\partial^2 T}{\partial r^2} + \frac{2}{r} \frac{\partial T}{\partial r} \right) \quad (27)$$

*conduction only
(no convection)
also: symmetric field*

with initial and boundary conditions:

$$T(r, 0) = T_i = \text{const} \quad , \quad 0 \leq r \leq R_i \quad (28)$$

$$T(R, t) = f(R, t) \quad , \quad t > 0 \quad (29)$$

The heat balance across the droplet interface yields

$$h_{app}(T_M - T_S) = -k \left(\frac{\partial T}{\partial r} \right)_{r=R} \quad (30)$$

and the symmetry condition may be expressed as:

$$\frac{\partial T}{\partial r} = 0 \quad \text{at} \quad r = 0 \quad (31)$$

There is an additional condition imposed by the mass transfer causing a droplet radius increase, according to

$$\frac{dR}{dt} = \frac{N_S M_S}{\rho_D} \quad (32)$$

This problem is known in the literature as the Stefan problem. A number of situations where this problem arises is treated by Rubinstein [68]. Since there is no available analytical solution (i.e. with R and h_{app} varying with time) of the differential equation (27) with the conditions (28) to (32), an approximate numerical technique is accepted using constant coefficients over short intervals of time. Thus a dimensionless temperature profile solution for a sphere of constant diameter a short time after exposure is [66,67]:

$$\frac{T - T_M}{T_M - T_i} = \sum_{n=1}^{n=\infty} \frac{2R}{\psi_n} \frac{(\sin \psi_n - \psi_n \cos \psi_n)}{(\psi_n - \sin \psi_n \cos \psi_n)} \frac{\sin(\psi_n r/R)}{r} \exp(-\psi_n^2 Fo) \quad (33)$$

where:

ψ_n - the roots of the transcendental equation (34)

$$1 - \psi_n \cot \psi_n = N_{Bi} = h_{app} R/k \quad (34)$$

The dimensionless droplet surface temperature is then (for $r = R$)

$$\frac{T - T_M}{T_M - T_i} = \sum_{n=1}^{\infty} \frac{2}{\psi_n} \frac{(\sin \psi_n - \psi_n \cos \psi_n) \sin \psi_n}{\psi_n - \sin \psi_n \cos \psi_n} \exp(-\psi_n^2 N_{Fo}) \quad (35)$$

The average temperature of the droplet \bar{T} is determined by

$$\bar{T} = \frac{3}{4\pi R^3} \int_0^R 4\pi T r^2 dr \quad (36)$$

which after integration yields

$$\bar{T} = T_M - (T_M - T_i) \sum_{n=1}^{\infty} \frac{6}{\psi_n^3} \frac{(\sin \psi_n - \psi_n \cos \psi_n)^2}{\psi_n - \sin \psi_n \cos \psi_n} \exp(-\psi_n^2 N_{Fo}) \quad (37)$$

It should be emphasized that these equations are based on the assumption that the apparent heat transfer coefficient is also constant during the time increment.

2.6 The Droplet Diameter Change

As it was pointed out the above derivations are valid for the case of a sphere of a constant radius, an assumption which is not quite true in this problem where steam is condensing on the droplet. However, over sufficiently small droplet surface temperature increases, the droplet size can be considered constant and for

repeated calculations over a succession of temperature (hence time) increments the mean droplet diameter can be adjusted according to the equation:

$$\frac{\Delta d}{\Delta t} = \frac{2N_S M_S}{\rho_D} \quad (38)$$

(For the sake of completeness it will be pointed out that the maximum change of a droplet diameter when fully utilized, i.e. heated uniformly to the surrounding temperature, is less than 4% for $x_S \leq 0.5$.) This unsteady state phenomenon representation by quasi-steady state conditions is adopted for all the correlations used for heat and mass transfer. In addition the steady state drag coefficients are assumed to be valid in the unsteady conditions provided the relevant non-dimensional numbers are calculated by use of the instantaneous values of the variables representing the condition of the droplet and its surroundings. This practice is exercised by many investigators, e.g. Frössling [69], El Wakil et al [62,70], Burstein et al [4], Ross and Hoffman [12], Groenewegh[32], Domingos [71], etc. The validity of this assumption is verified experimentally prior to this study by El Wakeil et al [62] and Priem et al [72] who studied the evaporation of fuel droplets in air.

2.7 Droplet Temperature Response with Internal Resistance and No Mixing

Strictly speaking the solution presented in paragraph 2.6 can only be used in the first time interval, since the initial

condition $T_i = \text{const}$ for the subsequent time increments is not satisfied. To avoid this problem at the end of every time increment the average droplet temperature is determined and used in the next step as the uniform initial droplet temperature. Clearly, this approximation introduces higher temperature driving forces than exist in a solid sphere, or in other words, the solution represents the response of a droplet which is periodically well mixed. This is the reason why the solution is called the internal mixing solution, there being as many mixings as there are time increments in the solution. A limit to the above model is the model which is now introduced. Basically this solution does not allow for any internal mixing, i.e. the droplet behaves like a solid sphere. At the end of every time increment the existing temperature profile within the sphere is determined, and used in the subsequent step as the initial temperature profile.

The general solution of a temperature field in a sphere suddenly exposed to a convective heating or cooling, and having a temperature profile $T_i = T(r)$ initially, is described by the following analytical solution [73]:

$$\theta(r,t) = T_M - T(r,t) = \sum_{n=1}^{n=\infty} \frac{2\psi_n}{\psi_n - \sin \psi_n \cos \psi_n} \frac{\sin(\psi_n r/R)}{r \cdot R} \cdot \exp(-\psi_n^2 N_{Fo}) \int_0^R r f_1(r) \sin(\psi_n r/R) dr \quad (39)$$

where:

$T(r, t)$ - temperature at any point of a sphere.

Assuming that the initial droplet temperature profile can be approximated by the polynomial

$$T_i(r) = \sum_{i=0}^{i=n} A_i r^i \quad (40)$$

where n is the polynomial order, equation (39) can be solved. The function $f_1(r)$ in equation (39) can then be written

$$f_1(r) = T_M - T_i(r) \quad (41)$$

Introducing (40) and (41) into (39) and performing the necessary algebraic operations (see Appendix C) yields the following temperature profile of a sphere when a seventh order polynomial for the initial temperature profile is used:

$$\begin{aligned} \theta(r, t) = & \sum_{n=1}^{n=\infty} \frac{2}{\psi_n} \frac{\psi_n}{\psi_n - \sin \psi_n \cos \psi_n} \frac{\sin(\psi_n r/R)}{r} \exp(-\psi_n^2 N_{Fo}) \cdot \\ & \left\{ (T_M - A_0)(\sin \psi_n - \psi_n \cos \psi_n) - A_1 \frac{R}{\psi_n} [2\psi_n \sin \psi_n - (\psi_n^2 - 2) \cos \psi_n - 2] - \right. \\ & - A_2 \frac{R^2}{\psi_n^2} [3(\psi_n^2 - 2) \sin \psi_n - \psi_n(\psi_n^2 - 6) \cos \psi_n] - A_3 \frac{R^3}{\psi_n^3} [4\psi_n(\psi_n^2 - 6) \\ & \cdot \sin \psi_n - (\psi_n^4 - 12\psi_n + 24) \cos \psi_n + 24] - A_4 \frac{R^4}{\psi_n^4} [(5\psi_n^4 - 60\psi_n + 120) \end{aligned}$$

$$\begin{aligned}
& \sin \psi_n - \psi_n (\psi_n^4 - 20\psi_n^2 + 120) \cos \psi_n] - A_5 \frac{R^5}{\psi_n^5} [\psi_n (6\psi_n^4 - 120\psi_n^2 + 720) \sin \psi_n - (\psi_n^6 - 30\psi_n^4 + 360\psi_n^2 - 720) \cos \psi_n - 720] - \\
& - A_6 \frac{R^6}{\psi_n^6} [(7\psi_n^6 - 210\psi_n^4 + 2520\psi_n^2 - 5040) \sin \psi_n - \psi_n (\psi_n^6 - 42\psi_n^4 + 840\psi_n^2 - 5040) \cos \psi_n] - A_7 \frac{R^7}{\psi_n^7} [\psi_n (8\psi_n^6 - 336\psi_n^4 + 6720\psi_n^2 + \\
& - 40320) \sin \psi_n - (\psi_n^8 - 56\psi_n^6 + 1680\psi_n^4 - 20160\psi_n^2 + 40320) \cos \psi_n + 40320] \} \quad (42)
\end{aligned}$$

During the numerical calculations it was found that it was necessary to use the seventh order polynomial in equation (40) to approximate the very steep profiles at $r = R$ in the beginning of the process. Denoting the term in the curly bracket of equation (42) by $I^{(7)}$ the surface temperature of the droplet can be written as:

$$\theta(R, t) = \sum_{n=1}^{n=\infty} \frac{2}{\psi_n} \frac{\sin \psi_n}{\psi_n - \sin \psi_n \cos \psi_n} I^{(7)} \exp(-\psi_n^2 N_{Fo}) \quad (43)$$

The average temperature of the droplet can be determined from

$$\bar{\theta}(t) = \frac{3}{4\pi R^3} \int_0^R 4\pi r^2 \theta(r, t) dr \quad (44)$$

Introducing (42) into (44) and performing the necessary algebraic operations the following is obtained:

$$\bar{\theta}(t) = \sum_{n=1}^{n=\infty} \frac{6}{\psi_n^3} \frac{\sin \psi_n - \psi_n \cos \psi_n}{\psi_n - \sin \psi_n \cos \psi_n} I^{(7)} \exp(-\psi_n^2 Fo) \quad (45)$$

If the initial temperature T_0 of a sphere is uniform, then the solutions (42), (43) and (45) evolve into:

$$\theta(r,t) = (T_M - T_0) \sum_{n=1}^{n=\infty} \frac{2R}{\psi_n} \frac{\sin \psi_n - \psi_n \cos \psi_n}{\psi_n - \sin \psi_n \cos \psi_n} \frac{\sin(\psi_n r/R)}{r} \exp(-\psi_n^2 Fo) \quad (46)$$

$$\theta(R,t) = (T_M - T_0) \sum_{n=1}^{n=\infty} \frac{2}{\psi_n} \frac{(\sin \psi_n - \psi_n \cos \psi_n) \sin \psi_n}{\psi_n - \sin \psi_n \cos \psi_n} \exp(-\psi_n^2 Fo) \quad (47)$$

$$\bar{\theta}(t) = (T_M - T_0) \sum_{n=1}^{n=\infty} \frac{6}{\psi_n^3} \frac{(\sin \psi_n - \psi_n \cos \psi_n)^2}{\psi_n - \sin \psi_n \cos \psi_n} \exp(-\psi_n^2 Fo) \quad (48)$$

Equations (46) to (48) are thus identical with equations (33), (35) and (37) used in the short time interval mixing model. This comparison confirms the validity of the use of the polynomial function in the no internal mixing model.

2.7.1 Summary of Solutions

The solutions using different models of the combined heat and mass transfer problem have been presented above. The first one is the case when the droplet is behaving as if it is perfectly

mixed, i.e. the internal temperature profile is always uniform and there is no internal resistance to heat transfer. The second model represents the situation when the droplet is periodically perfectly mixed and therefore exhibits a partial internal resistance to heat transfer. The third model is based on the assumption that the droplet is behaving as a solid sphere having the maximum possible internal resistance to heat transfer depending on the thermal conductivity and the size of the droplet itself. Clearly, the real behaviour of a droplet must lie in the domain of these three models and it remains to be determined experimentally which model best describes the behaviour of the droplet.

2.8 Thermodynamic and Transport Properties of Air, Water, Steam and Air/Steam Mixtures

In all the calculations reported in this thesis the thermodynamic and transport properties were determined from references [74,75,76,77 and 78]. The thermodynamic properties of air were determined from the ideal gas law and the transport properties from [79,80]. The transport properties of the air/steam mixture were calculated using correlations given in [79] and [81].

Appendix D contains specific details for every property calculated.

2.9 Outline of the Numerical Algorithm used in the No Internal Resistance Calculations

Before the algorithm outline is started some pertinent assumptions (besides those already introduced) will be listed.

- i) Heat transfer by radiation is assumed negligible in the range of conditions relevant to this work. This assumption has been adopted by previous workers [9,71,84]. (In higher temperature situations its contribution could be easily incorporated by use of the Spalding dimensionless group, see [12].)
- ii) The thermodynamic and physical properties of the air/steam mixture are considered uniform and evaluated at the arithmetic average temperature between droplet surface and surrounding medium temperature [81,85 and 86].
- iii) The effects of natural convection are negligible compared to those of forced convection [12].
- iv) The non-uniformity of heat and mass transfer around the sphere is taken into account by the use of the averaged heat and mass transfer coefficient correlations.
- v) The air/steam mixture is always saturated.

Equation (21) was solved by the method of short interval integration. Firstly the difference between the temperature of the surroundings and the initial droplet temperature (the total temperature range through which the droplet passes) was divided into a large number of increments (typically 40) and the physical, thermodynamic and transport properties of the vapour phase at the mean film

temperatures $(T_M + T_S)/2$ in each increment were calculated. In addition the velocities, Reynolds numbers, convective heat and mass transfer coefficients were also calculated. Then the time taken for the droplet temperature to be raised through each increment was calculated from equation (21). Some results of these calculations are shown in Figures 9, 10, 11 and 12, where the mean temperature responses of droplets injected at their terminal velocities and subjected to different saturated air/steam concentrations are shown as solid lines. The same calculations were performed using a fourth order Runge-Kutta technique [36] but there was no significant difference in the results.

The computer program developed for this purpose (short interval integration) is given in Appendix E. The Runge-Kutta procedure computer program is not included since it does not contain anything essentially new over the previous program.

2.10 Outline of the Numerical Algorithm used in the Partial Internal Resistance and Mixing Model

A droplet of radius R and initial temperature T_i was selected and assumed to be exposed to an air/steam mixture of known steam volume fraction x_{SM} and temperature T_M . From the gas phase data the bulk transport properties were calculated. A small increase in surface temperature ΔT_S was assumed. This enabled the calculation of the mean vapour film temperature and corresponding thermodynamic and transport properties followed by the heat and mass

$P_T = 1 \text{ BAR}$

$T_i = 20^\circ\text{C}$

$T_s = 81.35^\circ\text{C}$

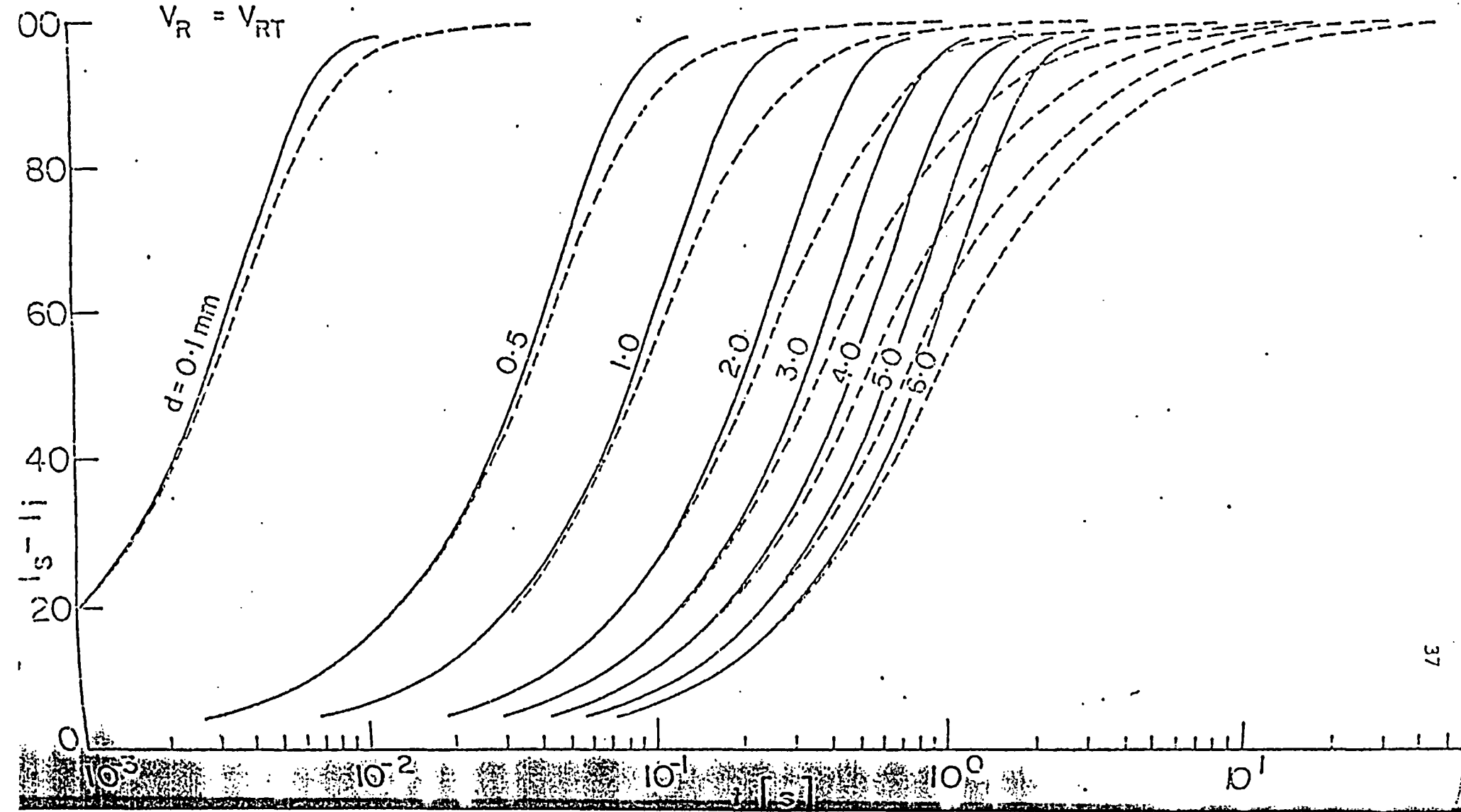
$X_S = 0.5$

$V_R = V_{RT}$

— NO RESISTANCE SOLUTION

- - - SOLUTION WITH PARTIAL INTERNAL RESISTANCE

Figure 9. Thermal Utilization vs. Time for $x_s = 0.5$



$P_T = 1 \text{ BAR}$

$T_i = 20^\circ\text{C}$

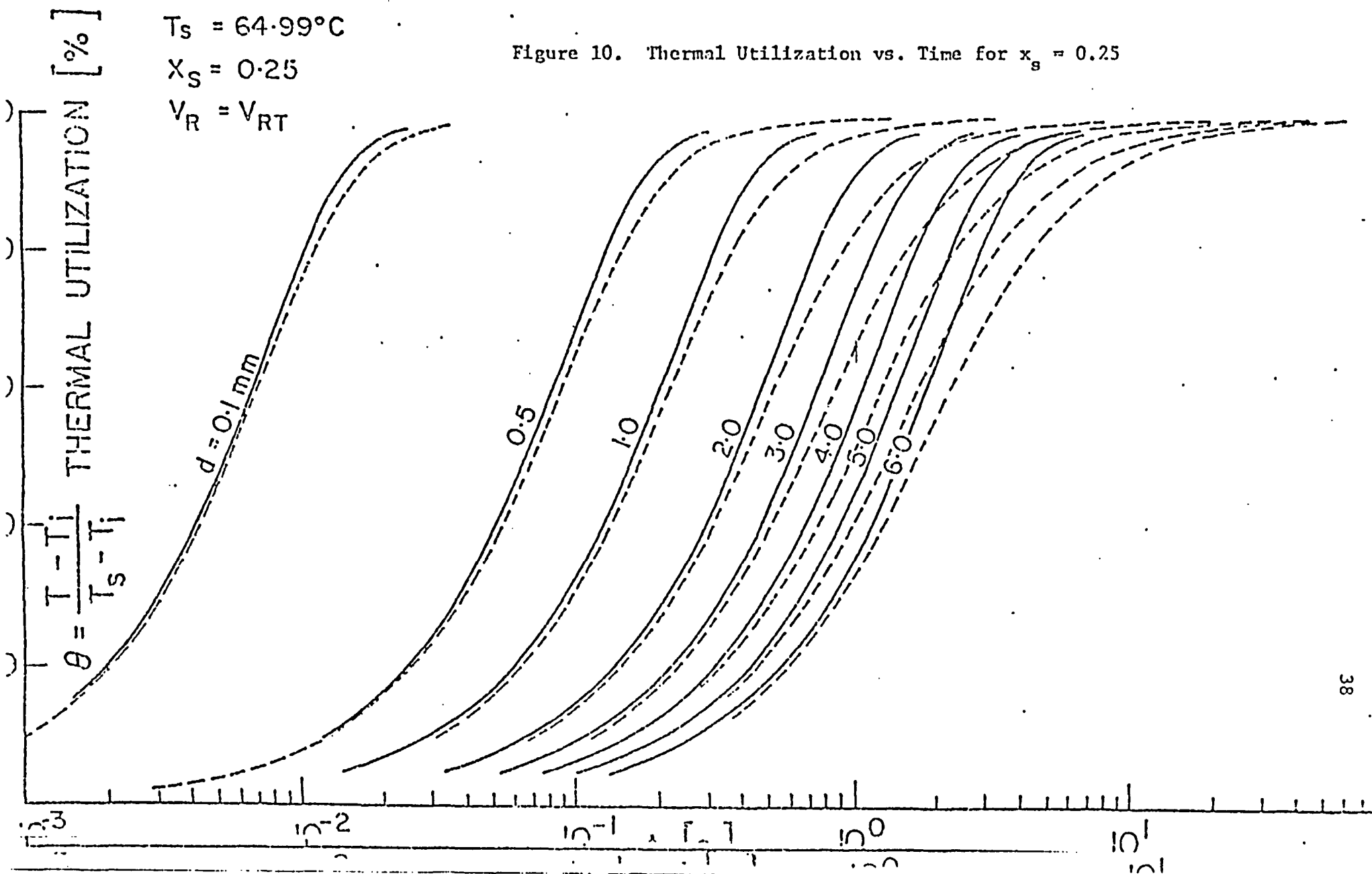
$T_s = 64.99^\circ\text{C}$

$X_S = 0.25$

$V_R = V_{RT}$

— SOLUTION WITHOUT INTERNAL RESISTANCE
- - - SOLUTION WITH PARTIAL INTERNAL RESISTANCE

Figure 10. Thermal Utilization vs. Time for $x_g = 0.25$



$P_T = 1 \text{ BAR}$

$T_i = 20^\circ\text{C}$

$T = 53.99^\circ\text{C}$

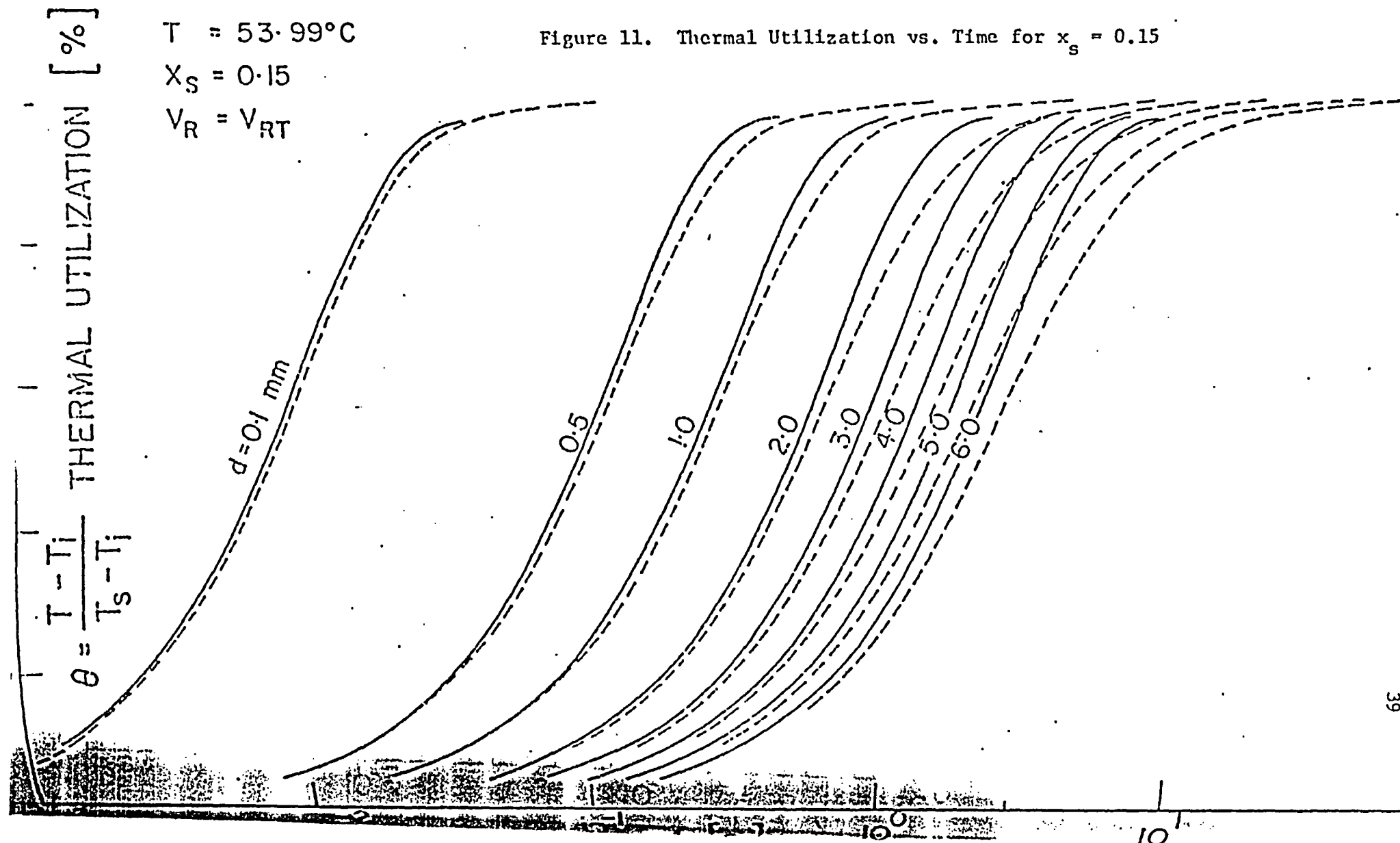
$X_S = 0.15$

$V_R = V_{RT}$

— NO RESISTANCE SOLUTION

- - - SOLUTION WITH PARTIAL INTERNAL RESISTANCE

Figure 11. Thermal Utilization vs. Time for $x_s = 0.15$



$P_T = 1 \text{ BAR}$

$T_i = 20^\circ\text{C}$

$T_s = 31.93^\circ\text{C}$

$X_s = 0.05$

$V_R = V_{RT}$

— NO RESISTANCE SOLUTION

- - - SOLUTION WITH PARTIAL INTERNAL RESISTANCE

Figure 12. Thermal Utilization vs. Time for $x_s = 0.05$

$\theta = \frac{T - T_i}{T_s - T_i}$ THERMAL UTILIZATION [%]

$d = 0.1 \text{ mm}$

0.5

1.0

2.0

3.0

4.0

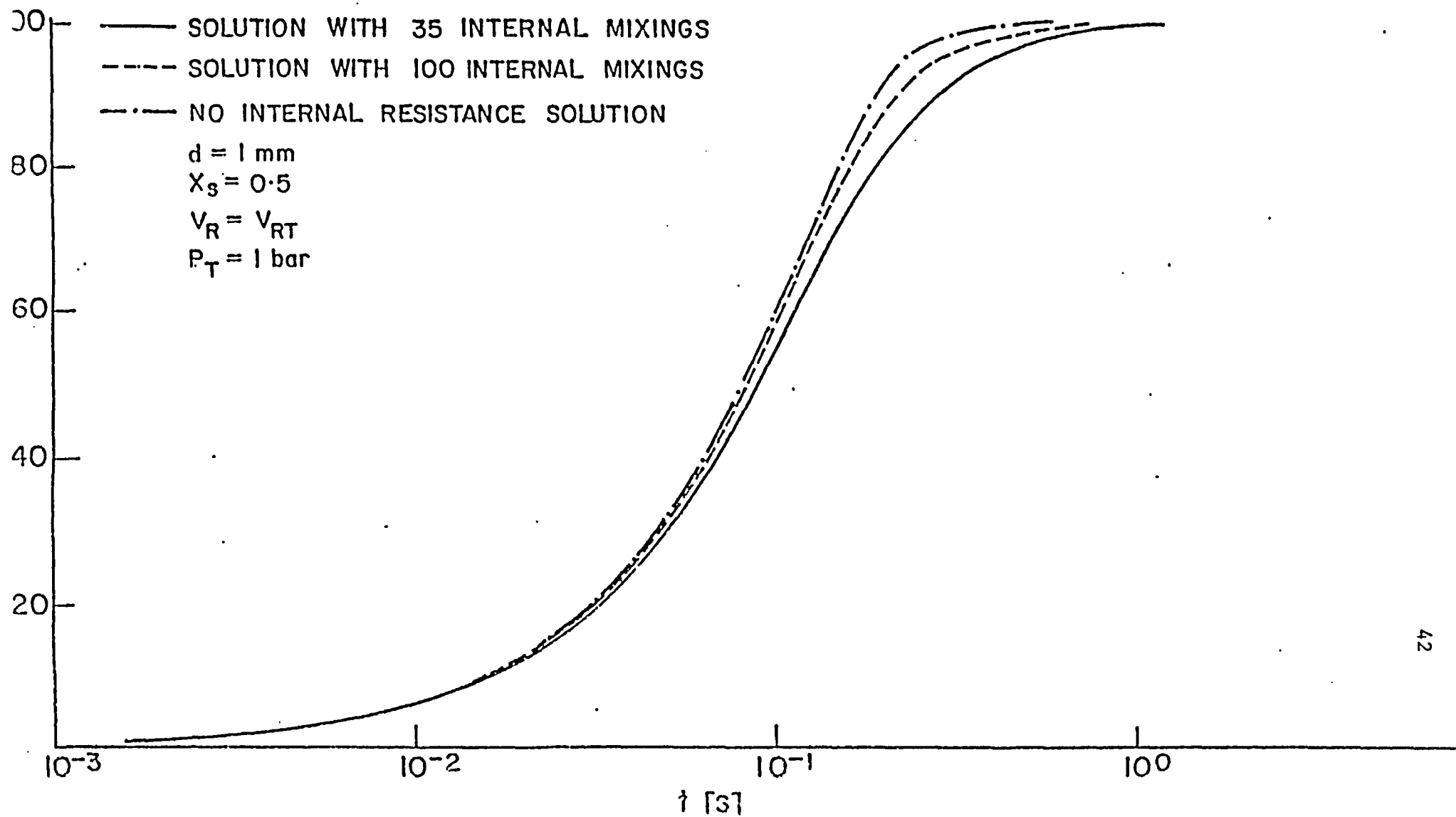
5.0

6.0

transfer coefficient using forms of equations (18) and (19). Thus an apparent heat transfer coefficient could be determined from equation (26). This heat transfer coefficient was then incorporated into the transcendental equation (34) to furnish a set of roots ψ_1 to ψ_n . The procedure for solving this transcendental equation was the "Half Interval Search" iterative technique [36]. From equation (35) the time taken for the specified surface temperature increase was determined, using the same iterative technique. The average temperature of the droplet was determined from equation (37). Finally the droplet diameter increase Δd was determined from equation (38) and the new radius was used for the next iterative step when the whole calculation was repeated using a new assumed surface temperature increase and a new uniform initial temperature profile equal to the mean temperature of the droplet calculated above. Figures 9, 10, 11 and 12 contain some typical predicted droplet temperature responses (dashed lines) taking into account the partial internal resistance.

To see the influence of the number of mixings on the iteration steps Figure 13 is drawn. The solid line represents the case of ~ 35 mixings while the dashed line represents the situation with ~ 100 mixings. As it is expected the higher the number of mixing is this model goes closer to the previous one, and in the limit with an infinite number of mixings would probably coincide with it. All the calculations with this model were otherwise performed with a constant number of mixings (usually 35).

Figure 13. Influence of a Number of Mixings on Droplet Temperature Response



Appendix F contains the relevant computer program with all the corresponding subroutines included.

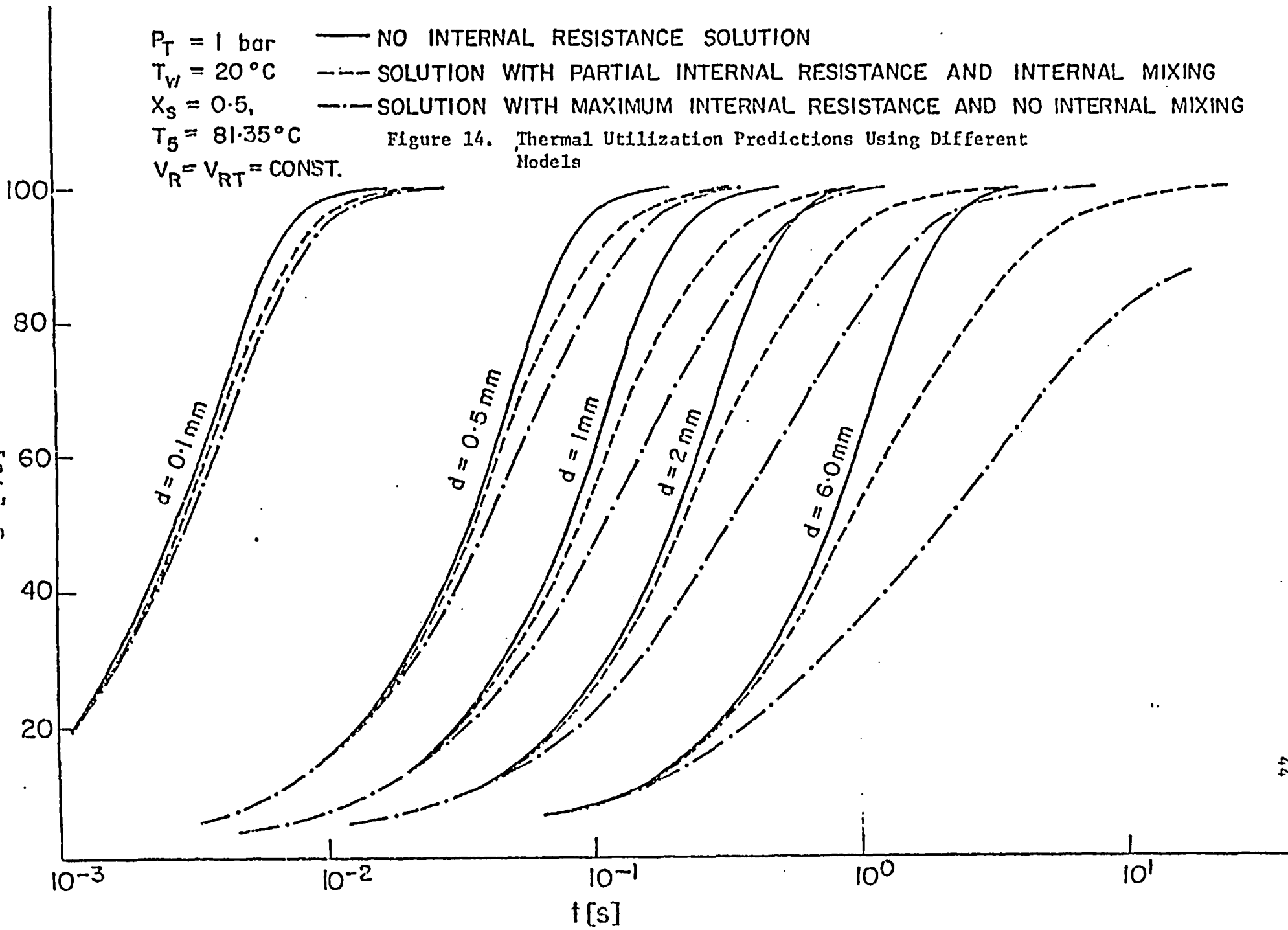
2.11 Outline of the Numerical Algorithm with Maximum Internal Resistance and No Mixing

In the first time step, this algorithm is basically the same as the previous one, however in the second and subsequent time steps, the initial temperature profile is obtained by curve fitting the temperature profile obtained at the end of the previous time interval. For this purpose, the droplet radius is divided into 20 intervals beginning at $r = 0$ and ending at $r = R$, and the droplet temperature determined at each of these nodal points. A linear regression subroutine is introduced to determine the unknown polynomial coefficients A_0 to A_7 (see equation (42)). This specifies the initial temperature profile for the second time step. In this time step (and in every subsequent one) the temperature at any point inside the droplet, at the surface and also average temperature are determined from equations (42), (43) and (45), respectively. The droplet diameter increase is determined in the same fashion as in the previous algorithm.

Since computer time required for this algorithm was excessive, only a few curves representing the thermal utilization as a function of time are shown in Figure 14. The maximum internal resistance solutions are represented by the dotted curves farthest to the right for each of the diameters considered. Thus the model

$P_T = 1 \text{ bar}$
 $T_w = 20^\circ\text{C}$
 $X_s = 0.5,$
 $T_5 = 81.35^\circ\text{C}$
 $V_R = V_{RT} = \text{CONST.}$

Figure 14. Thermal Utilization Predictions Using Different Models



predicts considerably slower response time, especially for the larger droplets. Since the droplet will probably experience some internal circulation the experimental results should fall into the region between the no internal resistance and no internal mixing solutions.

The discussed solution procedure seems to be much simpler and more general than the one proposed by Banerjee and Crosbie [87 and 88], since there is no need to introduce their assumptions:

- i) physical properties are independent of temperature
- ii) the heat transfer coefficient independent of the diameter of the sphere.

All the necessary details and subroutines used in the maximum internal resistance calculations can be found in Appendix G.

2.12 Discussion of Droplet Temperature Response Predictions

By comparison of Figures 9 to 12 it can be seen that the predicted response of the droplet temperature is much faster for droplets in saturated mixtures of 0.5 volume fraction than for a mixture of 0.05 volume fraction. This is to be expected because the temperature and mass driving forces are greater at the higher steam concentrations. The time taken for the larger droplets to almost achieve the temperatures of the surroundings is of the order of seconds and since the terminal velocity of such droplets is of the order of 9 m/s the droplets may not be fully utilized for condensing steam, even in a very high dousing chamber.

Hence : use significantly small drops!

The effect of the internal resistance of the droplets is illustrated by comparing the solid, dashed and dotted response curves in Figures 9 to 12 and 14. The internal resistance is most significant for the larger drops. In addition, as the gas phase heat and mass transfer resistance increases, that is, as the air concentration increases, the relative importance of the droplet internal resistance is reduced (i.e. dashed and solid lines are closer to each other).

Figure 15 illustrates the effect of the initial droplet velocity on droplet temperature response. The curve representing the fastest response is for a 1 mm droplet injected at three times its relative terminal velocity. When the droplet is injected at its terminal velocity its response is considerably slower and the trend continues for droplets entering at velocities less than the terminal velocity. These results might suggest that in steam dousing the droplets should be injected with a high downwards velocity. However, since this would also shorten the effective lifetime of the droplets in a particular chamber, the optimum injection velocity may be quite low. This will be discussed further in part II of this study.

Just for the sake of the completeness the effect of downwards and upwards movement of the droplet is compared in Figure 16, for the case when the internal resistance of the droplet is taken into account. The peculiar shape of the thermal utilization curve in the case of upwards movement of the droplet can be explained as

Uncertain

Figure 15. Initial Velocity Influence on Response Times

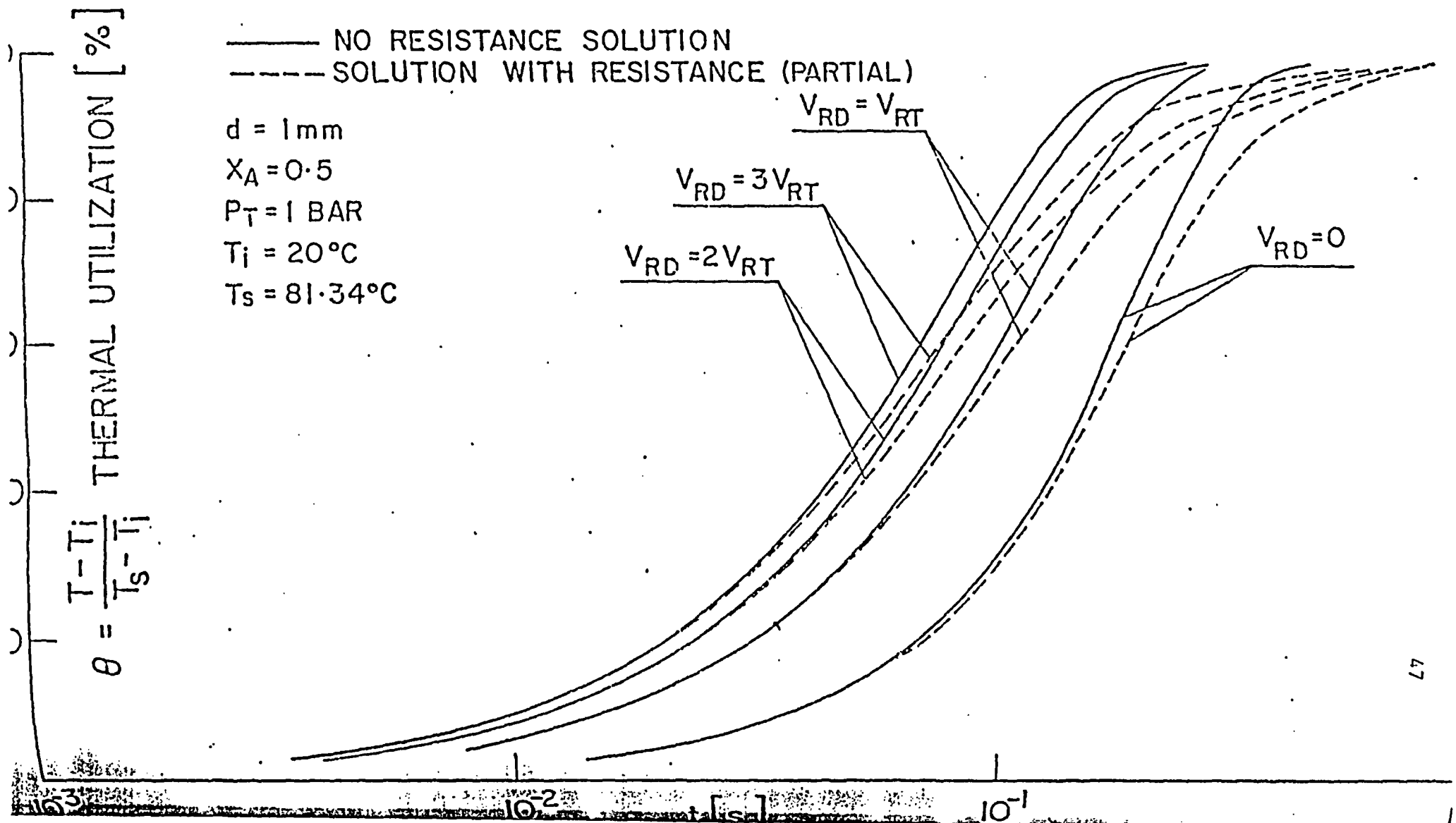
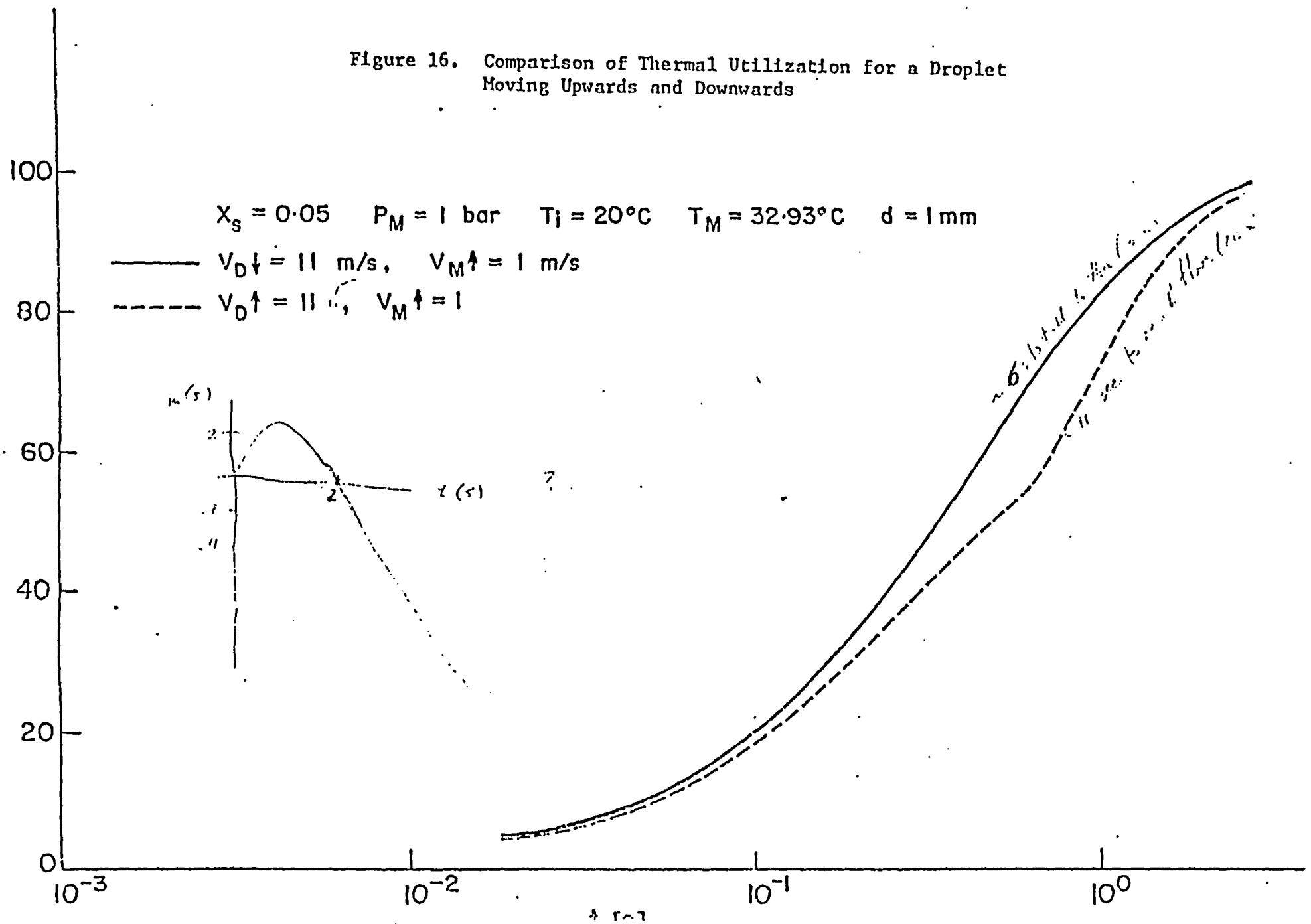


Figure 16. Comparison of Thermal Utilization for a Droplet Moving Upwards and Downwards



follows: in the beginning, both the curves are close together. The downwards moving droplet has a decreasing velocity until it reaches its relative terminal velocity. However, the upwards moving droplet goes through the moment when $v_R = 0$, and then accelerates towards the same relative terminal velocity as the other droplet.

Incomplete for following reasons:

- a) We need droplet times to reach floor for various sizes, initial velocities
- b) we need more results on utilization
 - different x_{stop} ratios
 - longer drops possibly

3. THE EXISTING EXPERIMENTAL EVIDENCE AND PREDICTIONS

The purpose of this chapter is to compare the heat transfer coefficients predicted and confirmed experimentally in this study with those cited in the literature for various experimental situations. The vapour phase or "external" heat transfer coefficient h_{app} is defined by equation (26) as:

$$h_{app} = Q_T / (T_M - T_S) \quad (26)$$

The predicted values of heat transfer coefficients which were later indirectly confirmed by measuring thermal utilization for our system (droplets and an air/steam mixture) are drawn in Figure 17. Thus the predicted average values of the apparent (with mass transfer) and convective (with no mass transfer) heat transfer coefficients for the droplets of various sizes (injected at terminal velocities) are presented over the range of concentrations $0.5 < x_A < 1$ which is the practical range of interest in this research program. The most striking feature of the apparent heat transfer coefficients is their rapid decline in the more dilute end of the range. The enhancement of the heat transfer coefficient caused by the steam condensation is clearly illustrated by comparing the two sets of curves.

To see what influence the different heat and mass transfer correlations might have on h_{app} , the predictions of Berman's [45] and Ranz and Marshall's [46] heat and mass transfer analogy correlations (curves 6 and 1 in Figure 8) for droplet evaporation are shown

— HUGHMARK'S CORRELATION
 - - - BERMAN'S CORRELATION
 - · - RANZ & MARSHALL'S CORRELATION

Figure 17. Predicted Values of the External and Convective Heat Transfer Coefficient

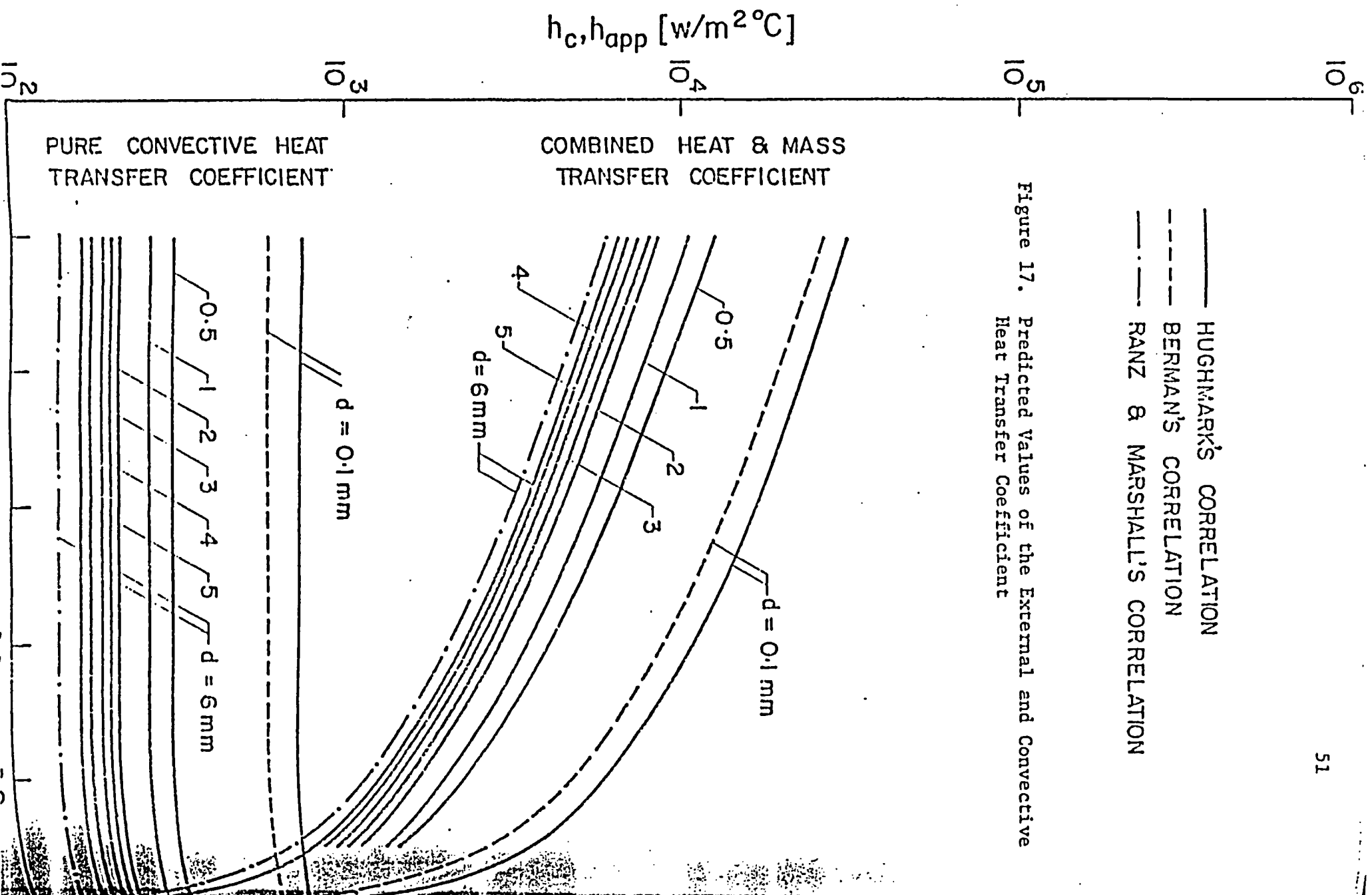


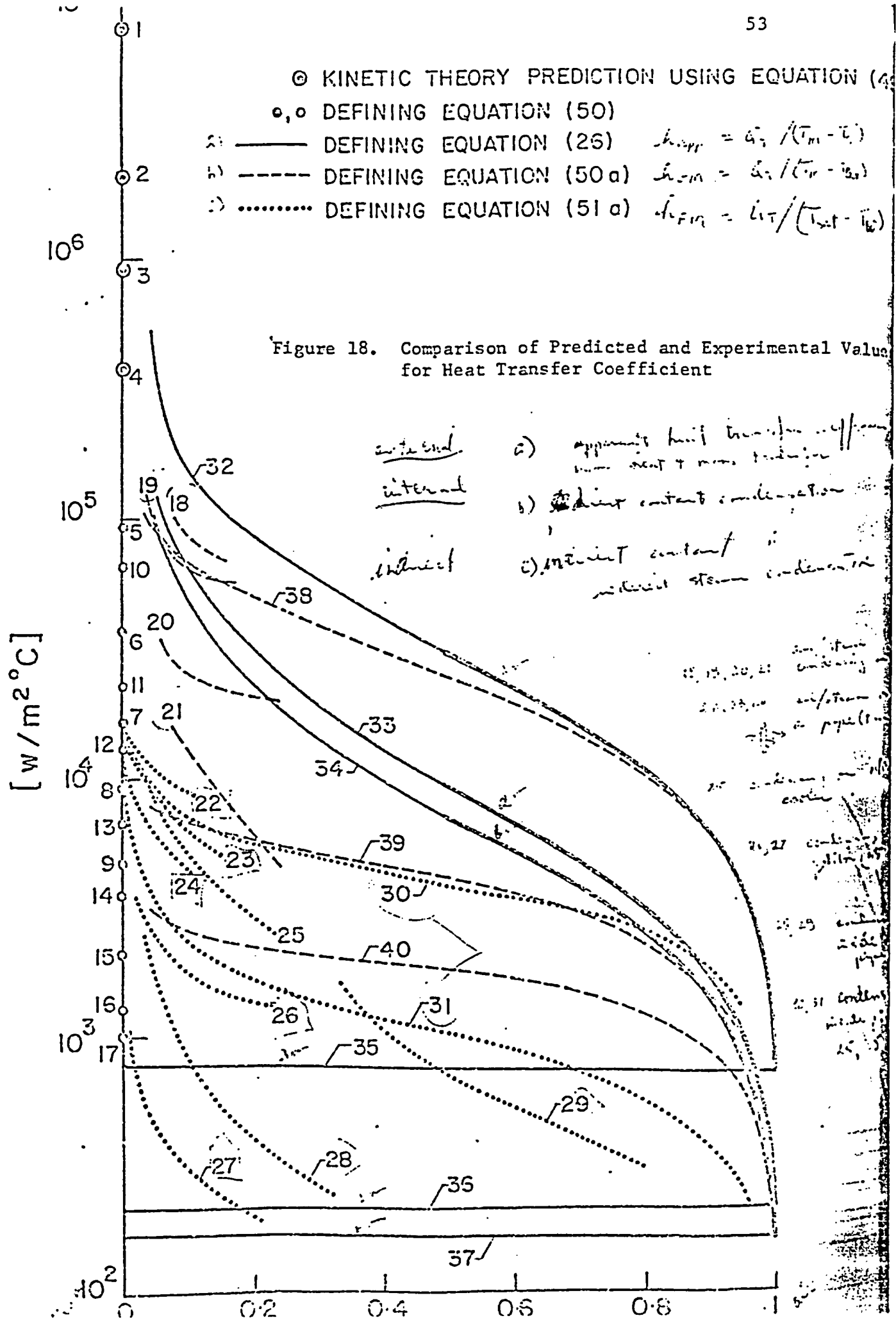
(Figure 17) by the dashed and by the dash-point lines for 0.1 and 6 [mm] droplets, respectively. They are very close to the predictions (solid lines in Figure 17) obtained when using Hughmark's correlations represented by curves 7 and 8 in Figure 8. This was expected since the Berman's, Ranz and Marshall's and Hughmark's correlations are very close together in Figure 8.

Before comparing heat transfer coefficients arising in different experimental situations it is always necessary to carefully define them. This has to be done in order to clarify which experimental values can be compared, and avoid possible confusion.

The first basis of comparison for the apparent heat transfer coefficient h_{app} is the interfacial heat transfer coefficient h_i predicted by the kinetic theory for pure steam condensation [89].

$$h_i = f \left(\frac{M_S}{2\pi R_g T_{sat}} \right)^{1/2} \left[\frac{\lambda}{T_{sat}} \frac{\lambda}{v_g - v_l} - \frac{P_{sat}}{2} \right] \quad (49)$$

Clearly, a comparison with this heat transfer coefficient is possible only in the limit where an inert gas concentration tends to the value zero, and when the liquid internal resistance is negligible. Calculated kinetic theory predictions of the heat transfer coefficients at the interface h_i are represented by points 1 to 4 in Figure 18 (on the pure steam line) for pressures 0.983, 0.167, 0.0689 and 0.0334 Bar, respectively [89]. These h_i values were obtained using the value of the condensation coefficient $f = 1$, see Mills and Seban [90].



The second basis of comparison could be the "internal" or "overall" heat transfer coefficient definition which has been used in cases of direct contact condensation of pure steam on water jets, sprays, etc.:

$$h_{\sigma} = Q / (T_{\text{sat}} - \bar{T}_L) \quad (50)$$

where:

Q - heat flux,

\bar{T}_L - average temperature of the liquid.

An analogous definition of this heat transfer coefficient in our case for the saturated air/steam mixture would be:

$$h_{\sigma M} = Q_T / (T_M - T_{\text{av}}) \quad (50a)$$

Lekic's [89] pure steam experimental results for the "internal" heat transfer coefficients (defined by equation (50)) are represented by points 5 to 9 for droplet diameters 0.1, 0.25, 0.5, 1 and 2 [mm], respectively. Points 10 to 17 represent the same type of heat transfer coefficient for the pure steam condensation on water droplets (predicted by Brown [91]), for droplet diameters of 0.1, 0.3, 0.5, 1, 2, 3.175, 4.76 and 6.35 [mm], respectively. To distinguish between these "internal" heat transfer coefficients (equation (50)) and external ones (equation (49)) they are represented differently in Figure 18, and the latter are denoted by double circles, i.e. as \odot .

A third basis of comparison could be the heat transfer coefficient usually defined for the case of "indirect" condensation of pure steam on a liquid film flowing over some surface (tubes, walls, etc.). The following definition of this heat transfer coefficient is customary:

$$h_F = Q/(T_{\text{sat}} - T_W) \quad (51)$$

where:

T_W - wall temperature.

Similarly, if the steam is condensing from a mixture on a liquid film an analogous definition applies:

$$h_{FM} = Q_T/(T_{\text{sat}} - T_W) \quad (51a)$$

In order to distinguish among the three heat transfer coefficients defined by equations (26), (50a) and (51a) in the case of condensation from vapour-inert gas mixtures, the coefficients are represented in Figure 18 by solid, dashed and dotted lines, respectively. It should be noted that these coefficients were introduced and defined in order as their values decreased. The highest values represent "external" heat transfer coefficients (equations (49) and (26)) followed by "internal" or "overall" ones used in cases of "direct" steam condensation (equations (50) and (50a)) and subsequently by those used for cases of "indirect" steam condensation (equations (51) and (51a)).

Now that the heat transfer coefficient definitions have been clarified, the corresponding experimental results (for mixtures) can be properly represented in Figure 18 and compared with our predicted and experimental values for droplets.

Curves 18, 19, 20 and 21 represent heat transfer coefficients obtained for an air/steam mixture at atmospheric pressure condensing on a jet of water for a mixture (flowing parallel to the initial direction of the jet) with relative velocities 45, 36, 26 and 14 m/s, respectively (see Kutateladze, Figure 11.9, page 196, [92]). Curves 22, 23 and 24 represent the heat transfer coefficients h_{FM} for the case of transverse flow past a horizontal pipe [53]. Curve 25 illustrates the values obtained in reactor building coolers (finned tubes with water flowing inside) for rich mixtures of air and steam and for a frontal velocity 3.4 m/s [93]. The condensation of steam from an air/steam mixture on a vertical film is represented by curves 26 and 27 for wall temperatures of 55 and 10°C, respectively [94]. The condensation of steam from an air/steam mixture inside a pipe is represented by curves 28 and 29 obtained by Ackermann [95].

The only data available over practically the whole range of inert gas volume fractions are those of Renker [96], and these data are for the condensation of steam inside a pipe. Curves 30 and 31 in Figure 18 illustrate these data for the mixture velocities 25 and 5 m/s, respectively.

It is now of interest to compare the results of this study with those of the other investigators cited above. The thicker

parts ($x_A > 0.5$) of the solid lines 32, 33 and 34 represent the h_{app} predictions of this study using Hughmark's [48] correlations (for Nusselt and Sherwood numbers) for droplet diameters 0.1, 2 and 6 mm falling at their respective terminal velocities and for a total mixture pressure of 1 Bar. These predictions have been confirmed experimentally in this study (see below). The thinner parts ($x_A < 0.5$) of these lines illustrate the predictions of this work using the same approach (as for $x_A > 0.5$). However, no experiments were performed in this region of steam concentrations. Our curve 32 for a 0.1 mm droplet has the lowest internal resistance and tends most rapidly to the kinetic theory prediction for the corresponding pressure of 1 Bar (point 1) as expected.

does it
reach the
point?

Pure convective heat transfer coefficients (no condensation) as predicted by this study are represented by curves 35, 36 and 37 for droplet diameters 0.1, 2 and 6 mm, respectively, and for pure air ($x_A \rightarrow 1$) they are the same as the heat transfer coefficients calculated allowing for mass transfer (curves 32, 33 and 34).

To be able to compare the heat transfer coefficients predicted (and confirmed experimentally for $x_A > 0.5$) in this study with the pure steam values obtained by Brown [91] and Ford and Lekić [97] our heat transfer coefficients have been recalculated using equation (50a). The results of these calculations are represented by lines 38, 39 and 40 in Figure 18. Point 5 represents the heat transfer coefficient for a 0.1 mm droplet obtained by Ford and Lekić, while point 10 represents the value predicted by Brown. Our prediction

for a 0.1 mm droplet (based on the heat and mass transfer analogy extension in the region of very high steam concentrations) is represented by curve 38 in Figure 18 and tends to extrapolate to somewhat higher values in the limit as x_A approaches zero. The same is true for the 2 mm droplet value represented by the point 9 (Ford and Lekić) and by the point 14 (Brown) while our prediction is represented by curve 30. The same applies for a 6 [mm] droplet (compare points 15, 17 and curve 40). Brown's experiments were performed on sprays, while his theory was for single drops, thus there is some doubt about the comparability of his predictions and experiments. Ford and Lekić's experimental and theoretical results are in good agreement and they are for single droplets, and it is believed that their results are more reliable. Comparison of our predictions (curves 38 and 39) with Ford and Lekić's results (points 5 and 9) shows reasonable agreement.

Thus the final conclusion of this comparison is that the predictions of the heat and mass transfer analogy (for an air/steam mixture) applied to mixtures with inert gas concentrations of $0 < x_A < 0.5$ tend to the corresponding values of the "external" heat transfer coefficients predicted by the kinetic theory and the values of the "internal" heat transfer coefficient for the pure steam, when the heat transfer coefficients are carefully and properly defined.

Finally it should be pointed out that the importance of the droplet internal resistance is illustrated once more in this figure. For a 0.1 mm droplet and $x_A > 0.5$ the resistance to heat

transfer is practically all in the gas phase (compare curves 32 and 38), however for a 6 mm droplet the internal resistance is quite important (compare curves 34 and 40) almost as far as $x_A = 0.95$.

To conclude this chapter it should be pointed out that this survey of experimental results is probably the most exhaustive collection of the data in the area of the condensation in the presence of non-condensables. It is very useful to have these data together enabling the distinction between the different experimental situations, and avoiding possible confusion by improper use of the defining equations.

4. EXPERIMENTAL APPARATUS

The purpose of the single drop experiments was to obtain measurements of thermal utilization, i.e. to measure as a function of time the percentage of the total possible heat pick-up of a droplet. This is the same as the time dependence of the mean dimensionless droplet temperature (expressed as a percentage).

To make this measurement two possible techniques were at first considered. These were:

- i) the suspension of a droplet on a thermocouple or thermistor tip in an air/steam gas stream,
- ii) the free suspension of a droplet in a wind tunnel.

The second approach (used by Garner and Kendrick [101] successfully in mass transfer experiments) was abandoned because

- a) it was necessary to deal with the saturated air/steam mixture and problems of wet apparatus surfaces were unmanageable; for more details see Ford and Lekić [90,97],
- b) it was practically impossible to measure the temperature response of such a droplet, since it did not stay in a fixed position in the tunnel, on the contrary it tended to oscillate and move in all the directions inside the wind tunnel cross sectional area,
- c) only the relative terminal velocity could be investigated whereas it was necessary to investigate relative velocities less than this value in this work.

The first arrangement is much simpler and has been used by several previous investigators [69,62,12] to study the evaporation process. The general apparatus arrangement is shown in Figure 19. Figure 20 shows the air and steam lines together with air heater and calming chamber, while Figure 21 shows the general view of the apparatus, including the droplet producing unit, metering pump, cooling and feeding water lines, recorder and humidity meter.

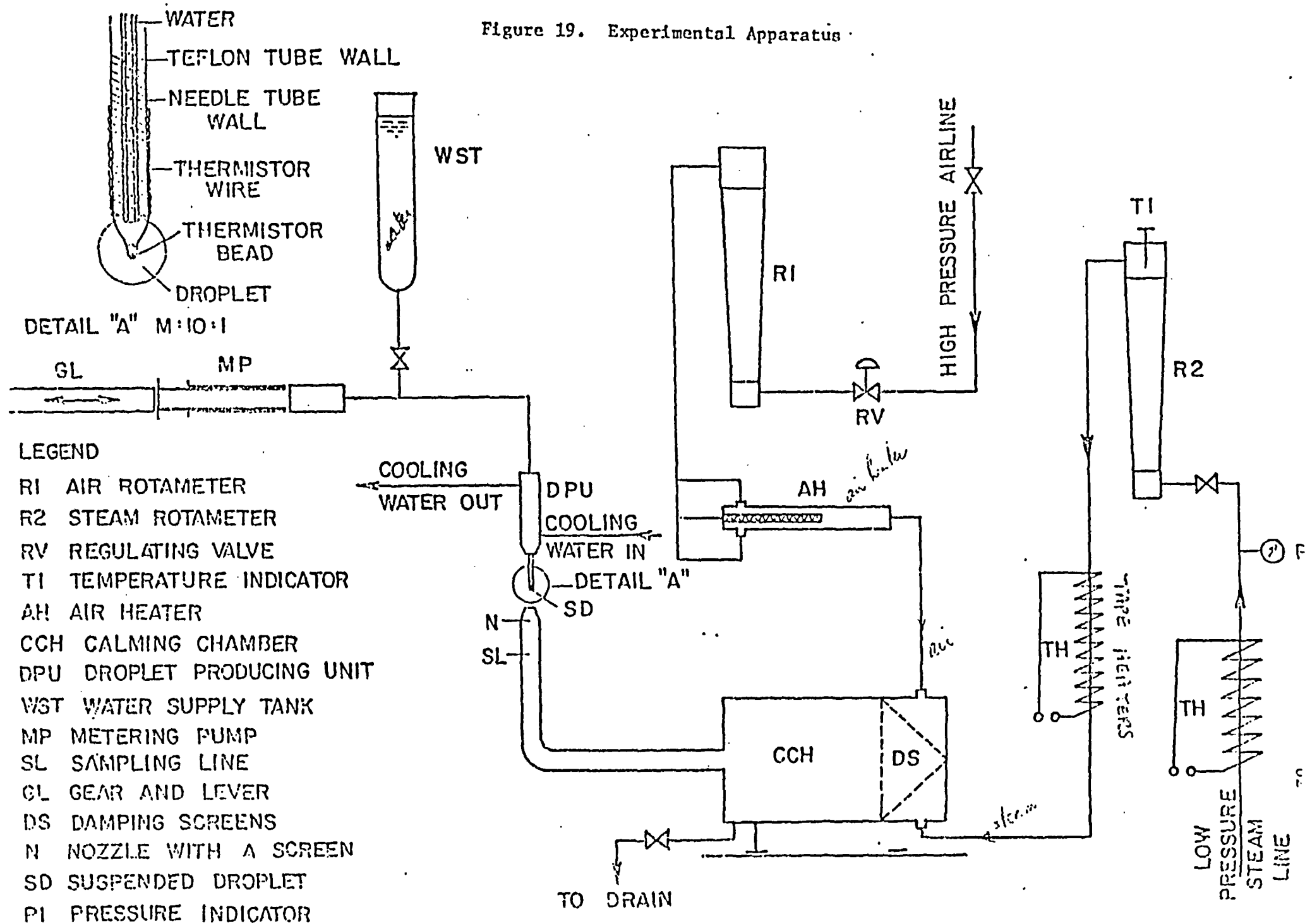
4.1 Air System

Air was taken from the laboratory high pressure line. Its pressure was decreased to 20 psig by passing it through the regulating valve RV and passing it through the rotameter R_1 . The calibration curve of this rotameter is in Appendix H. The calibration was performed with two American Aluminum case meters AL-600 and AL-350 Cfh. Both the calibration points are shown on the graph in Appendix H. From the rotameter R_1 the air stream was split into three parts (1/4" PVC tubing used) to feed the air heater AH. The electrical heater (GTE Sylvania Incorporated) was connected to a variac which varied the power to the heater over a range from zero to 500 watts. From the air heater the air was led to the calming chamber CCH.

4.2 Steam System

In a similar fashion steam was taken from the low pressure steam line and led to the steam rotameter R_2 . This rotameter was previously calibrated by the supplier Schutte Koerting Co. (the

Figure 19. Experimental Apparatus



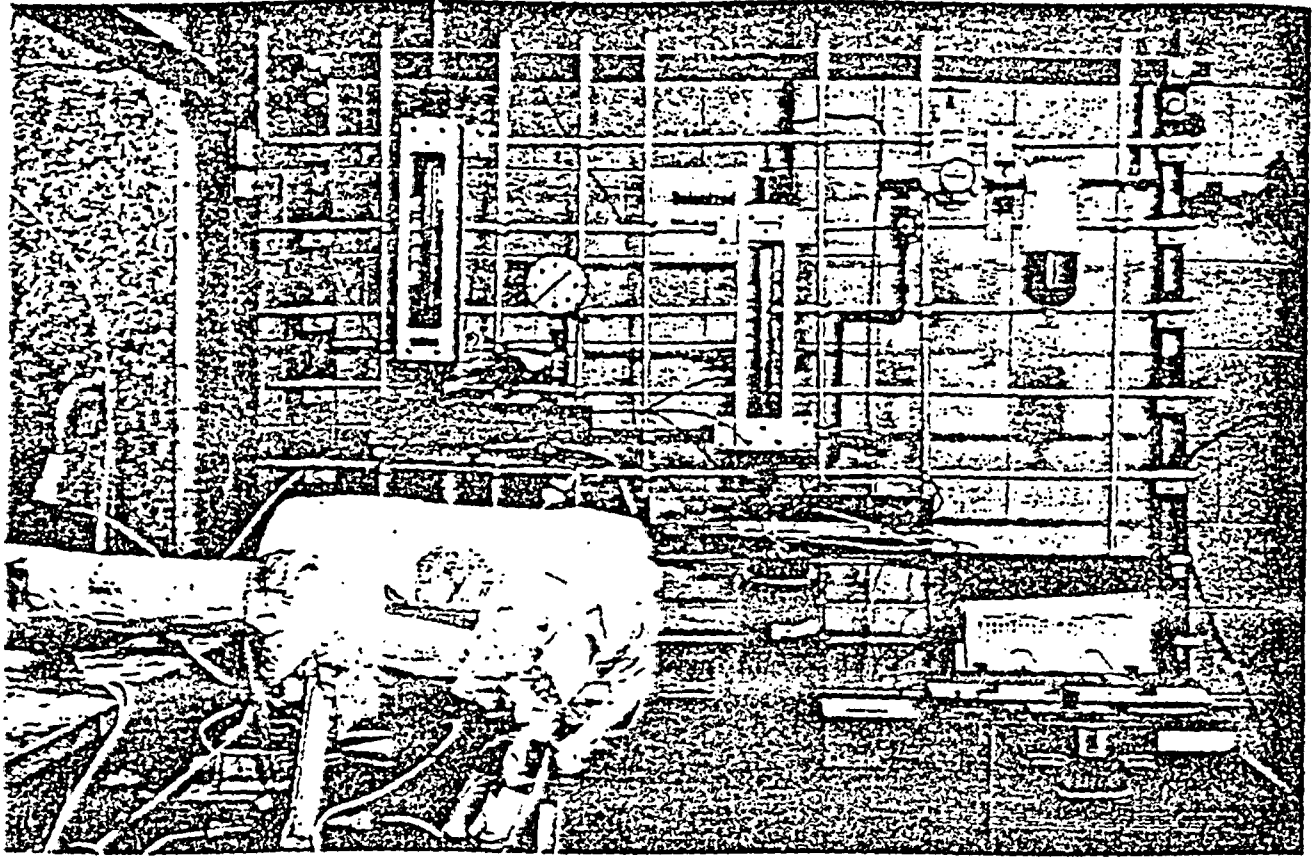


Figure 20. Side-view of Experimental Apparatus with Steam and Air Lines.

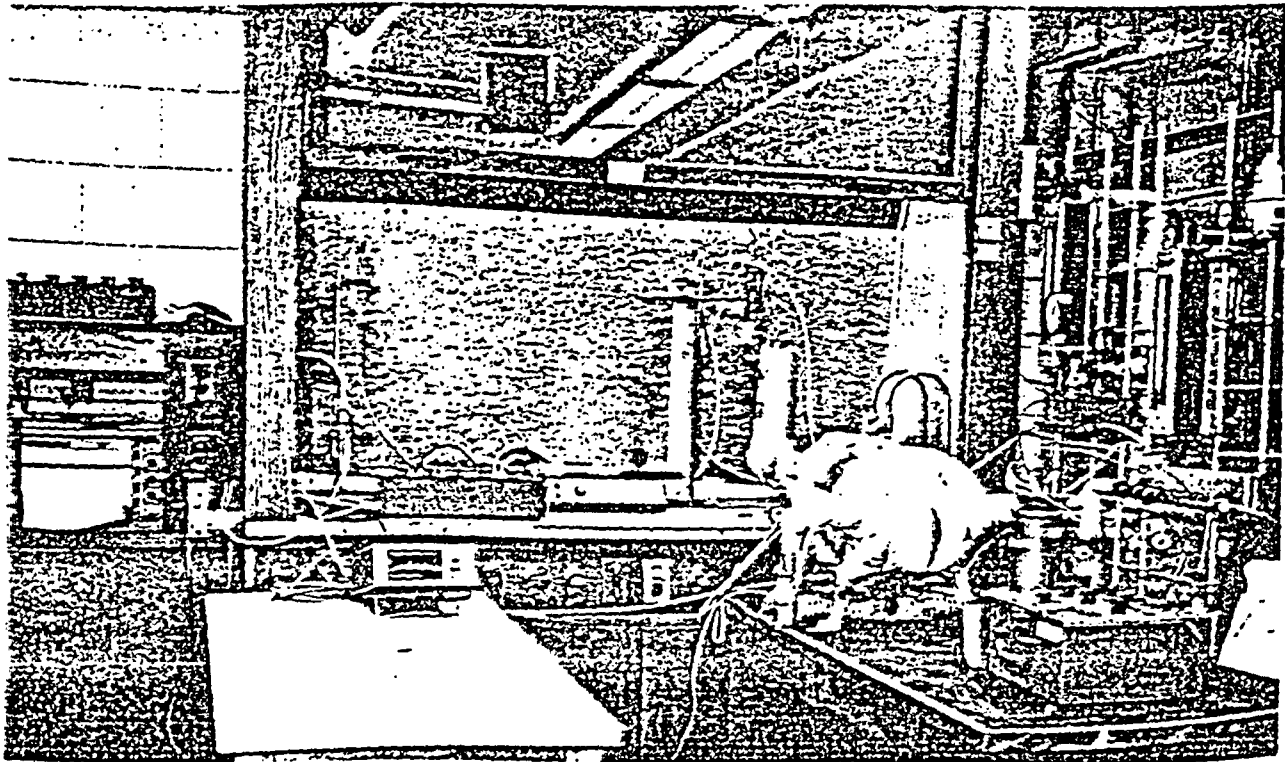


Figure 21. Side-view of Experimental Apparatus with the Test Section and Droplet Producing Unit.

supplier of the rotameter R_1 , also) for a steam pressure of 15 psig and temperature 212°F. The temperature indicator T_1 in the rotameter's exit showed the temperature ~ 212°F during all the experimental runs. The pressure indicator PI (range 0-30 psig) was used to determine the steam pressure before the rotameter. From the rotameter R_2 the steam stream was also led to the calming chamber. The steam line tubing was heated by tape heaters and insulated carefully to prevent the steam condensation.

4.3 Test Section

Air and steam were introduced through 3/4" pipes into the calming chamber CCH, which was made from a 20" long pipe with 10" OD. After being thoroughly mixed and calmed using a 80 mesh screen as shown in Figure 19, the stream was led through a 2" ID pipe to the nozzle especially designed to ensure a flat velocity profile of mixture. 140 mesh screen was provided at the end of the nozzle to decrease free stream turbulence [102]. Two nozzles were used having 1" and 1-1/2" ID, respectively.

4.4 Droplet Producing Unit

The droplet was produced in the droplet producing unit DPU. Essentially it consisted of a feed and a cooling water system. More details can be found elsewhere [89]. The feed water (deionized) was supplied through a very precise syringe metering pump MP (model 341), a product of Sage Instruments a Division of Orion Research Inc. With a 50 cc syringe size the flow rate could be varied

between 0.33 and 13 ml/min or ml/hr, depending on the gears selected. With a 10 μ L syringe this could be reduced to 0.000092-0.0036 ml/min or m./hr, respectively. With the cooling water, the feed water could be cooled practically to the temperature of city supply water. A droplet was produced by starting and stopping the syringe piston using the gear and lever arrangement. Droplets ranging in size from 1.3 to 4 mm could thus be produced.

4.5 Measurement Techniques

The flow rates of air and steam were determined by the rotameters R_1 and R_2 respectively. The steam and water temperature were measured using iron-constantan thermocouples.

The air/steam mixture velocity was determined by use of the continuity equation using measured flow rates. A pitot tube velocity measurement showed that the velocity profile just after the nozzle was flat.

The humidity of the air/steam mixture was determined using a digital humidity and temperature sensing system supplied by Thunder Scientific Corporation. This system uses the Brady Array Humidity Sensor [103] which is a semiconductor device which changes its resistivity as "water content" of the array increases. The digital readout is obtained just by exposing the sensor to the air/steam mixture. Although this instrument was extremely handy and simple to use it was also very temperamental even though AECL's experience with this instrument had previously been very satisfactory. The instrument

calibration was tested as follows: an air/steam mixture sample was sucked from the main air/steam line (about 5" before the exit nozzle) using the sample tap, provided. This mixture was passed through three containers filled with water cooled by city water inside glass cooling coils. Steam from the mixture in an intimate contact with water condensed, and the remaining air was fed to a precise gas meter to determine its flow rate. The bottles were weighed before and after the sample run. The difference in weight gave the amount of the steam condensed from the air/steam mixture and this allowed the calculation of the humidity of the air/steam mixture. When the Brady Array System was working correctly the agreement between the two measurement techniques was very good (within $\pm 5\%$).

The calibration curve for the Brady Array instrument was supplied by the instrument manufacturer and it is given in Appendix I.

The temperature measurement arrangements are shown schematically in Figure 22. The temperatures of the feed water and steam were measured in a normal manner therefore they are not discussed in any detail. The calibration curve for feed water thermocouple is given in Appendix J together with tabulated values for electromotive forces. For the temperature readings of the steam thermocouple tabulated values of electromotive forces were used.

The droplet temperature measurement deserves some comment since this measurement took some time to be developed. After several trials the following technique was adopted. Tiny thermistor wires

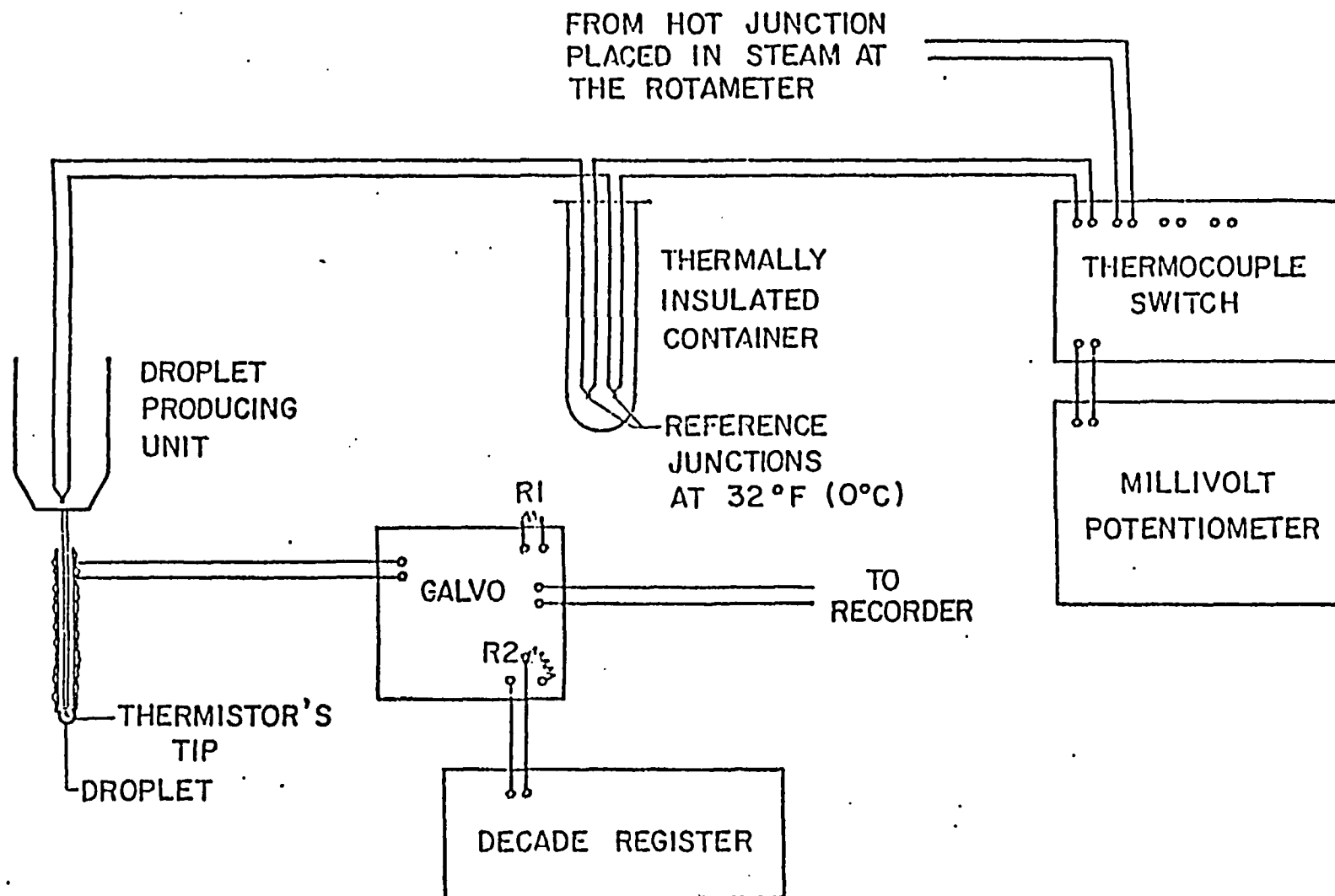


Figure 22. Temperature Measurements Scheme

(~ 0.025 mm) were glued onto a teflon tube which was slid over the drop producing needle. Detail "A" in Figure 19 represents the needle end (enlarged ten times) together with the 1.3 mm droplet (smallest diameter obtained experimentally) suspended at it. The thermistor bead is a spheroid with the longer axis length 0.3 mm. The thermistor is produced by Fenwal Electronics. Two needles were used. They were made of Popper and Sons Inc. aerospace stainless steel type 304 tubes as specified in the next table.

Table I.1

Needle #	Gauge	OD		ID		Wall Thickness	
		mm	inch	mm	inch	mm	inch
1	30	0.3048	0.012	0.1524	0.006	0.0762	0.003
2	26	0.4572	0.018	0.2413	0.0095	0.10795	0.00425

The corresponding thermistors were termed Nos. 1 and 2. For their calibration a liquid-in-glass thermometer serial No. SC2118, manufactured by Fisher, range -1 to 101°C, graduation 0.1°C, was used. The thermistor calibration curves together with the corresponding calibrations of the recorder charts are given in Appendix K.

4.6 Experimental Procedure

The experimental and measurement procedure was as follows. A previously decided air/steam mixture was fed to the nozzle and all

the parameters defining the mixture were measured and recorded. A droplet was formed on the needle tip and photographed. (The camera used was Nikkormat FTN 35 mm with 55 mm Micro-Nikkor f 3.5 Lens and Braun 240 LS Electronic flash. Elements used f .32 exposure and flash duration 1/1000 sec.) The films developed were subsequently projected on a wall using a film strip projector. The diameter of the needle was known. This gave the reference dimension for the droplet determination. The droplets were prolate spheroids and the equivalent sphere diameter d was determined from (equal volumes of the spheroid and the sphere)

$$d = (ab^2)^{1/3} \quad (52)$$

where, a and b are the longer and shorter spheroid axes, respectively. The estimated accuracy of the droplet diameter measurement is ± 0.1 mm.

The high speed recorder was switched on and the droplet was exposed by moving it quickly into the air/steam mixture where it remained for about ten seconds. The recorded time intervals were 0.01 sec at a chart speed 5 in. per second. The chart paper used was Type 1895 Standard Kodak, 8 in. by 200 ft., specification 1. This type of paper showed the best recording for the specified elements on the recorder (0.01 sec time recording at 5 in. per second chart speed).

Before proceeding to the evaluation and discussion of experimental results the possible influence of radiation, condensation

and heat transfer on and through the needle with respect to the droplet temperature histories will be discussed.

4.7 Heat Conduction and Radiation Influence on the Droplet

Temperature Response Measurement

As was mentioned earlier, radiation effects can be neglected safely in this range of temperatures (maximum surrounding temperature in the experiments was $\sim 88^{\circ}\text{C}$ and the lowest droplet temperature $\sim 12^{\circ}\text{C}$ and this difference decreases as the process goes on). Ranz [104] found that the radiation effects are negligible in the case of droplet evaporation at 260°C surrounding medium temperature. Even in the case of liquid fuel burning, the radiant energy from the flame to the drop is less than 15% of the total heat transfer [9].

With respect to the possible effect of the needle on the temperature response, the first fact to be noted is that the whole wake region contribution to the total droplet heat and mass transfer is expected to be in the order of 10%, Hoffman and Ross [17]. Thus the needle presence at the droplet rear would be expected to have a relatively small influence on the total heat and mass transfer. However, due to the fact that the needles were made from stainless steel there existed the possibility that they might conduct a fair amount of heat away from the rapidly heating droplet.

The hypodermic needle is represented as a semi-infinite rod with thermal insulation of its lateral surfaces (see Luikov [73],

p. 203) at a uniform temperature equal to the initial surrounding medium temperature. For the most severe approximation of the real problem it can be assumed that:

- i) the tip of the needle (droplet itself) experiences an infinite heat transfer coefficient with the surrounding medium bringing its temperature instantaneously to T_M and
- ii) there is no heat transfer towards the lateral surface of the needle (covered by a teflon tube) from the surroundings.

The differential equation describing the problem is

$$\frac{\partial T(x,t)}{\partial t} = \alpha \frac{\partial^2 T(x,t)}{\partial x^2}, \quad 0 < x < \infty \quad (53)$$

with initial condition

$$T(x,0) = T_0 = \text{const} \quad (54)$$

and boundary conditions

$$T(\infty, t) = T_0, \quad \frac{\partial T(\infty, t)}{\partial x} = 0 \quad (55)$$

The solution of this problem may be written as:

$$\theta = \frac{T(x,t) - T_0}{T_M - T_0} = \text{erfc} [x/2(\alpha t)^{1/2}] \quad (56)$$

which can be written as:

$$\theta = \text{erfc} [x/B)/2(N_{Fo})^{1/2}] \quad (57)$$

where

$$B = \frac{c}{P} = \frac{d}{4} - \text{ratio of the needle cross-sectional area to its perimeter}$$

$$N_{Fo} = \frac{\alpha t}{B^2} - \text{Fourier number.}$$

To obtain some numerical values it will be assumed that the needle and its enclosed water represent the rod which has the physical properties of the needle which is made of stainless steel type 304. The outside diameter of the needle is 0.3 mm (0.012"). The physical properties of this steel are

$$\alpha = \frac{\lambda}{\rho c_p} = \frac{16.6147}{502.3 \cdot 8027.08} = 4.12 \cdot 10^{-6} \text{ [m}^2/\text{s]}$$

$$\text{Hence, for } t = 10 \text{ sec and } B = 0.3 \cdot 10^{-3}/4 = 7.5 \cdot 10^{-5} \text{ [m]}$$

$$N_{Fo} = \frac{4.12 \cdot 10^{-6} \cdot 10}{7.5^2 \cdot 10^{-10}} = 7325.77$$

At the end of the needle $x = L = 5 \text{ cm}$

$$\frac{x}{B} = \frac{5 \cdot 10^{-2}}{7.5 \cdot 10^{-5}} = 666.6$$

Introducing these values into (57) it yields

$$\theta = \text{erfc} [666.6/2(7325.77)^{1/2}] = \text{erfc}(3.89)$$

$$= 1 - \text{erf}(3.89) \approx 1 - 1 = 0$$

and

$$T(L, 10) = T_0$$

This implies that the water on the other end of the needle does not "feel" what is happening to the droplet after the "droplet" is kept at its maximum possible temperature for 10 sec.

By use of the theoretical models discussed earlier, the heat fluxes to the droplet surface have been predicted as a function of time. Thus, the heat fluxes through the end of the rod may be compared with previously predicted fluxes to the droplet. Before this is done the areas of the rod end and the droplet will be compared.

Areas of the rod end

$$A_R = d^2 \pi / 4 = 0.3^2 \cdot 3.14 / 4 = 7.0685 \cdot 10^{-2} \text{ mm}^2$$

Surface area of the 1 mm droplet

$$A_{D1} = d^2 \pi = 1^2 \cdot 3.14 = 3.14159 \text{ mm}^2$$

and the surface area of the 3 mm droplet

$$A_{D3} = 3^2 \cdot 3.14 = 28.27 \text{ mm}^2.$$

The area of the rod end is ~ 2.2% of the 1 mm and ~ 0.25% of the 3 mm droplet total area. (The smallest droplet diameter achieved in the experiments was $d = 1.3 \text{ mm}$.)

To determine the heat flux through the rod end the following approach will be used:

$$q = -k \frac{\partial \theta(0, \tau)}{\partial x} \quad (58)$$

Differentiating the solution for θ wrt x (equation (56)) and introducing it into (58) yields:

$$q = -k(T_M - T_0) \exp(-x^2/4\alpha t)/(\pi\alpha t)^{1/2} \quad (59)$$

The heat flux entering the rod is found by taking $x = 0$ and is

$$q_0 = -k(T_M - T_0)/(\pi\alpha t)^{1/2} \quad (60)$$

and the total heat flux entering in the time interval from $t = 0$ to $t = t$ becomes

$$Q_0 = \int_{t=0}^{t=t} q_0 dt = -2k(T_M - T_0) \cdot (t/\pi\alpha)^{1/2} \quad (61)$$

Anticipating $t = 0.2$ sec and the 3 mm droplet being exposed to an air/steam mixture $x_s = 0.5$. After 0.2 sec the droplet temperature is 38°C (used instead of T_M). Thus

$$\begin{aligned} q_0 &= 2 \cdot 16.6(38-20)(0.2/3.14 \cdot 4.12 \cdot 10^{-6})^{1/2} \\ &= 74285 \text{ [J/m}^2\text{]} \end{aligned}$$

or the amount of heat entering the rod is

$$Q_0 = q_0 \cdot A_R = 74285 \cdot 7.0685 \cdot 10^{-2} \cdot 10^{-6} = 5.25 \cdot 10^{-3} \text{ [J]}$$

The total heat flux entering the 3 mm droplet in the same time interval (taken from our predictions) is:

$$q_{D3} \approx 4 \cdot 10^4 \text{ [J/m}^2\text{]}$$

and the amount of heat entering the 3 mm droplet

$$Q_{D3} = q_{D3} \cdot A_{D3} = 4 \cdot 10^4 \cdot 28.27 \cdot 10^{-6} = 1.13 \text{ [J]}$$

Thus the amount of heat conducted through the rod is less than 0.5 percent of the total heat entering the droplet. In a similar manner it can be shown that the amount of heat conducted by the rod is less than 3 percent of the total heat entering the 1 mm droplet at the same conditions (0.2 sec and $x_s = 0.5$).

Keeping in mind all the simplifications introduced in this treatment, i.e.:

- i) the sudden change of the rod and temperature; in the experiments the rod end was "protected" by the droplet itself and its temperature can only change as the droplet temperature changes,
- ii) the physical properties of steel; in the experimental situation the needle is filled with water whose thermal conductivity is much lower than that of the steel,

one can safely presume that the heat conduction along the needle can be neglected.

5. EVALUATION AND DISCUSSION OF EXPERIMENTAL RESULTS

Since the droplet temperature was recorded continuously, it was possible to produce smooth experimental thermal utilization curves. Using the recorded experimental parameters (air/steam mixture temperature, velocity, droplet diameter and initial droplet temperature) the thermal utilization of a droplet experiencing these parameters could also be predicted by use of the various computer algorithms discussed above. The experimental and predicted responses could then be plotted together.

Before we proceed to the evaluation and the discussion of the experimental results the range of experimental variables will be specified. These are:

- droplet diameter: $d = 1.3$ to 4 [mm]
- air/steam mixture velocity: $v_R = 108$ to 691 cm/s
- steam concentration by volume: $x_S = 5$ to 66%
- water initial temperature: $T_{Wi} = 15.8$ to 22.5°C .

*mentioned ranges
verified*

There were 90 runs altogether which covered the above range of variations. For presentation purposes, only a few typical responses are selected and shown in Figures 23 to 27. However, all the experimental data have been considered in the following discussion and are tabulated in Table 1 of Appendix L.

It was pointed out in the paragraph 2.11 that the droplets would most likely experience some internal mixing and it was expected that the second model (internal resistance with periodic mixing)

would probably provide a good approximation to the real situation. This intuitive prediction agrees very well with the experiments as one can see from Figures 23 to 28.

Figure 23 represents the typical dimensionless temperature response θ for the run 3 (see Table I in Appendix L) and its comparison with all the three theoretical models:

- no internal resistance (solid line),
- internal resistance with periodic mixing (dashed line),
- internal resistance and no mixing (dashed line).

From this figure (a typical one) it is clear that the experimental results are represented the best by the second model. In all the calculations around 35 mixings were used.

To see the droplet diameter influence on the thermal utilization (keeping steam concentration constant ~ 6%) Figure 24 was drawn. The dashed lines represent the thermal utilization predictions using the second model (internal resistance with periodic mixings) while the points represent the experimental results. The agreement between predictions and the experiments is very good for all the curves, which show a significant influence of the droplet diameter on the droplet dimensionless temperature response.

A similar graph of the approximately 15% steam concentration data is shown in Figure 25. This figure shows the same trend as the previous one which is that the bigger the droplet diameter, the slower its temperature change.

Figure 23. Comparison of Experimental Results with Different Models

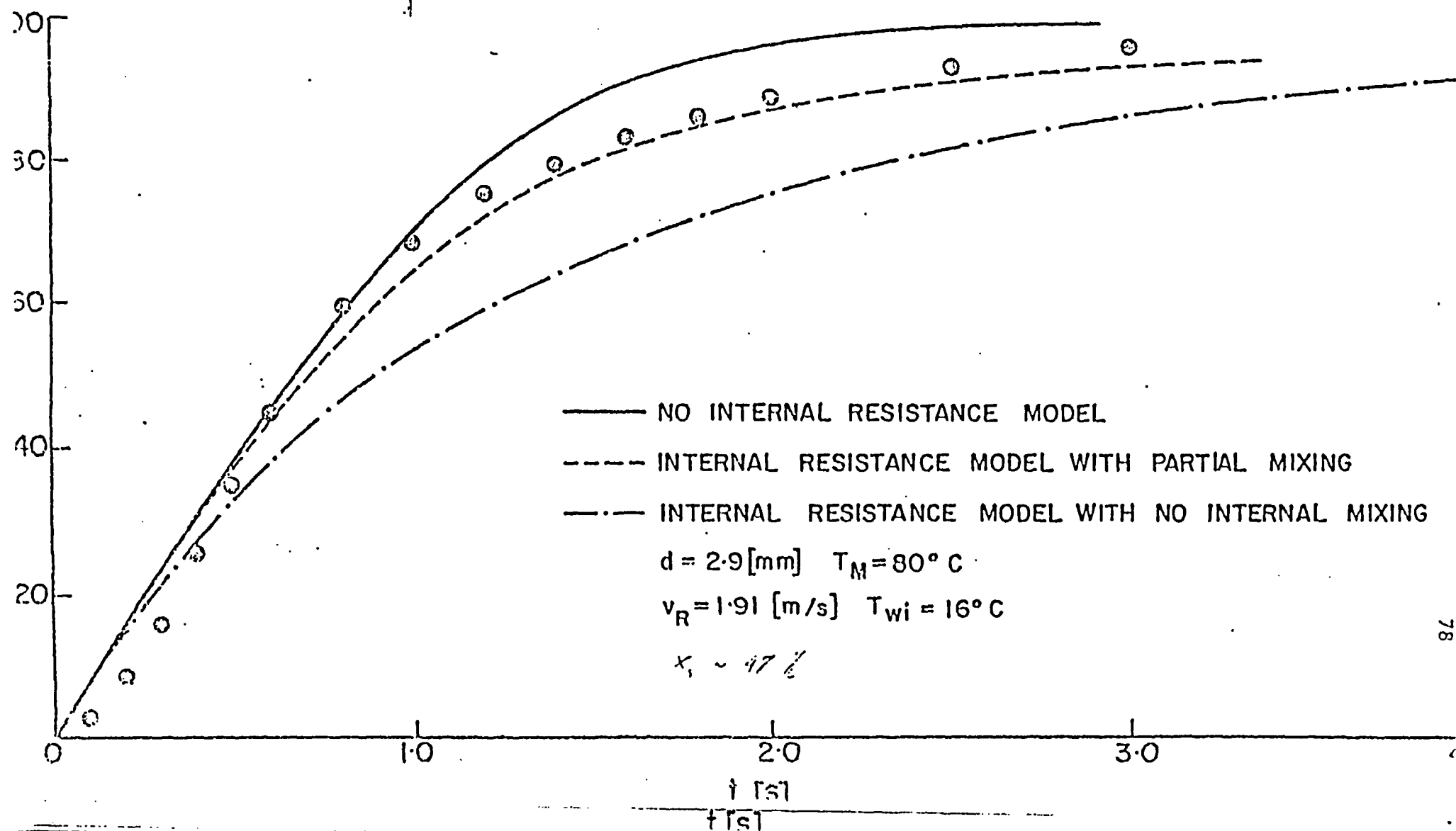


Figure 24. Comparison of Experimental Results with Predictions Using Internal Resistance Model with Partial Mixing for Different Droplet Sizes at $x_s \sim 6\%$

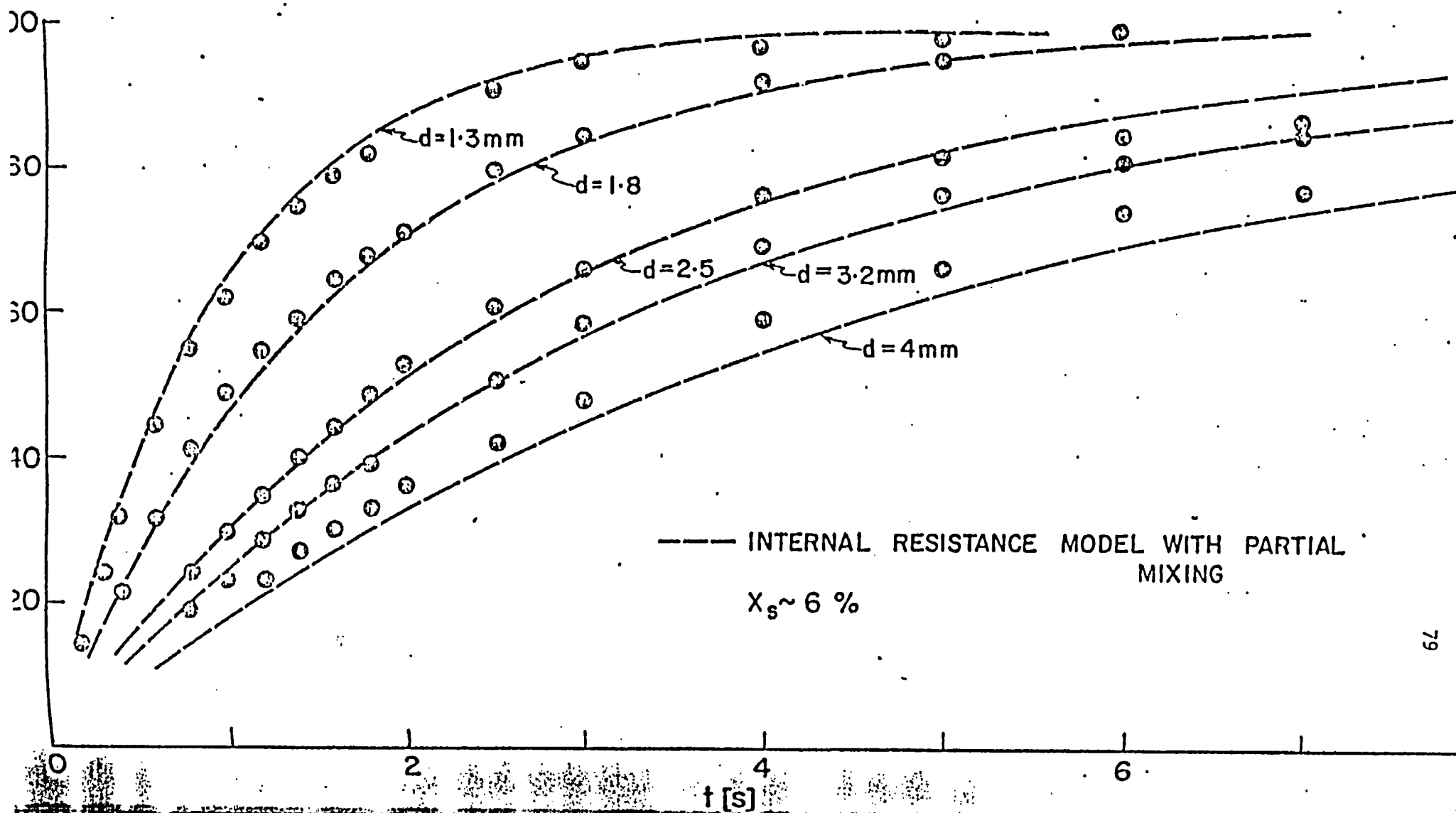
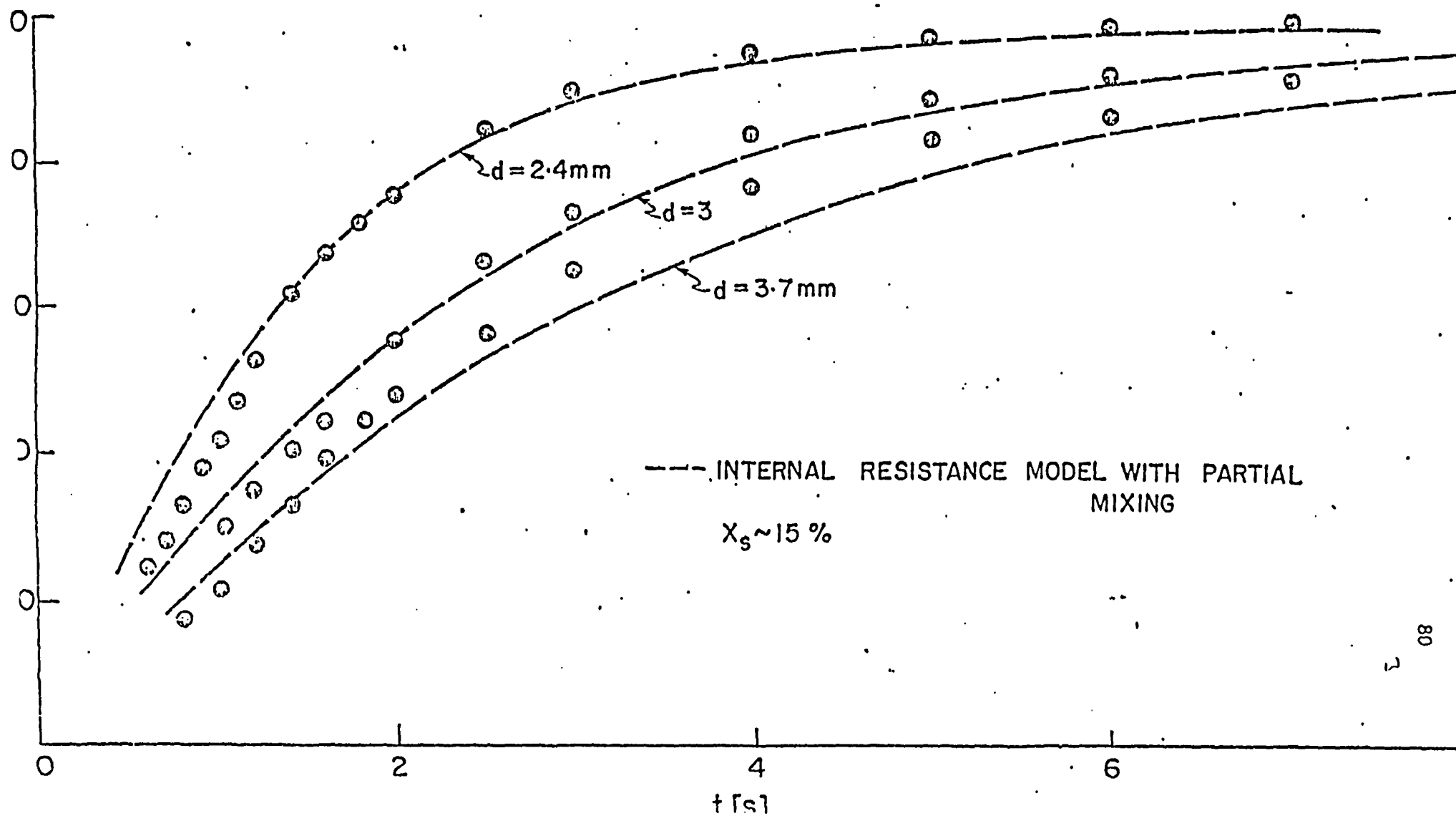


Figure 25. Comparison of Experimental Results with Predictions
Using Internal Resistance Model with Partial
Mixing for Different Droplet Sizes at $x_s \sim 15\%$



To show how the thermal utilization of the droplet is affected by the value of the steam concentration in an air/steam mixture, Figure 26 is plotted. In this figure the thermal utilization vs. time for the 2.5 mm droplet diameter for different steam concentrations (varying from 65% to 5%) is shown. Again the agreement between the experiment and the second model predictions is very good confirming the fact that the higher the steam concentration is the "faster" the droplet temperature response.

The influence of the mixture velocity on the droplet temperature response (droplet diameter ~ 2.8 [mm] and steam concentration ~ 35% by volume) is shown in Figure 27. Once more the agreement between the predictions and the experiments is very good, showing that the relative velocity is very important factor, i.e. the higher the relative velocity the faster the droplet temperature change.

The agreement of the rest of the experimental runs (see Table I in Appendix L) with the predictions is good in the whole range of the variables.

To obtain a measurement of the spread of the experimental data and the accuracy of the predictions, two values of the thermal utilization, 50% and 75% were chosen (on the theoretical curves) and the difference between the experimental values of thermal utilization θ_E and the chosen predicted ones θ_P are shown in Figure 28 plotted against the time taken to reach θ_P . From this figure it

Figure 26. Comparison of Experimental Results with Predictions
Using Internal Resistance Model with Partial Mixing
for Different Steam Concentrations $d \sim 2.5$ mm

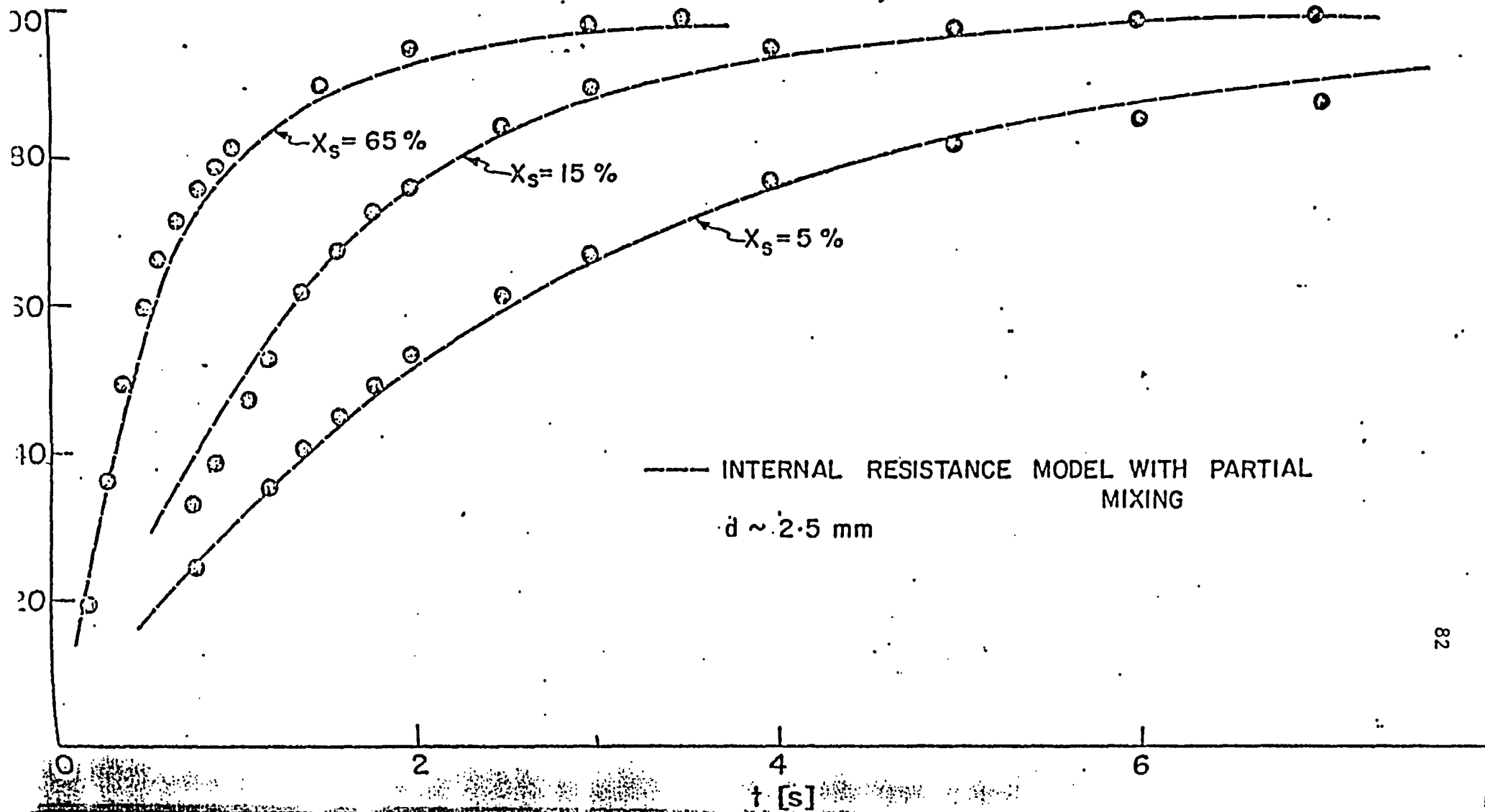
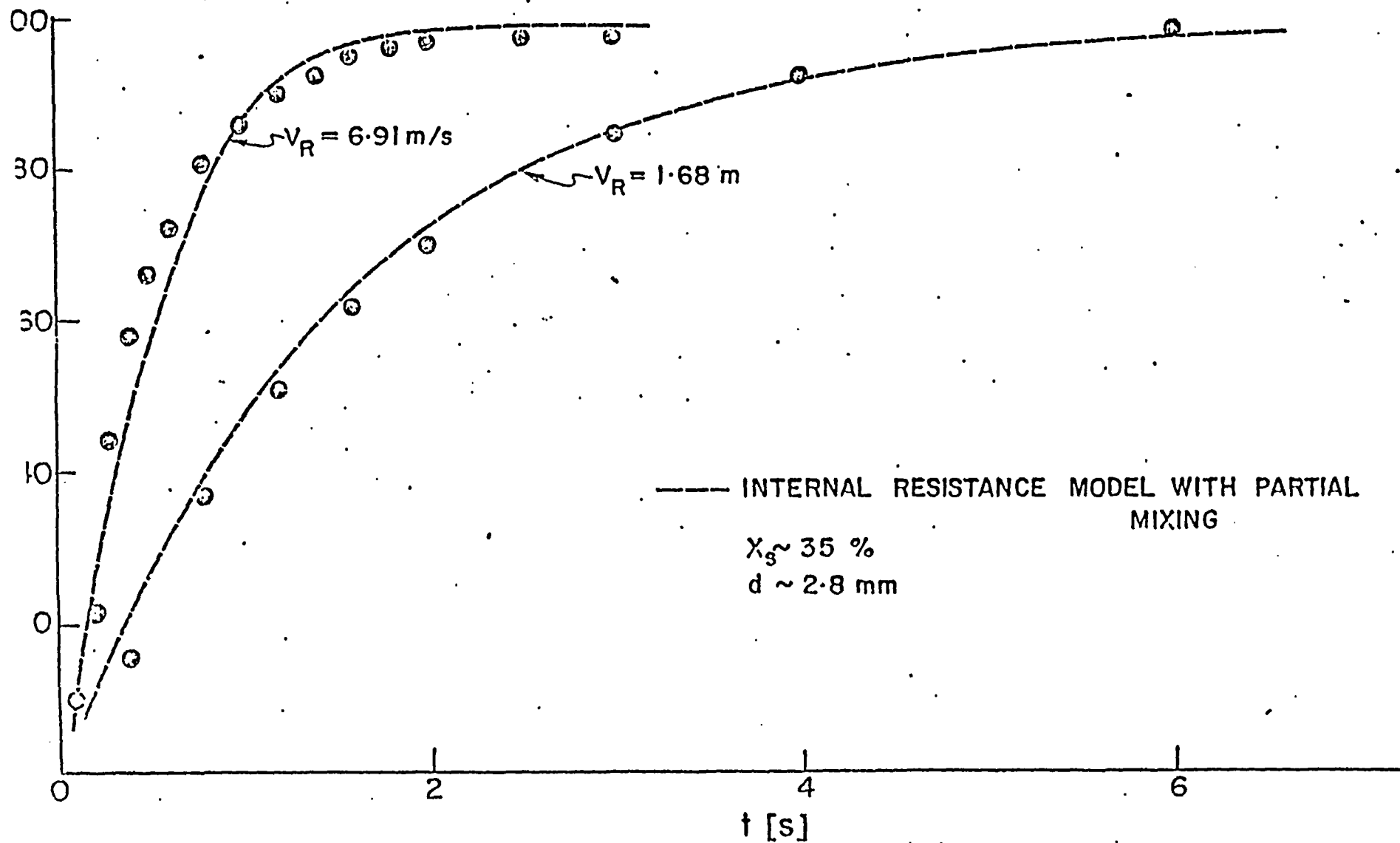


Figure 27. Comparison of Experimental Results with Predictions Using Internal Resistance Model with Partial Mixing for Different Velocities of the Air/Steam Mixture and $d \sim 2.8 \text{ mm}$ and $x_s \sim 35\%$



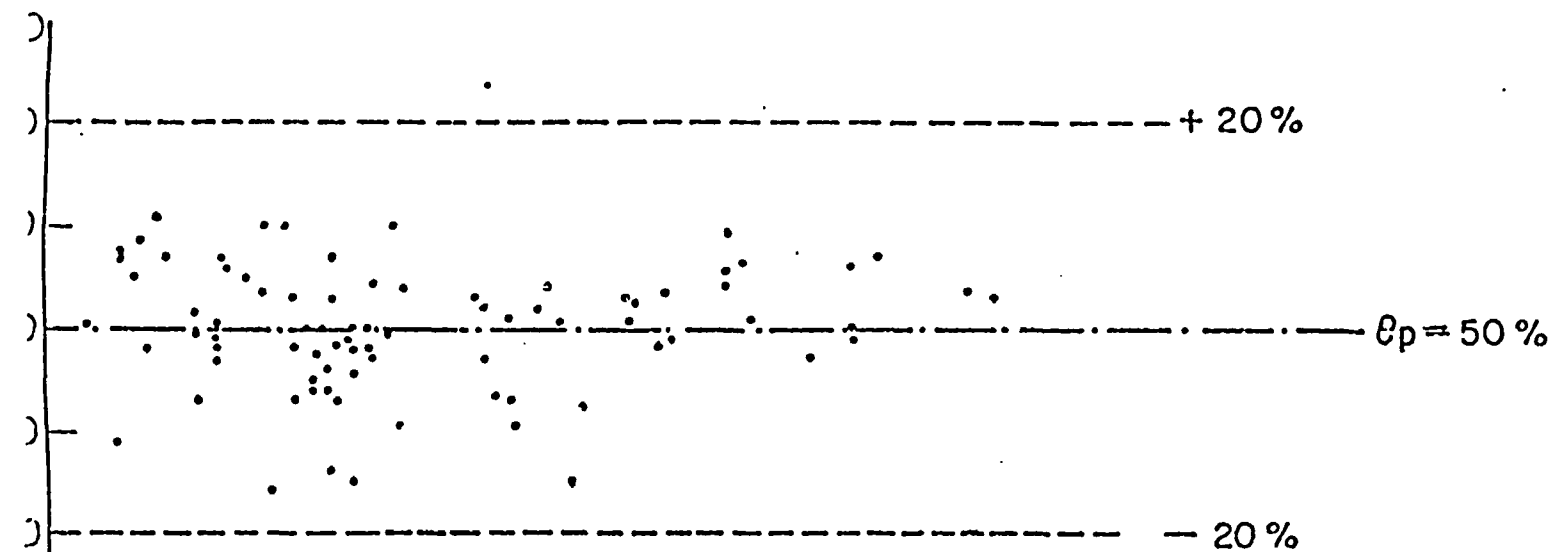
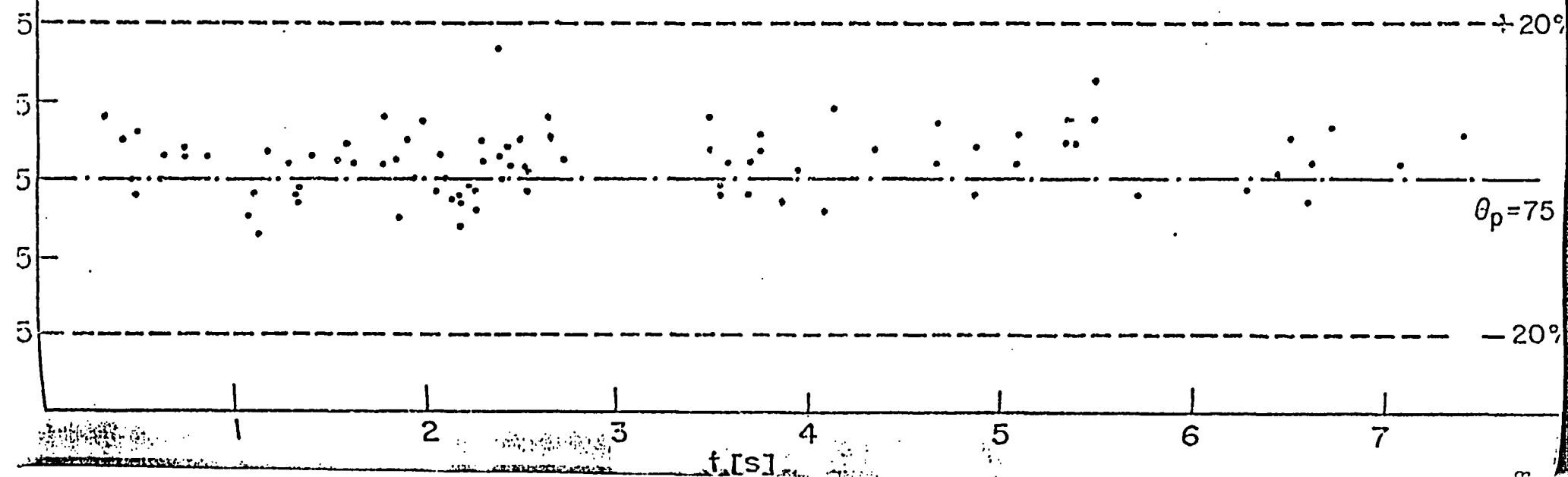


Figure 28. Comparison of Predicted Values of Thermal Utilization ($\theta_p = 50\%$ and $\theta_p = 75\%$) with Experimental Results



can be seen that the maximum difference between the predictions and experiments is enclosed by the $\pm 20\%$ thermal utilization lines for both the values of the thermal utilization (50% and 75%). A simple statistical analysis of these data gave a value for the standard deviation of about 5% for both chosen values of the thermal utilization.

To find out if the theoretical values of the thermal utilizations (50% and 75% chosen) differ significantly from the experimental average values $\bar{\theta}_{50}$ and $\bar{\theta}_{75}$ a simple student's t-test was performed [105]. From Table I (Appendix L) the average values of $\bar{\theta}_{50}$ and $\bar{\theta}_{75}$ are calculated as:

$$\bar{\theta}_{50} = 49.927 \quad \text{and} \quad \bar{\theta}_{75} = 76.716$$

The point estimates of the corresponding standard deviations are:

$$s_{50} = 6.0609 \quad \text{and} \quad s_{75} = 3.968$$

When s is known t is then calculated from the formula

$$t_{50} = \frac{\theta_{50} - \bar{\theta}_{50}}{s/\sqrt{n}} = \frac{50 - 49.927}{6.0609/\sqrt{90}} = 0.114$$

and

$$t_{90} = \frac{\bar{\theta}_{75} - \theta_{75}}{s/\sqrt{n}} = \frac{76.716 - 75}{3.96845/\sqrt{90}} = 4.102$$

The value of t thus obtained is compared to the tabulated value for t_a at the required confidence level (95% chosen) with $n = 90$ degrees

of freedom. Thus:

$$t_a (.95, 90) = 1.99$$

The experimental value of the thermal utilization $\bar{\epsilon}_{50}$ is therefore not different from the predictions since

$$t_{50} = 0.114 < t_a = 1.99$$

however the $\bar{\theta}_{75}$ value is significantly different from the predicted one, since

$$t_{75} = 4.102 > t_a = 1.99$$


This simple statistical analysis implies that there is some bias in our predictions. It is felt that this bias lies in the number of mixings used in the calculations of the predicted values of the thermal utilization θ_p . The value 35 was used in all the calculations in spite of the fact that the bigger droplets would probably experience higher numbers of mixings. A trend of this kind could be observed when comparing the experimental results and the predictions. In Figure 24 the experimental results tend towards the no internal resistance model (infinite number of mixings) as the droplet diameter increases. This has been noticed in most of the other runs which can be seen from Figure 28, where the bigger droplets are represented by longer response times and more of the experimental values tend to be higher than the predicted ones, implying that they

are "more" mixed. From Figure 13 one can see that the higher number of mixings (~ 100 compared to ~ 40) gives bigger differences for higher values of thermal utilization. Thus, using the greater number of mixings for the bigger droplets the difference between experimental results and predictions would decrease and the "cause" of the bias in the predictions would disappear. However, it is not possible to say what number of circulations or mixings should be used for any particular case. In any case our findings are in agreement with Harriot [106] who has found that the velocity of circulation increases with the diameter of the droplet.

To conclude this section it can be said in general that the experimental results agree closely with the second model predictions over the whole range of the experiments. The predicted influence of all the important parameters (steam concentration, droplet diameter, air/steam mixture velocity) are confirmed experimentally.

6. CONCLUSIONS AND RECOMMENDATIONS OF PART I

From the material presented so far the following conclusions can be drawn:

- i) The model with internal thermal resistance in a droplet and internal mixing (sometimes referred to as "partial internal mixing" or "second model") describes very well the effects of combined momentum heat and mass transfer to a single droplet since in a large majority of the experimental results correspond closely to the predictions of this model.
- ii) The predicted effects of all the parameters in the theoretical part of this study were confirmed experimentally:
An increase of the droplet diameter (see Figure 24) increases the response time.
The higher the concentration, the faster the droplet temperature response (Figure 25).
The higher the relative droplet velocity, the faster the droplet temperature response (Figure 26).
- iii)  Bigger droplets are experiencing more circulation (see Figures 24 and 28).
- iv) The results tend to confirm that it is correct to calculate the external (equation (49)) and internal (equation (50)) heat transfer coefficients by use of heat and mass transfer analogy, and Hughmark's [48] or Ranz and Marshall's [46] correlations for Nusselt and Sherwood numbers (see Figure 18)

give practically the same excellent results over the whole range of the experimental Reynolds numbers (100 to 1200).

- v) The resistance to heat transfer in this situation may occur significantly in both phases. The internal resistance of the droplet is most significant for fast moving large droplets in concentrated steam-air mixtures. The external heat transfer resistance is most significant for small, slow moving droplets in dilute mixtures.
- vi) The unsteady state temperature response calculations done by use of the quasi-steady state approach work out satisfactorily.
- vii) The analogy method of calculation may be extrapolated to the pure steam situation and predicts the "pure" steam heat transfer coefficients reasonably well (see Figure 18 and discussion of Chapter 3).

Some possible suggestions and recommendations for future work are:

- i) To extend the range of experiments to the higher steam concentrations, since very few runs were done in this range due to excessive condensation on the cold surfaces of the droplet producing unit. For this purpose the unit should be redesigned.
- ii) To modify the existing theoretical approach for the case of non-saturated air/steam mixtures when the droplet tends to reach the wet bulb mixture temperature rather than the dry bulb one.

- iii) The apparatus could be used to study simultaneous heat and mass transfer inside the droplet by using different mixtures for the surrounding medium.
- iv) Instead of the mass transfer towards the droplet the opposite process could be studied, i.e. droplet evaporation. The results of such work would be widely applicable to many operations such as drying, air-conditioning, etc.

PART II

SIMULATION OF THE SPRAY SYSTEM AND DESIGN

SYNTHESIS OF A DOUSING CHAMBER

7. INTRODUCTION

We are now in a position to attempt to solve a more complex and realistic problem involving the combined momentum, heat and mass transfer in an experimental pilot plant, which was set up to provide a basis for the real dousing chamber design. The problem of the full size dousing chambers (see Figure 3) is even more complex due to the existence of the chamber internals and the fact that the air/steam mixture enters the building tangentially. There will be no attempts in this study regarding the possible simulation of the real dousing chamber.

The experimental pilot plant was designed by AECL and the experimental results from this plant were provided by that company [107]. The droplet size distribution measurements reported below were initiated as a result of the findings of the first part of this work. The experiments were carried out at AECL and the results obtained so far were analysed at Waterloo. The drop size distribution measurements are still in progress as an essential part of the general research project. For more details see K. McLean [108] who is continuing this part of the work.

The second part of this thesis is thus only concerned with the problem of the steam dousing simulation of the pilot plant. Chapter 8 will deal with the experimental part of the problem, while Chapter 9 will treat the theoretical approach to this problem. Chapter 10 will deal with the problem solution technique and the

corresponding numerical algorithm outline. Chapter 11 is devoted to the experimental results and their comparison with the theoretical predictions while Chapter 12 deals with the conclusions and possible suggestions and recommendations.

8. EXPERIMENTAL

The following two paragraphs will be devoted to short reviews of the pilot plant and droplet size distribution experiments. More details can be found in [107] and [108].

8.1 Dousing Chamber Tests

Figure 29 shows a schematic representation of the pilot plant experimental apparatus (as reported in [107]). Essentially, the plant consisted of a large vessel (56 [m³] and 5 [m] high) pump and motor unit and hot water header. The latter was used to provide live steam to the dousing chamber at a specified total pressure in the vessel. The pump and motor unit was used to provide the prescribed flow rate (and pressure drop) across the spray nozzles. The experiments were performed with one and subsequently with five swirl nozzles type TF48FC, produced by BETE FOG NOZZLES, INC., Greenfield, Massachusetts.

The experimental procedure was as follows:

- i) The vessel was filled with air and its pressure recorded.
- ii) The steam was introduced into the vessel from the hot-water header until a desired total pressure was reached.
- iii) The pump was switched on and the water flow rate and temperature were recorded.
- iv) The change of total pressure in the vessel (due to the steam condensation) was recorded as a function of time.

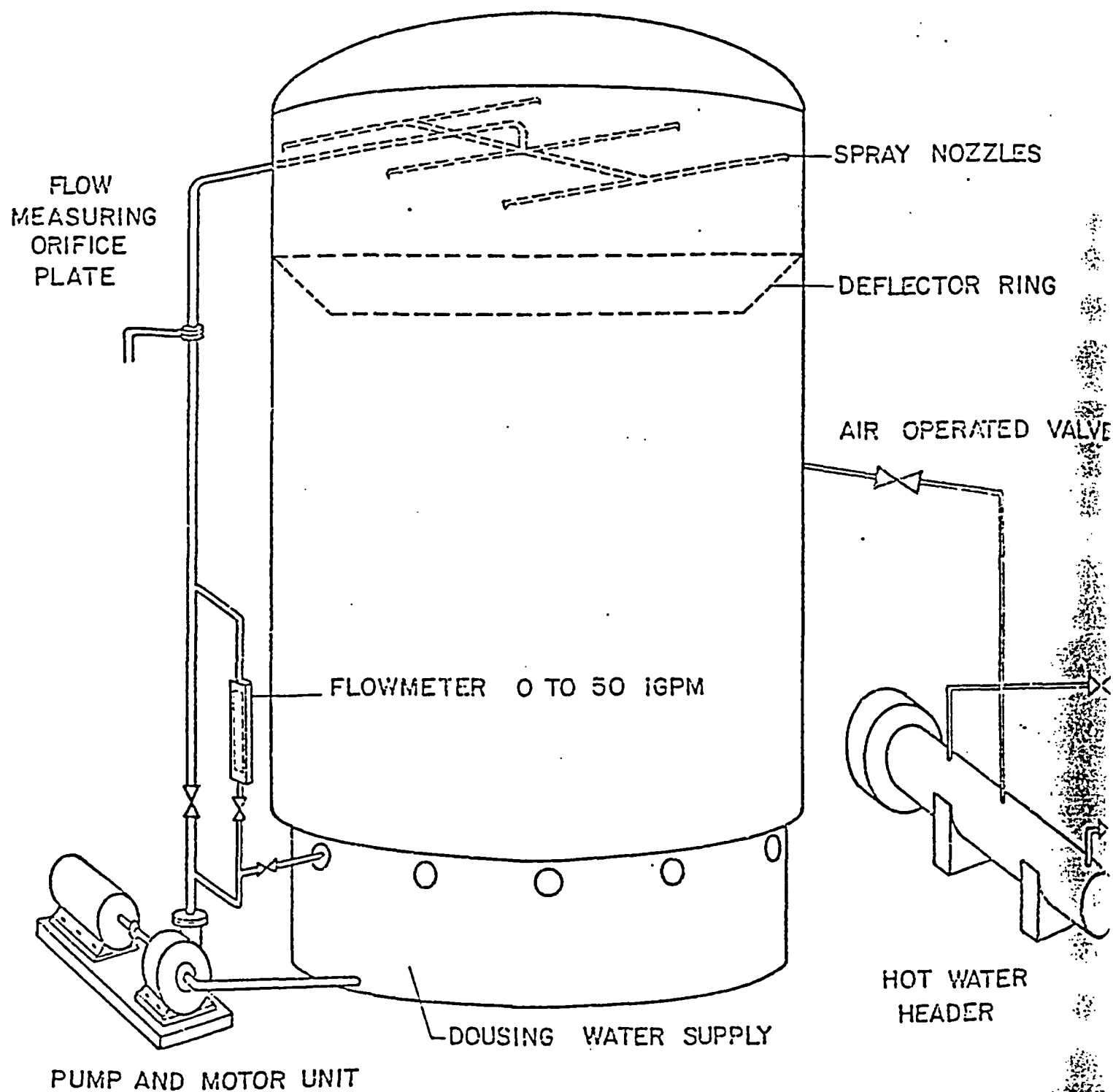


Figure 29. Pilot Plant Test Facility

Using this technique curves 1A to 3E (solid lines) shown in Figures 39, 40 and 41 were obtained. To provide an estimate of the heat losses from the vessel to the surrounding medium curve 1 (obtained with no water flow) in Figure 39 was recorded. In this case the condensation and the vessel pressure change was caused just by the cooling effect of the vessel, since the water pump and thus the nozzles were not used.

The flow rates of water with a single nozzle were 45 IGPM and for the five nozzles case it was five times greater, i.e. 225 IGPM.

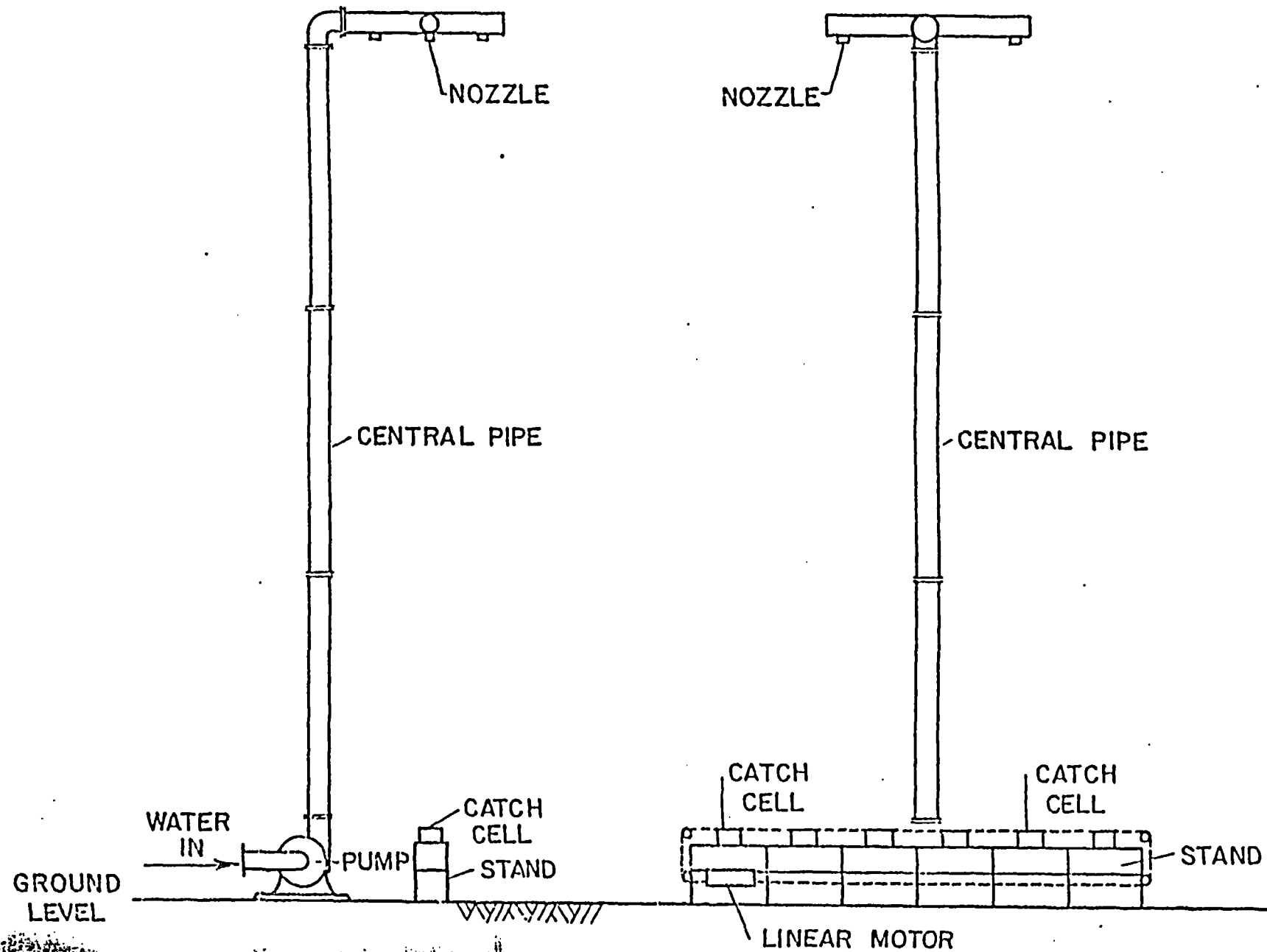
8.2 Droplet Size Distribution Measurements

The experiments on the droplet size distribution of the particular nozzles used in the pilot plant tests are just a small part of an extensive study of droplet size distributions of the different spray producing equipment used by AECL such as spray plates and different spray nozzles.

The experimental apparatus (see Figure 30) consists of a central adjustable height tower 45 feet high. In this manner it is possible to measure the droplet size distribution at different heights. On the top of the central water supply pipe is a flange to connect the cross arrangement with the outlets for the nozzles. There is a pump to provide the necessary water flow rates and the pressure drop across the nozzles.

Preliminary review of drop size measurement techniques showed that the "catch in oil" technique, used by Brown [91],

Figure 30. Experimental Apparatus for Droplet Size Distribution Measurement



Syhre [109], Kushnyrev [110] and Gelperin [111], had been found to be satisfactory and simple to deal with. After several oils for the cells were tried it was found that castor oil had the best characteristics for the intended purpose of catching the drops. High speed movies showed there was very little splashing when the droplets fell into the oil and the droplets were retained just at the interface and after a short time period would start to move slowly to the bottom of the shuttered catching box. This time period was long enough for shadow photographs of the drops to be taken. A special stand was designed for the purpose of mounting the catch cells [108]. On top of the stand could be mounted up to eight catch cells made of acrylic plates. Below each box was a special water and light proof compartment where the photographic plates (8" x 10") were placed. The tops of the cells could be exposed with sliding plates connected to a linear motor. These sliding plates were provided with slits which when slid over the box, exposed the oil to the spray for a while. Hence the following simple experimental procedure was as follows:

- i) The stand was placed in position beneath the spray and the boxes were loaded with the photographic plates and the castor oil layer.
- ii) The spray was formed by switching on the pump.
- iii) The linear motor was started moving the covering plates and opening the boxes for a while and allowing the droplets to

hit the oil and be suspended just beneath its surface.

- iv) The specially designed light source was placed over the boxes. This was essentially a long metal duct (8 feet) fitting over the box. The duct had an electronic flash built into the top.
- v) The flash was switched on exposing the plates to give a real size shadow (black and white) image of the droplets on the plates.

The catch in cell technique worked quite satisfactorily in the range of flow rates (30 to 50 IGPM) with the BETE nozzle placed 15 ft above the catch cells as the water distributor. However, when the dousing plates were used very large droplets were formed and the splashing and the back splashing was so intensive that the reliability of the technique was questionable. To avoid this problem a direct photography technique is being developed [108] to produce an image of the moving droplets in air. In preliminary experiments, this technique has been tried out simultaneously with "the catch in cell" technique. The development of this technique is still in progress and certain refinements such as a decrease of the depth of the photographed droplet layer, light source distance, better image of smaller droplets, etc., will be necessary before it can be judged reliable. In spite of the necessity for the further improvements of this technique it is felt that the comparison of the results obtained by both methods is useful, even at this stage of the development. This will be pursued in paragraph 11.2.

9. THEORETICAL ANALYSIS

9.1 Problem Definition and Simplifying Assumptions

It was decided that the experimental pilot plant vessel could be represented by a chamber containing an air/steam mixture as shown in Figure 31. Thus the state of the air/steam mixture in the vessel is specified by its pressure P_M , temperature T_M and the chamber's volume V_M . The parameters of the entering water are specified by its flow rate $m_{W,E}$ and its temperature $T_{W,E}$. Similarly the parameters of the leaving water are $m_{W,L}$ and $T_{W,L}$.

The problem can be stated briefly as follows: It is necessary to predict the pressure in the chamber as a function of time when the initial conditions of the air/steam mixture are known as well as the conditions of the entering and leaving dousing water. To enable this, certain simplifying assumptions are necessary. These assumptions are:

1. The air/steam mixture in the vessel is perfectly mixed and always saturated with steam.
2. The air/steam mixture velocity in the vessel is zero during the dousing process.
3. The thermodynamic properties of the mixture components are determined from the ideal gas law since the total pressure in the experiments was $P_M \leq 2$ Bar. (Steam is saturated vapor)
4. The spray immediately upon injection into the chamber breaks up into droplets of known size distribution whose defining parameters are specified in advance.

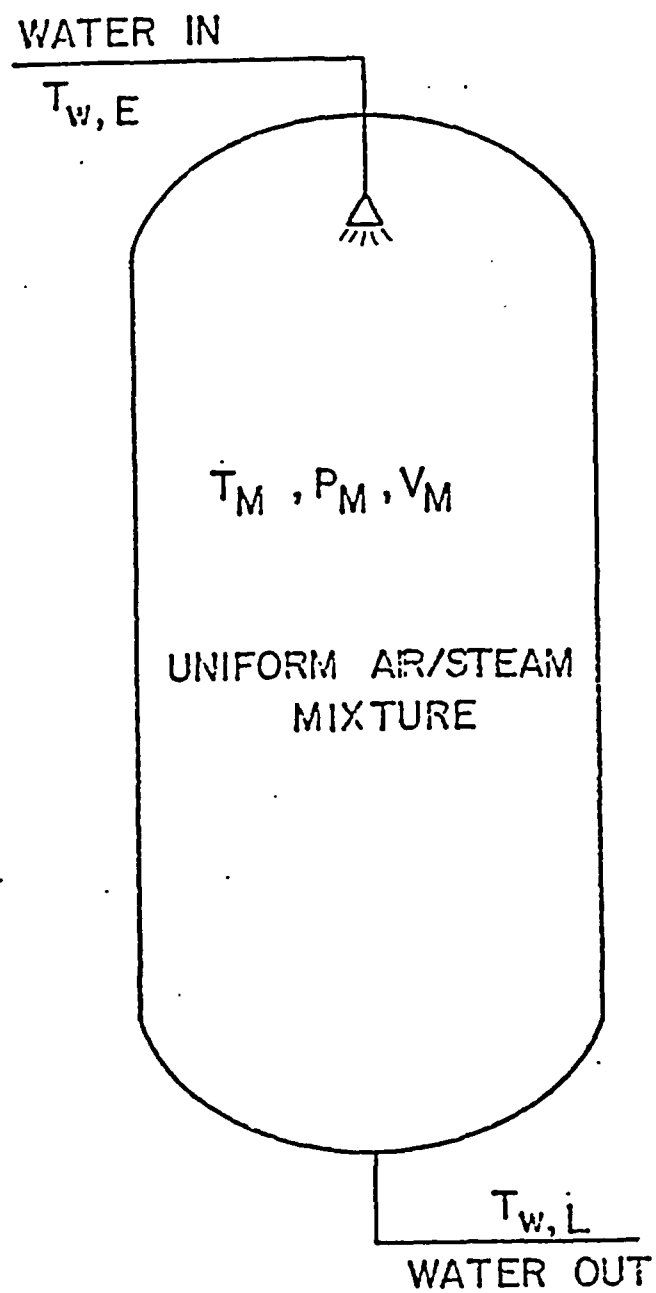


Figure 31. Pilot Plant Dousing Chamber Model

5. The increase in a droplet diameter due to condensation was neglected, since its increase is less than 5% as found in Part I of this study.
6. Each droplet maintains its identity in the vessels, implying there is no:
 - i) shattering, whatever the cause may be (e.g., a) the distribution of aerodynamic pressures, see Hinze [112]; b) waves and oscillations, see Levich and Krylov (in [113], p. 299); c) turbulence, see Hinze [112] and Brodkey [114]).
 - ii) colliding which can cause: a) coalescence; b) separation and c) disintegration.
7. The void fraction of the system is very close to unity, and the amount of the droplet interaction can be neglected, thus each droplet is treated as a single one in an infinite medium for the purpose of its transport coefficient evaluations. The problem of interacting droplets is discussed by Yaron and Gal-or [115].
8. The dousing water supply source has constant temperature.
9. The flow rate of dousing water into the chamber remains constant.
10. The volume of water on the chamber floor is negligible as compared to the volume of the vessel.
11. The pressure drop due to condensation of steam on the walls and obstructions of the chamber can be modelled from an experimental test (curve 1 in Figure 39 where tank pressure versus time was obtained without the use of a dousing spray). This effect can thus be incorporated into the model in the form of heat losses to the surroundings.

9.2 Basis of the Simulation

Consider the dousing system shown in Figure 30, consisting of a vessel filled with an air/steam mixture of known pressure, P_M , temperature, T_M , and the steam volume fraction X_{SM} corresponding to a saturation temperature T_M . The total pressure of the system will change due to the condensation of steam on the injected water droplets. The rate of pressure change in the vessel will depend on many factors governing the rates of heat and mass transfer from the gas phase to the liquid phase. For example, the local size, temperature and velocity distributions of droplets, the temperature and air concentration in the gas phase are all factors influencing the vessel pressure change.

In order to utilize the information developed in Part I for a single droplet, to solve this complex dousing problem the following approach is adopted. A known initial droplet size distribution is discretized into M droplet diameters and the height of the chamber is divided into N increments. Applying the energy conservation law (for a time interval $\Delta t = t_2 - t_1$) we can say that the water energy change (increase) ΔE_W is equal to the air/steam mixture energy change (decrease) ΔE_M . Allowing for energy losses to the surrounding Q_{LS} , we can write

$$\Delta E_M = \Delta E_W + Q_{LS} \Big|_{t_1}^{t_2} \quad (62)$$

If the internal energy of the mixture in the chamber at the time $t = t_1$ is

$$u_{M1} = c_{v1} T_1, \text{ kJ/kg} \quad (63)$$

and at the time $t = t_2$

$$u_{M2} = c_{v2} T_2, \text{ kJ/kg} \quad (64)$$

then the energy change of the air/steam mixture can be written as

$$\Delta E_M = m_{M1} u_{M1} - m_{M2} u_{M2} \quad (65)$$

The energy of all the water droplets in the chamber at the time $t = t_1$ is

$$E_{M1} = \sum_{i=1}^{i=M} \sum_{j=1}^{j=N} m_{W_{i,j}} h_{W_{i,j}} \Big|_{t_1} \quad (66)$$

and at the time $t = t_2$

$$E_{M2} = \sum_{i=1}^{i=M} \sum_{j=1}^{j=N} m_{W_{i,j}} h_{W_{i,j}} \Big|_{t_2} \quad (67)$$

where, the corresponding enthalpies are

$$h_{W_{i,j}} = c_{p_{i,j}} T_{i,j} \quad (68)$$

Now, the energy of the droplets entering the system during the time

increment is

$$E_{WE} = \sum_{i=1}^M m_{WE,i,1} h_{W,i,1} \Big|_{t_1}^{t_2} \quad (69)$$

and similarly the energy of water leaving the dousing system

$$E_{WL} = \sum_{i=1}^M m_{WE,i,N} h_{W,i,N} \Big|_{t_1}^{t_2} \quad (70)$$

Thus the energy change of water phase due to heat pick-up from the air/steam mixture is

$$\Delta E_W = E_{W2} - E_{W1} + E_{WL} - E_{WE} \quad (71)$$

In the last equation the effects of kinetic energy, potential energy and work are neglected.

Hence, combining equations (62), (65) and (71) yields

$$m_{M1} u_{M1} - m_{M2} u_{M2} = E_{W2} - E_{W1} + E_{WL} - E_{WE} + Q_{LS} \Big|_1^2 \quad (72)$$

or written in the same form as presented in [116]

$$\begin{array}{ccccccc} m_{M1} u_{M1} & + & E_{W1} & + & E_{WE} & = & m_{M2} u_{M2} + E_{W2} + E_{WL} + Q_{LS} \Big|_1^2 \\ \textcircled{1} & & \textcircled{2} & & \textcircled{3} & & \textcircled{4} \quad \textcircled{5} \quad \textcircled{6} \quad \textcircled{7} \end{array} \quad (72a)$$

Equations (72) or (72a) which basically represent a statement of the first law of thermodynamics for the dousing system can be used to determine state 2 of the air/steam mixture in the chamber a short

period of time (0.5 sec say) after starting from the specified state 1.

However, before we proceed to the description of the numerical algorithm itself it is necessary to detail how each term in these equations, (72) or (72a), can be determined.

Term ① represents the internal energy of the air/steam mixture and it is easily determined using equation (63) since the initial state of the air/steam mixture is specified.

Terms ② and ⑤ represent the energy of all the droplets in the chamber at the beginning (specified) and at the end of the time increment, respectively. When the droplet size distribution is specified (paragraph 9.3) and discretized the equation of motion solution (paragraph 9.4) enables us to determine the number of droplets in each height increment at the end of each increment. Finally, the temperatures of droplets (paragraph 9.5) combined with their numbers in each height increment allow us the determination of the energy of all the droplets in the chamber at the end of each time increment.

Term ③ is easily determined from the specified flow rate and the temperature of the entering water.

The energy of water leaving the chamber represented by term ⑥ is determined by summing the energies of the droplets which left the last height increment ($N = 100$) during the time interval.

The dousing chamber heat losses (term ⑦) are determined from the experimental data on heat losses (paragraph 9.6).

Thus in effect the only unknown term in equation (72a) is ④ representing the total energy of the air/steam mixture in the chamber at the end of the time increment. This term is determined from equation (72a) by a trial and error procedure. For more details see Chapter 10 which describes the calculation algorithm.

9.3 Droplet Size Distribution

To determine the total mass of any droplet size at any height increment in the system it is necessary to prescribe the initial droplet size distribution. Because none of the equations for droplet size distribution are derived on the basis of a physical model of atomization the choice of which relation to use rests on its ability to represent the experimental data. A recent study [117], in that regard, showed that the upper limit function, proposed by Mugele and Evans [118], and chi-square distribution give good approximations for drop size distributions. It can be shown that the other models [117] such as Nukiyama and Tanasawa, Rosin-Ramler, the log-probability function, which are often used to represent the experimental data on droplet size distributions, are in fact special cases of χ -square and upper-limit distributions. Since the last two distribution models are the most general, the other models have not been considered. The upper-limit function has been finally selected on the following grounds:

- i) a preliminary drop size analysis showed that for the nozzles used in the experimental tests [107] this function correlated local drop size distribution reasonably well;

- ii) it is relatively simple to determine the defining parameters, see Mugele and Evans [118];
- iii) it is the only drop size distribution allowing for a maximum droplet size.

The upper-limit normalized volumetric drop size distribution function is expressed as

$$\frac{dv}{dx} = \frac{\delta}{\pi^{1/2}} \frac{x_m}{(x_m - x)x} \exp \left[-\delta^2 \left(\ln \frac{bx}{x_m - x} \right)^2 \right] \quad (73)$$

where: b , δ and x_m , being the maximum droplet diameter, are distribution defining parameters,

dv - is the normalized volume of droplets with diameters between $x - \frac{dx}{2}$ and $x + \frac{dx}{2}$.

A normalized upper limit number distribution function could also be used to represent the experimental spray data, however the number distribution function gave worse approximations to the same data as shown in [117], and therefore only the normalized upper limit volume distribution function was used in the evaluation of our experimental data.

9.4 Equation of Motion Solution

Now when the droplet size distribution function is specified the problem of the droplet size distributions throughout the chamber can be solved by using the momentum equation for droplets.

The specified droplet size distribution is discretized into M droplet

diameters, the mass and the number of droplets of i -th diameter ($i = 1, \dots, M$) can be determined. By solving the equation of motion for every droplet diameter it is possible to determine the number of all droplets in the j -th ($j = 1, \dots, N$) height increment in the vessel. In this manner the water droplet distribution throughout the chamber is specified in each time increment. The equation of motion for droplets is solved numerically using the fourth order Runge-Kutta technique [36] and Reinhart's [33] correlations for droplet drag coefficients.

The results of these computations are shown in Figures 32 to 34. Figure 32 represents the droplet velocity distribution at different positions in a chamber, for a spray injected with the initial velocity 10 m/s in an air/steam system at $P_M = 2.23$ Bar, $P_{SM} = 0.95$ Bar and $T_M = 98.25^\circ\text{C}$ (initial state in experiments 1A). Figure 33 shows the fall times of different diameter droplets necessary to reach a specific position in a chamber for the same spray as in Figure 32. Figure 34 represents the position of different diameter droplets (the same spray as in previous two figures) in a chamber for different times starting from time zero. From this figure it can be seen that all the droplets bigger than 1.2 [mm] reach the bottom of the chamber after only 1 [sec], while the 0.5 [mm] droplet does not reach the chamber bottom until 2.5 [sec] have elapsed. Thus the smaller droplets have a better chance of being fully utilized than the larger droplets.

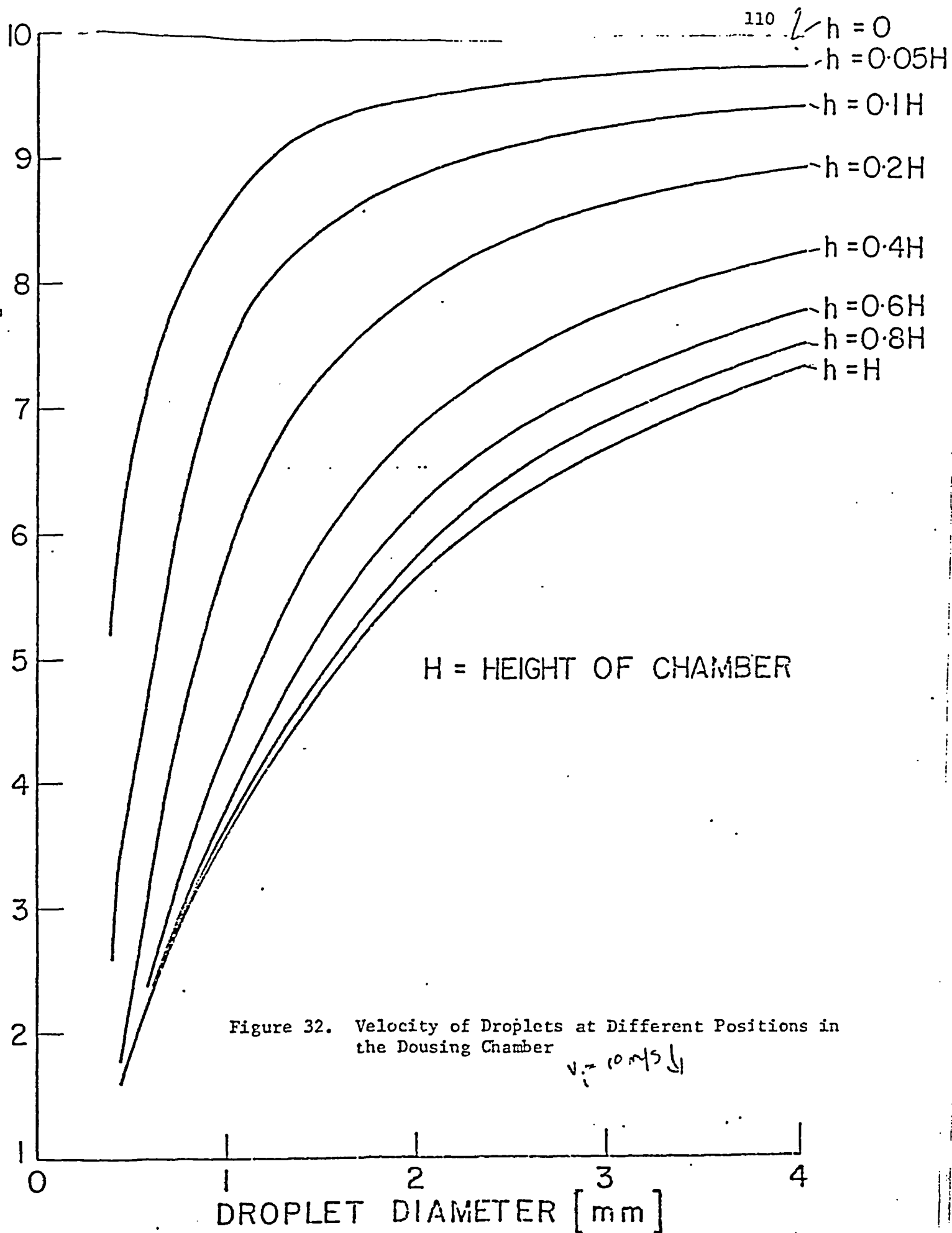


Figure 33. Times Taken by Different Droplets to Reach a Certain Position in the Chamber

$H = \text{HEIGHT OF A CHAMBER}$

$v_i = 10 \text{ m/sec} \downarrow$

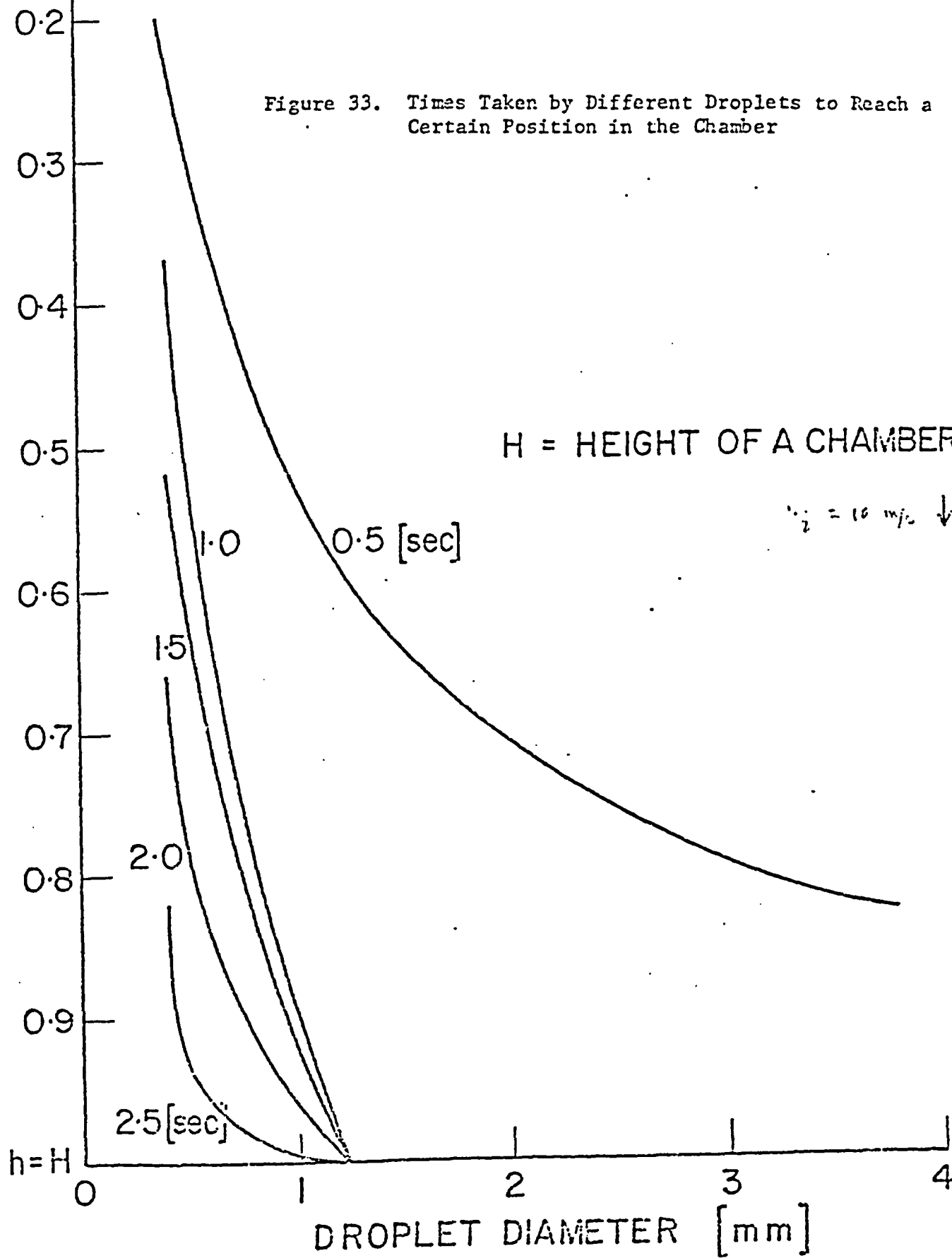
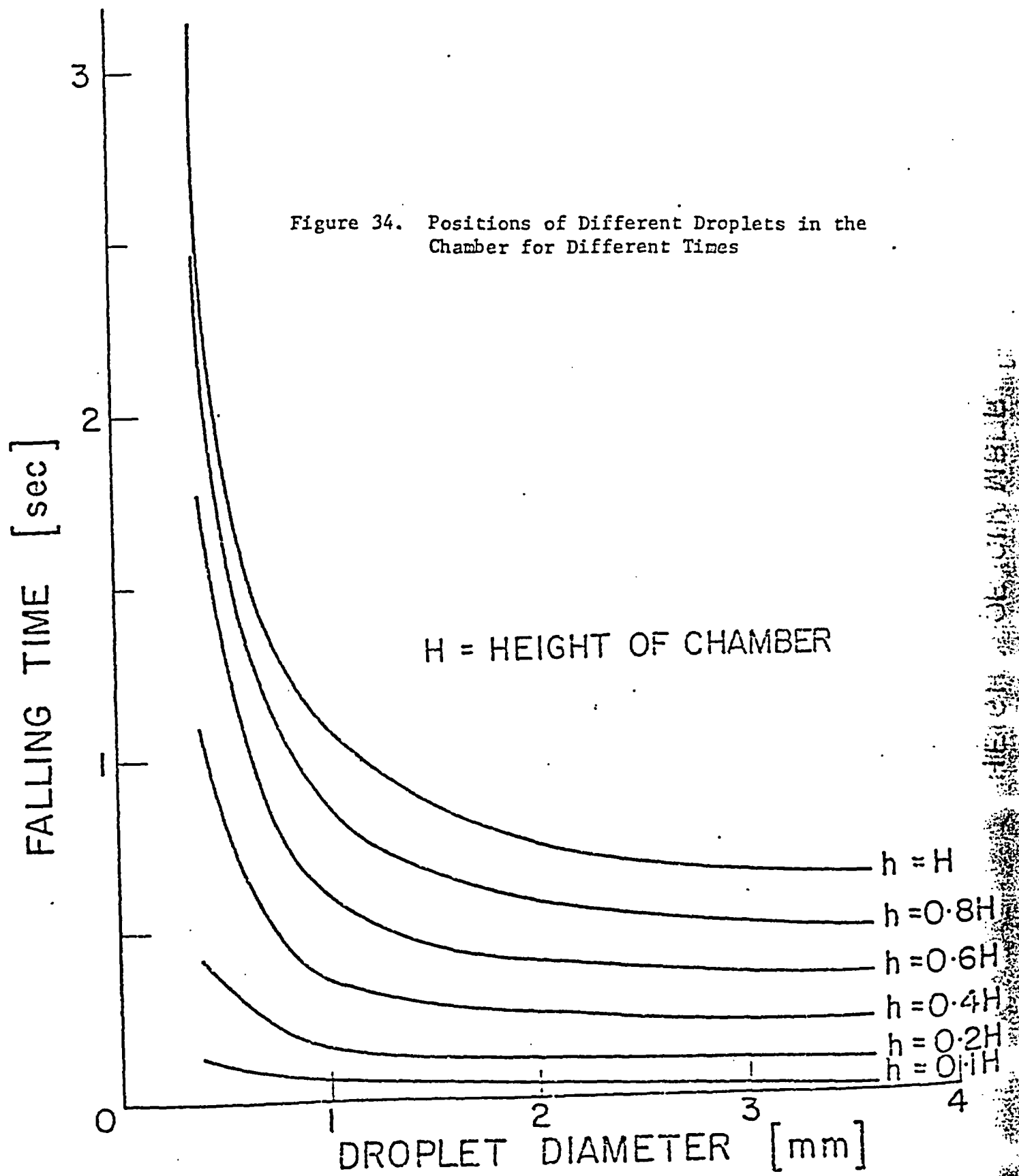


Figure 34. Positions of Different Droplets in the Chamber for Different Times



9.5 Droplet Temperature Distributions

In order to predict the temperature response of the water droplets in the same manner as was done in Part I of this study, it would be necessary to solve $M \times N$ ($M = 10$, $N = 100$) times the single droplet problem in every time increment (0.5 sec). This is not feasible because it would require excessive computational time and a huge computer memory. To overcome this problem some other means of calculating droplet temperature responses have been considered. The "collocation method" [119] was tried, for a single droplet response. This method was subsequently abandoned, since it did not offer any advantage over the procedure outlined earlier, because it was necessary to solve a system of algebraic equations at the collocation points for each sphere for every time interval.

The striking similarity of all curves representing the individual dimensionless temperature responses (see Figures 9 to 12) suggested that they might be fitted by the equation

$$\theta = 1 - \exp(-A_1 Z) \quad (74)$$

where A_1 is an adjustable parameter. Simple dimensional analysis of certain important parameters (see Appendix M) gave the following expression for the dimensionless parameter Z

$$Z = \left(\frac{P_{SM} v_{Ro}}{m} \right)^{1/3} \cdot t \quad (75)$$

The correlation (75), however, was found to be too simple

to enable the fitting of the thermal utilization curves reasonably well. Several other curve fits were tried (see Table II.1) using the Waterloo Computer Center Library Subroutines GEPLSD or DPENLN which are optional routines. Some of the curve fits were more successful than others. A dimensional five parameter model of the type

$$\theta = 1 - \exp \left[- A_1 P_M^{A_2} v_{Ro}^{A_3} \left(\frac{x_{SH}}{m} \right)^{A_4} t^{A_5} \right] \quad (76)$$

gave the best agreement with the predictions. The results of the least squares estimates (for 1230 points) of parameters A_1 to A_5 are:

$$A_1 = 2.317 \cdot 10^{-3}, A_2 = 1.22549, A_3 = 0.262816, A_4 = 0.519932$$

$$A_5 = 0.102082 \quad (77)$$

To compare the correlation predictions with calculated droplet temperature histories, Figure 35 is drawn. This shows that the correlation predictions (points) are in fairly good agreement with the temperature responses over a wide range of air/steam mixture parameters. Now, using equation (76) and equalities (77) it is possible to calculate the temperature of the droplets in the dousing system at any time and position. This has been done and the results are illustrated in Figure 36 where, after a 0.5 sec exposure, typical temperatures of different diameter droplets at different positions in the chamber are shown, for the same spray used to produce Figures 32 to 34, after a 0.5 [sec] exposure.

TABLE II.1

Droplet Temperature Response Model Fits

Model	Subroutine Used
$\theta = 1 - \exp(b_1 Z + b_2)$ $\theta = 1 - \exp(b_1 Z^2 + b_2 Z + b_3)$ $\theta = 1 - \exp(b_1 Z^3 + b_2 Z^2 + b_3 Z + b_4)$ $\theta = 1 - \exp(b_1 Z^4 + b_2 Z^3 + b_3 Z^2 + b_4 Z + b_5)$ $\theta = 1 - \exp(b_1 Z^5 + b_2 Z^4 + b_3 Z^3 + b_4 Z^2 + b_5 Z + b_6)$	GEPLSD
$\theta = 1 - (b_1 Z + b_2)$ $\theta = 1 - (b_1 Z^2 + b_2 Z + b_3)$ $\theta = 1 - (b_1 Z^3 + b_2 Z^2 + b_3 Z + b_4)$ $\theta = 1 - (b_1 Z^4 + b_2 Z^3 + b_3 Z^2 + b_4 Z + b_5)$ $\theta = 1 - (b_1 Z^5 + b_2 Z^4 + b_3 Z^3 + b_4 Z^2 + b_5 Z + b_6)$	GEPLSD
$\theta = 1 - b_1 Z$ $\theta = 1 - \exp(b_1 Z + b_2)$ $\theta = 1 - \exp(-b_1 Z^{b_2})$ $\theta = 1 - \exp(b_1 Z^{b_2} + b_3)$ $\theta = 1 - b_2 \exp(-b_3 Z^{b_4})$	DPENLN

(Cont'd)

Table II.1 (Cont'd)

Model	Subroutine Used
$\theta = 1 - \exp (b_1 z^{b_2}) + b_3 z^{b_4}$ $\theta = 1 - \exp (b_1 z + b_2 z^2 + b_3 z^3 + b_4)$ $\theta = b_1 - b_2 \exp (b_e p^{b_4} v_R^{b_5} m^{b_6} t^{b_7})$ $\theta = 1 - \exp (b_1 p^{b_2} v_R^{b_3} m^{b_4} t^{b_5} x_S^{b_6})$	DPENLN

where

$P[N/m^2]$, $v_R [m/s]$, $t [s]$ and $m [kg]$.

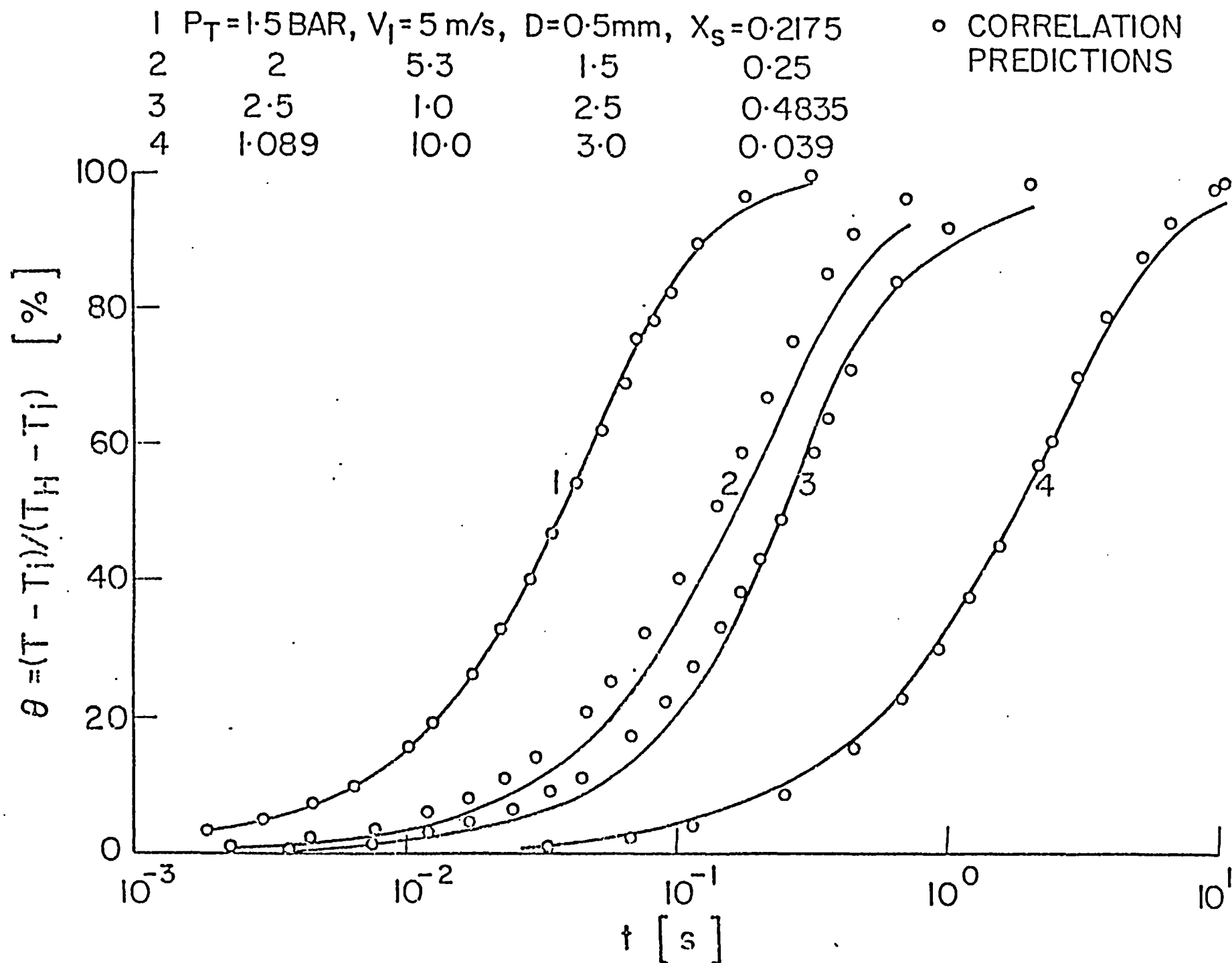


Figure 35. Thermal Utilization Predictions Compared to Experimental Values

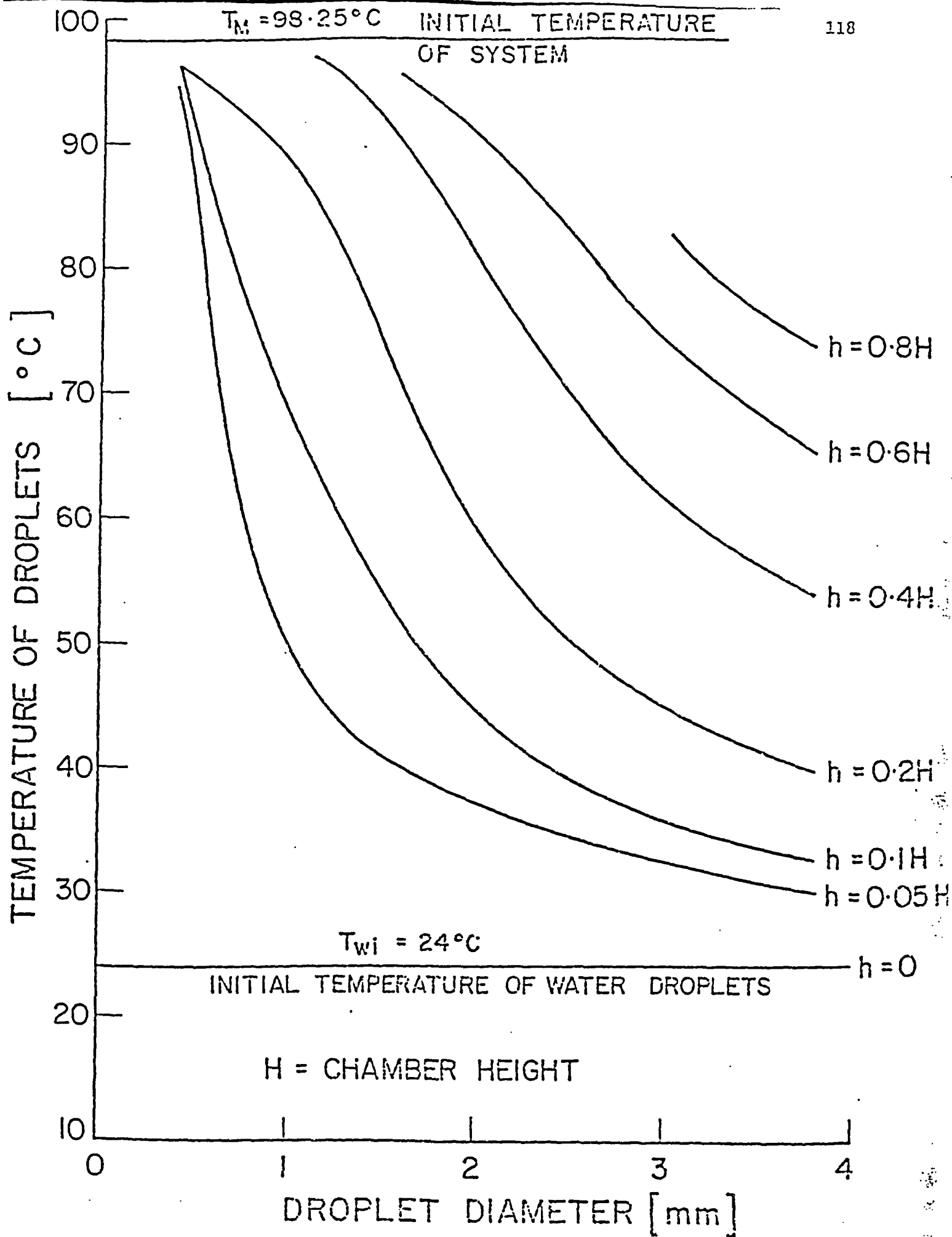


Figure 36. Different Diameter Droplets Temperature at

The only quantity in equation (72a) left unspecified is the heat loss to the surrounding medium which will be dealt with in the next paragraph.

9.6 Heat Losses Simulation

The heat losses to the surroundings Q_L were determined experimentally, see Figure 39, curve 1. These experimental results were fitted by

$$P = P_i \exp(-kt) \quad (78)$$

where:

P_i - initial chamber pressure,

k - adjustable constant,

t - time.

In this manner, the chamber pressure decrease due to heat losses was calculated rather than the corresponding heat losses. The least square estimate for the nonlinear model (77) of the parameter k is 0.002.

Thus all the necessary terms in equation (72a) are specified and we can proceed to the outline of the numerical algorithm itself.

10. THE NUMERICAL ALGORITHM OUTLINE

The only unknown term in equation (72a) is the term (4) which represents the total energy of the chamber after a certain time increment (0.5 sec used). This can therefore be determined from equation (72a). By a trial and error procedure the corresponding temperature and pressure of the air/steam mixture is determined and subsequently used as the initial state for the new time increment. This implies the repetition of the procedure until the pressure change in the dousing chamber is satisfactorily decreased to a preselected value. This is the essential step in the algorithm, however before it can be taken, there are a number of steps involved as shown in the program contained in Appendix N.

The algorithm entry data are:

- (i) chamber volume and height
- (ii) initial state of air/steam mixture in the chamber
- (iii) inlet water flow rate, temperature and velocity
- (iv) droplet size distribution parameters: x_m , b and δ
- (v) number of droplet sizes M and chamber height increments N
- (vi) a time increment.

The program then proceeds through the following steps:

1. From the known droplet size distribution, the volume fraction distribution of droplets of a given mean diameter in each of the diameter intervals is calculated.
2. The numbers of droplets of each of the diameters in a unit volume of water is calculated.

3. The temperature of the system is determined from the partial pressure of steam present in the tank.
4. The density and heat capacity of water at the inlet conditions is determined.
5. The chamber is divided into a number of 5 cm height increments.
6. The velocity profile of each droplet size as it falls through the chamber is calculated by using a Runge-Kutta technique.
7. The time (sec) for droplets of a given diameter to fall to a specific height increment in the chamber is calculated.
8. The energy (kJ) of the dousing water entering the chamber in a single time increment (0.5 sec) is calculated.
9. The total residence time (sec) in the chamber of a droplet of given diameter is calculated.
10. The amount of air in the chamber at the start of test is calculated.
11. The initial energy content (kJ) of the air/steam mixture is calculated.
12. Time is incremented by Δt (used value was 0.5 sec).
13. At the end of the time increment the new local drop size distribution is calculated, i.e. the number of droplets of given diameters that are in the various height increments of the chamber.
14. If any droplets have left the chamber then the volume fraction of droplets of that particular diameter is calculated.

15. The local droplet temperature distribution is calculated. The new temperature ($^{\circ}\text{C}$) of all droplets at all height increments of the chamber is determined from the generalized correlation of thermal utilization (equation (77)).
16. Then using the temperatures of the droplets of given diameter the program then determines the energy (kJ) of all the droplets in the chamber at the end of the time increment. The density and heat capacity of each droplet is first determined from the droplet temperature and the total pressure of the system.
17. The energy (kJ) of any droplets that have left the chamber during the time increment is calculated. The value of volume fraction determined from step 14 is used if it is the first time for droplets of a given diameter to leave the chamber.
18. The energy reduction of the air/steam mixture is calculated by use of equation (72a).
19. The partial pressure of steam is determined by trial and error. The procedure requires that the energy of air + energy of steam approximates the new energy of the mixture. Both energy of air and energy of steam are determined indirectly through functions of the partial pressure of steam.
20. A new system temperature is determined from the partial pressure of steam.
21. Total pressure of the system is determined and printed out.
22. Steps 12 to 21 are repeated by advancing the time increment.

More details about every step can be found in the program
given in Appendix N.

11. EXPERIMENTAL RESULTS AND DISCUSSION

In this chapter the experimental results concerning the droplet size distributions will be treated firstly in paragraph 11.1. The next paragraph 11.2 will deal with the problem of the dousing chamber test predictions on the basis of the information on droplet size distributions supplied in paragraph 11.1.

11.1 Droplet Size Distribution

Experimental runs were performed at three flow rates ~ 30, ~ 40 and ~ 50 IGPM and the corresponding photographs (using the catch in cell technique) are shown in Figures 1 to 6 of Appendix O (two for each flow rate taken at different horizontal positions inside the spray). Each of these photographs is analysed on the departmental Quantimeter. The results of these analyses are shown in Figures 7 to 12 in the same Appendix corresponding to flow rates 30, 40 and 50 IGPM. The defining parameters \bar{x}_m , \underline{b} and $\underline{\delta}$ of the upper limit distribution function were obtained by the least square fit by linearization of the upper limit function model, see P. M. Reilly [121]. The least square fit estimates are represented by solid lines in Figures 7 to 12. The results of these calculations are shown in Table II.2.

From this table it can be seen that the maximum measured droplet size decreases as the flow rate through the nozzle increases (corresponding to increasing pressure drops across the nozzle) which is expected. The curve-fitted values of the maximum droplet sizes

TABLE II.2

Flow Rate IGPM	Run #	Number of Droplets Measured	Maximum Droplet Diameter Measured [mm]	Predicted Values		
				\bar{x}_m [mm]	δ	b
30.8	130	126	5.6	5.25	1.265	0.292
30.8	132	127	4.5	3.49	0.902	0.399
40.42	131	48	4.0	2.935	1.47	1.68
40.42	133	132	4.0	5.295	2.172	1.008
50.05	134	143	3.7	4.629	0.677	1.569
50.05	136	181	3.7	3.917	0.822	0.779

differ from the measured ones, however, they correspond to the so-called maximum stable droplets (Mugele [122], one of the originators of the upper limit distribution function theory).

The dousing chamber tests were performed with 45 IGPM per nozzle, and therefore it was necessary to find some kind of average droplet size distribution for this flow rate. But before this was done it was also necessary to find an average droplet size distribution for one flow rate from the results obtained at different horizontal positions in the spray. Comparing the defining coefficients in Table II.2 for the corresponding pairs of distributions, it can be seen that they differ considerably. A reasonable way to

find an average distribution at the same flow rate is to take weighted values of the frequency distributions depending upon the amount of a liquid caught in the cells at the different positions in the spray. Thus for the 40 IGPM flow rate (Runs 131 and 133) the liquid volumes caught in the cells (during the same period of time) were $\sim 15 \text{ mm}^3$ and $\sim 2646 \text{ mm}^3$, respectively. Hence the sampled amount of water in the spray having distribution 131 (Figure 9 in Appendix C) was negligible, and the distribution 133 (Figure 10 in Appendix O, and circles O and the least square fitted curve 1 in Figure 39) is taken to be the representative one for this flow rate. Similarly, for the 50 IGPM flow rate the volumes caught in the cells were 707 and 1647 mm^3 for distribution 134 and 136 (Figures 11 and 12 in Appendix O), respectively. The weighted (30% and 70%) frequency distribution is shown in Figure 37 by dots e, while curve 2 represents the least square fitted line. The estimated parameters are:

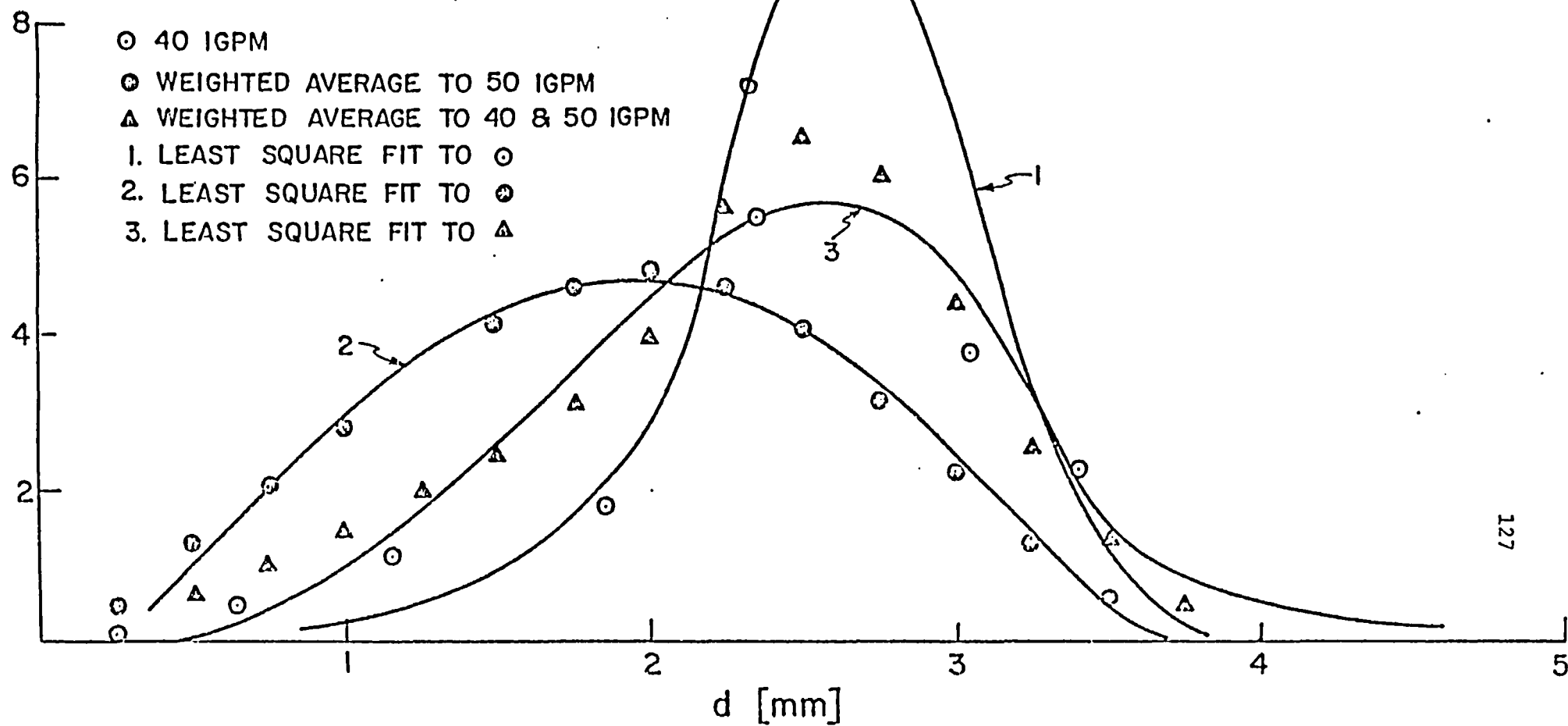
$$x_m = 3.82 \quad b = 0.9859 \quad \delta = 0.793 \quad (79)$$

To obtain a representative distribution for the 45 IGPM flow rate (dousing chamber experiments flow rate) the frequency distribution for 40 IGPM (Figure 10 in Appendix O, and curve 1 in Figure 37) and the averaged frequency distribution for 50 IGPM (curve 2 in Figure 37) were weighted by a 50% to 50% correspondence, to produce the triangles A in Figure 37. The least square fitted curve to this data represented by curve 3 (in Figure 37) and its defining

Figure 37. Comparison of Different Droplet Size Distributions Obtained by the Catch in Cell Technique

CATCH IN CELL TECHNIQUE

- 40 IGPM
- ⊙ WEIGHTED AVERAGE TO 50 IGPM
- △ WEIGHTED AVERAGE TO 40 & 50 IGPM
- 1. LEAST SQUARE FIT TO ○
- 2. LEAST SQUARE FIT TO ⊙
- 3. LEAST SQUARE FIT TO △



parameters are:

$$x_m = 3.847 \text{ [mm]}, \quad b = 0.605, \quad \delta = 0.886 \quad (80)$$

These are the defining parameters (obtained by using the catch in cell technique) for the upper limit distribution function to be used in the simulation of the dousing chamber runs.

It was pointed out in paragraph 8.2 that a comparison of droplet size distributions obtained by the catch in cell technique and direct photography will certainly be interesting. For that purpose the direct photography method was attempted simultaneously with the experiments with the catch in cell technique. The photographs of the spray in air at the flow rates 30, 40 and 50 IGPM are shown in Figures 13 to 15 (Appendix O), respectively. These figures (13 to 15 of Appendix O) represent the droplet images above the outer catch cell, i.e. they correspond to droplet sizes in cells represented by runs 132, 133, and 136 (Figures 2, 4 and 6 and distributions in Figures 8, 10 and 12 in Appendix O). The photographs for the flow rates 40 and 50 IGPM had to be analysed manually, since the droplets did not appear as solid dots against the background, thus preventing analysis by the Quantimeter. The results of this analysis are shown in Figures 16 and 17 of Appendix O for 40 and 50 IGPM, respectively. The solid lines represent the least squares fit of the upper limit distribution function model. The parameter estimates are given in Table II.3.

TABLE II.3

Flow Rate [IGPM]	Maximum Droplet Diameter Measured [mm]	Predicted Values		
		x_m [mm]	b	δ
30.8	3.8	not analysed		
40.42	3.5	3.31	0.7697	1.1071
50.05	3	$\bar{x} = 1.452$	—	1.9978

The 50 IGPM case (Figure 17 of Appendix O) is best fitted by the log-probability distribution function, which is a special case of the upper limit one. The volume log-probability distribution function is defined as

$$\frac{dv}{dx} = \frac{\delta}{\sqrt{\pi}} \frac{1}{x} \exp(-\delta^2 y^2) \quad (81)$$

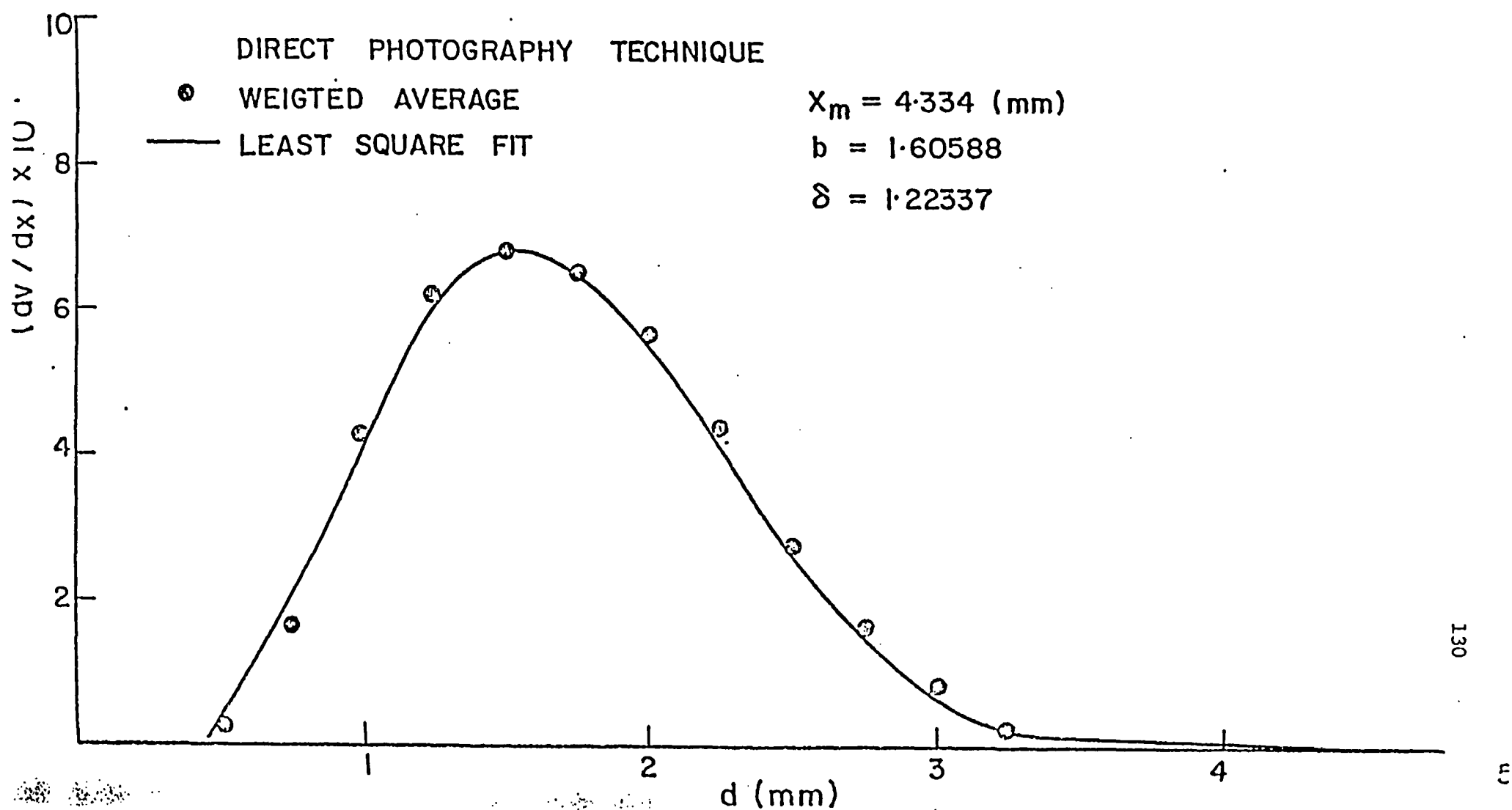
with

$$y = \ln(x/\bar{x}) \quad (82)$$

$$\bar{x} = \frac{x_m}{b} \quad (83)$$

The representative droplet size distribution at 45 IGPM is obtained by weighting the frequency droplet size distributions at 40 IGPM (Figure 16 of Appendix O) and 50 IGPM (Figure 17 of Appendix O) in the 50% to 50% correspondence. In this manner the droplet size distribution shown in Figure 38 by the solid line is

Figure 38. Droplet Size Distribution Obtained by the Direct Photography Technique



obtained. The upper limit distribution function model fitted to these data is represented by the dashed line in Figure 38, and the defining parameters are

$$x_m = 4.334 \text{ [mm]} \quad b = 1.606 \quad \delta = 1.223 \quad (84)$$

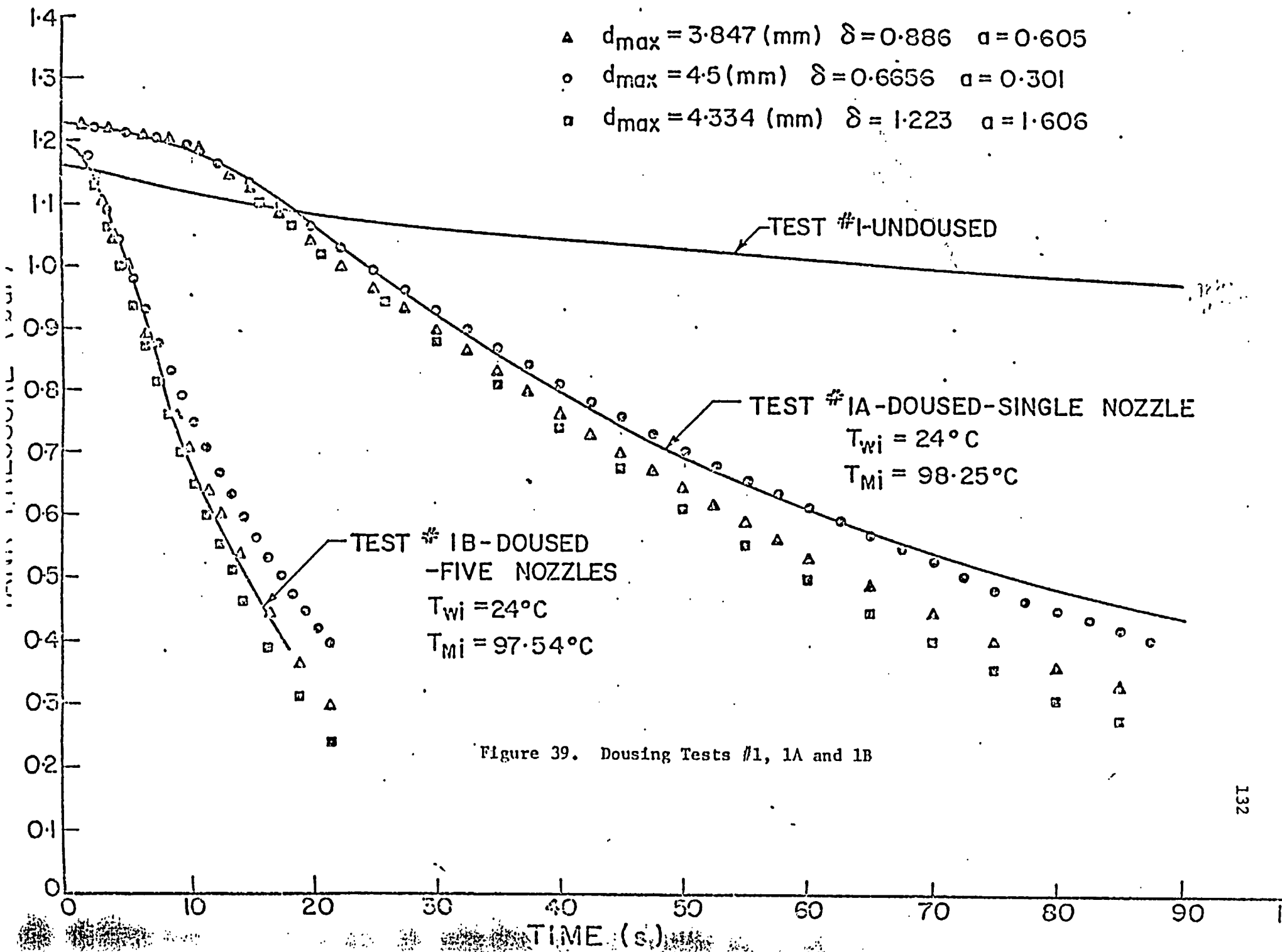
Thus, the equalities (80) and (84) represent the upper limit distribution function defining parameters for the two different methods of droplet size distribution measurements, namely "the catch in cell" and "the direct photograph" methods, respectively.

In the next paragraph it is shown how these parameters were used in the computer algorithm to predict the dousing chamber pressure changes as a function of time.

11.2 Dousing Test Predictions

Dousing tests were undertaken [107] in the enclosed chamber of total volume $56 \text{ [m}^3\text{]}$ (see Figure 29) provided firstly with single spray nozzles (experiments 1A, 2A, 2B, 2C and 3A, Figures 39 and 40) and then a group of five spray nozzles (experiments 2D, 2E, 2F, 3D and 3E, Figures 39 and 41). The experimental results are represented by the solid lines while the triangles represent predictions using the droplet size distribution obtained using the catch in cell technique and the squares represent the predictions using the droplet size distribution obtained using the direct photography technique.

From Figures 39 to 41 it can be seen that the predicted



SINGLE NOZZLE

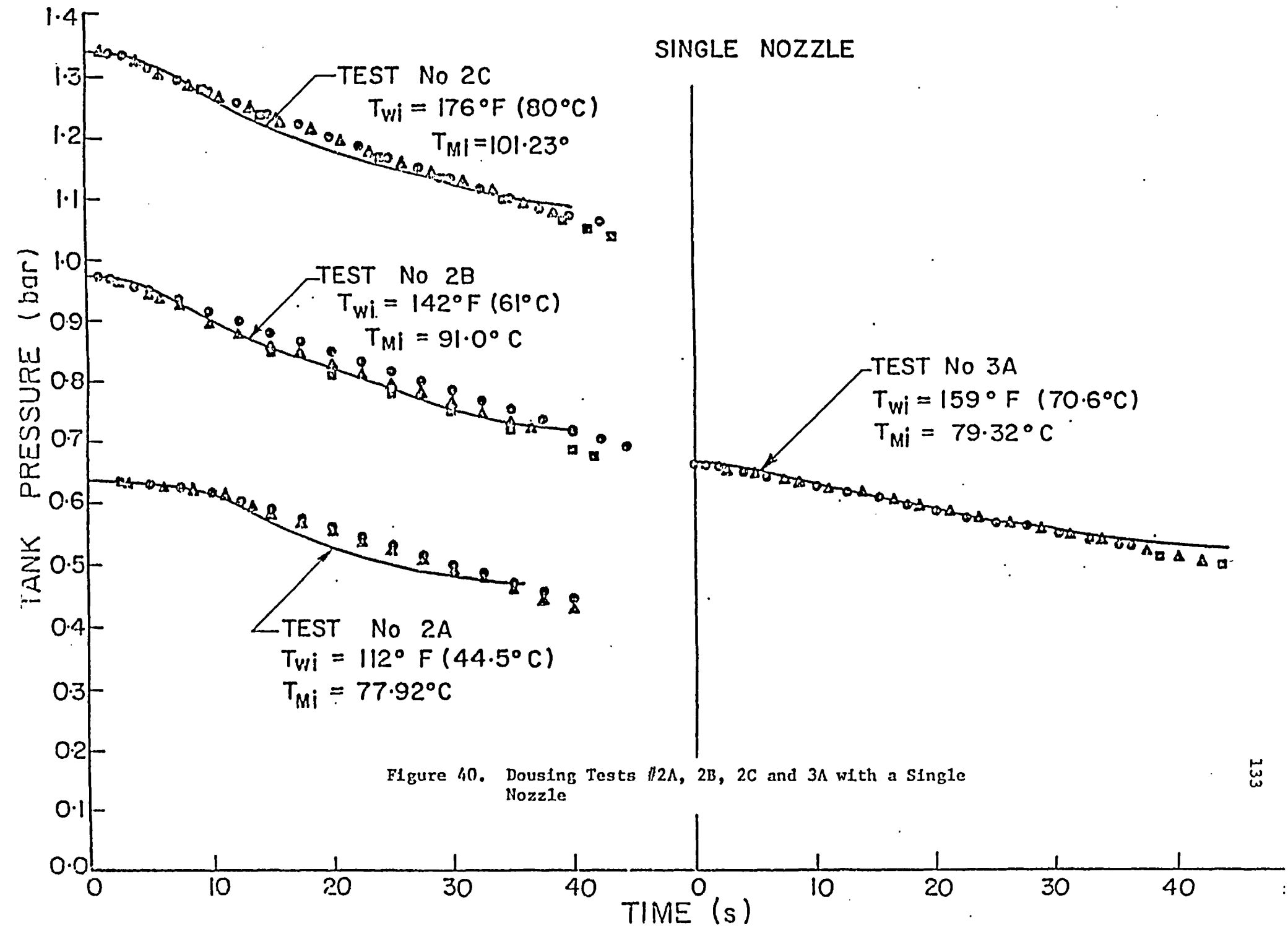
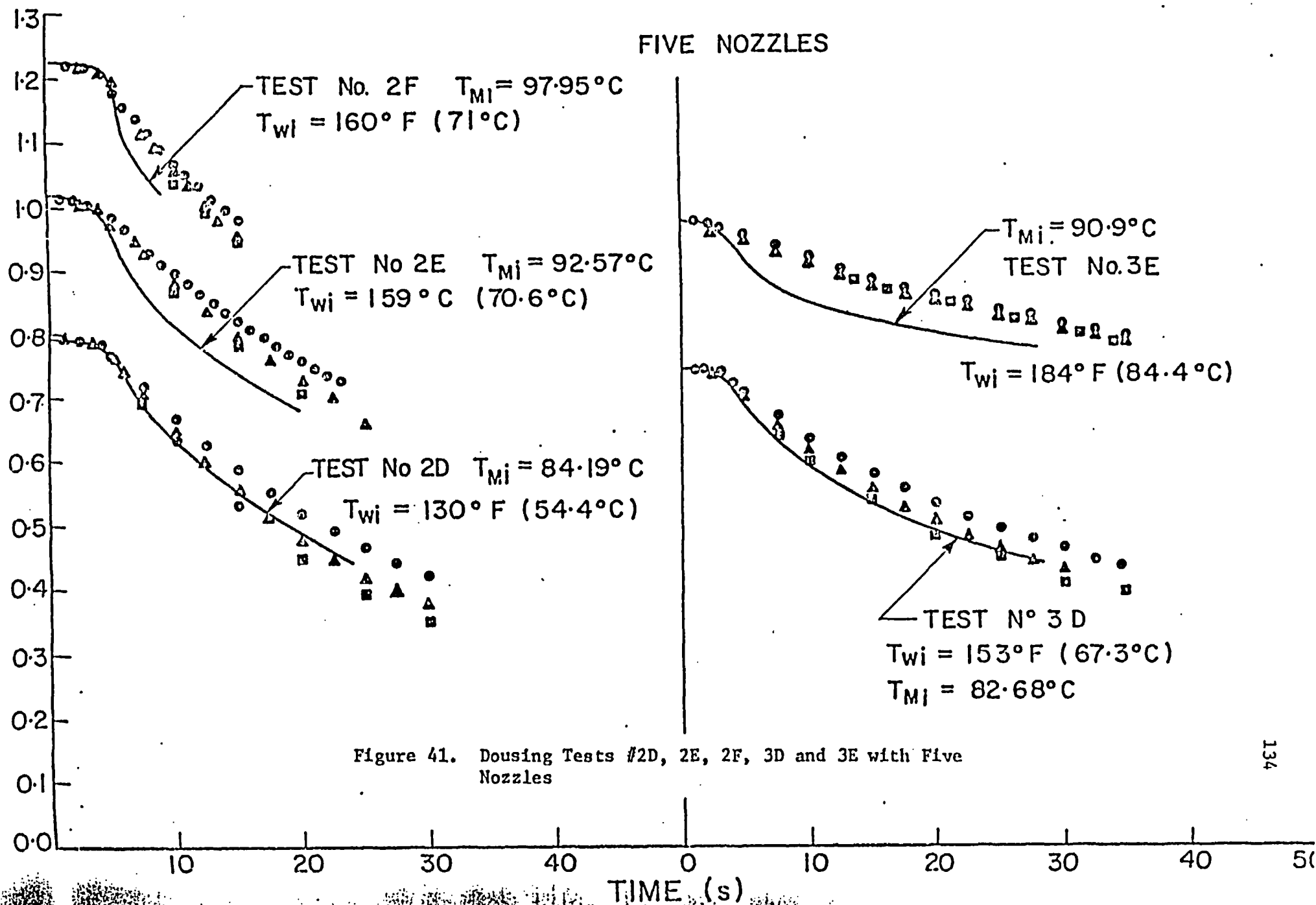


Figure 40. Dousing Tests #2A, 2B, 2C and 3A with a Single Nozzle



results (triangles) show very good agreement for all the tests. The difference between the predicted and measured pressures at any time is within $\pm 7\%$ of the measured value for all the runs except 1A, for times greater than 50 seconds. All the runs (except 1A) were recorded for time periods of from 10 to 40 seconds. The recording time length may be an important factor affecting the accuracy of the predictions because of the following two phenomena which are bound to show increasing influences later in the dousing process. These phenomena are acting in the same direction, i.e. they both tend to increase the predicted pressure drop rate in the dousing chamber if they are not taken into account in the simulation algorithm. These phenomena are explained as follows:

- 1) In Figure 38 the curve for the test #1 is shown, where a reduction in system pressure was obtained without the use of dousing water. The experimental curve shows that the steam condensation on the walls of the chamber contributes to the overall pressure drop at a rate of about 0.0021 [Bar/sec] for conditions similar to test #1. These conditions were always above 0.97 Bar, however, in the absence of other experimental information, this curve was used to estimate the heat losses in all the other dousing runs involving water sprays when the dousing chamber temperature and pressure changes were much more rapid which would mean lower actual heat losses to the surrounding medium than were allowed for.

ii) No attempt has been made to theoretically determine the effect of steam condensation on the water film which must inevitably be formed by droplet impingement on the walls and the obstructions of the chamber. In the initial time period of this film formation this effect may not be so important, but as time progresses this effect probably becomes more pronounced as the walls become completely wetted. In the simulation runs however, it is presumed that all the water entering the dousing chamber flows in the form of spray which is certainly predicting a more rapid pressure drop in the chamber than would occur if part of the water flowed as a film on the walls and obstructions.

In spite of this it can be said in general that the simulation model predictions for such a complex problem are highly satisfactory over the wide range of experimental conditions.

The simulation model predictions using the droplet size distribution obtained from the direct photography technique predict slightly lower values (represented by squares in Figures 38 to 41) of dousing chamber pressures as compared to the values obtained by use of droplet size distribution obtained using the catch in cell technique. Further work on the direct photography technique will probably improve its reliability over the catch in cell technique. In any case the dousing chamber pressure drop predictions using the droplet size distribution obtained from the catch in cell technique are conservative, if compared with the droplet size distribution obtained using the direct photography technique.

Finally, the sensitivity of the simulation model to the effects of droplet size distribution should be mentioned. To show the effects of the size distribution, the simulation has been run with three different imaginary droplet size distributions.

The first droplet size distribution is represented by the parameters

$$x_m = 8.847 \text{ [mm]}, \quad b = 0.605 \quad \text{and} \quad \delta = 0.88 \quad (85)$$

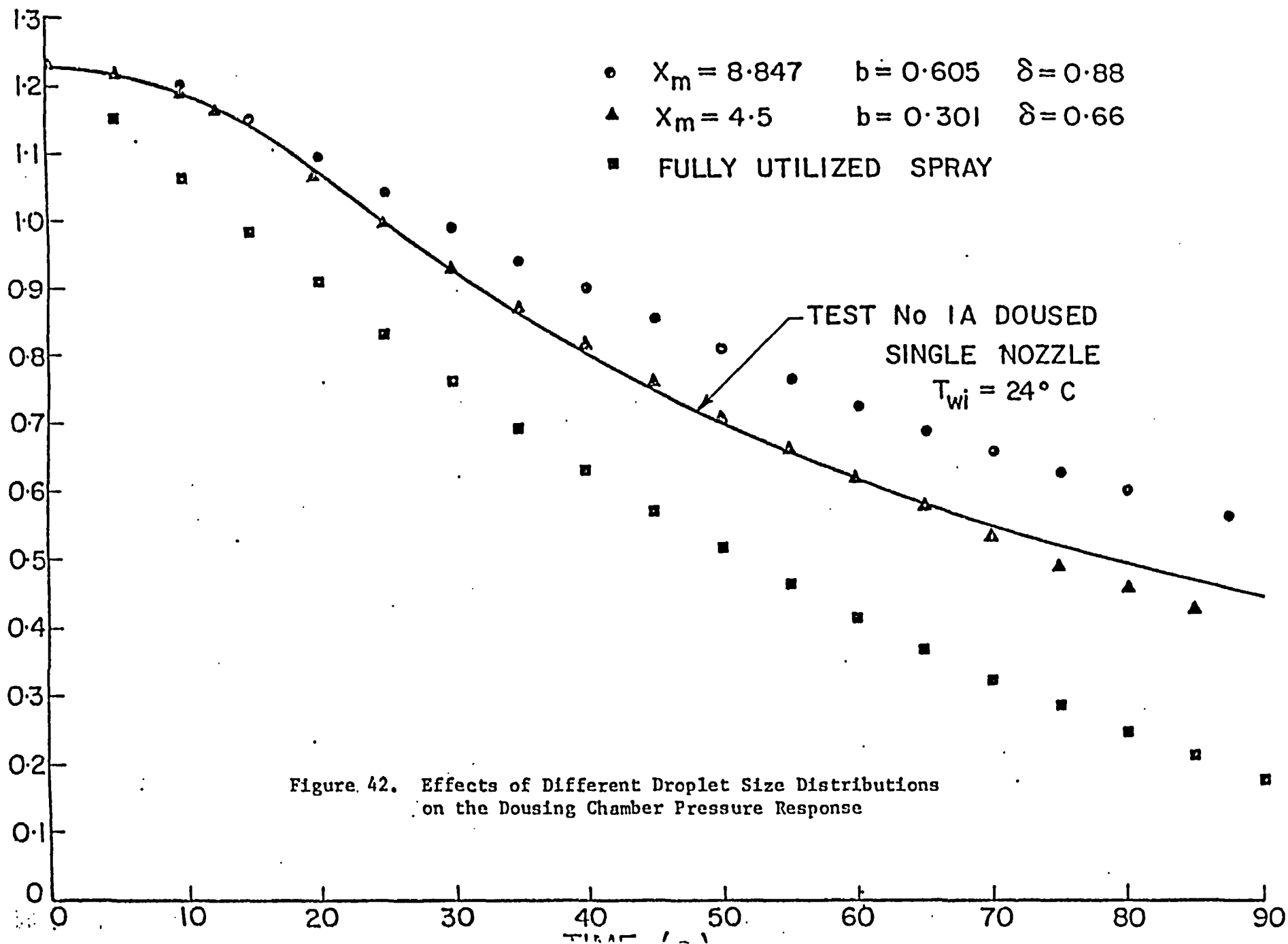
which has the same "shape" as the one measured using the catch in cell technique but a larger maximum diameter x_m . This droplet size distribution prediction (for the conditions of the run 1A) are represented by circles in Figure 42.

The second size distribution is a very small diameter spray, so small that all the droplets will be fully utilized in the chamber. This represents the heat balance on the chamber when all the water is utilized. The pressure in the chamber cannot be decreased any faster than the pressure decrease represented by this curve, which is illustrated by squares in Figure 42.

Finally, by a trial and error method a droplet size distribution was selected which gave a very good fit to the experimental results (for the conditions of the run 1A). Its defining parameters are:

$$x_m = 4.5, \quad b = 0.301, \quad \delta = 0.66 \quad (86)$$

Figure 42 gives an indication of the sensitivity of the simulation to the different droplet size distributions. The



difference between simulated and predicted values can be very high. The heat balance curve predicts the pressure in the chamber 0.515 Bar after at $t = 50$ sec, while in the experiments at this time the pressure was 0.7 Bar. The droplet size distribution represented by circles (Figure 42) would predict a pressure of 0.81 Bar at this time. This sensitivity of the dousing chamber response curves to the droplet size distributions highlights the need for accurate drop size data. Obviously more effort needs to be put into the acquisition of such data to lend confidence to future scale-up and full size dousing chamber simulations.

12. CONCLUSIONS AND RECOMMENDATIONS OF PART II

As demonstrated in Figures 39 to 41 the simulation model developed in the second part of this report gives very good predictions of the dousing chamber pressure drops over the wide range of inlet water and dousing chamber conditions. The ability of the model to predict practically all the runs within a few percent is very encouraging for the simulation of the real dousing chambers.

The correlation between thermal utilization and the initial droplet and gas phase variables (equation (76)) is a good practical way of getting around gigantic computer requirements of the dousing chamber simulation. The comparison between the correlation values of thermal utilization and the theoretically and experimentally confirmed values shows excellent agreement.

// if it's possible

At this stage of the project it can be concluded that the catch in cell technique of droplet size distribution measurements gives bigger average droplet sizes than the direct photography technique. However, more experiments and some improvements in both techniques will give a firmer answer as to the question of the reliability of the techniques.

The recommendations for future work are:

- i) modelling of the dousing chamber heat losses to the surroundings;
- ii) modelling of the condensation on dousing chamber walls and obstructions;

iii) droplet size distribution measurement under the real conditions in a dousing chamber, which surely differ considerably from those in the pilot plant tests. Which of the measurement techniques will be more advantageous is not possible to assess at this stage of the project.

13. FINAL SUMMARY

The following is a summary of the accomplishments of this project.

1. It has been demonstrated that the only practical way to solve the droplet combined heat and mass transfer problem for N_{Re} over a wide range of values is by the macroscopic balance treatment involving the transport rate equations.
2. A survey of the literature on drag coefficients for droplets has led to the conclusion that the Reinhart's drag coefficient correlations appear to be the best.
3. Droplet velocity trajectories have been calculated using Reinhart's drag coefficient correlations for upwards and downwards freely moving droplets. This could only be done numerically. Solutions using Reinhart's drag coefficient correlations agree with existing data on droplet terminal velocities. These trajectories were the ones eventually used in the simulation of droplet temperature responses for free falling droplets (see below for summary).
4. Some analytical solutions for trajectories of solid spheres in free fall were either obtained from the literature or newly derived, however, it was decided in the end to use the "Reinhart's trajectories" instead of the solid sphere ones.
5. The sensible and latent heat transfer contributions to gas side heat transfer coefficients were discussed. It was shown that

mass transfer coefficients are very often not known. A detailed discussion of previous workers' use of the analogy led to the conclusion that its use in this work could be valid.

6. A comparison of the external heat and mass transfer analogy equations for different systems was enabled by collecting the correlations in Figure 8.
7. A model was developed in the form of an analytical solution based on the combined heat and mass transfer analogy to predict the temperature of a free falling droplet which is perfectly mixed (i.e. no internal resistance).
8. A model was developed in the form of a numerical solution based on the combined heat and mass transfer analogy to predict the temperature of a free falling droplet which is partially mixed. This involves the combination of the external heat and mass transfer analogy with the internal conduction problem where the internal temperature profile is renewed periodically.
9. A third model was developed in the form of a combined analytical and numerical solution based on the combined heat and mass transfer analogy to predict the temperature of a free falling droplet which behaves as a solid sphere internally. This model describes the droplet having no internal mixing and the maximum possible internal droplet resistance.
10. It was shown that as the number of internal mixings increased the partial internal resistance model became asymptotic to the no internal resistance model (see Figure 13).

11. It was shown that in the limit as the number of internal mixings was decreased to zero and the initial temperature profile was uniform, the partial internal resistance model would become asymptotic to the no internal mixing model (see Chapter 2.7).
12. The maximum effect of a change of droplet size was investigated and although this was found to be small it was incorporated in the models.
13. All the necessary thermodynamics and physical properties for the air/water system were collected on one place (Appendix D).
14. Computer algorithms for each of the models were developed.
15. The effects of steam concentration, initial velocity and diameter, on the temperature response (thermal utilization) of free falling droplets were predicted. The possible range of effects on thermal utilization caused by internal mixing of varying degrees was shown.
16. Various ways of defining the heat transfer coefficient in the condensing process were carefully discussed.
17. The experimental results of many workers dealing with condensation from pure steam and also from air/steam mixtures were collected together in one place for comparison purposes.
18. It was shown that the predictions using the analogy theory extrapolate reasonably well to the pure steam measured and theoretical heat transfer coefficients.
19. An apparatus was built to enable the measurement of temperature responses of single droplets suspended in air/steam jets.

20. Experimentally measured mean temperature responses of droplets (using tiny thermistors glued on teflon tubing) were obtained.
21. The possible effects on the temperature responses of the needle used to create the droplets were shown to be negligible.
22. Comparison of the experimental results and the theoretical models confirmed that a droplet appears to behave as if it is partially mixed internally.
23. The predictions of the partial internal mixing model and the results of 90 experiments showed standard deviations of 6% and 4% in the temperature response at 50 and 75% utilization respectively.
24. A slight trend in the data suggested that the larger droplets behaved as if they were experiencing more internal circulation than the smaller droplets.
25. It was concluded that the analogy theory could be applied with confidence to the problem of combined heat and mass transfer to droplets moving relative to an air/steam mixture provided that some internal resistance to heat transfer was allowed for.
26. Experimental data representing the size distribution of sprays produced by a typical dousing chamber nozzle were obtained by two methods, namely "the catch in cell" and the "direct photography" methods. The data were fitted by upper limit distribution functions.
27. A simulation model of a pilot plant dousing chamber was developed based on the previously obtained knowledge of the thermal utilization of droplets and a step by step energy balance.

28. In order to make the use of the model feasible from the point of view of computer time usage, a generalized dimensional correlation relating the thermal utilization, air/steam mixture pressure, initial droplet velocity, mass of droplet, steam concentration and time was obtained by use of an optimal curve fitting procedure.
29. The dousing chamber simulations and the experimental data supplied by Atomic Energy of Canada were compared and found to be in reasonable agreement.
30. The sensitivity of the simulation model to spray size distributions was illustrated and it was concluded that although the simulations of the pilot plant chamber were very good, it is expected that more data on droplet size distributions ~~expected~~ in the full-scale dousing chamber would be needed for scale-up purposes.

LITERATURE:

1. W. R. Marshall, Jr.: Atomisation and Spray Drying, Chem. Eng. Progress Monograph Series, No. 2, Vol. 50, 1956.
2. J. K. Pylant and H. A. Walls: Numerical Simulation of Large-Scale Spray Cooling Systems, 13th Nat. Heat Transf. Conf., AIChE-ASME, Denver, Colorado, Aug. 6-9, 1972.
3. J. Dlouhi and W. H. Gauvin: Heat and Mass Transfer in Spray Drying, 6, No. 1 (1960), pp. 29-34.
4. S. Z. Burstein, S. S. Hammer and V. D. Agosta: Spray Combustion Model with Droplet Breakup: Analytical and Experimental Results, pp. 243-267 in the book: Detonation and Two-Phase Flow, editors S. S. Penner and F. A. Williams, Academic Press, 1962.
5. K. G. T. Hollands: An Analysis of Counterflow Spray Cooling Tower, Int. J. Heat & Mass Transfer, 17 (1974), pp. 1227-1239.
6. G. Atagündüz: Tropfengrößenverteilung und Verdunstungskühlung (Droplet Size Distribution and Evaporative Cooling), Ph.D. Thesis, TH Stuttgart, 1965.
7. J. L. Threllkeld: Thermal Environmental Engineering, Prentice Hall, 1970.
8. K. K. McKelvey and M. Brooke: The Industrial Cooling Tower, Elsevier, Amsterdam, 1959.
9. A. B. Hedley, A. S. M. Nuruzzaman and G. F. Martin: Combustion of Single Droplets and Simplified Spray Systems, Progress Review No. 62, Journal of the Institute of Fuel, No. 1 (1971), pp. 38-54.
10. J. H. Kopp: Wärme-und Stoffaustausch bei Mischkondensation (Heat and Mass Transfer in Direct Contact Condensation), BWK, 18, No. 3 (1966), pp. 128-129.
11. A. Williams: Combustion of Droplets of Liquid Fuels, A Review, Combustion and Flame, 21, No. 1 (1973), pp. 1-31.
12. L. L. Ross and T. W. Hoffman: Evaporation of Droplets in High Temperature Environment, Proceedings AIChE 3rd Int. Heat Transfer Conference, Chicago, 5, 50, 1966.
13. A. E. Hamielec, T. W. Hoffman and L. L. Ross: Numerical Solution of the Navier Stokes Equation for Flow Past Spheres, AIChE J1., 13 (1967), pp. 212-219.

14. B. P. LeClair, A. E. Hamielec, H. R. Pruppacher: A Numerical Study of the Drag on a Sphere at Low and Intermediate Reynolds Number, *J. of the Atmosph. Sci.*, 27, No. 2 (1970), pp. 308-315.
15. J. H. Masliyah and N. Epstein: Numerical Study of Steady Flow Past Spheroids, *J. Fluid Mech.*, 44 (1970), 493-512.
16. S. E. Woo and A. E. Hamielec: A Numerical Method of Determining the Rate of Evaporation of Small Water Drops Falling at Terminal Velocity of Air, *J. of the Atmosph. Sciences*, 28, No. 8 (1971), pp. 1448-1454.
17. T. W. Hoffman and L. L. Ross: A Theoretical Investigation of the Effect of Mass Transfer on Heat Transfer to an Evaporating Droplet, *Int. J. Heat & Mass Transfer*, 15 (1972), pp. 599-617.
18. B. P. LeClair, A. E. Hamielec, H. R. Pruppacher and W. D. Hall: A Theoretical and Experimental Study of the Internal Circulation in Water Drops Falling at Terminal Velocity in Air, *J. of the Atmosph. Sciences*, 29, No. 4 (1972), pp. 728-740.
19. J. H. Masliyah and N. Epstein: Numerical Solution of Heat and Mass Transfer from Spheroids in Steady Axisymmetric Flow, *Progress in Heat and Mass Transfer*, Vol. 6 (1972), pp. 613-632.
20. R. L. Pitter, H. R. Pruppacher and A. E. Hamielec: A Numerical Study of Viscous Flow Past a Thin Oblate Spheroid at Low and Intermediate Reynolds Numbers, *J. of the Atmosph. Sci.*, 30, No. 1 (1973), pp. 125-134.
21. L. J. Snyder, T. W. Spriggs and W. Stewart: Solution of the Equations of Change by Galerkin's Method, *AIChE Journal* 10 (1964), pp. 535-540.
22. D. B. Spalding and S. V. Patankar: *Heat and Mass Transfer in Boundary Layers*, Intertext Books, London, 1970.
23. S. V. Patankar: ME 780-Numerical Prediction of Elliptic Flows, Class Notes, Mechanical Engineering Department, University of Waterloo, Winter 1974.
24. C. E. Lapple and C. B. Shepherd: Calculation of Particle Trajectories, *Ind. Engng. Chem.* 32 (1940), pp. 605-617.
25. H. Schlichting: *Boundary Layer Theory*, Pergamon Press, 1955.
26. L. B. Torobin and W. H. Gauvin: Fundamental Aspects of Solid-Gas Flow, *The Can. J. of Chem. Eng.* 37 (1959), pp. 129-141, 167-176, 224-236; 38 (1960), pp. 142-153, 189-200; 39 (1961), pp. 113-120.

27. R. D. Ingebo: Drag Coefficients for Droplets and Solid Spheres in Clouds Accelerating in Air Streams, NACA TN 3762.
28. R. Gunn and G. D. Kinzer: The Terminal Velocity of Fall for Water Droplets in Stagnant Air, Journal of Meteorology, 6 (1949), pp. 243-248.
29. E. Kulic, E. Rhodes, G. Sullivan: Heat Transfer Rates Predictions in Condensation on Droplets from Air/Steam Mixture, The Can. J. of Chem. Eng., 53 (1975), pp. 252-258.
30. R. R. Hughes and E. R. Gilliland: The Mechanics of Drops, Chem. Eng. Prog., 49 (1952), pp. 497-504.
31. K. G. T. Hollands: An Analysis of Counterflow Spray Cooling Tower, Int. J. Heat & Mass Transfer, 17 (1974), pp. 1227-1239.
32. J. F. Groeneweg: The Statistical Description of a Spray in Terms of Droplet Velocity, Size and Position, Ph.D. Thesis, University of Wisconsin, 1967.
33. A. Reinhart: Das Verhalten fallender Tropfen (The Behaviour of Falling Droplets) Prom. Nr. 3412, Eidgenössischen Technischen Hochschule in Zürich, 1964.
34. A. Reinhart, Das Verhalten fallender Tropfen, Chemie Ing.-Techn., 36, No. 7 (1964), pp. 740-746.
35. J. H. Perry: Chemical Engineers Handbook, McGraw-Hill (1950).
36. S. S. Kuo: Computer Applications of Numerical Methods, Addison Wesley, 1972.
37. G. F. Foote and P. S. DuToit: Terminal Velocity of Raindrops Aloft, Journal of Appl. Meteorology, 8, No. 2 (1969), pp. 249-253.
38. R. E. Treybal: "Mass Transfer Operations", McGraw-Hill (1968).
39. A. W. P. Skelland: "Diffusional Mass Transfer", John Wiley (1974).
40. G. Ackermann: Das Lewische Gesetz für das Zusammenwirken von Wärmeübergang und Verdunstung (The Lewis Law for Combined Heat Transfer and Evaporative Cooling), Forsch. Ing.-Wes. 5 (1935), p. 95.
41. G. Ackermann: Theorie der Verdeunstungskühlung (The Theory of Evaporative Cooling), Ing. Arch., 5 (1934), pp. 124-146.

42. G. Ackermann: "Wärmeübergang und molekulare Stoffübertragung im gleichen Feld bei grossen Temperatur und Partialdruck differenzen (Heat Transfer and Molecular Mass Transfer in the Same Field in the Presence of High Temperature and Partial Pressure Differences), Forschungsheft 382, Forsch. Geb. Ing.-Wes. (1937).
43. W. K. Lewis: The Evaporation of Liquid into a Gas, Trans. ASME, 44 (1922), pp. 455-476.
44. E. R. Gilliland and T. K. Sherwood: Diffusion of Vapors into Air Streams, Ind. Eng. Chem. 26, No. 5 (1934), pp. 516-523.
45. L. D. Berman: Evaporative Cooling of Circulating Water, Pergamon Press, 1967.
46. W. E. Ranz and W. R. Marshall, Jr.: Evaporation from Drops, Parts I and II, Chem. Eng. Prog. 48 (1952), pp. 141-146, 173-180.
47. W. R. Marshall: Heat and Mass Transfer in Spray Drying, Trans. ASME, 77 (1955), pp. 1377-1385.
48. G. A. Hughmark: Mass and Heat Transfer from Rigid Spheres, AIChE Journal, 13 (1967), pp. 1219-21.
49. L. S. Bobe, D. D. Malyshev: Calculating the Condensation of Steam with a Cross-Flow of Steam Gas Mixture over Tubes, Thermal Engineering, 18, No. 12 (1971), pp. 126-130.
50. V. M. Semeyin: Teplootdacha Vlazhnovo vozduha pri kondensatsii para (Heat Transfer from Wet Air by Vapour Condensation), Teploenergetika, 4 (1956), pp. 11-15.
51. J. T. Schrodtt and E. R. Gerhard: Condensation of Water Vapour from a Non-Condensing Gas on Vertical Tubes in a Bank, Ind. Engng. Chem. Fundamentals, 4, No. 1 (1965), pp. 46-49.
52. L. D. Berman: Vliyanie potoka veshchestva na konvektivnuyu teplootdachu pri isparenii i kondensatsii (Mass Transfer Influence on Convective Heat Transfer in the Evaporation and the Condensation), Teploenergetika, 4, No. 2 (1956), pp. 25-30.
53. L. D. Berman: Eksperimentalnye isledovaniya kondensatsii para v prisustvii nekondensiruyushchihsya gazov (An Experimental Study of the Condensation of a Vapour in the Presence of Non-Condensable Gases), Teploenergetika, 5, No. 6 (1957), pp. 43-50.
54. L. D. Berman: Determining the Mass Transfer Coefficient in Calculations on Condensation of Steam Containing Air, Thermal Engineering, 16, No. 10 (1969), 95-99.

55. L. D. Berman: Generalization of Experimental Data Relating to Heat and Mass Transfer During the Condensation of Vapour in the Presence of a Non-Condensing Gas, *High Temperature*, 10, No. 3 (1972), pp. 520-526.
56. L. D. Berman: Simultaneous Process of Heat and Mass Transfer in Evaporation and Condensation, Paper No. E2.20 in Heat Transfer Session, 5. International Congress of Chemical Engineering Chemical Equipment Design and Automation, CHISA '75, Prague, Aug. 1975.
57. B. S. Bobe, V. A. Solouhin: Heat and Mass Transfer with Steam Condensation from Steam-Gas Mixture with Turbulent Flow Inside a Pipe, *Thermal Engineering*, 19, No. 9 (1972), pp. 40-43.
58. H. Kramers: Heat Transfer from Spheres to Flowing Media, *Physica* 12 (1946), pp. 61-80.
59. R. B. Keey and Glen: Mass Transfer from Solid Spheres, *Can. J. Che. Eng.*, 42 (1964), pp. 227-232.
60. R. Darke, Jr.: Discussion on the Paper of G. C. Vliet and G. Leippert, *Trans. ASME Ser. C, Heat Transfer*, 83 (1961), pp. 170-173.
61. D. M. Ward, O. Trass, A. I. Johnson: Mass Transfer from Fluid and Solid Spheres at Low Reynolds Numbers, *Can. J. Chem. Eng.*, 40 (1962), pp. 164-168.
62. M. M. El-Wakil, O. A. Uyehara and P. S. Myers: "A Theoretical Investigation of the Heating-Up Period of Injected Fuel Droplets Vaporizing in Air", NACA TN3179 (1954).
63. S. Lambiris and L. B. Combs: "Steady-State Combustion Measurements in Lox/RP-1 Rocket Chamber and Related Spray Burning Analysis," pp. 269-304, in the book: *Detonation and Two-Phase Flow*, edited by S. S. Penner and F. A. Williams, Academic Press (1962).
64. P. N. Rowe, K. T. Claxton and J. B. Lewis: "Heat and Mass Transfer from a Single Sphere in an Extensive Flowing Fluid", *Trans. Inst. Chem. Engrs.*, 43 (1965), pp. T14-T31.
65. E. N. Lightfoot: Estimation of Heat and Mass Transfer Rates, Chapter 2 in *A.I.Ch.E. Continuing Education Series #4* (1969).
66. M. Jakob: "Heat Transfer", Vol. 1, John Wiley (1949).
67. V. Arpaci: "Conduction Heat Transfer", Addison-Wesley (1966).

68. L. I. Rubinstein: The Stefan Problem, Vol. 27, Translation of Mathematical Monographs, American Mathematical Society, 1971.
69. N. Frösling: "The Evaporation of Falling Drop (Über die Verdunstung fallender Tropfen), A.E.R.E., Harwell, translation August, 1963, Beitr. Geophys., 52 (1938).
70. M. M. El-Wakil, R. J. Priem, H. J. Brikowski, P. S. Myers and O. A. Uyehara: "Experimental and Calculated Temperature and Mass Histories of Vaporizing Fuel Drops", NACA TN 3490 (1956).
71. J. J. Domingos; L. F. C. Roriz: The Prediction of Trajectories of Evaporating or Burning Droplets, 5th International Heat Transfer Conference, Vol. V, Sept. 1974, Tokyo.
72. R. J. Priem, G. L. Borman, M. M. El-Wakil, O. A. Uyehara and P. S. Myers: Experimental and Calculated Histories of Vaporizing Fuel Drops, NACA TN 3988 (1957).
73. A. V. Luikov, "Analytical Heat Diffusion Theory", Academic Press (1968).
74. The 1967 IFC Formulation for Industrial Use, The International Committee of 6th Conference of the Properties of Steam.
75. J. Juza: "Formulas for Thermodynamic Properties of Water and Steam for Industrial Calculation", Praha (1966).
76. H. Vesper: Näherungsgleichungen für die Zustandgrößen des Wassers und des Dampfes an den Grenzkurven zur Verwendung in elektronischen Rechenmaschinen (Approximate Equation for State Values of Water and Steam on the Upper and the Lower Boundary Curve for the Application in Electronic Calculators), Brennstoff-Wärme-Kraft, 15, No. 1 (1963), pp. 20-23.
77. VDI - Wasserdampfataeln, Berlin (1963).
78. A Lekić: "The Analysis of the Accuracy of the Equations of Thermodynamic Properties of Water and Steam in the Comparison with the International and Other Tables", Energoinvest, ITEN (1967).
79. F. A. Holland, et al: "Heat Transfer", Heineman Educational Books, London (1970).
80. R. C. Reid and J. K. Sherwood: "The Properties of Gases and Liquids", McGraw-Hill (1956).
81. R. B. Bird, W. E. Stewart and E. L. Lightfoot: Transport Phenomena, John Wiley, 1960.

82. W. M. Rohsenow, J. P. Hartnett: Handbook of Heat Transfer, McGraw-Hill, 1973.
83. N. B. Vargaftik: Spravotschnik po teplofizitscheskim svoystvam gasov, zhidhostey (Handbook of Physical Properties of Gases and Liquids), Nauka, Moscow, 1972.
84. C. L. Tien: Heat Transfer by a Turbulently Flowing Fluid-Solids Mixture in a Pipe, Journal of Heat Transfer, 3, No. 5 (1961), pp. 183-188.
85. W. P. Manning and W. H. Gauvin: Heat and Mass Transfer to Decelerating Finely Atomized Sprays, A.I.Ch. Jl., 6, No. 2 (1960), pp. 184-190.
86. E. R. G. Eckert: Engineering Relations for Heat Transfer and Friction in High Velocity Laminar and Turbulent Boundary Layer Flow over Surfaces and Constant Pressure and Temperature, Trans. ASME, 78 (1959), pp. 1273-1283.
87. S. K. Banerjee: Transient Cooling of a Sphere Due to Boiling, M.S. Thesis, University of Missouri-Rolla (1972).
88. A. L. Crosbie and S. K. Banerjee: Quenching of a Solid Sphere in Oil, Wärme-und Stoffübertragung 7 (1974), pp. 113-120.
89. A. Lekić, "The Rate of Growth of Drop During Condensation", M.A.Sc. Thesis, University of Waterloo (1970).
90. A. F. Mills and R. A. Seban: The Condensation Coefficient of Water, Int. Jl. of Heat & Mass Transfer, 10 (1967), pp. 1815-1827.
91. G. Brown, "Heat Transmission by Condensation of Steam on a Spray of Water Drops", Ph.D. Thesis, Imperial College of Science and Technology (1948).
92. S. S. Kutateladze, V. H. Borishanskii, "A Concise Encyclopedia of Heat Transfer", Pergamon (1966).
93. Internal AECL Documentation.
94. M. Jakob: Heat Transfer, Vol. 2, John Wiley (1956).
95. D. Ackermann: Wärme und Stoffübergangskoeffizienten bei der Abkühlung von dampf/Gas Gemischen in Oberflächenkondensatoren (Heat and Mass Transfer Coefficients by Cooling of Steam/Gas Mixtures in Surface Condensers), Chemie Ingr. Techn., 44, No. 5 (1972), pp. 274-280.

96. W. Renker: Der Wärmeübergang bei der Kondensation von Dämpfen in Anwesenheit nichtkondensierender Gase (Heat Transfer in Condensation of Steam in the Presence of Noncondensable Gases), Chem. Techn., 7, No. 8 (1955), pp. 451-461.
97. J. D. Ford and A. Lekić: Rate of Growth of Drops During Condensation, Int. J. Heat Mass Transfer, 16 (1973), pp. 61-64.
98. E. M. Sparrow and S. H. Lin: Condensation Heat Transfer in the Presence of a Non-Condensable Gas, Trans. ASME (Series C), No. 8 (1964), pp. 430-436.
99. D. G. Kroger and W. M. Rohsenov: Condensation Heat Transfer in the Presence of Non-Condensable Gas, Int. J. Heat & Mass Transfer, 11 (1968), pp. 15-26.
100. E. Marshall and R. Meyder: On Condensation Mass Transfer in the Presence of Non-Condensables, Wärme-und Stoffübertragung, 3 (1970), pp. 191-196.
101. F. H. Garner and P. Kendrick: Mass Transfer to Drops of Liquid Suspended in a Gas Stream, Part I: A Wind Tunnel for the Study of Individual Liquid Drops, Trans. Instn. Chem. Engrs. (London), 37 (1959), pp. 155-161.
102. H. L. Dryden and G. B. Schubauer: The Use of Damping Screens for the Reduction of Wind-Tunnel Turbulence, J. Aero. Sci., 14 (1947), pp. 221-228.
103. P. F. Bennewitz: The Brady Array - A New Bulk-Effect Humidity Sensor, Society of Automotive Engineers, Automobile Engineering Meeting, Detroit, May 14-18, 1973.
104. W. E. Ranz: On the Evaporation of a Drop of Volatile Liquid in High Temperature Surrounding, Trans. ASME, 78 (1956), pp. 909-913.
105. P. M. Reilly: Introduction to Statistical Methods, University of Waterloo, Chemical Engineering Department, 1974.
106. P. Harriot: A Review of Mass Transfer Interfaces, Can. J. Chem. Eng., 40 (1962), pp. 60-69.
107. The Atomic Energy of Canada Ltd., Internal Publication.
108. K. McLean: M.A.Sc. Thesis, University of Waterloo, Chemical Engineering Department, in preparation.
109. H. Syhre: Einige theoretische Betrachtungen zur Kondensation an wassertropfen (Some Theoretical Treatments of the Condensation on Water Droplets), Energietechnik, 11, No. 9 (1961), pp. 401-406.

110. V. I. Kushnyrev: Eksperimentalnoe issledovanie processa dispergovania zhidkosti primenitelno k smesitelnoy kondensacii (Experimental Investigation of the Disintegration Processes of the Liquids Applied to the Direct Contact Condensation), Trudy MEI Teploenergetika i mashinostroenie, vip. 104, 1972.
111. N. I. Gelperin, B. N. Basargin, V. S. Galustov, V. V. Shuvalov: Issledovanie dispersnosti raspyla centribezno struynoi forsunki (Examination of Atomization by Centrifugal Nozzle), Himitscheskoe and neftnoe mashinostroenie, No. 11, 1972, pp. 15-16.
112. J. O. Hinze: Fundamentals of the Hydrodynamic Mechanism of Splitting in Dispersion Processes, A.I.Ch.E. Journal, 1 (1955), pp. 289-295.
113. W. R. Sears, M. Van Dyke, editors: Annual Review of Fluid Dynamics, Vol. 1, Annual Review Inc., 1969.
114. R. S. Brodkey: The Phenomena of Fluid Motions, Addison-Wesley, 1967.
115. I. Yaron, B. Gal-or: Convective Mass and Heat Transfer from Size Distributed Drops, Bubbles or Solid Particles, Int. J. Heat Mass Transfer, 14 (1971), pp. 727-737.
116. E. Kulic, E. Rhodes, G. Sullivan, K. McLean: Direct Contact Condensation from Air/Steam Mixtures on Falling Sprays, 5.- International CHISA Congress, Heat Transfer Section, Paper #E2.1, Prague, Aug. 25-29, 1975.
117. A. Lekić, R. Bajramović, J. D. Ford: Droplet Size Distribution: An Improved Method for Fitting Experimental Data, Submitted for publication in The Canadian Journal of Chemical Engineering.
118. R. A. Mugele and H. D. Evans: Droplet Size Distribution in Sprays, Ind. Eng. Ch., 43, No. 6 (1951), pp. 1317-1324.
119. W. E. Stewart: Solution of Transport Problems by Collocation Methods, A.I.Ch.E. Continuing Education Series #4 (1969).
120. R. A. Greenkorn and D. P. Kessler: Transfer Operations, McGraw-Hill, 1972.
121. P. M. Reilley: Engineering Statistics, Ch. E. 622, University of Waterloo, 1975.
122. R. A. Mugele: Maximum Stable Droplets in Dispersoids, A.I.Ch.E. Journal, 6, No. 1 (1960), pp. 3-8.

NOMENCLATURE

a	Ratio of heat fluxes caused by the concentration and temperature driving forces, defined by the equation (11)
a_1	Constant defined in Table 1, see Appendix B
$b = \frac{x_m - x_{50}}{x_{50}}$	Skewness parameter in upper limit equation (73)
A	Area of a droplet m^2
A, B	Constants in equations (18) and (19)
A_1, A_2, A_3, A_4, A_5	Constants in equation (81)
C_1, C_2, C	Constants defined by the equations (21), (22), and (23), respectively
$C_M, C_{AM}, C_{SM}, C_{Si}$	Molar concentrations of: an air/steam mixture; air in a mixture; steam in a mixture; steam at the interface, respectively $kg\ moles/m^3$
C_D, C_D^D, C_D^S	Drag coefficient of: a droplet, a disk and a sphere, respectively
C_{Dmax}	Drag coefficient value at the maximum value d^* , see Table 1 of Appendix B
c_v	Specific heat at constant volume, $J/kg^\circ C$
c_{pw}	Specific heat at constant pressure of a droplet $J/kg^\circ C$
C_{PA}, C_{PS}	Molar heat capacities of air and steam, respectively $J/kg\ mole\ ^\circ K$

d	Droplet diameter m
$d^* = N_{Re}^2 / N_{Fr}$ $= 3\rho_M^2 g / \mu^2$	Reinhart's dimensionless diameter
d_{max}^*	Maximum value of d^* , see Table 1 of Appendix B
D_{AB}	Diffusivity of steam in air m^2/s
E_M, E_W	Energy content of mixture and water, respectively kJ
E_{WE}, E_{WL}	Energy of water entering and leaving dousing chamber, respectively kJ
f	Condensation coefficient
$f(x)$	Distribution function
F	Mass transfer coefficient $kg\ moles/m^2s$
F_b	Body force N
$g = 9.80665$	Gravity acceleration m/s^2
$h_\sigma, h_{\sigma M}, h_F, h_{FM}$	Heat transfer coefficients defined by equations (50) and (50a), (51) and (51a), respectively $J/m^2s^\circ K$
h_c	Convective or sensible heat transfer coefficient $J/m^2s^\circ K$
h_{app}	Apparent heat transfer coefficient defined by equation (26), $J/m^2s^\circ K$
h_M, h_w	Enthalpies of air/steam mixture and water, respectively kJ/kg
j_s	Mass flux defined by equation (17), kg/m^2s

k	Thermal conductivity of a droplet	$J/ms^{\circ}K$
$m = (1/6)\pi d^3 \rho_D$	Mass of a droplet	kg
m_M, m_W	Masses of air/steam mixture and water, respectively	kg
M_A, M_S	Molecular weights of air and steam, respectively	kg/kg mole
N_A, N_S	Molar fluxes of air and steam, respectively	kg moles/ m^2s
N_{AC}	Ackermann number defined by equation (10)	
$N_{Bi} = h_{app} d / 2k$	Biot number	
$N_{FO} = \frac{\alpha t}{R^2}$	Fourier number	
$N_{Fr} = \frac{V_R^2}{dg}$	Froud number	
N_{Gr}	Grashof number	
$N_{Nu} = \frac{hd}{k}$	Nusselt number	
$N_{Pr} = \frac{C_p \mu}{k} = \frac{\nu}{\alpha}$	Prandtl number	
$N_{Re} = \frac{V_R d \rho_M}{\mu} = d^* V_R^*$	Reynolds number	
$N_{Sc} = \frac{\mu}{\rho D_{AB}} = \frac{\nu}{D_{AB}}$	Schmidt number	
$N_{Sh} = \frac{Fd}{C_M D_{AB}}$	Sherwood number	
$N_{Su} = \frac{c d \rho_M}{2 \mu_M} = N_{Re} / We$	Drop deformation number	

$N_{We} = \frac{V_R^2 d \rho_M}{\sigma}$	Weber number
P_M	Total pressure of a mixture N/m^2 , Bar
P_{AM}, P_{SM}	Partial pressure of air and steam in a mixture, respectively N/m^2 , Bar
P_{sat}	Saturation pressure of steam N/m^2 , Bar
P_{Si}	Partial pressure of steam at the interface N/m^2 , Bar
Q_T, Q_L, Q_S	Total, latent and sensible heat fluxes to a droplet $J/m^2 s$
Q_{LS}	Heat losses to surrounding fluid, kJ
r	Distance from any point in a droplet to its centre m
R	Radius of a droplet m
R_g	Universal gas constant $J/kg^\circ K$
R_M, R_S	Mixture and steam constant, respectively, $J/kg^\circ K$
$S = N_{Re}^4 N_{Fr} / N_{We}^3 = \rho_M \sigma^3 / g \mu^4$	Reinhart's system constant
t	Time s
T_i, \bar{T}, T	Initial, average temperatures and a temperature at any time instant of droplet, respectively $^\circ C$
T_M	Initial temperature of air-steam mixture $^\circ C$
T_{sat}	Saturation temperature of steam, $^\circ C$
T_w	Wall temperature, $^\circ C$
u_M	Internal energy of mixture, kJ/kg

v_D, v_M	Velocity of a droplet and the mixture, respectively, [m/s]
v_{D0}	Initial velocity of a droplet, [m/s]
v_R, v_{R0}, v_{RT}	Relative, initial and terminal relative velocity, [m/s]
v_g, v_l	Specific volumes of the vapour and water at saturation pressure m^3/kg
v	Volume fraction of droplets having diameter $< x$
$V_R^* = \frac{3}{\sqrt{N_{Re} N_{Fr}}} = V_R \frac{3}{\rho_M \mu g}$	Reinhart's dimensionless velocity
x	Diameter of particles
\bar{x}	Average droplet diameter defined by equation (84)
x_m	Maximum stable droplet diameter
x_{50}	Droplet diameter at $V = 0.5$
X_A, X_S	Volume fractions of air and steam in a mixture, respectively
y	Dimensionless function of x (equation (83))
z	Distance travelled m
$Z = \frac{(P_{SM} V_R)^{1/3} t}{m^{1/3}}$	Dimensionless parameter used in equation (75)
Π_W, Π_g	Dimensionless numbers defined by equation (16)

Greek Letters

$\alpha = k/\rho_D C_p$	Thermal diffusivity of a droplet m^2/s
δ	Size distribution parameter used in equation (73) and (82)
Δ	Difference
$\theta = \frac{T - T_i}{T_M - T_i}$	Thermal utilization
λ	Latent heat of water vaporization J/kg
μ_M	Dynamic viscosity of a mixture Ns/m^2
π	3.14159
ν	Kinematic viscosity m^2/s
σ	Surface tension N/m
ρ_D, ρ_M	Density of a droplet and mixture kg/m^3
ϵ_s	Dimensionless number defined by equation (12)

APPENDIX A

SOME ANALYTICAL SOLUTIONS OF THE MACROSCOPIC
MOMENTUM EQUATION FOR A SPHERE

In this approach are presented solutions obtained either from the literature or by the author for the relative velocity v_R and position z of a sphere after it has been injected in an air/steam mixture with an initial velocity v_{Ro} .

CASE 1. In the Stokes region ($N_{Re} < 0.1$) the drag coefficient can be represented by

$$C_D = N_{Re}/24 \quad C_D = \frac{24}{N_{Re}} \quad (A.1)$$

The solutions obtained are the same as those obtained by Lapple [24].

$$v_R = g/A + (v_{Ro} - g/A) \exp(-At) \quad (A.2)$$

$$z = (g/A - v_M)t + (v_{Ro}/A - g/A^2)[1 - \exp(-At)] \quad (A.3)$$

where

$$A = 18\mu_M/\rho_D d^2 \quad (A.4)$$

CASE 2. In the region of $0.1 < N_{Re} < 2$ the standard solid sphere drag coefficient curve can be approximated by:

$$C_D = \frac{24}{N_{Re}} \left(1 + \frac{3}{16} N_{Re} \right) \quad (A.5)$$

Thus

$$v_R = \frac{G + H \exp(Dt/2)}{F \exp(Dt/2) - E} \quad (A.6)$$

and

$$z = (2G/DE + 2H/DF) \ln \frac{F \exp(Dt/2) - E}{F - E} - (G/E + v_M)t \quad (A.7)$$

where

$$B = \frac{27}{8} \frac{\rho_M}{d\rho_D}, \quad \Delta = -4Bg - A^2; \quad D_2 = D_1 + 2D \quad (A.8)$$

$$D = (-\Delta)^{1/2}, \quad D_1 = -2Bv_{Ro} - A - D; \quad E = -2BD_1 \quad (A.9)$$

$$F = -2BD_2, \quad G = D_1(D - A); \quad H = D_2(D + \Delta) \quad (A.10)$$

These expressions were not found in literature and were derived by the author by solving the equation of motion of the sphere.

CASE 3. In the range of $2 < N_{Re} < 500$ the standard solid sphere drag coefficient curve can be represented [25] by:

$$C_D = 16/N_{Re}^{1/2} \quad \text{for} \quad 2 < N_{Re} < 10 \quad (\text{A.11})$$

$$C_D = 11.5/N_{Re}^{1/2} \quad \text{for} \quad 10 < N_{Re} < 500 \quad (\text{A.12})$$

In this case, only an implicit relationship could be derived for the droplet velocity as a function of time t . This is given in equation (A.12).

$$t = \frac{2}{3IJ^{1/3}} \left\{ \frac{1}{2} \ln \left[\frac{(J^{2/3} + J^{1/3}v_R^{1/2} + v_R)(J^{1/3} - v_{Ro}^{1/2})^2}{(J^{1/3} - v_R^{1/2})^2(J^{2/3} + J^{1/3}v_{Ro}^{1/2} + v_{Ro})} \right] - \sqrt{3} \tan^{-1} \frac{2(v_R^{1/2} - v_{Ro}^{1/2})}{\sqrt{3} J^{1/3} + (2v_R^{1/2} + J^{1/3})(2v_{Ro} + J^{1/3})} \right\} \quad (\text{A.13})$$

with

$$I = g/J \quad (\text{A.14})$$

$$J = gd^{3/2} \rho_D / 12 \rho_M^{1/2} \mu_M^{1/2} \quad \text{for} \quad 2 < N_{Re} < 10 \quad (\text{A.15})$$

and

$$J = gd^{3/2} \rho_D / 8.625 \cdot \rho_M^{1/2} \mu_M^{1/2} \quad \text{for} \quad 10 < N_{Re} < 500 \quad (\text{A.16})$$

In this case it was not possible to obtain an analytical solution for the distance travelled.

CASE 4. In the region where the Newton's law applies, i.e.

$500 < N_{Re} < 2 \cdot 10^5$, the drag coefficient is

$$C_D = 0.44 \quad (\text{A.17})$$

an elegant solution can be obtained for both the velocity and the distance travelled

$$v_R = \frac{\tanh(Cgt) + C v_{Ro}}{C[1 + C v_{Ro} \tanh(Cgt)]} \quad (\text{A.18})$$

where

$$C = 0.33 \cdot \rho_M / \rho_D \cdot g \cdot d \quad (\text{A.19})$$

The distance travelled depends upon the initial relative velocity:

- a) When the initial relative velocity of a drop v_{Ro} is smaller than its terminal relative velocity v_{RT} , then:

$$z = \frac{1}{C^2 g} \ln \frac{\cosh[Cg(t - C_1)]}{\cosh[-CC_1g]} - v_M \cdot t \quad (\text{A.20})$$

- b) When the initial relative velocity of a drop v_{Ro} is greater than its terminal relative velocity v_{RT} , then: *

$$z = \frac{1}{C^2 g} \ln \frac{\sinh[Cg(t - C_1)]}{\sinh[-CC_1g]} - v_M \cdot t \quad (\text{A.21})$$

where

$$C_1 = -\frac{1}{2gC} \ln \left| \frac{1 + C v_{Ro}}{1 - C v_{Ro}} \right| \quad (\text{A.22})$$

The relative terminal velocity is in both the cases

$$v_{RT} = 1/C \quad (A.23)$$

It was first believed that derivations of the last two cases were new, however it has been recently discovered that a similar approach was used in [6] which confirms the validity of the solution.

It is possible to obtain corresponding analytical solutions for a sphere initially moving upwards. The solutions are slightly different from those already derived for a downwards movement of a sphere until the moment when the droplet reaches its maximum height. From this moment on the derived equations will hold.

APPENDIX B

REINHART'S CORRELATIONS FOR DROPLET DRAG COEFFICIENT

$$S = N_{Re}^7 N_{Ti} / N_{Re}^3 = \frac{\rho_M c}{g_{Ti}}$$

APPENDIX B

REINHART'S DRAG COEFFICIENT FOR DROPLETS

DOMAIN	$C_D = f(N_{Re}, S, \Delta\rho/\rho)$	UPPER LIMIT OF VALIDITY	
		$d^* = f(\Delta\rho/\rho, S)$ AND/OR $N_{Re} = f(\Delta\rho/\rho, S)$	
I	$C_D = 24/N_{Re}$	$d^* = 1.216/(\Delta\rho/\rho_M)^{1/3}$	$N_{Re} = 0.1$
II ^a $S < 44 \cdot 10^{12}$	$C_D = \frac{24}{N_{Re}} (1 + 0.15 N_{Re}^{0.687})$	$d^* = 70 \left(\frac{\Delta\rho}{\rho_M}\right)^{-1/3} (10^{-12} S)^{-0.111}$	$N_{Re} = 974 (10^{-12} S)^{-0.192}$
II ^b $S > 44 \cdot 10^{12}$	OR ANY OTHER VALID CORRELATION FOR SOLID SPHERES	$d^* = 30.8 \left(\frac{\Delta\rho}{\rho_M}\right)^{-1/3} (10^{-12} S)^{-0.111}$ \uparrow S	$N_{Re} = 236 (10^{-12} S)^{0.192}$
III ^a $S < 44 \cdot 10^{12}$	$C_D = 0.43 (10^{-12} S)^{0.05}$	$d^* = 122 \left(\frac{\Delta\rho}{\rho_M}\right)^{-0.535} (10^{-12} S)^{0.275}$	$N_{Re} = 2240 \left(\frac{\Delta\rho}{\rho_M}\right)^{-0.303} (10^{-12} S)^{0.388}$
III ^b $S > 44 \cdot 10^{12}$	$C_D = 0.7 (10^{-12} S)^{-0.05}$	$d^* = 300 \left(\frac{\Delta\rho}{\rho_M}\right)^{-0.535} (10^{-12} S)^{0.0367}$	$N_{Re} = 7160 \left(\frac{\Delta\rho}{\rho_M}\right)^{-0.303} (10^{-12} S)^{0.08}$
IV	$C_D = 0.0657 d^* \left(\frac{\Delta\rho}{\rho_M}\right)^{0.224} (10^{-12} S)^{-0.065}$	$d^* = 160 \left(\frac{\Delta\rho}{\rho_M}\right)^{-0.447} (10^{-12} S)^{0.114}$	$N_{Re} = 3190 \left(\frac{\Delta\rho}{\rho_M}\right)^{-0.173} (10^{-12} S)^{0.18}$
V MAXIMUM	$C_D = 0.00335 \left(\frac{\Delta\rho}{\rho_M}\right)^{0.447} (10^{-12} S)^{-0.131} d^*$ $C_{Dmax} = 0.75 \left(\frac{\Delta\rho}{\rho_M}\right)^{-0.0232} (10^{-12} S)^{0.036}$	$d^*_{max} = 224 \left(\frac{\Delta\rho}{\rho_M}\right)^{-0.5} (10^{-12} S)^{1/6}$	$N_{Re} = N_{Re_{max}} = 4470 \left(\frac{\Delta\rho}{\rho_M}\right)^{-0.238} (10^{-12} S)^{0.232}$
VI	$C_D = C_{Dmax} + a_1 (d^* - d^*_{max})$ $a_1 = 0.035 - \frac{1}{29.54} \log \left\{ \left[\frac{S^{0.5}}{\Delta\rho \rho_M} \right] 10^3 \right\}$	HYDRODYNAMIC STABILITY OF A DROPLET	HYDRODYNAMIC STABILITY OF A DROPLET

APPENDIX C

EVALUATION OF THE DROPLET TEMPERATURE RESPONSE
WITH INTERNAL RESISTANCE AND NO INTERNAL MIXING

Equation (36) can be rewritten as (for the seventh order polynomial)

$$f_1(r) = T_M - (A_0 + A_1 r + A_2 r^2 + A_3 r^3 + \dots + A_7 r^7) \quad (C.1)$$

Introducing this into equation (34) it yields

$$\begin{aligned} \theta(r, t) = \sum_{n=1}^{n=\infty} \frac{2\psi_n}{\psi_n - \sin \psi_n \cos \psi_n} \frac{\sin(\psi_n r/R)}{rR} \exp(-\psi_n^2 N_{Fo}) \cdot \\ \cdot \int_0^R r [T_M - (A_0 + A_1 r + A_2 r^2 + A_3 r^3 + \dots + A_7 r^7)] \cdot \\ \cdot \sin(\psi_n r/R) dr \end{aligned} \quad (C.2)$$

Considering just the integral in the last equation, one obtains

$$\begin{aligned} I = T_M \int_0^R r \sin(\psi_n r/R) dr - A_0 \int_0^R r \sin(\psi_n r/R) dr - \\ - A_1 \int_0^R r^2 \sin(\psi_n r/R) dr + A_2 \int_0^R r^3 \sin(\psi_n r/R) dr + \\ + \dots + A_7 \int_0^R r^8 \sin(\psi_n r/R) dr \end{aligned} \quad (C.3)$$

Denoting the integrals with T_M and A_0 to A_7 by $I_M, I_0, I_2, \dots, I_7$, the last integral can be rewritten as

$$I = I_M + \sum_{i=0}^7 I_i \quad (C.4)$$

It is possible now to evaluate every single integral by the simple integration by parts. Thus

$$I_M = T_M \int_0^R r \sin(\psi_n r/R) dr \quad (C.5)$$

and

$$\int u dv = uv - \int v du \quad (C.6)$$

$$dv = \sin(\psi_n r/R) dr \quad ; \quad u = r$$

or

$$v = -\frac{R}{\psi_n} \cos(\psi_n r/R) \quad ; \quad dv = dr$$

and

$$I_M = T_M \left\{ -\frac{rR}{\psi_n} \cos(\psi_n r/R) \Big|_0^R + \int \frac{R}{\psi_n} \cos(\psi_n r/R) dr \right\}$$

and

$$\begin{aligned} I_M &= T_M \left\{ -\frac{R^2}{\psi_n} \cos \psi_n + \frac{R}{\psi_n} \left[\frac{R}{\psi_n} \sin(\psi_n r/R) \right] \Big|_0^R \right\} \\ &= T_M \left\{ \frac{R^2}{\psi_n^2} (\sin \psi_n - \psi_n \cos \psi_n) \right\} \end{aligned}$$

and finally

$$I_M = T_M \frac{R^2}{\psi_n^2} (\sin \psi_n - \psi_n \cos \psi_n) \quad (C.7)$$

Similarly, the second integral yields

$$I_0 = A_0 \frac{R^2}{\psi_n^2} (\sin \psi_n - \psi_n \cos \psi_n) \quad (C.8)$$

The next integral is

$$I_1 = A_1 \int_0^R r^2 \sin(\psi_n r/R) dr$$

Performing the integration by parts twice gives:

$$I_1 = A_1 \frac{R^3}{\psi_n^3} [2\psi_n \sin \psi_n - (\psi_n^2 - 2) \cos \psi_n - 2] \quad (C.9)$$

Furthermore, the integral I_2 is

$$I_2 = A_2 \int_0^R r^3 \sin(\psi_n r/R) dr$$

After the first integration is performed, the integral with lower power of r is obtained. Thus one can use the previous integration step in the evaluation of the higher power integral, to obtain

$$I_2 = A_2 \frac{R^4}{\psi_n^4} [3(\psi_n^2 - 2) \sin \psi_n - \psi_n(\psi_n^2 - 6 \cos \psi_n)] \quad (C.10)$$

Using the same technique the remaining integrals are evaluated

$$\begin{aligned} I_3 &= A_3 \int_0^R r^4 \sin(\psi_n r/R) dr \\ &= A_3 \frac{R^5}{\psi_n^5} [4\psi_n(\psi_n^2 - 6) \sin \psi_n - (\psi_n^4 - 12\psi_n^2 + 24) \cos \psi_n + 24] \end{aligned} \quad (C.11)$$

$$\begin{aligned} I_4 &= A_4 \int_0^R r^5 \sin(\psi_n r/R) dr = A_4 \frac{R^6}{\psi_n^6} [5\psi_n^4 - 60\psi_n^2 + 120) \sin \psi_n - \\ &\quad - \psi_n(\psi_n^4 - 20\psi_n^2 + 120) \cos \psi_n] \end{aligned} \quad (C.12)$$

$$\begin{aligned}
I_5 = A_5 \int_0^R r^6 \sin(\psi_n r/R) dr &= A_5 \frac{R^7}{\psi_n^7} [\psi_n (6\psi_n^4 - 120\psi_n^2 + 720) \sin \psi_n \\
&- (\psi_n^6 - 30\psi_n^4 + 360\psi_n^2 - 720) \cos \psi_n - 720] \quad (C.13)
\end{aligned}$$

$$\begin{aligned}
I_6 = A_6 \int_0^R r^7 \sin(\psi_n r/R) dr &= A_6 \frac{R^8}{\psi_n^8} [(7\psi_n^6 - 210\psi_n^4 + 2520\psi_n^2 \\
&- 5040) \sin \psi_n - \psi_n (\psi_n^6 - 42\psi_n^4 + 840\psi_n^2 - 5040) \cos \psi_n] \\
&\quad (C.14)
\end{aligned}$$

and finally

$$\begin{aligned}
I_7 = A_7 \int_0^R r^8 \sin(\psi_n r/R) dr &= A_7 \frac{R^9}{\psi_n^9} [\psi_n (8\psi_n^6 - 336\psi_n^4 + 6720\psi_n^2 \\
&- 40320) \sin \psi_n - (\psi_n^8 - 56\psi_n^6 + 1680\psi_n^4 - 20160\psi_n^2 \\
&+ 40320) \cos \psi_n + 40320] \quad (C.15)
\end{aligned}$$

Introducing the values of integrals $I_M, I_0, I_1, \dots, I_7$ into equation (34), equation (37) is obtained.

APPENDIX DTHERMODYNAMICS AND TRANSPORT PROPERTIES OF WATER,
AIR, STEAM AND THEIR MIXTURE

viscosity of steam μ_s
 viscosity of air μ_a
 viscosity of steam-air mixture μ_{mix}
 thermal conductivity of air k_a
 " " " steam k_s
 " " " mixture k_{mix}
 diffusivity of water vapor through air D
 surface tension of water σ

saturation pressure P_s
 saturation temperature T_s
 density of water ρ
 specific volume of water v
 density of saturated steam ρ_s
 specific volume of " " steam v_s
 density of saturated water ρ_w
 specific volume of " " water v_w
 enthalpy of saturated water h_w
 " " " steam h_s
 heat capacity of water c_p
 " " " steam c_{ps}
 thermal conductivity of water k_w
 " " " steam k_s

D.1 Saturation Pressure

Steam saturation pressure $P_s = f(T)$ is determined from Vesper's (76) correlation

$$\ln P_s = \sum_{i=0}^{i=9} A_i X^i \quad (\text{Bar}) \quad (\text{D.1.1})$$

where

$$X = \frac{t}{100}$$

t - temperature in $^{\circ}\text{C}$

$$\begin{aligned} A_0 &= -5.0982373 \cdot 10^0 & A_5 &= 2.4775634 \cdot 10^{-1} \\ A_1 &= 7.2704899 \cdot 10^0 & A_6 &= -8.6590250 \cdot 10^{-2} \\ A_2 &= -3.0337268 \cdot 10^0 & A_7 &= 2.0153393 \cdot 10^{-2} \\ A_3 &= 1.2567591 \cdot 10^0 & A_8 &= -2.6934527 \cdot 10^{-3} \\ A_4 &= -5.6086594 \cdot 10^{-1} & A_9 &= 1.5531799 \cdot 10^{-4} \end{aligned} \quad (\text{D.1.2})$$

Equation (D.1.1) is valid for $0 \leq t \leq 374.15^{\circ}\text{C}$. Accuracy of this equation is less than 0.02% for $t < 300^{\circ}\text{C}$ and less than 0.01% for $t > 300^{\circ}\text{C}$, see Lekić [78].

D.2 Saturation Temperature

Steam saturation temperature $T_s = f(P)$ is determined using Vesper's [76] correlation

$$T_s = \sum_{i=0}^{i=11} A_i [\ln (1.01972 P)]^i \quad ^{\circ}\text{C} \quad (\text{D.2.1})$$

where

P - pressure in Bar

$$\begin{aligned}
 A_0 &= 9.9092712 \cdot 10^1 & A_6 &= - 3.7393484 \cdot 10^{-4} \\
 A_1 &= 2.7854242 \cdot 10^1 & A_7 &= - 1.7417752 \cdot 10^{-5} \\
 A_2 &= 2.7537565 \cdot 10^0 & A_8 &= 2.2071712 \cdot 10^{-5} \\
 A_3 &= 2.1077805 \cdot 10^{-1} & A_9 &= 1.5343731 \cdot 10^{-6} \\
 A_4 &= 2.1296820 \cdot 10^{-2} & A_{10} &= - 4.2685685 \cdot 10^{-7} \\
 A_5 &= 1.3283773 \cdot 10^{-1} & A_{11} &= - 4.2924603 \cdot 10^{-8}
 \end{aligned} \tag{D.2.2}$$

Equation (D.2.1) is valid for $0.006108 \leq P \leq 221.2$ Bar, and agreement with the table values is less than 0.06°C .

D.3 Density and Specific Volume of Water

Density of water is determined from

$$\rho = \frac{1}{v} \quad \text{kg/m}^3 \tag{D.3.1}$$

where v - specific volume of water, m^3/kg .

A specific volume of water is determined using the Tratz [77] equation

$$\begin{aligned}
 v &= \frac{G}{W^{1/3.4}} - H - K \cdot \tau + (n - \tau)^2 [L + (n - \tau)^8 M] \\
 &\quad - \frac{N(q + r\sigma + \sigma^2)}{z + \tau^{11}}
 \end{aligned} \tag{D.3.2}$$

where:

$$W = U - [kU^2 + l(\sigma - m\tau)]^{1/2} \tag{D.3.3}$$

$$U = f - g\tau^2 - h\tau^{-6} \quad (D.3.4)$$

$$\tau = \frac{T}{T_c} = \frac{t + 273.15}{647.3} \quad (D.3.5)$$

$$\sigma = \frac{P}{P_c} = \frac{P}{221.286} \quad (D.3.6)$$

P_c, T_c - critical pressure and temperature

t - temperature in $^{\circ}\text{C}$

P - pressure in Bar.

$$\begin{array}{lll} A = 4.17 \cdot 10^{-1} & M = 7.676621 \cdot 10^{-1} & g = 3.122199 \cdot 10^8 \\ H = 1.139706 \cdot 10^{-4} & N = 1.052358 \cdot 10^{-11} & h = 1.999850 \cdot 10^5 \\ K = 9.949927 \cdot 10^{-5} & f = 3.7 \cdot 10^8 & k = 1.72 \cdot 10^0 \\ L = 7.24165 \cdot 10^{-5} & n = 6.537154 \cdot 10^{-1} & r = 1.310268 \cdot 10^1 \\ l = 1.362926 \cdot 10^{16} & q = 6.25 \cdot 10^1 & z = 1.5108 \cdot 10^{-5} \\ m = 1.500705 \cdot 10^0 & & \end{array} \quad (D.3.7)$$

Comparison of the values obtained using the Tratz equation with The 1967 IFC Formulation shows the differences less than 0.05% for $t < 300^{\circ}\text{C}$ and $P < 400$ Bar.

D.4 The Density and the Specific Volume of the Saturated Steam

The specific volume of the saturated steam ^(v'') is determined from the product $P_s v''$ as proposed by Vesper [76] according to:

$$P_s v'' = \sum_{i=0}^{i=8} A_i X^i, \quad \text{Bar} \frac{\text{m}^3}{\text{kg}} \quad (D.4.1)$$

where

$$X = \frac{t_s}{100}$$

t_s - saturation temperature in °C

$$\begin{aligned} A_0 &= 1.2602044 \cdot 10^0 & A_5 &= 3.3488548 \cdot 10^{-2} \\ A_1 &= 4.5905064 \cdot 10^{-1} & A_6 &= -1.5087828 \cdot 10^{-2} \\ A_2 &= -7.0419435 \cdot 10^{-3} & A_7 &= 3.1565330 \cdot 10^{-3} \\ A_3 &= 1.1476149 \cdot 10^{-4} & A_8 &= -2.4890060 \cdot 10^{-4} \\ A_4 &= -3.8647589 \cdot 10^{-2} \end{aligned} \quad (D.4.2)$$

and

$$v'' = \frac{(P_s v'')}{P_s}, \quad \text{m}^3/\text{kg} \quad (D.4.3)$$

and the density

$$\rho = \frac{1}{v''}, \quad \text{kg/m}^3 \quad (D.4.4)$$

D.5 The Density of and the Specific Volume of Saturated Water

The specific volume of saturated water ^(v') was determined from Vesper [76] equation:

$$v' = \sum_{i=10}^{i=9} A_i X^i \quad (D.5.1)$$

where

$$X_1 = \frac{t}{100}$$

$$\begin{aligned}
 A_0 &= 1.0001189 \cdot 10^{-3} & A_5 &= 5.2428875 \cdot 10^{-4} \\
 A_1 &= 5.3740533 \cdot 10^{-6} & A_6 &= - 2.8652450 \cdot 10^{-4} \\
 A_2 &= - 2.67941471 \cdot 10^{-5} & A_7 &= 9.0664926 \cdot 10^{-5} \\
 A_3 &= 3.0237718 \cdot 10^{-4} & A_8 &= - 1.5437041 \cdot 10^{-5} \\
 A_4 &= - 5.5126569 \cdot 10^{-4} & A_9 &= 1.0968357 \cdot 10^{-6}
 \end{aligned} \quad (D.5.2)$$

D.6 The Enthalpy of Saturated Water

The enthalpy of the saturated water ^(h') is calculated using Vesper's [76] approximation of table values.

$$h' = \sum_{i=0}^{i=9} A_i X^i, \quad \text{kJ/kg} \quad (D.6.1)$$

where

$$X = \frac{t_s}{100}$$

t_s - saturation temperature in °C

$$\begin{aligned}
 A_0 &= - 4.7554093 \cdot 10^{-2} & A_5 &= 1.5159421 \cdot 10^2 \\
 A_1 &= 4.2490349 \cdot 10^2 & A_6 &= - 7.8226638 \cdot 10^1 \\
 A_2 &= - 4.4519838 \cdot 10^1 & A_7 &= 2.3865162 \cdot 10^1 \\
 A_3 &= 1.2080923 \cdot 10^2 & A_8 &= - 3.9629482 \cdot 10^0 \\
 A_4 &= - 1.7579053 \cdot 10^2 & A_9 &= 2.7663765 \cdot 10^{-1}
 \end{aligned} \quad (D.6.2)$$

D.7 Saturated Steam Enthalpy (h'')

Vesper's [76] approximation of steam tables values will be used again

$$h'' = \sum_{i=0}^{i=6} A_i X^i, \quad \text{kJ/kg} \quad (\text{D.7.1})$$

where

$$X = \frac{t_s}{100}$$

t_s - saturation temperature in $^{\circ}\text{C}$

$$A_0 = 2.5006256 \cdot 10^3$$

$$A_4 = 2.7974559 \cdot 10^1$$

$$A_1 = 1.8150666 \cdot 10^2$$

$$A_5 = -9.4307509 \cdot 10^0$$

$$A_2 = 1.5749571 \cdot 10^1$$

$$A_6 = 1.0285952 \cdot 10^0$$

$$A_3 = -4.3077814 \cdot 10^1$$

D.8 Heat Capacity of Water

The heat capacity of water is determined by differentiating Juza's expression for water enthalpy, Lekić [78]:

$$C_{PW} = A + By + C \left(\frac{1}{y+2} - 0.24927 + 0.021y \right), \quad \frac{\text{kJ}}{\text{kg}^{\circ}\text{K}} \quad (\text{D.8.1})$$

where

$$\begin{aligned} A = & 4.1982594 - 0.1304363 \cdot X + 0.19097088 \cdot X^2 \\ & - 0.07403256 \cdot X^3 + 0.02259985 \cdot X^4 \end{aligned} \quad (\text{D.8.2})$$

$$B = 0.0307256 + 0.033444712 \cdot X - 0.024208803 \cdot X^2 + 0.004837208 \cdot X^3 - 0.001100455 \cdot X^4 \quad (D.8.3)$$

$$C = 0.032 + 0.003264 \cdot X^5 + 0.26912 \cdot 10^{-6} \cdot X^{15} \quad (D.8.4)$$

$$X = \frac{t}{100} \quad (D.8.5)$$

$$y = \frac{P}{100} \quad (D.8.6)$$

t - temperature in °C

P - pressure in Bar

D.9 Heat Capacity of Steam

The heat capacity of steam is determined from the equation (see Lekić [78]):

$$C_{ps} = \sum_{i=1}^{i=4} 1A_i \tau^{i-1} - I_1 \left\{ \left[\frac{-10.7724A}{\tau^{3.82}} + 5.1324 \cdot E \left(C - \frac{\sigma}{2} \right) \tau^{1.82} \right] \tau + \left[\frac{9\tau^3 D \sigma - 70B + 52(d \cdot \tau - \tau^3) \cdot D \cdot \sigma - \frac{352 \cdot C}{\tau^{33}}}{\tau^{15}} \right] \sigma^3 \right\} \quad (D.9.1)$$

where

$$\begin{aligned} A_1 &= 1.1698648 \cdot 10^3 & A_3 &= 7.3765806 \cdot 10^1 \\ A_2 &= -8.0553613 \cdot 10^0 & A_4 &= 1.3026684 \cdot 10^1 \end{aligned} \quad (D.9.2)$$

$$\tau = \frac{T}{T_c} = \frac{t + 273.15}{647.3} \quad (D.9.3)$$

$$\sigma = \frac{P}{P_c} = \frac{P}{221.287} \quad (D.9.4)$$

$$\begin{aligned} A &= 4.7331 \cdot 10^{-3} & C &= 1.55108 \\ B &= 2.93945 \cdot 10^{-3} & d &= 1.26591 \\ C &= 4.35507 \cdot 10^{-6} & & \\ D &= 6.70126 \cdot 10^{-4} & & \\ E &= 3.17362 \cdot 10^{-5} & & \\ I_1 &= 2.21287034 \cdot 10^4 & & \end{aligned} \quad (D.9.5)$$

D.10 Thermal Conductivity of Water

The thermal conductivity of water was determined by the 1967 IFC Formulation [74].

$$k_w = \sum_{i=0}^{i=4} A_i X^i + (P - P_s) \sum_{i=0}^{i=3} B_i X^i + (P - P_s)^2 \sum_{i=0}^{i=3} C_i X^i, \quad (D.10.1)$$

$\frac{J}{ms^{\circ}K}$

where

$$X = \frac{t + 273.15}{273.15} \quad (D.10.2)$$

t - temperature in $^{\circ}C$

$$\begin{aligned} A_0 &= -0.92247 & B_0 &= -9.4730 \cdot 10^{-4} & C_0 &= 1.6560 \cdot 10^{-6} \\ A_1 &= 2.8395 & B_1 &= 2.5186 \cdot 10^{-3} & C_1 &= -3.8929 \cdot 10^{-6} \\ A_2 &= -1.8007 & B_2 &= -2.0012 \cdot 10^{-3} & C_2 &= 2.9323 \cdot 10^{-6} \\ A_3 &= 0.52577 & B_3 &= 5.1536 \cdot 10^{-4} & C_3 &= -7.1693 \cdot 10^{-7} \\ A_4 &= -0.07344 & & & & \end{aligned}$$

D.11 Thermal Conductivity of Steam

The thermal conductivity of steam was determined from [74]

$$k_s = 0.0176 + 5.87 \cdot 10^{-5} t + 1.04 \cdot 10^{-7} \cdot t^2 - 4.51 \cdot 10^{-11} \cdot t^3, \quad \frac{\text{J}}{\text{ms}^\circ\text{K}} \quad (\text{D.11.1})$$

where

t = temperature in $^\circ\text{C}$.

D.12 Viscosity of Steam

The viscosity of steam is determined using [74]

$$\mu_s = 80.4 + 0.407 \cdot t - \rho_s (1858. - 5.9 \cdot t) / 100, \quad 10^7 \cdot \frac{\text{NS}}{\text{m}^2} \quad (\text{D.12.1})$$

where

t - temperature in $^\circ\text{C}$

ρ - density of steam in kg/m^3 .

D.13 Viscosity of Air

The viscosity of air was determined from

$$\mu_A = 173.6 + 0.454 \cdot t, \quad 10^7 \cdot \frac{\text{NS}}{\text{m}^2} \quad (\text{D.13.1})$$

where

t - temperature in $^\circ\text{C}$.

D.14 Viscosity of Air/Steam Mixture

The viscosity of an air/steam mixture was determined following the procedure proposed by Bird et al [81]:

$$\mu_{mix} = \sum_{i=1}^{i=n} \frac{x_i \mu_i}{\sum_{j=1}^{j=3} x_j \phi_{ij}} \quad (D.14.1)$$

where

x_i, x_j - mole fractions of the mixture components

μ_i - viscosities of the mixture components

$$\phi_{ij} = \frac{1}{\sqrt{8}} \left(1 + \frac{M_i}{M_j} \right)^{-1/2} \left[1 + \left(\frac{\mu_i}{\mu_j} \right)^{1/2} \left(\frac{M_i}{M_j} \right)^{1/4} \right]^2 \quad (D.14.2)$$

M_i, M_j - molecular weight of the mixture components.

D.15 Thermal Conductivity of Air

The thermal conductivity of air was determined using the procedure outlined in Holland et al [79]. It is assumed that air consists of 78% of nitrogen N_2 , 21% of oxygen and 1% of Argon, thus

$$k_A = \frac{\sum_{i=1}^{i=3} r_i M_i^{1/3} k_i}{\sum_{i=1}^{i=3} r_i M_i^{1/3}}, \quad \frac{J}{ms^{\circ}K} \quad (D.15.1)$$

where

r_i, M_i - volume functions and molecular weights of N_2, O_2 and A_r , respectively.

The thermal conductivity of the components was determined as

$$k_1 = \mu_{01} (1.32 \cdot C_{V1} + 508 - 104.6/X_1) \quad (D.15.2)$$

$$k_2 = \mu_{02}(1.32 \cdot C_{V2} + 444.8 - 91.59/X_2) \quad (D.15.3)$$

$$k_3 = 2.5 \cdot \mu_{03} \cdot C_{V3} \quad (D.15.4)$$

$$M_1 = 28.02, \quad M_2 = 32, \quad M_3 = 39.94 \frac{\text{kg}}{\text{kmol}} \quad (D.15.5)$$

The viscosities μ_{01} were determined

$$\mu_{01} = 8.175(4.58 \cdot X_1 - 1.67)^{5/8} \cdot 10^{-11} / \xi_1 \quad (D.15.6)$$

$$\xi_1 = 1.873 \cdot 10^{-5} \cdot K^{1/6} / [(kg/kmol)^{1/2} (N/m^2)^{2/3}]$$

$$\xi_2 = 1.393 \cdot 10^{-5} \quad (D.15.7)$$

$$\xi_3 = 1.272 \cdot 10^{-5}$$

$$X_1 = \frac{t + 273.15}{126.1}, \quad X_2 = \frac{t + 273.15}{154.4}, \quad X_3 = \frac{t + 273.15}{151.2} \quad (D.15.8)$$

The specific heat at constant volume C_{Vi} was determined from

$$C_{Vi} = (C_{pi} - 8315) / M_i, \quad \frac{J}{kg \cdot K} \quad (D.15.9)$$

The specific heat at the constant pressure C_{pi} is

$$\begin{aligned} C_{P1} &= 27214 + 4.18(t + 273.15), \quad J/kmol \cdot K \\ C_{P2} &= 34625 + 1.082(t + 273.15) - 78586 \cdot 10^4 / (t + 273.15)^2 \\ C_{P3} &= 20808, \quad J/kmol \cdot K \end{aligned} \quad (D.15.10)$$

D.16 The Thermal Conductivity of the Air/Steam Mixture

The thermal conductivities of gas mixtures at low density may be estimated by a method analogous to that previously given for viscosity (see equations (D.13.1) and (D.13.2)):

$$k_{\text{mix}} = \frac{\sum_{i=1}^{i=n} x_i k_i}{\sum_{j=1}^{j=n} x_j \phi_{ij}}, \quad \frac{\text{J}}{\text{ms}^\circ\text{K}} \quad (\text{D.16.1})$$

The x_i are mole fractions and the k_i are the thermal conductivities of the pure components. The coefficients ϕ_{ij} are identical with those that appeared in the viscosity equation:

$$\phi_{ij} = \frac{1}{\sqrt{8}} \left(1 + \frac{M_i}{M_j} \right)^{-1/2} \left[1 + \left(\frac{\mu_i}{\mu_j} \right)^{1/2} \left(\frac{M_j}{M_i} \right)^{1/4} \right]^2 \quad (\text{D.16.2})$$

D.17 The Diffusivity of Water Vapour Through Air

The diffusivity of water vapour through air was determined from [79]

$$D = \frac{(1 - Y_w)(T^\circ\text{K})^{1.81} \cdot 10^{-9}}{\frac{Y_1}{0.7577} + \frac{Y_2}{0.7794} + \frac{Y_3}{0.7503}}, \quad \text{m}^2/\text{s} \quad (\text{D.17.1})$$

where

$$Y_1 = 0.78, \quad Y_2 = 0.21, \quad Y_3 = 0.01$$

Y_w - volume fraction of water vapour in air.

D.18 The Surface Tension of Water in Air

The least square fit through the data of Rohensow and Hartnett [82] gave the following relations for surface tension σ as a function of temperature in °C

$$\sigma = 75.448 - 0.13071 \cdot T - 3.5056 \cdot 10^{-4} \cdot T^2 \quad (\text{D.18.1})$$

or

$$\sigma = 75.671 - 0.16131 \cdot T + 4.3348 \cdot 10^{-4} T^2 - 5.2269 \cdot 10^{-6} \cdot T^3 \quad (\text{D.18.2})$$

Since the differences of water surface tension in air and steam are negligible (see Vargaftik [83]), the water surface tension in air/steam mixture can be calculated using either of equations (D.18).

APPENDIX E

THE COMPUTER PROGRAM FOR NO INTERNAL RESISTANCE

SOLUTION OF THE SINGLE DROPLET RESPONSE

3JOB WAIFIV ***** ,KP=29,P=100

```

C *****
C *****
C *
C * THIS PROGRAM SOLVES THE PROBLEM OF SIMULTANEOUS HEAT & MASS
C * TRANSFER FROM AN AIR/STEAM MIXTURE TO A DROPLET MOVING WITH
C * A CONSTANT VELOCITY, NO INTERNAL RESISTANCE TO A HEAT TRANSFER
C * IN A SPHERE
C * SI--UNITS
C *
C *****
C *****
C
C A=THERMAL DIFFUSIVITY M2/SEC
C AMBMF=THERMAL CONDUCTIVITY OF MIXTURE -- FILM J/M OK SEC
C ANHMF=THERMAL CONDUCTIVITY OF STEAM -- FILM J/M OK SEC
C AMBMV=THERMAL CONDUCTIVITY OF AIR -- FILM J/M OK SEC
C CPA = HEAT CAPACITY OF AIR J/KMOLOK
C CPMF = HEAT CAPACITY OF MIXTURE AT FILM TEMPERATURE J/KG OK
C CPP = HEAT CAPACITY OF STEAM KJ/KG OK
C CPV = HEAT CAPACITY OF WATER KJ/KG OK
C DIFMF=DIFFUSIVITY OF MIXTURE -- FILM M2/SEC
C DT=TEMPERATURE INCREASE OC
C F=MASS TRANSFER COEFFICIENT KMOL/M2 SEC
C G=MOLEULAR MASS VELOCITY KMOL/M2 SEC
C H=HEAT TRANSFER COEFFICIENT J/M2 OK SEC
C HVAPE=HEAT OF VAPORIZATION KJ/KG
C KE = THE NUMBER OF DIAMETERS
C KF = THE NUMBER OF STEAM/(AIR+STEAM) RADIUS
C PEN = PECLET NUMBER
C PPP = PARTIAL PRESSURE OF THE STEAM BAR
C PRN = PRANDTL NUMBER
C PT = TOTAL PRESSURE OF THE MIXTURE BAR
C PV = PRODUCT OF PPP BY (1/ROP) BAR*M3/KG
C REMB=REYNOLDS NUMBER OF MIXTURE -- BULK
C REN = REYNOLDS NUMBER
C RMB = MIXTURE GAS CONSTANT - BULK J/KG OK
C ROMB = DENSITY OF MIXTURE - BULK KG/M3
C ROP = DENSITY OF VAPOUR - BULK KG/M3
C ROPF=DENSITY OF STEAM -- FILM KG/M3
C ROV = DENSITY OF WATER KG/M3
C RIND=RATIO OF THERMAL DIFFUSIVITY AND MOLECULAR DIFFUSION COEFF.
C SCN = SCHMIDT NUMBER
C SHN = SHERWOOD NUMBER
C TF=TEMPERATURE OF FILM OC
C THUT--THERMAL UTILIZATION
C TRA=MASS TRANSFER RATE KMOL/M2 SEC
C TV = WATER DROPLET TEMPERATURE OC
C TZ = SATURATION TEMPERATURE CORRESPONDING TO PPP OC
C USM = NUSSLETT NUMBER
C VISMB = VISCOSITY OF MIXTURE - BULK 10**7*NS/M2
C VISPM = VISCOSITY OF STEAM - BULK 10**7*NS/M2
C VISVM = VISCOSITY OF AIR - BULK 10**7*NS/M2
C VISMF=VISCOSITY OF MIXTURE -- FILM 10.**7 *N SEC/M2
C VISVF=VISCOSITY OF AIR -- FILM 10.**7 *N SEC/M2
C VISPF=VISCOSITY OF STEAM -- FILM 10.**7 *N SEC/M2
C VRT = TERMINAL VELOCITY M/SEC
C WMMF=MOLECULAR WEIGHT OF MIXTURE -- FILM KG/KMOL
C *****
C *****

```

```

C -----
2      VREXP=0.
3      VREXP=100.
C -----
4      READ 1,KE,KF,PT
5      1  FORMAT(215,F10.5)
6      DO 80 I=1,KE
7      DO 90 J=1,KF
8      2  FORMAT(5F10.5)
9      IF(VREXP.GT.0.) GO TO 43
10     READ 2,D(I),R(J),VREXP,I1,I0
11     GO TO 44
12     43 READ 2,D(I),TZ,VREXP,I1,I0
13     44 CONTINUE
14     IV=I1
15     THELO=0.
16     HAPPO=0.
17     HAPSTP=0.
18     HAPINT=0.
19     HQ=0.
20     HSTEP=0.
21     HJNT=0.
22     HAPCHO=0.
23     HAPCHI=0.
24     PI=3.14159
25     VU=VREXP
26     VINF=0.
C
C      DENSITY OF MIXTURE__BULK
C
27     IF(VREXP.GT.0.) GO TO 46
28     PPP=R(J)*PT
29     CALL TEMP1(PPP,TZ)
30     GO TO 47
31     46 CONTINUE
32     CALL PZAS(TZ,PPP)
33     R(J)=PPP/PT
34     47 CONTINUE
35     RMB=8314.7/(R(J)*18.02+(1.-R(J))*28.96)
36     ROMB=100000.*PT/(RMB*(TZ+273.15))
C
C      VISCOSITY OF MIXTURE__BULK
C
37     CALL SEKPV(TZ,PV)
38     ROP=P1/PV
39     VISV=80.4+0.407*TZ-ROP*(1858.-5.9*TZ)/1000.
40     VISV=173.4+0.454*TZ
41     F112=0.3536/SQRT(1.+0.6222)*(1.+SQRT(VISP/VISV)*1.12593)**2
42     F121=0.3536/SQRT(1.+1.0071)*(1.+SQRT(VISV/VISP)*0.82814)**2
43     VISMB=R(J)*VISP/(R(J)+(1.-R(J))*F112)+(1.-R(J))*VISV/(R(J)*F121-R(J))
44     CALL VVODE5(F1,I1,VVOD)
45     ROV=1./VVOD
46     OM=ROV*PI*D(I)**3/(6.*10.**9)
47     AREA=PI*D(I)**2*10.**(-6)
C
C      TERMINAL VELOCITY OF MIXTURE
C
48     IF(VREXP.GT.0.) GO TO 17
49     IF(D(I)-0.5)3,3,5
50     3  FN1=8.625*SQRT(VISMB*BAROMR/10.**7)/(D(I)/1000.)*1.5/ROV

```

```

53      REMB=VR1*(D(1)*R0MB*10000./VISMb
54      IF (REMB-10.)6,6,4
55      4   VR1=(9.40665/FR2)**(2./3.)
56      REMb=REMB*VR11/VR1
57      VR1=VR11
58      GO TO 6
59      5   VR1=9.43*(1.-EXP(-(D(1)/1.77)**1.147))
60      GO TO 18
61      17  CONTINUE
62      VR1=VREXP
63      18  CONTINUE
64      REMb=VR1*(D(1)*10000./VISMb
65      6   CONTINUE
66      PRINT 11,D(1),R(J),PI,T1,VD,VINF
67      11  FORMAT(/,2X,5HD(1)=,F10.5,2X,5HR(J)=,F10.5,2X,3HPT=,F10.5,2X,3H
1=,F10.5,2X,3HVD=,F10.5,2X,'VINF=',F10.5)
68      KI=30
69      DT=(T2-T1)/KI
70      DT1=DT
71      BDT=0.99
72      KJ=KJ+10
      C
      C
73      DO 100 K=1,KJ
      C
      C
      C
74      IVOLD=IV
75      IF(K.GT.(KJ-11)) GO TO 12
76      GO TO 13
77      12  CONTINUE
78      IF(K.GT.(KJ-7)) GO TO 14
79      DT=DT1/5.
80      GO TO 13
81      14  BDT=BDT+9./10.**(K-31)
82      IVN=BDT*12
83      DT=IVN-IV
84      13  CONTINUE
85      IV=IV+DT
86      IVM=IV-DT/2.
87      IF(IV.GT.0.9999*12) GO TO 34
88      TF=(T2+IV-DT/2.)/2.
89      IFM=(T2+IVM-DT/4.)/2.
90      CALL PZAS(TF,PZF)
91      CALL PZAS(IFM,PZFM)
92      RF=PZF/PI
93      RFM=PZFM/PI
94      CALL SERPV(TF,PV)
95      CALL SERPV(IFM,PVM)
96      RUPF=PI/PV
97      RUPFM=PI/PVM
      C
      C
      C
      C
98      CALL VISASM(TF,RF,RUPF,VISMF)
99      CALL VISASM(IFM,RFM,RUPFM,VISMFM)
      C
      C
      C
      C
100     CALL AMBASM(TF,RF,CPN2,CPU2,CPAN,AMBMF)
101     CALL AMBASM(IFM,RFM,CPN2M,CPU2M,CPANM,AMBMM)
      C
      C
      C
      C
102     CALL DIFFUSIVITY-OF MIXTURE -- FILM

```

```

102      CALL DIFASF(1F,RF,DIFMF)
103      CALL DIFASF(1FM,RFM,DIFMF)

      C
      C
      C      DENSITY OF MIXTURE -- FILM
104      RMF=4314.7/(RF*18.02+(1.-RF)*28.96)
105      RFM=4314.7/(RFM*18.02+(1.-RFM)*28.96)
106      RUMF=100000.*PI/(RMF*(1F+273.15))
107      RUMFM=100000.*PI/(RFM*(1FM+273.15))

      C
      C
      C      HEAT CAPACITY OF MIXTURE -- FILM
108      CALL CPPAR(PZF,1F,CPF)
109      CALL CPPAR(PZFM,1FM,CPPM)
110      CPA=0.7*CPN2+0.21*CPU2+0.01*CPAR
111      CPAN=0.7*CPN2M+0.21*CPU2M+0.01*CPARM
112      CPMF=RF*CPF*1000.+(1.-RF)*CPA/28.96
113      CPMFM=RFM*CPPM*1000.+(1.-RFM)*CPAM/28.96

      C
      C
      C      PRANDTL NUMBER
114      PRN=CPMF*VISMF/AMHMF/10.**7
115      PRNM=CPMFM*VISMF/AMHMF/10.**7

      C
      C
      C      REYNOLDS NUMBER
116      REN=VR1*D(1)*RUMF*10000./VISMF
117      RENM=VR1*D(1)*RUMFM*10000./VISMF

      C
      C
      C      SCHMIDT NUMBER
118      SCN=VISMF/RUMF/DIFMF/10.**7
119      SCNM=VISMF/RUMFM/DIFMF/10.**7

      C
      C
      C      PECLET NUMBER
120      PEN=REN*SCN
121      PENM=RENM*SCNM

      C
      C
      C      NUSSELT NUMBER
122      IF(REN<450.)7,7,6
123      USN=2.+0.6*(REN**0.5)*(PRN**(1./3.))
124      USN1=2.+0.6*(REN**0.5)*(PRNM**(1./3.))

      C
      C
      C      SHERWOOD NUMBER
125      SHN=2.+0.6*(REN**0.5)*(SCN**(1./3.))
126      SHNM=2.+0.6*(RENM**0.5)*(SCNM**(1./3.))
127      GO TO 9
128      6
129      USN=2.+0.27*(REN**0.62)*(PRN**(1./3.))
130      USNM=2.+0.27*(RENM**0.62)*(PRNM**(1./3.))
131      SHN=2.+0.27*(REN**0.62)*(SCN**(1./3.))
132      SHNM=2.+0.27*(RENM**0.62)*(SCNM**(1./3.))

      C
      C
      C      HEAT TRANSFER COEFFICIENT
132      9      H=1000.*AMHMF*USN/D(1)
133      HM=1000.*AMHMF*USNM/D(1)

      C
      C      MASS TRANSFER COEFFICIENT

```

```

135      M=VR1*ROMH/AMM8
136      F=SHM**A/PEM
137      FM=SHM**A/PEM

      C
      C      MASS TRANSFER RATE
      C
138      CALL PZAS(TV,PZV)
139      INA=F*(ALOG((1.-PZV/PT)/(1.-PPP/P)))
140      CALL PZAS(TVM,PZVM)
141      INAM=FM*(ALOG((1.-PZVM/PT)/(1.-FPP/PT)))

      C
      C      HEAT OF VAPORIZATION
      C
142      CALL SEKI(TF,HSEK)
143      CALL PRINI1(TF,HPRIM)
144      HVAP=HSEK-HPRIM
145      CALL SEKI(TFM,HSEK)
146      CALL PRINI1(TFM,HPRIM)
147      HVAPM=HSEK-HPRIM

      C
      C      SENSIBLE HEAT TRANSFER
      C
148      ACC=INA*18020.*CPP/H
149      ACN=ACC/(1.-EXP(-ACC))
150      QS=ACN*H*(TZ-TV+DT/2.)
151      ACCM=INAM*18020.*CPPM/HM
152      ACM=ACCM/(1.-EXP(-ACCM))
153      QSM=ACM*HM*(TZ-TV+DT/2.)

      C
      C      LATENT HEAT TRANSFER
      C
154      QL=HVAP*INA*18020.
155      QLM=HVAPM*INAM*18020.

      C
      C      TOTAL HEAT TRANSFER
      C
156      QT=QL+QS
157      QTM=QLM+QSM

      C
      C      APPARENT HEAT TRANSFER COEFFICIENT
      C
158      HAP=QT/(TZ-TV+DT/2.)
159      HAPM=QTM/(TZ-TVM+DT/2.)

      C
      C      BIOT NUMBER
      C
160      CALL ARDA(PT,TV,VLA*8)
161      B1=HAP*B(1)/VLA*8/2000.

      C
      C      TIME NECESSARY TO TEMPERATURE INCREASE DT
      C
162      CALL VVODE5(PT,TV,VVOD)
163      ROV=1./VVOD
164      CALL CPVOD2 (PT,TV,CPV)
165      C1=6./(ROV*CPV*B(1))
166      C2=(INA*18.02*CPP*1000./(1.-EXP(-INA*18.02*CPP*1000./H)))
167      C=C1+C2
168      ARGUM1=(C*(TZ-TV+DT)+C1*HVAP*INA*18020.)/(C*(TZ-TV)+C1*HVAP*INA*
169      118020.)
169      IF (ARGUM1<1.0.) GO TO 36
170      THE1A=(1./C)*ALOG(ARGUM1)
171      THE1U=THE1U+THE1A

```



```

C      THERMAL UTILIZATION
C
172      THUT=(TV-11)/(TZ-11)
C
C      RATIO OF THERMAL DIFFUSIVITY AND DIFFUSION COEFFICIENT
C
173      A=ANMF/(RDMF*CPMF)
174      RTMD=A/DIFMF
C
C      APPARENT HEAT TRANSFER COEFFICIENT--CHECK UP
C
175      HAPCH=D*CPV*(TV-TVULD)*1000./AREA/(TZ-TV+DT/2.)/THETA
C
C      AVERAGE APPARENT HEAT TRANSFER COEFFICIENT
C
176      HAPSTP=HAPSTP+HAPP
177      HAPAVS=HAPSTP/K
178      HAPINI=HAPINI+(HAPPO+4.*HAPPH+HAPP)*THETA/6.
179      HAPAVI=HAPINI/THETU
180      HAPPO=HAPP
181      HAPCHT=HAPCHT+(HAPCHO+HAPCH)*THETA/2.
182      HAPCHO=HAPCH
183      HAPCTR=HAPCHT/THETU
C
C      AVERAGE SENSIBLE HEAT TRANSFER COEFFICIENT
C
184      HSTEP=HSTEP+H
185      HAVSTP=HSTEP/K
186      HINI=HINI+(H+4.*HH+H)*THETA/6.
187      HAVINI=HINI/THETU
188      HO=H
C
C      ENHANCEMENT FACTOR
C
189      EFSTEP=HAVAVS/HAVSTP
190      EFINI=HAVAVI/HAVINI
191      EF=EFINI
C
C      H ALL STEAM TO H MIXTURE RATIO
C
192      HAS=914190.2
193      HSHNR=HAVAVI/HAS
194      TAV=TV
C
C      *****
195      PRINT 25,TV,TAV,U(1),RTMD,THUT,THETU
196      25      FORMAT(2X,3HIV=,E14.7,1X,4HTAV=,E14.7,1X,5HDT(1)=,E14.7,1X,5HRTMD=,E14.7,1X,5HTHUT=,E14.7,1X,6HTHETU=,E14.7)
197      PRINT 26,THA,F,RI,HAPP,HAPAVS,HAPAVI
198      26      FORMAT(2X,'T.A.=',E14.7,1X,'F=',E14.7,1X,'RI=',E14.7,1X,'HAPP=',E14.7,1X,'HAPAVS=',E14.7,1X,'HAPAVI=',E14.7)
199      PRINT 24,H,HAVSTP,HAVINI,EFSTEP,EFINI,HAPCTR
200      24      FORMAT(2X,'H=',E14.7,1X,'HAVSTP=',E14.7,1X,'HAVINI=',E14.7,1X,'EFSTEP=',E14.7,1X,'EFINI=',E14.7,1X,'HAPCTR=',F10.1)
201      PRINT 29,PRN,SCN,SHN,USN,UL,ACN,HAPCH
202      29      FORMAT(2X,'PRN=',F10.5,1X,'SCN=',F10.5,1X,'SHN=',F10.5,1X,'USN=',F10.5,1X,'UL=',F10.5,1X,'ACN=',F10.5,1X,'HAPCH=',F10.1)
203      100      CONTINUE
204      34      CONTINUE

```

TIME SURROUNDING TEMPERATURE',/)

207 36 CONTINUE
 208 PRINT 27,PPP,TZ,ROF,VISP,VISV,VISMb
 209 27 FORMAT(2X,4HPPP=,E14.7,1X,3HTZ=,E14.7,1X,4HROF=,E14.7,1X,5HVISP=,
 114.7,1X,5HVISV=,E14.7,1X,6HVISMb=,E14.7//)

C
 210 40 PRINT24,ROV,VRI,REMB,OT,EF,HSHMR
 211 26 FORMAT(2X,4HROV=,E14.7,1X,4HVRI=,E14.7,1X,5HREMB=,E14.7,1X,3HOT=,
 114.7,1X,3HEF=,E14.7,1X,6HSHMR=,E14.7//)

C
 212 80 CONTINUE
 213 STOP
 214 END

C
 C *****

215 SUBROUTINE FZAS(1,PS)

C
 C *****

216 X=T/100.
 217 PS((((((((1.55318/10000.*X-2.6934527/1000.)*X+2.0153393/100.)*
 16.659025/100.)*X+2.4775634/10.)*X-5.6086594/10.)*X+1.2567591)*X-
 2033727)*X+7.2704894)*X-5.07871)
 218 PS=EXP(PS)/1.01972
 219 RETURN
 220 END

C
 C *****

221 SUBROUTINE TEMP1(PPP,TZ)

C
 C *****

222 X=ALOG(1.01972*PPP)
 223 TZ(((((((((-4.2924603/10000./10000.*X-4.2665665/10000000.)*X+1.
 1343731/1000000.)*X+2.2071712/100000.)*X-1.7417752/100000.)*X-3.7:
 23454/10000.)*X+1.3283773/1000.)*X+2.129682/100.)*X+2.1077605/10.
 3X+2.3753577)*X+27.854242)*X+99.092712
 224 RETURN
 225 END

C
 C *****

226 SUBROUTINE VV00F5(PT,Iv,VV00)

C
 C *****

227 A=(Iv+273.15)/647.3
 228 S=PI/221.286
 229 U=100.*(3700000.-3122199.*A*A-1999.85/A**6)
 230 W=(U+SQRT(1.72*U*U+1362926.*10.**10*(S-1.500705*A)))*0.2941177
 231 B=1.052355*(62.5+S*(13.10268+S))/10.**11/(1.5108/100000.+A**11)
 232 C=(0.6537154-A)**2
 233 C=C*(7.241105/100000.+0.7676621*C**4)
 234 VV00=0.417/W+C-B-(11.39706-9.94927*A)/100000.
 235 RETURN
 236 END

C
 C *****

237 SUBROUTINE SEKPV(TZ,PV)

C
 C *****

238 X=T/100.

1.3444546/100.) * x - 3.8647549/100.) * x + 1.1476149/10000.) * x - 7.04144
2000.) * x + 4.5905064/10.) * x + 1.2602044

240

RETURN

241

END

C

C

242

SUBROUTINE CPV002(PT,TV,CPV)

C

C

243

X=TV/100.

244

Y=PT/100.

245

Z=X**5

246

CPV=1./(Y+2.)+0.021*Y-0.24927

247

CPV=CPV*(0.032+Z*(0.003264+0.026912*Z+Z/100000.))

248

Z=(((-1.100455*X+4.03/204)*X-24.208603)*X+33.444712)*X+30.72521

249

CPV=Z*Y/1000.+CPV

250

Z=((2.254485*X-7.403256)*X+19.097088)*X-13.04363)*X+419.62594

251

CPV=Z/100.+CPV

252

RETURN

253

END

C

C

254

SUBROUTINE CPPAK(PT,TF,CPP)

C

C

255

X=(TF+273.15)/647.3

256

S=PT/221.246

257

b=1.6266287*(1.55106-S/2.)*X**1.62/10000.-5.0986846/100./X**3.

258

C=(2.010376*S*(17.72274*S-11.*X**3)/1000.-0.2057615)/X**15

259

D=22124.703*(b*S+(C-1.5329446/X**33/1000.)*S**3)

260

CPP=(1169.6644-D*X*(-16.110723+X*(221.29742-X*52.106/36)))/647

261

RETURN

262

END

C

C

263

SUBROUTINE SEKI(1,ENTIA)

C

C

264

X=1/100.

265

ENTIA((((((1.0285952*X-4.4307509)*X+27.974559)*X-43.077814)*X+1
19571)*X+181.50666)*X+2500.6256

266

RETURN

267

END

C

C

268

SUBROUTINE PRIM11(1,ENTIA)

C

C

269

X=1/100.

270

ENTIA(((((((2.7553765/10.*X-3.9624482)*X+23.865152)*X-78.2260
1X+151.59421)*X-175.79053)*X+120.80923)*X-44.519836)*X+425.1734
2-7.45540093/100.

271

IF(1-350.)2,2,1

272

ENTIA=ENTIA+0.388/39*EXP(0.225556*(1-350.))

273

RETURN

274

END

C

```

275 SUBROUTINE AMDA(P,I,VLAMH)
C
C
276 X=1.+I/273.15
277 CALL PZAS(I,PS)
278 VLAMH=((0.24323-0.071693*X)*X-0.36929)*X+0.1656)*(P-PS)/100000.
279 VLAMH=(VLAMH+((0.1536*X-20.012)*X+25.166)*X-9.473)/10000.)*(P-PS)
280 VLAMH=VLAMH+((0.52577-0.07344*X)*X-1.6007)*X+2.8395)*X-0.42247
281 RETURN
282 END
C
C
283 SUBROUTINE VISASM(TF,RF,ROPF,VISMF)
C
284 VISPF=50.4+0.407*TF-ROPF*(1858.-5.9*TF)/1000.
285 VISVF=173.6+0.454*TF
286 F112F=0.3536/SQRT(1.+0.6222)*(1.+SQRT(VISPF/VISVF)+1.12593)**2
287 F121F=0.3536/SQRT(1.+1.6071)*(1.+SQRT(VISVF/VISPF)+0.88814)**2
288 VISMF=RF*VISPF/(RF+(1.-RF)*F112F)+(1.-RF)*VISVF/(RF*F121F+1.-RF)
289 RETURN
290 END
C
C
291 SUBROUTINE AMBASM(TF,RF,CPO2,CPO2,CPAR,AMBVF)
C
292 AMBPF=0.0176+5.67/100000.*TF+1.04/10.*TF*TF-0.451*TF*TF*TF/10.
293 AMN2=28.02
294 AMO2=32.
295 AMAR=39.94
296 TRN2=(TF+273.15)/126.1
297 TRQ2=(TF+273.15)/154.4
298 TRAR=(TF+273.15)/151.2
299 SIN2=1.673/100000.
300 SIQ2=1.393/100000.
301 SIAR=1.272/100000.
302 CPO2=27214.+4.167*(TF+273.15)
303 CPO2=34025.+1.0602*(TF+273.15)-76580.*10000./(TF+273.15)**2
304 CPAR=20808.
305 CVN2=(CPO2-6315.)/AMN2
306 CVO2=(CPO2-6315.)/AMO2
307 CVAR=(CPAR-6315.)/AMAR
308 VISN2=8.175*(4.56*TRN2-1.67)*(5./8.)/SIN2/10.**11
309 VISQ2=8.175*(4.56*TRQ2-1.67)*(5./8.)/SIQ2/10.**11
310 VISAR=8.175*(4.56*TRAR-1.67)*(5./8.)/SIAR/10.**11
311 AMHN2=VISN2*(1.32*CVN2+500.-104.6/TRN2)
312 AMHO2=VISQ2*(1.32*CVO2+444.6-91.59/TRQ2)
313 AMBAR=2.5*VISAR*CVAR
314 AMBVF=(0.76*(AMN2*(1./3.))*AMHN2+0.21*(AMO2*(1./3.))*AMHO2+0.01
315 1*(AMAR*(1./3.))*AMBAR)/(0.76*(AMN2*(1./3.))+0.21*(AMO2*(1./3.))
316 20.01*(AMAR*(1./3.)))
315 F112L=0.3536/SQRT(1.+0.6222)*(1.+SQRT(AMBPF/AMBVF)+1.12593)**2
316 F121L=0.3536/SQRT(1.+1.6071)*(1.+SQRT(AMBVF/AMBPF)+0.88814)**2
317 AMBVF=RF*AMBPF/(RF+(1.-RF)*F112L)+(1.-RF)*AMBVF/(RF*F121L+1.-RF)
318 RETURN
319 END
C
C
320 SUBROUTINE DIFASM(TF,RF,DIFMF)

```

```
321      DIFMF=(1.-RF)*((TF+273.15)**1.81)/10.**9/((1.-RF)*0.78/0.7577+  
322      1RF)*0.21/0.7794+(1.-RF)*0.01/0.7503)  
323      RETURN  
      END
```

C

\$ENTRY

APPENDIX F

THE COMPUTER PROGRAM FOR INTERNAL RESISTANCE AND
MIXING MODEL OF THE SINGLE DROPLET RESPONSE

```

C *****
C *****
C *
C *THIS PROGRAMME SOLVES THE PROBLEM OF SIMULTANEOUS MOMENTUM, HEAT &
C *MASS TRANSFER DURING CONDENSATION OF STEAM FROM SATURATED AIR-STEAM
C *MIXTURE ON A DROPLET WITH RESISTANCE TO HEAT FLOW IN A DROPLET
C *STEADY STATE DRAG COEFFICIENTS FOR WATER DROPLETS USING REINHART'S
C *CORRELATION--INITIALLY DROPLET MOVES EITHER UPWARDS OR DOWNWARDS
C *
C *SI--UNITS
C *
C *****
C *****
C *****
C A=THERMAL DIFFUSIVITY M2/SEC
C AMBMF=THERMAL CONDUCTIVITY OF MIXTURE -- FILM J/M OK SEC
C AMBMP=THERMAL CONDUCTIVITY OF STEAM -- FILM J/M OK SEC
C AMBMV=THERMAL CONDUCTIVITY OF AIR -- FILM J/M OK SEC
C AMDA=THERMAL CONDUCTIVITY OF WATER J/M SEC OC
C BI=BIOT NUMBER
C CUCDN=DRAG COEFFICIENT OF A DROPLET
C CDD =DRAG COEFFICIENT OF A DISK
C CUSS =DRAG COEFFICIENT OF A SOLID SPHERE
C CK0,CK1,CK2,CK3=RUNGE KUTTA'S COEFFICIENTS
C CPA = HEAT CAPACITY OF AIR J/KMOLOK
C CPMF = HEAT CAPACITY OF MIXTURE AT FILM TEMPERATURE J/KGOK
C CPP = HEAT CAPACITY OF STEAM KJ/KGOK
C CPV=HEAT CAPACITY OF WATER KJ/KG OK
C DD=DROPLET DIAMETER INCREASE M
C DIFMF=DIFFUSIVITY OF MIXTURE -- FILM M2/SEC
C DT=TEMPERATURE INCREASE OC
C F=MASS TRANSFER COEFFICIENT KMOL/M2 SEC
C FUN=FOURIER NUMBER
C G=GRAVITY ACCELERATION M2/SEC
C H=HEAT TRANSFER COEFFICIENT J/M2 OK SEC
C HVAP=HEAT OF VAPORIZATION KJ/KG
C KE = THE NUMBER OF DIAMETERS
C KF = THE NUMBER OF STEAM/(AIR+STEAM) RATIOS
C PEN = PECLET NUMBER
C PPP = PARTIAL PRESSURE OF THE STEAM BAR
C PRN = PRANDTL NUMBER
C PT = TOTAL PRESSURE OF THE MIXTURE BAR
C PV = PRODUCT OF PPP BY (1/ROP) BAR*M3/KG
C QL=LATENT HEAT TRANSFER J/M2 SEC
C QS=SENSIBLE HEAT TRANSFER J/M2 SEC
C QT=QS+QL -- TOTAL HEAT TRANSFER J/M2 SEC
C RENB=REYNOLDS NUMBER OF MIXTURE -- BULK
C REN = REYNOLDS NUMBER
C RMB = MIXTURE GAS CONSTANT - BULK J/KGOK
C RMDR=RATIO OF THERMAL DIFFUSIVITY AND MOLECULAR DIFFUSION COEFF.
C ROMH = DENSITY OF MIXTURE - BULK KG/M3
C ROP = DENSITY OF VAPOUR - BULK KG/M3
C ROV = DENSITY OF WATER KG/M3
C ROPF=DENSITY OF STEAM -- FILM KG/M3
C SCN = SCHMIDT NUMBER
C SHN = SHERWOOD NUMBER
C SURFT-SURFACE TENSION OF A DROPLET IN AN AIR/STEAM MIXTURE N/M
C TF=TEMPERATURE OF FILM OC
C TNA=MASS TRANSFER RATE KMOL/M2 SEC
C TV = WATER DROPLET TEMPERATURE OC
C TZ = SATURATION TEMPERATURE CORRESPONDING TO PPP OC

```

```

C      VISMH - VISCOSITY OF MIXTURE - BULK      10**7*NS/M2
C      VISMF=VISCOSITY OF MIXTURE -- FILM      10.**7 *N SEC/M2
C      VISPH - VISCOSITY OF STEAM - BULK      10**7*NS/M2
C      VISPF=VISCOSITY OF STEAM -- FILM      10.**7 *N SEC/M2
C      VISVB - VISCOSITY OF AIR - BULK      10**7*NS/M2
C      VISVF=VISCOSITY OF AIR -- FILM      10.**7 *N SEC/M2
C      VD=VELOCITY OF A DROPLET      M/SEC
C      VINP=VELOCITY OF SURROUNDING MIXTURE      M/SEC
C      VR=RELATIVE VELOCITY OF A DROPLET      M/SEC
C      VRO=INITIAL RELATIVE VELOCITY      M/SEC
C      VRT - TERMINAL VELOCITY      M/SEC
C      WM=MOLAR MASS VELOCITY      KMOL/M2 SEC
C      WMMF=MOLECULAR WEIGHT OF MIXTURE -- FILM      KG/KMOL
C      WMPF=MOLECULAR WEIGHT OF MIXTURE -- FILM      KG/KMOL
C      Z=DISTANCE TRAVELLED BY A DROPLET      M
C
C
C

```

```

1      DOUBLE PRECISION RI,Y
2      COMMON K,VRTI,NE,VRR,ZRK,ROMH,VISMH,G,NJ,NM,NN,THETA,VINF,VDUP,
3      1SURFT,ROV,D,VRO,I,VR,Z,THETU,VRRS
4      DIMENSION D(20),R(20),X(200),Y(200)

```

```

C-----
4      VRTI=100.
5      VREXP=0.
6      VREXP=100.

```

```

C-----
7      READ 1,KE,KF
8      1      FORMAT(2I5)
9      DO 50 J=1,KE
10     READ 37,PT
11     37      FORMAT(F10.5)
12     DO 90 J=1,KF
13     IF(VREXP.GT.0.) GO TO 43
14     READ 2,D(I),R(J),T0,T1,TH1
15     2      FORMAT(5F10.5)
16     GO TO 44
17     43      READ 45,D(I),I2,VREXP,T0,T1,TH1
18     45      FORMAT(6F10.5)
19     44      CONTINUE
20     IF(VRTI.GT.0.) GO TO 501
21     VDUP=0.
22     VINF=1.
23     IF(VDUP.GT.0.) GO TO 502
24     VDDOWN=11.
25     VD=VDDOWN
26     VRU=VINF+VD
27     GO TO 501
28     502      VRO=ABS(VDUP-VINF)
29     VD=VDUP
30     501      CONTINUE
31     TV=T1
32     THFID=0.
33     HAPPO=0.
34     HAPSIP=0.
35     HAPINT=0.
36     RO=0.
37     RSTEP=0.
38     HINT=0.
39     HAPLRO=0.
40     HAPCHI=0.
41     TIME=0.
42     RI=0

```



```

43      RM=0
44      NN=0
45      ZKK=0.
46      VPKK=0.
47      G=9.80665
48      PI=3.14159
49      TAVULD=10

      C
      C      DENSITY OF MIXTURE__HULK
      C
50      IF(VREXP.GT.0.) GO TO 46
51      PPP=R(J)*PI
52      CALL TEMPI(PPP,IZ)
53      GO TO 47
54      46      CONTINUE
55      CALL PZAS(IZ,PPP)
56      R(J)=PPP/PI
57      47      CONTINUE
58      RMB=6314.7/(R(J)*18.02+(1.-R(J))*28.96)
59      ROMB=100000.*PI/(RMB*(IZ+273.15))

      C
      C      VISCOSITY OF MIXTURE__HULK
      C
60      CALL SEKPV(IZ,PV)
61      ROP=PI/PV
62      VISP=80.4+0.407*IZ-ROP*(1858.-5.9*IZ)/1000.
63      VISV=173.6+0.454*IZ
64      FI12=0.3536/SQRT(1.+0.0222)*(1.+SQRT(VISP/VISV))*1.12593)**2
65      FI21=0.3536/SQRT(1.+1.0071)*(1.+SQRT(VISV/VISP))*0.85814)**2
66      VISM=R(J)*VISP/(R(J)+(1.-R(J))*FI12)+(1.-R(J))*VISV/(R(J)+FI21-
1-R(J))

      C
      C      MASS OF A DROPLET
      C
67      CALL VVODES(PI,T1,VVOD)
68      ROV=1./VVOD
69      OM=ROV*PI*O(1)**3/(6.*10.**9)
70      AREA=PI*O(1)**2*10.**(-6)
71      PRINT 11,O(1),R(J),PI,T1,VD,VINF
72      11      FORMAT(/,2X,SHO(1)=,F10.5,2X,SHR(J)=,F10.5,2X,3HPT=,F10.5,2X,3
1=,F10.5,2X,3HVD=,F10.5,2X,'VINF=',F10.5)

      C
      C      TERMINAL VELOCITY OF MIXTURE
      C
73      IF(VREXP.GT.0.) GO TO 17
74      IF(O(1)-1.0)3,3,5
75      3      FK1=6.025*SQRT(VISM*ROMB/10.**7)/(O(1)/1000.))*1.5/ROV
76      FK2=1.3913*FK1
77      VRT=(9.80665/FK1)**(2./3.)
78      REMB=VRT*O(1)*ROMB*10000./VISM
79      IF(REMB-10.)6,6,4
80      4      VRT1=(9.80665/FK2)**(2./3.)
81      REMB=REMB*VRT1/VRT
82      VRT=VRT1
83      GO TO 6
84      5      VRT=9.43*(1.-EXP(-(O(1)/1.77)**1.147))
85      GO TO 18
86      17      CONTINUE
87      VRT=VREXP
88      18      CONTINUE
89      REMB=VRT*O(1)*10000./VISM
90      6      CONTINUE

```

```

92      GO TO 16
93      15  CONTINUE
94          VR=VRT
95          VRU=VRT
96          Z=0.
97      16  CONTINUE
98          KJ=30
99          DT=(12-T1)/KJ
100         DT1=DT
101         KJ=KJ+10
102         BOT=0.99
103      C
104      C *****
105      C DO 100 K=1,KJ
106      C *****
107      C
108      IF(K.GT.(KJ-11)) GO TO 12
109      GO TO 13
110      12  CONTINUE
111      IF(K.GT.(KJ-7)) GO TO 14
112      DT=DT1/5.
113      GO TO 13
114      14  HD1=HDT+9./10.*(K-31)
115          TVN=HD1*12
116          DT=TVN-TV
117      13  CONTINUE
118          TV=TV+DT
119          TVN=TV-DT/2.
120          IF(TV.GT.0.9999*12) GO TO 34
121          TF=(12+TV-DT/2.)/2.
122          TFM=(12+TVN-DT/4.)/2.
123          CALL PZAS(TF,PZF)
124          CALL PZAS(TFM,PZFM)
125          RF=PZF/PT
126          RFM=PZFM/PT
127          CALL SEAPV(TF,PV)
128          CALL SEAPV(TFM,PVM)
129          RUPF=PT/PV
130          RUPFM=P1/PVM
131      C
132      C VISCOSITY OF MIXTURE--FILM
133      C
134      CALL VISASM(TF,RF,RUPF,VISMF)
135      CALL VISASM(TFM,RFM,RUPFM,VISMFM)
136      C
137      C THERMAL CONDUCTIVITY OF MIXTURE -- FILM
138      C
139      CALL ANBASM(TF,RF,CPN2,CP02,CPAN,ANBME)
140      CALL ANBASM(TFM,RFM,CPN2M,CP02M,CPANM,ANBMM)
141      C
142      C DIFFUSIVITY-OF MIXTURE -- FILM
143      C
144      CALL DIFASM(TF,RF,DIFMF)
145      CALL DIFASM(TFM,RFM,DIFMFM)
146      C
147      C DENSITY OF MIXTURE--FILM
148      C
149      RNF=8314.7/(RF*18.02+(1.-RF)*28.96)
150      RNFN=8314.7/(RFN*18.02+(1.-RFN)*28.96)
151      RUMF=100000.*P1/(RNF*(TF+273.15))
152      RUMFM=100000.*P1/(RNFN*(TFM+273.15))
153      C
154      C HEAT CAPACITY OF MIXTURE -- FILM

```

```

C
137 CALL CPPAR(PZF,TF,CPF)
138 CALL CPPAR(PZFM,TFM,CPFM)
139 CPA=0.7A*CPN2+0.21*CPD2+0.01*CPAR
140 CPAN=0.7A*CPN2M+0.21*CPD2M+0.01*CPARM
141 CPNF=RF*CPN+1000.+(1.-RF)*CPA/28.96
142 CPNFM=RFM*CPNM+1000.+(1.-RFM)*CPAM/28.96

C
C PRANDTL NUMBER
C
143 PRN=CPNF*VISNF/AMNMF/10.**7
144 PRNM=CPNFM*VISFM/AMNFM/10.**7

C
C REYNOLDS NUMBER
C
145 REN=VRT*D(1)*RDMF*10000./VISNF
146 RENM=VRTM*D(1)*RDMFM*10000./VISFM
147 AMMF=KF*18.02+(1.-KF)*28.96
148 AMFM=RFM*18.02+(1.-RFM)*28.96
149 AMMH=R(J)*18.02+(1.-R(J))*28.96
150 K=VRT*RDMH/AMMH
151 RE=1
152 IF(VRTT.GT.0.) GO TO 600
153 IF(K-1)404,404,405
154 405 REN=VR*D(1)*RDMF*10000./VISMF
155 RENM=VRM*D(1)*RDMFM*10000./VISFM
156 K=VR*RDMH/AMMH
157 TOLD=THE TU+INETA
158 600 CONTINUE

C
C SCHMIDT NUMBER
C
159 404 SCN=VISMF/RDMF/DIFMF/10.**7
160 SCNM=VISFM/RDMFM/DIFFM/10.**7

C
C PECLET NUMBER
C
161 PEN=REN*SCN
162 PENM=RENM*SCNM

C
C NUSSELT NUMBER
C
163 IF(REN-450.)7,7,H
164 7 USN=2.+0.6*(REN**0.5)*(PRN**(1./3.))
165 USNM=2.+0.6*(RENM**0.5)*(PRNM**(1./3.))

C
C SHERWOOD NUMBER
C
166 SHN=2.+0.6*(REN**0.5)*(SCN**(1./3.))
167 SHNM=2.+0.6*(RENM**0.5)*(SCNM**(1./3.))
168 GO TO 9
169 6 USN=2.+0.27*(REN**0.62)*(PEN**(1./3.))
170 USNM=2.+0.27*(RENM**0.62)*(PENM**(1./3.))
171 SHN=2.+0.27*(REN**0.62)*(SCN**(1./3.))
172 SHNM=2.+0.27*(RENM**0.62)*(SCNM**(1./3.))

C
C HEAT TRANSFER COEFFICIENT
C
173 9 H=1000.*AMMF*USN/D(1)
174 HM=1000.*AMFM*USNM/D(1)

C
C MASS TRANSFER COEFFICIENT

```

```

175      KMMB=R(J)*18.02+(1.-R(J))*28.96
176      KMMF=RF*18.02+(1.-RF)*28.96
177      F=SHH*W/PEN
178      FM=SHHM*W/PFDM

```

```

C
C
C      MASS TRANSFER RATE

```

```

179      CALL PZAS(TV,PZV)
180      TNA=F*(ALOG((1.-PZV/PT)/(1.-PPP/PT)))
181      CALL PZAS(TVM,PZVM)
182      TNAM=FM*(ALOG((1.-PZVM/PT)/(1.-PPP/PT)))

```

```

C
C
C      HEAT OF VAPORIZATION

```

```

183      CALL SEKI(TF,HSEK)
184      CALL PRIM11(TF,HPRIM)
185      HVAP=HSEK-HPRIM
186      CALL SEKI(TFM,HSEK)
187      CALL PRIM11(TFM,HPRIM)
188      HVAPM=HSEK-HPRIM

```

```

C
C
C      SENSIBLE HEAT TRANSFER

```

```

189      ACC=TNA*18020.*CFF/H
190      ACN=ACC/(1.-EXP(-ACC))
191      QS=ACN*H*(TZ-TV+DT/2.)
192      ACCM=TNAM*18020.*CFFM/HM
193      ACNM=ACCM/(1.-EXP(-ACCM))
194      QSM=ACNM*HM*(TZ-TV+DT/4.)

```

```

C
C
C      LATENT HEAT TRANSFER

```

```

195      QL=HVAP*TNA*18020.
196      QLM=HVAPM*TNAM*18020.

```

```

C
C
C      TOTAL HEAT TRANSFER

```

```

197      QT=QL+QS
198      QTM=QLM+QSM

```

```

C
C
C      APPARENT HEAT TRANSFER COEFFICIENT

```

```

199      HAPP=QT/(TZ-TV+DT/2.)
200      HAPPM=QTM/(TZ-TV+DT/4.)

```

```

C
C
C      BIOT NUMBER

```

```

201      CALL AMDA(PT,TV,VLANH)
202      BI=HAPP*D(1)/VLANH/2000.

```

```

C
C
C      THE ROOTS OF TRANSCENDENTAL EQUATION  $\tan(x) + x/(BI-1.) = 0$ .

```

```

203      CALL TRANEN(BI,Y)

```

```

C      *****
C      TIME TAKEN FOR DROPLET TEMPERATURE INCREASE DT--HALF INTERVAL
C      SEARCH METHOD
C      *****

```

```

204      EPS=0.0001
205      THA=0.00001
206      THB=THJ
207      TEMPR=(TZ-TV)/(TZ-T0)

```

```

C
C      THERMAL DIFFUSIVITY OF WATER DROPLET

```

```

C
208 CALL CPV002(P1,IV,CPV)
209 CALL VV00F5(P1,IV,VV00)
210 ROV=1./VV00
211 ALFA=VLAPH/CPV/ROV/1000.

C
C
C FOURIER NUMBER

212 FONA=4.*ALFA*THA*(10**6)/(D(1)**2)
213 FOMB=4.*ALFA*THB*(10**6)/(D(1)**2)
214 SUMA=0.
215 SUMB=0.
216 DO 110 L=1,200
217 IF(L.GT.20) GO TO 109
218 X(L)=S*GL(Y(L))
219 GO TO 108
220 109 X(L)=X(L-1)+PI
221 108 CONTINUE
222 AISA=(SIN(X(L))-X(L)*COS(X(L)))/(X(L)-SIN(X(L))*COS(X(L)))*(SIN(X(L))/X(L))
223 STEPA=(X(L)**2)*FONA
224 IF(STEPA.GT.175.) GO TO 107
225 SA=2.*AISA*EXP(-STEPA)
226 SUMA=SUMA+SA
227 IF(ABS(SUMA/10.**6).GT.ABS(SA)) GO TO 107
228 110 CONTINUE
229 107 FIHA=TEMPH-SUMA
230 DO 111 L=1,200
231 IF(L.GT.20) GO TO 112
232 X(L)=S*GL(Y(L))
233 GO TO 113
234 112 X(L)=X(L-1)+PI
235 113 CONTINUE
236 AISB=(SIN(X(L))-X(L)*COS(X(L)))/(X(L)-SIN(X(L))*COS(X(L)))*(SIN(X(L))/X(L))
237 STEPB=(X(L)**2)*FOMB
238 IF(STEPB.GT.175.) GO TO 114
239 SB=2.*AISB*EXP(-STEPB)
240 SUMB=SUMB+SB
241 IF(ABS(SUMB/10.**6).GT.ABS(SB)) GO TO 114
242 111 CONTINUE
243 114 FIHB=TEMPB-SUMB
244 N=0
245 207 N=N+1
246 XTH=(THA+THB)/2.
247 IF(XTH.GT.0.4995*TH1)GO TO 91
248 TEMP=TEMPH
249 FONX=4.*ALFA*XTH*(10.**6)/(D(1)**2)
250 SUMX=0.
251 DO 120 L=1,200
252 IF(L.GT.20) GO TO 115
253 X(L)=S*GL(Y(L))
254 GO TO 116
255 115 X(L)=X(L-1)+PI
256 116 CONTINUE
257 AISX=(SIN(X(L))-X(L)*COS(X(L)))/(X(L)-SIN(X(L))*COS(X(L)))*(SIN(X(L))/X(L))
258 STEPX=(X(L)**2)*FONX
259 IF(STEPX.GT.175.) GO TO 117
260 SX=2.*AISX*EXP(-STEPX)
261 SUMX=SUMX+SX
262 IF(ABS(SUMX/10.**6).GT.ABS(SX)) GO TO 117

```

```

264 117 FTHX=TEMP-SUMX
265 IF(FTHX)212,210,211
266 212 IF(FTHX+EPS)203,210,210
267 211 IF(FTHX-EPS)210,210,203
268 203 IF(FTHX*FTHA)205,206,206
269 205 THB=XTH
270 FTHB=FTHX
271 GO TO 207
272 206 THA=XTH
273 FTHA=FTHX
274 GO TO 207
275 208 PRINT 209
276 209 FORMAT(14HA IS TRUE ROUT)
277 GO TO 196
278 210 CONTINUE
279 GO TO 197
280 198 XTH=A
281 197 THETA=XTH
282 IF(VRT1.GT.0.) GO TO 407
283 NE=NE+1
284 IF(NE.LE.3) GO TO 406
285 T=THETA+THETA
286 IF(NE.GE.8) GO TO 413
287 IF(ABS(T/TOLD-1.).LT.0.001) GO TO 407
288 GO TO 406
289 413 CONTINUE
290 IF(NE.GE.20) GO TO 414
291 IF(ABS(T/TOLD-1.).LT.0.02) GO TO 407
292 GO TO 406
293 414 CONTINUE
294 IF(NE.GE.30) GO TO 415
295 IF(ABS(T/TOLD-1.).LT.0.03) GO TO 407
296 GO TO 406
297 415 CONTINUE
298 IF(NE.GE.40) GO TO 407
299 IF(ABS(T/TOLD-1.).LT.0.04) GO TO 407
C
C SURFACE TENSION OF WATER IN AIR
C
300 406 SURFT=(75.6-0.145*TV-0.25*10.**(-3)*TV**2)/1000.
C
C SURFACE TENSION GROUP
C
301 IF(VDUP.GT.0.) GO TO 505
302 CALL VELDDU
303 GO TO 405
304 505 CONTINUE
305 CALL VELDUP
306 GO TO 405
307 407 CONTINUE
308 IF(VRT1.GT.0.) GO TO 408
309 IF(VDUP.EQ.0.) GO TO 408
310 IF(VRRS.GT.0.) GO TO 408
311 NI=1
C
C AVERAGE TEMPERATURE OF DROPLET
C
312 408 CONTINUE
313 THETAU=THETA+THETA
314 FUNAV=4.*ALFA*THETA*(10.**6)/(D(1)**2)
315 SUMAV=0.
316 DO 151 L=1,200
317

```

```

318      X(L)=SIN(L(Y(L)))
319      GO TO 153
320 152    X(L)=X(L-1)+PI
321 153    CONTINUE
322      AISAV=((SIN(X(L))-X(L)*COS(X(L)))*2)/(X(L)-SIN(X(L))*COS(X(L))
323      STEP AV=(X(L)**2)*FORAV
324      IF(STEP AV.GT.175.) GO TO 154
325      SAV=6.*AISAV*EXP(-STEP AV)/X(L)**3
326      SUMAV=SUMAV+SAV
327      IF(ABS(SUMAV/10.**6).GT.ABS(SAV)) GO TO 154
328 151    CONTINUE
329 154    TAV=TZ-(TZ-T1)*SUMAV
330      T1=TAV
331      IF(VR11.GT.0.) GO TO 409
332      GO TO 410
333 409    CONTINUE
334      Z=Z+VR1*THETA
335 410    CONTINUE
      C
      C      DROPLET DIAMETER INCREASE
      C
336      DD=(2.*TNA*18.02/ROV)*THETA*1000.
337      D(1)=D(1)+DD
      C
      C      THERMAL UTILIZATION
      C
338      THU1=(TAV-T0)/(TZ-T0)
      C
      C      RATIO OF THERMAL DIFFUSIVITY AND DIFFUSION COEFFICIENT
      C
339      A=AMJMF/(RUMF*CPMF)
340      RTMD=A/DIFMF
      C
      C      AVERAGE APPARENT HEAT TRANSFER COEFFICIENT
      C
341      HAPSTP=HAPSTP+HAPP
342      HAPAVS=HAPSTP/K
343      HAPINT=HAPINT+(HAPPO+4.*HAPPN+HAPP)*THETA/6.
344      HAPAVI=HAPINT/THETU
345      HAPPO=HAPP
      C
      C      AVERAGE APPARENT HEAT TRANSFER COEFFICIENT--CHECK UP
      C
346      HAPCH=0.*CPV*(TAV-TAVOLD)*1000./AREA/(TZ-TV+DT/2.)/THETA
347      HAPCH1=HAPCH1+(HAPCH0+HAPCH)*THETA/2.
348      HAPCH0=HAPCH
349      HAPCTR=HAPCH1/THETU
350      TAVOLD=TAV
      C
      C      AVERAGE SENSIBLE HEAT TRANSFER COEFFICIENT
      C
351      HSTEP=HSTEP+H
352      HAVSTP=HSTEP/K
353      H1NT=H1NT+(H0+4.*HN+H)*THETA/6.
354      HAVINT=H1NT/THETU
355      H0=H
      C
      C      ENHANCEMENT FACTOR
      C
356      EFSTEP=HAPAVS/HA VSTP
357      EFINT=HAPAVI/HA VINT
      C
358      C1CTO=(TZ-TAV)/(TZ-T0)

```

```

359      DLSRHS=(VMT*PPP*THE10**3)/(U(1)**3)
360      PRINT 25,IV,IAV,U(1),RIMD,THUT,THE10
361      25      FORMAT(2X,3HTV=E14.7,1X,4HTAV=E14.7,1X,5HD(1)=,E14.7,1X,5HTING.
1E14.7,1X,5HTINT=F14.7,1X,6HTHE10=E14.7)
362      PRINT 26,INA,F,FI,HAPP,HAPAVS,HAPAVI
363      26      FORMAT(2X,'INA=',E14.7,1X,'F=',E14.7,1X,'FI=',E14.7,1X,'HAPP=',
1E14.7,1X,'HAPAVS=',E14.7,1X,'HAPAVI=',E14.7)
364      PRINT 24,H,HAVSTP,HAVINT,EFSIEP,EFINT,FONAV
365      24      FORMAT(2X,'H=',E14.7,1X,'HAVSTP=',E14.7,1X,'HAVINT=',F14.7,1X,
1'EFSIEP=',E14.7,1X,'EFINT=',E14.7,1X,'FONAV=',E14.7)
366      PRINT 23,IOLD,VF,Z,REN,NE,DI,HAPCTR
367      23      FORMAT(2X,5HIOLD=E14.7,1X,'VF=',E14.7,1X,'Z=',E14.7,1X,'REN=',
1E14.7,1X,'NE=',13,1X,'DI=',F10.5,1X,'HAPCTR=',F10.1)
368      PRINT 29,PRN,SCN,SHN,USN,WS,QL,ACN,HAPCH
369      29      FORMAT(2X,'PRN=',F10.5,1X,'SCN=',F10.5,1X,'SHN=',F10.5,1X,'USN=
1',F10.5,1X,'US=',F10.2,1X,'QL=',F10.2,1X,'ACN=',F10.5,1X,'HAPCH=
2,F10.1,/)
370      100      CONTINUE
371      GO TO 33
372      91      PRINT 55
373      55      FORMAT('0','ITERATION CANT BE ACCOMPLISHED BETWEEN THE LIMITS
1THA8THH','0')
374      GO TO 33
375      34      CONTINUE
376      PRINT 35
377      35      FORMAT('0','WATER SURFACE TEMPERATURE IS GREATER THAN 99.99% OF
1THE SURROUNDING TEMPERATURE',/)
378      33      CONTINUE
379      PRINT 27,PPP,TZ,RGP,VISP,VISV,VISMH
380      27      FORMAT(2X,4HPPP=E14.7,1X,3HTZ=E14.7,1X,4HRGP=E14.7,1X,5HVISP=,
114.7,1X,5HVISV=E14.7,1X,6HVISMH=E14.7/)
381      90      PRINT 28,VRI,REMH,DI,EFINT,HAPAVI,HAVINT
382      28      FORMAT(2X,4HVRI=E14.7,1X,5HREMH=E14.7,1X,3HDI=E14.7,1X,'EFINT=
1,E14.7,1X,'HAPAVI=',E14.7,1X,'HAVINT=',E14.7///)
383      C
384      60      CONTINUE
385      STOP
386      END
387      C
388      C      *****
389      SUBROUTINE PZAS(T,PS)
390      C      *****
391      C
392      X=T/100.
393      PS(((((((1.55318/10000.*X-2.6934527/1000.)*X+2.0153393/100.)*X
18.659025/100.)*X+2.4775634/10.)*X-5.6086594/10.)*X+1.2567591)*X-3
2033727)*X+7.2704899)*X-5.07671)
394      PS=EXP(PS)/1.01972
395      RETURN
396      END
397      C
398      C      *****
399      SUBROUTINE TEMPL(PPP,TZ)
400      C      *****
401      C
402      X=ALOG(1.01972*PPP)
403      TZ((((((-4.2924603/10000./10000.*X-4.2625685/10000000.)*X+1.
1343731/1000000.)*X+2.201712/100000.)*X-1.7417752/100000.)*X-3.73
23484/10000.)*X+1.4283773/1000.)*X+2.129682/100.)*X+2.1677605/10.)*
3X+2.3753577)*X+27.854242)*X+99.042712
404      RETURN

```


C
C
C

397

SUBROUTINE VVODES(P1,IV,VVOD)

C
C

398

A=(IV+273.15)/647.3

399

S=PI/221.286

400

U=100.*(3700000.-3122149.*A*A-1999.85/A**6)

401

W=(U+SQRT(1.72*U*U+1352925.*10.**10*(S-1.500705*A)))*.244117

402

B=1.052358*(62.5+S*(13.10268+S))/10.**11/(1.5108/100000.+A**11)

403

C=(0.053/154-A)**2

404

C=C*(7.241165/100000.+0.7676021*C**4)

405

VVOD=0.417/W+C-B-(11.39706-9.94427*A)/100000.

406

RETURN

407

END

C
C

408

SUBROUTINE SEKPV(TZ,PV)

C
C

409

X=TZ/100.

410

PV=((((-2.489006/10000.*X+3.156533/1000.)*X-1.5087829/100.)
1.3488548/100.)*X-3.8647589/100.)*X+1.1476149/10000.)*X-7.04194
2000.)*X+4.5905064/10.)*X+1.2602044

411

RETURN

412

END

C
C

** ***** **

413

SUBROUTINE CPVOD2(P1,IV,CPV)

C
C

414

X=IV/100.

415

Y=PI/100.

416

Z=X**5

417

CPV=1./(Y+2.)+0.021*Y-0.24927

418

CPV=CPV*(0.032+Z*(0.003264+0.026912*Z*Z/100000.))

419

Z=(((-1.100455*X+4.837200)*X-24.208803)*X+33.444712)*X+30.7252

420

CPV=Z*Y/1000.+CPV

421

Z=((2.259485*X-7.403256)*X+19.097088)*X-13.04363)*X+419.82594

422

CPV=Z/100.+CPV

423

RETURN

424

END

C
C

425

SUBROUTINE CPPAN(P1,IF,CPP)

C
C

426

X=(IF+273.15)/647.3

427

S=PI/221.286

428

B=1.6268287*(1.55108-S/2.)*X**1.82/10000.-5.0986646/100./X**3.

429

C=(2.010378*S*(17.722/4*S-11.*X**3)/1000.-0.2057615)/X**15

430

D=22128.703*(B*S+(C-1.5324846/X**33/1000.)*S**3)

431

CPP=(1169.8646-D+X*(-16.110723+X*(221.29742-X*52.106736)))/647

432

RETURN

433

END

C
C

```

434      SUBROUTINE SEKI(T,ENTA)
C      *****
C
435      X=1/100.
436      ENTA=((((1.0285952*X-9.4307509)*X+27.974559)*X-43.077814)*X+15.
19571)*X+161.50666)*X+2500.0256
437      RETURN
438      END
C
C      *****
439      SUBROUTINE PRIM11(T,ENTA)
C      *****
C
440      X=1/100.
441      ENTA=(((((((2.7663765/10.*X-3.9629482)*X+23.665162)*X-78.226638)
1X+151.59421)*X-175.79053)*X+120.80923)*X-44.519838)*X+425.17349)*
2-7.4554093/100.
442      IF(T-350.)2,2,1
443      1 ENTA=ENTA+0.348739*EXP(0.225556*(T-350.))
444      2 RETURN
445      END
C
C      *****
446      SUBROUTINE ANDA(P,T,VLAMB)
C      *****
C
447      X=1.+T/273.15
448      CALL PZAS(T,PS)
449      VLAMB=((0.24323-0.071643*X)*X-0.38929)*X+0.1656)*(P-PS)/100000.
450      VLAMB=(VLAMB+((15.1536*X-20.017)*X+25.146)*X-9.473)/10000.)*(P-PS)
451      VLAMB=VLAMB+((0.52577-0.07344*X)*X-1.8007)*X+2.8395)*X-0.92247
452      RETURN
453      END
C
C      *****
454      SUBROUTINE TRANEG(M1,X1)
C      TRANSCENDENTAL EQUATION SOLUTION -- TAN(X)+X/(R1-1.)=0.--HALF
C      INTERVAL SEARCH METHOD
C      *****
C
455      IMPLICIT REAL*8(A-H,O-Z)
456      DIMENSION X1(20)
457      C=M1-1.
458      P1=3.1415926535
459      IF(DABS(C).LT.0.005) GO TO 79
460      79 CONTINUE
461      DO 13 I=1,20
462      IF(DABS(C).LT.0.005) GO TO 21
463      IF(R1-1.)20,21,22
464      20 A=(1-I)*P1+0.000001
465      R=(2*I-1)*P1/2.
466      EPS=0.00001*(A+R)/2./(1.-R1)
467      GO TO 23
468      21 Y=(2*I-1)*P1/2.
469      GO TO 25
470      22 P1=3.1415926537
471      A=(2*I-1)*P1/2.
472      R=I*P1-0.00001
473      EPS=0.0001*(A+R)/2./(R1-1.)
474      23 FA=NTAN(C)-A/(1.-R1)

```

```

475      FD=DTAN(H)-C/(1.-H1)
476      K=0
477      7      K=K+1
478      Y=(A+H)/2.
479      TA=DTAN(Y)
480      CX=Y/C
481      F=TA+CX
482      IF(F)12,10,11
483      12      IF(F+EPS)3,10,10
484      11      IF(F-EPS)10,10,3
485      3      IF(F+FA)5,8,6
486      5      H=Y
487      FH=F
488      GO TO 7
489      6      A=Y
490      FA=F
491      GO TO 7
492      8      PRINT 9
493      9      FORMAT(14H4 IS TRUE ROOT)
494      GO TO 13
495      25     PRINT 9H,Y
496      98     FORMAT(10X,5HX(L)=,F15.8)
497      GO TO 13
498      10     CONTINUE
499      13     X1(I)=Y
500      RETURN
501      END

```

```

C
C
C      *****
502      SUBROUTINE VELODD
C      *****
C      NUMERICAL SOLUTION OF THE EQUATION OF MOTION FOR A DROPLET MOV
C      DOWNWARDS RUNGE--KUTTA TECHNIQUE
C
503      COMMON K,VRT,NE,VRR,ZRR,RUMH,VISMH,G,NI,NM,NN,THETA,VINF,VOLD,
ISURF1,ROV,D,VRO,I,VH,Z,THETU,VRES
504      DIMENSION U(20)
505      IF(K-1)408,408,409
506      408     VR=VRO
507      Z=0.
508      GO TO 410
509      409     IF(NE.LE.2) GO TO 415
510      VR=VRRK
511      Z=ZRR
512      GO TO 410
513      415     VRRK=VR
514      ZRR=Z
515      410     IF(VRO-VRT)451,452,453
516      451     IF(VR-VRT)454,452,452
517      453     IF(VR-VRT)452,452,454
518      454     CONTINUE
519      REU=VR*D(1)*RUMH*10000./VISMH
520      CALL COREJA(REU,COCOR)
521      PRUD=3000.*RUMH*VR**2/(4.*D(1)*ROV)
522      CRU=G-PRUD*COCOR
523      RE1=(VR+CRU*THETA/2.)*D(1)*RUMH*10000./VISMH
524      RE1=(VR+CRU*THETA/4.)*D(1)*RUMH*10000./VISMH
525      CALL COREJA(RE1,COCOR)
526      PRUD=3000.*RUMH*(VR+CRU*THETA/2.)*2/(4.*D(1)*ROV)

```

```

528      CALL COREIN(HEM1,CDCDR)
529      PROD=3000.*RUMB*(VR+CK0*THE1A/4.)*2/(4.*D(1)*ROV)
530      RE2=(VR+CK1*THE1A/2.)*D(1)*RUMB*10000./VISMH
531      REM2=(VR+CK1*THE1A/4.)*D(1)*RUMB*10000./VISMH
532      LKM1=G-PROD*CDCDR
533      CALL COREIN(RE2,CDCDR)
534      PROD=3000.*RUMB*(VR+CK1*THE1A/2.)*2/(4.*D(1)*ROV)
535      CK2=G-PROD*CDCDR
536      CALL COREIN(REM2,CDCDR)
537      PROD=3000.*RUMB*(VR+CKM1*THE1A/4.)*2/(4.*D(1)*ROV)
538      CKM2=G-PROD*CDCDR
539      RE3=(VR+CK2*THE1A)*D(1)*RUMB*10000./VISMH
540      REM3=(VR+CKM2*THE1A/2.)*D(1)*RUMB*10000./VISMH
541      CALL COREIN(RE3,CDCDR)
542      PROD=3000.*RUMB*(VR+CK2*THE1A)*2/(4.*D(1)*ROV)
543      CK3=G-PROD*CDCDR
544      CALL COREIN(REM3,CDCDR)
545      PROD=3000.*RUMB*(VR+CKM2*THE1A/2.)*2/(4.*D(1)*ROV)
546      CKM3=G-PROD*CDCDR
547      Z1=VR-VINF
548      VRH=VR+(CK0+2.*CKM1+2.*CKM2+CKM3)*THE1A/12.
549      Z2=VRH-VINF
550      VR=VR+(CK0+2.*CK1+2.*CK2+CK3)*THE1A/6.
551      Z3=VR-VINF
552      Z=Z+(Z1+4.*Z2+Z3)*THE1A/6.
553      GO TO 405
554      452 VR=VRT
555      IF(K-1)468,468,469
556      468 TIME=0.
557      Z=0.
558      GO TO 470
559      469 IF(KE.LE.2) GO TO 475
560      TIME=TIMEC
561      Z=ZC
562      GO TO 470
563      475 TIMEC=TIME
564      ZC=Z
565      470 TIME=TIME+THE1A
566      Z=Z+(VR-VINF)*TIME
567      405 CONTINUE
568      RETURN
569      END

```

C
C
C

```

570      SUBROUTINE VELDUP
571      C
572      C *****
573      C
574      C NUMERICAL SOLUTION OF THE EQUATION OF MOTION FOR A DROPLET MOVING
575      C UPWARDS RUNGE-KUTTA TECHNIQUE
576      C
577      COMMON K,VRT,RE,VRRK,ZRK,ROMB,VISMH,G,N,NM,MN,DT,VAIR,VDU,SURFT,
578      1ROV,C,VRO,I,VR,Z,THE10,VRRS
579      DIMENSION D(20)
580      IF(K-1)408,408,409
581      408 VR=VRT
582      Z=0.
583      GO TO 410
584      409 IF(KE.LE.2) GO TO 415
585      VR=VRRK
586      Z=ZRK
587      GO TO 410

```

```

581      415  VRK=VR
582      ZK=Z
583      410  CONTINUE
584      RE0=VR*D(1)*RUMH*10000./VISMB
585      CALL COREIN(RE0,CDCDR)
586      PRD=3000.*RUMH*VR**2/(4.*D(1)*ROV)
587      IF(VAIR-VRI)60,61,60
588      61    VAIR=VAIR-0.001
589      60    IF(V00.LI.VAIR) GO TO 210
590      IF(4.LI.1) GO TO 116
591      GO TO 16
592      116   CONTINUE
593      IF(NM.GI.1) GO TO 201
594      GO TO 151
595      210   NM=NM+1
596      201   CONTINUE
597      GO TO 16
598      151   CONTINUE
599      CK0=-(G+PRD*CDCDR)
600      GO TO 17
601      16    CK0= G-PRD*CDCDR
602      17    RE1=(VR+CK0*DT/2.)*D(1)*RUMH*10000./VISMB
603      REM1=(VR+CK0*DT/4.)*D(1)*RUMH*10000./VISMB
604      CALL COREIN(RE1,CDCDR)
605      PRD=3000.*(VR+CK0*DT/2.)*2/(4.*D(1)*ROV)
606      IF(N.LI.1) GO TO 118
607      GO TO 18
608      118   CONTINUE
609      IF(NM.GI.0) GO TO 18
610      CK1=-(G+PRD*CDCDR)
611      GO TO 19
612      18    CK1= G-PRD*CDCDR
613      19    CALL COREIN(REM1,CDCDR)
614      PRD=3000.*(VR+CK0*DT/4.)*2/(4.*D(1)*ROV)
615      IF(N.LI.1) GO TO 120
616      GO TO 20
617      120   CONTINUE
618      IF(NM.GI.0) GO TO 20
619      CKM1=-(G+PRD*CDCDR)
620      GO TO 21
621      20    CKM1= G-PRD*CDCDR
622      21    RE2=(VR+CK1*DT/2.)*D(1)*RUMH*10000./VISMB
623      REM2=(VR+CK1*DT/4.)*D(1)*RUMH*10000./VISMB
624      CALL COREIN(RE2,CDCDR)
625      PRD=3000.*(VR+CK1*DT/2.)*2/(4.*D(1)*ROV)
626      IF(N.LI.1) GO TO 122
627      GO TO 22
628      122   CONTINUE
629      IF(NM.GI.0) GO TO 22
630      CK2=-(G+PRD*CDCDR)
631      GO TO 23
632      22    CK2= G-PRD*CDCDR
633      23    CALL COREIN(REM2,CDCDR)
634      PRD=3000.*RUMH*(VR+CKM1*DT/4.)*2/(4.*D(1)*ROV)
635      IF(N.LI.1) GO TO 124
636      GO TO 24
637      124   CONTINUE
638      IF(NM.GI.0) GO TO 24
639      CKM2=-(G+PRD*CDCDR)
640      GO TO 25
641      24    CKM2= G-PRD*CDCDR
642      25    RE3=(VR+CK2*DT/2.)*D(1)*RUMH*10000./VISMB

```

216

```

644      CALL COREIN(HE3,CDCDR)
645      PROD=3000.*RUMH*(VF+C*2*DT)**2/(4.*D(I)*ROV)
646      IF(N.LT.1) GO TO 126
647      GO TO 26
648 126    CONTINUE
649      IF(NM.GI.0) GO TO 26
650      CK3=-(G+PROD*CDCDR)
651      GO TO 27
652 26     CK3= G-PROD*CDCDR
653 27     CALL COREIN(HEM3,CDCDR)
654      PROD=3000.*RUMH*(VR+CK2*DT/2. )**2/(4.*D(I)*ROV)
655      IF(N.LT.1) GO TO 128
656      GO TO 28
657 128    CONTINUE
658      IF(NM.GI.0) GO TO 28
659      CKM3=-(G+PROD*CDCDR)
660      GO TO 29
661 28     CKM3= G-PROD*CDCDR
662 29     CONTINUE
663      IF(N.LT.1) GO TO 130
664      GO TO 7
665 130    CONTINUE
666      IF(NM.GI.0) GO TO 7
667      Z1=VR+VAIK
668      GO TO 51
669 7       Z1=VAIK-VR
670      GO TO 51
671 51     VRM=VR+(CK0+2.*CKM1+2.*CKM2+CKM3)*DT/12.
672      IF(N.LT.1) GO TO 132
673      GO TO 71
674 132    CONTINUE
675      IF(NM.GI.0) GO TO 71
676      Z2=VRM+VAIK
677      GO TO 53
678 71     Z2=VAIK-VRM
679      GO TO 53
680 53     CONTINUE
681      VR=VR+(CK0+2.*CK1+2.*CK2+CK3)*DT/6.
682      VRS=VF
683      IF(VR.LI.0.) GO TO 112
684      GO TO 111
685 112    CONTINUE
686      VR=ABS(VR)
687 111    CONTINUE
688      IF(N.LT.1) GO TO 134
689      GO TO 72
690 134    CONTINUE
691      IF(NM.GI.0) GO TO 72
692      Z3=VR+VAIK
693      GO TO 35
694 72     Z3=VAIK-VR
695      GO TO 35
696 35     CONTINUE
697      Z=Z+(Z1+4.*Z2+Z3)*DT/6.
698 56     CONTINUE
699      IF(N.LT.1) GO TO 145
700      GO TO 73
701 145    CONTINUE
702      IF(NM.GI.0) GO TO 73
703      VD=VR+VAIK
704      GO TO 41
705 73     VD=VAIK-VR
706 41     CONTINUE

```

```

707      T=THE10+DT
708      PRINT 102,CK0,CK1,CK2,CK3,RE0,RE1,RE2,RE3,N,K,L,N
709      102  FORMAT(1X,4HCK0=,F10.5,1X,4HCK1=,F10.5,1X,4HCK2=,F10.5,1X,4HCK3
110.5,1X,4HRE0=,F5.1,1X,4HRE1=,F5.1,1X,4HRE2=,F5.1,1X,4HRE3=,F5.
21X,2H=,13,1X,2H=,13,1X,3H=,13)
710      PRINT 101,1,VK,Z,VD,VHRS,Z1,Z2,Z3,CDCDR,FM
711      101  FORMAT(10X,2H=,F5.2,5X,3HVR=,F5.2,5X,2HZ=,F5.2,5X,3HVD=,F5.2,2
15HVHRS=,F5.2,2X,3H21=,F5.2,2X,3H22=,F5.2,2X,3H23=,F5.2,1X,6HCD
2,F5.1,1X,3H=,13)
712      RETURN
713      END

C
C      *****

714      SUBROUTINE CDREIN(RE1,CO)
C
C      *****

715      COMMON K,VRI,WE,VRK,ZRK,ROMB,VISMB,G,NI,NM,NN,THETA,VINF,VDUP,
1SURFT,KOV,D,VK0,1,VK,Z,THE10,VRPS
716      DIMENSION D(20)
717      RE1=ABS(RE1)
718      S=ROMB*SURF1**3*10.**2H/G/VISMB**4
719      DELRO=KOV-ROMB
720      DSTAR=10.*D(1)*((ROMB**2)*G*10.**2/VISMB**2)**(1./3.)
721      DSTAR1=1.21n/(DELRO/ROMB)**(1./3.)
722      DSTA2A=70.0*(DELRO/ROMB)**(-1./3.)*(S*10.**(-12))**(-0.111)
723      DSTA2B=50.8*(DELRO/ROMB)**(-1./3.)*(S*10.**(-12))**(-0.111)
724      DSTA3A=122.*(DELRO/ROMB)**(-0.535)*(S*10.**(-12))**(-0.275)
725      DSTA3B=300.*(DELRO/ROMB)**(-0.535)*(S*10.**(-12))**(-0.0367)
726      DSTA4A=160.*(DELRO/ROMB)**(-0.447)*(S*10.**(-12))**(-0.114)
727      RE2A=974.*(S*10.**(-12))**(-0.192)
728      RE2B=236.*(S*10.**(-12))**0.192
729      RE3A=2240.*(DELRO/ROMB)**(-0.303)*(S*10.**(-12))**0.388
730      RE3B=7160.*(DELRO/ROMB)**(-0.303)*(S*10.**(-12))**0.08
731      RE4=3190.*(DELRO/ROMB)**(-0.173)*(S*10.**(-12))**0.18
732      RE5=4470.*(DELRO/ROMB)**(-0.238)*(S*10.**(-12))**0.232
733      DMAXS=224.*(DELRO/ROMB)**(-0.5)*(S*10.**(-12))**(-1./6.)
734      CDMAX=0.75*(DELRO/ROMB)**(-0.0232)*(S*10.**(-12))**0.036
735      WSTAR=3.273*((DELRO/ROMB)*S**0.25)**0.262
736      WMAXS=RE5/DMAXS
737      WSTAR4=RE4/DSTAR4
738      WSTAR3A=RE3A/DSTAR3A
739      WSTAR3B=RE3B/DSTAR3B
740      WSTAR2A=RE2A/DSTAR2A
741      WSTAR2B=RE2B/DSTAR2B
742      WSTAR1=0.1/DSTAR1
743      DS1=DMAXS
744      A=0.065-(1./29.54)*ALOG10(S**0.5/(DELRO/ROMB)*10.**(-3))
745      IF(RE1.LE.0.5) GO TO 10
746      IF(S.GT.44.*10**12) GO TO 20
747      IF(RE1.GT.RE2A) GO TO 25
748      CD=(24./RE1)*(1.+0.150*RE1**0.687)
749      DSTA=(3.*RE1**2*CD*ROMB/(4.*DELRO))**(-1./3.)
750      WSTA=(4.*RE1*DELRO/(3.*CD*ROMB))**(-1./3.)
751      GO TO 210
752      20  CONTINUE
753      IF(RE1.GT.RE2B) GO TO 26
754      CD=(24./RE1)*(1.+0.150*RE1**0.687)
755      DSTA=(3.*RE1**2*CD*ROMB/(4.*DELRO))**(-1./3.)
756      WSTA=(4.*RE1*DELRO/(3.*CD*ROMB))**(-1./3.)
757      GO TO 210
758      25  CONTINUE
759      IF(RE1.GT.RE2A) GO TO 20

```

```

760      CD=0.45*(S*10.**(-12))*0.05
761      DSTA=(3.*RE1**2*CD*ROMH/(4.*DELRO))* (1./3.)
762      WSTA=(4.*RE1*DELRO/(3.*CD*ROMH))* (1./3.)
763      GO TO 210
764  26    CONTINUE
765      IF (RE1.GT.RE30) GO TO 50
766      CD=0.7*(S*10.**(-12))*(-0.05)
767      DSTA=(3.*RE1**2*CD*ROMH/(4.*DELRO))* (1./3.)
768      WSTA=(4.*RE1*DELRO/(3.*CD*ROMH))* (1./3.)
769      GO TO 210
770  10    CD=24./RE1
771      DSTA=(3.*RE1**2*CD*ROMH/(4.*DELRO))* (1./3.)
772      WSTA=(4.*RE1*DELRO/(3.*CD*ROMH))* (1./3.)
773      GO TO 210
774  50    CONTINUE
775      IF (RE1.GT.RE4) GO TO 60
776      DSTA=(RE1/(4.5*(DELRO/ROMH))*0.388*(S*10.**(-12))*0.0323))* (1./
11.29)
777      WSTA=DSTA**0.29*4.5*(DELRO/ROMH))*0.388*(S*10.**(-12))*0.0323
778      CD=0.06570*DSTA**0.42*(DELRO/ROMH))*0.224*(S*10.**(-12))*(-0.065
779      GO TO 210
780  60    CONTINUE
781      IF (RE1.GT.RE5) GO TO 70
782      WSTA=19.96*(DELRO/ROMH))*0.262*(S*10.**(-12))*0.0654
783      DSTA=RE1/WSTA
784      CD=0.00355*(DELRO/ROMH))*0.477*(S*10.**(-12))*(-0.131)*DSTA
785      GO TO 210
786  70    CONTINUE
787  11    GR=4.*DELRO*DST**3-3.*RE1**2*ROMH*(A*(DST-DMAXS)+CD*MAX)
788      GRPRIM=12.*DELRO*DST**2-3.*RE1**2*ROMH*A
789      DSTN=DST-GR/GRPRIM
790      IF (ABS((DSTN-DST)/DST).LT.0.001) GO TO 12
791      DST=DSTN
792      GO TO 11
793  12    CD=CD*MAX+A*(DSTN-DMAXS)
794      WST=SQRT(4.*DELRO*DSTN/(3.*ROMH*(A*(DSTN-DMAXS)+CD*MAX)))
795      DSTA=DSTN
796      WSTA=WST
797  210    CONTINUE
798      RETURN
799      END

```

C

C

```

*****

```

```

800      SUBROUTINE VISASM(TF,RF,ROPF,VISPF)
801  C      *****
802      VISPF=0.4+0.407*TF-ROPF*(1858.-5.9*TF)/1000.
803      VISVF=173.6+0.454*TF
804      F112F=0.3536/SQRT(1.+0.6222)*(1.+SQRT(VISPF/VISVF)*1.12593)**2
805      F121F=0.3536/SQRT(1.+1.6071)*(1.+SQRT(VISVF/VISPF)*0.48414)**2
806      VISPF=RF*VISPF/(RF+(1.-RF)*F112F)+(1.-RF)*VISVF/(RF*F121F+1.-RF)
807      RETURN
808      END

```

C

C

```

*****

```

```

808      SUBROUTINE AMBASM(TF,RF,CPN2,CP02,CPAR,AMBPF)
809  C      *****
810      AMBPF=0.0176+5.87/100000.*TF+1.04/10.**7*TF*TF-0.451*TF*TF/TF/10.
1*11
811      WPN2=28.02
812      WPU2=32.
      WPAR=39.90

```



```

813      TRN2=(TF+273.15)/126.1
814      TR02=(TF+273.15)/154.4
815      TRAR=(TF+273.15)/151.2
816      SIN2=1.873/100000.
817      SLO2=1.393/100000.
818      SIAR=1.272/100000.
819      CPN2=27214.+0.187*(TF+273.15)
820      CP02=34625.+1.0802*(TF+273.15)-75586.*10000./(TF+273.15)**2
821      CPAR=20000.
822      CVN2=(CPN2-8315.)/WNN2
823      CV02=(CP02-8315.)/PM02
824      CVAR=(CPAR-8315.)/VPAH
825      VISN2=N.175*(4.58*TRN2-1.67)**(5./8.)/SIN2/10.**11
826      VIS02=N.175*(4.58*TR02-1.67)**(5./8.)/SLO2/10.**11
827      VISAR=N.175*(4.58*TRAR-1.67)**(5./8.)/SIAR/10.**11
828      AMN2=VISN2*(1.32*CVN2+500.-104.6/TRN2)
829      AM02=VIS02*(1.32*CV02+444.8-91.59/TR02)
830      AMAR=2.5*VISAR*CVAR
831      AMBVF=(0.78*(WNN2**(1./3.))*AMN2+0.21*(PM02**(1./3.))*AM02+0.
1(WPAH**(1./3.))*AMAR)/(0.78*(WNN2**(1./3.))+0.21*(PM02**(1./3
20.01*(WPAH**(1./3.)))
832      F112L=0.3536/SQRT(1.+0.6222)*(1.+SQRT(AMBPF/AMBVF)*1.12593)**2
833      F121L=0.3536/SQRT(1.+1.6071)*(1.+SQRT(AMHVF/AMBPF)*0.44814)**2
834      AMBMF=RF*AMBPF/(RF+(1.-RF)*F112L)+(1.-RF)*AMBVF/(RF+F121L+1.-RF)
835      RETURN
836      END

```

C

C

```

*****

```

```

837      SUBROUTINE DIFASM(TF,RF,DIFMF)

```

C

```

838      DIFMF=(1.-RF)*((TF+273.15)**1.81)/10.**9/((1.-RF)*0.78/0.75774
1RF)*0.21/0.7744+(1.-RF)*0.01/0.7503)

```

```

839      RETURN

```

```

840      END

```

C

C

C

C

```

*****
*****

```

```

$ENTRY

```

APPENDIX G

THE COMPUTER PROGRAM FOR INTERNAL RESISTANCE AND
NO MIXING SOLUTION OF THE SINGLE DROPLET RESPONSE

```

C *****
C *****
C *
C *THIS PROGRAMME SOLVES THE PROBLEM OF SIMULTANEOUS MOMENTUM,HEAT
C *MASS TRANSFER DURING CONDENSATION OF STEAM FROM SATURATED AIR-S
C *MIXTURE ON A DROPLET WITH RESISTANCE TO HEAT FLOW IN A DROPLET
C *A NONUNIFORM TEMPERATURE OF A DROPLET
C *STEADY STATE DRAG COEFFICIENTS FOR WATER DROPLETS USING REINHART
C *CORRELATION--INITIALLY DROPLET MOVES EITHER UPWARDS OR DOWNWARDS
C *
C *SI--UNITS
C *
C *****
C *****
C *****
C A=THERMAL DIFFUSIVITY M2/SEC
C AMBMF=THERMAL CONDUCTIVITY OF MIXTURE -- FILM J/M OK SEC
C AMBMP=THERMAL CONDUCTIVITY OF STEAM -- FILM J/M OK SEC
C AMBMV=THERMAL CONDUCTIVITY OF AIR -- FILM J/M OK SEC
C AMDA=THERMAL CONDUCTIVITY OF WATER J/M SEC OC
C BI=BIOT NUMBER
C CDCDR=DRAG COEFFICIENT OF A DROPLET
C CDD -DRAG COEFFICIENT OF A DISK
C CDSS -DRAG COEFFICIENT OF A SOLID SPHERE
C CK0,CK1,CK2,CK3=RUNGE KUTTA'S COEFFICIENTS
C CPA - HEAT CAPACITY OF AIR J/KMOLOK
C CPMF - HEAT CAPACITY OF MIXTURE AT FILM TEMPERATURE J/KGOK
C CPP - HEAT CAPACITY OF STEAM KJ/KGOK
C CPV=HEAT CAPACITY OF WATER KJ/KG OK
C DD=DROPLET DIAMETER INCREASE M
C DIFMF=DIFFUSIVITY OF MIXTURE -- FILM M2/SEC
C DT=TEMPERATURE INCREASE OC
C F=MASS TRANSFER COEFFICIENT KMOL/M2 SEC
C FON=FOURIER NUMBER
C G=GRAVITY ACCELERATION M2/SEC
C H=HEAT TRANSFER COEFFICIENT J/M2 OK SEC
C HVAP=HEAT OF VAPORIZATION KJ/KG
C KE - THE NUMBER OF DIAMETERS
C KF - THE NUMBER OF STEAM/(AIR+STEAM) RATIOS
C PEN - PECLET NUMBER
C PPP - PARTIAL PRESSURE OF THE STEAM BAR
C PRN - PRANDTL NUMBER
C PT - TOTAL PRESSURE OF THE MIXTURE BAR
C PV - PRODUCT OF PPP BY (1/ROP) BAR*M3/KG
C QL=LATENT HEAT TRANSFER J/M2 SEC
C QS=SENSIBLE HEAT TRANSFER J/M2 SEC
C QT=QS+QL -- TOTAL HEAT TRANSFER J/M2 SEC
C REMH=REYNOLDS NUMBER OF MIXTURE -- BULK
C REN - REYNOLDS NUMBER
C RMB - MIXTURE GAS CONSTANT - BULK J/KGOK
C RTND=RATIO OF THERMAL DIFFUSIVITY AND MOLECULAR DIFFUSION COEFF.
C ROMB - DENSITY OF MIXTURE - BULK KG/M3
C ROP - DENSITY OF VAPOUR - BULK KG/M3
C ROV - DENSITY OF WATER KG/M3
C ROPF=DENSITY OF STEAM -- FILM KG/M3
C SCN - SCHMIDT NUMBER
C SHN - SHERWOOD NUMBER
C SURFT-SURFACE TENSION OF A DROPLET INAN AIR/STEAM MIXTURE N/M
C TF=TEMPERATURE OF FILM OC
C TNA=MASS TRANSFER RATE KMOL/M2 SEC
C TV - WATER DROPLET TEMPERATURE OC
C TZ - SATURATION TEMPERATURE CORRESPONDING TO PPP OC

```

C	USN - NUSSLEI NUMBER	
C	VISMB - VISCOSITY OF MIXTURE - BULK	10**7*NS/M2 222
C	VISMF=VISCOSITY OF MIXTURE -- FILM	10.**7 *N SEC/M2
C	VISPB - VISCOSITY OF STEAM - BULK	10**7*NS/M2
C	VISPF=VISCOSITY OF STEAM -- FILM	10.**7 *N SEC/M2
C	VISVB - VISCOSITY OF AIR - BULK	10**7*NS/M2
C	VISVF=VISCOSITY OF AIR -- FILM	10.**7 *N SEC/M2
C	VD=VELOCITY OF A DROPLET	M/SEC
C	VINF=VELOCITY OF SURROUNDING MIXTURE	M/SEC
C	VR=RELATIVE VELOCITY OF A DROPLET	M/SEC
C	VRO=INITIAL RELATIVE VELOCITY	M/SEC
C	VRT - TERMINAL VELOCITY	M/SEC
C	W=MOULAR MASS VELOCITY	
C	WMMF=MOLECULAR WEIGHT OF MIXTURE -- FILM	KMOL/M2 SEC
C	WMMF=MOLECULAR WEIGHT OF MIXTURE -- FILM	KG/KMOL
C	Z=DISTANCE TRAVELLED BY A DROPLET	KG/KMOL
C		M
C		
C		
C		

```

1  DOUBLE PRECISION BI,Y,RO,TN,A0,A1,A2,A3,A4,A5,A6,A7
2  COMMON K,VRT,NE,VFK,ZRK,ROMB,VISMB,G,NI,NM,NN,THETA,VINF,VDUP,
3  1SURFT,ROV,D,VRO,I,VR,Z,THETU,VRRS
4  DIMENSION RN(20),TN(20),TNP(20),RD(20)
5  DIMENSION D(20),R(20),X(200),Y(200)

```

```

5  VRTT=100.
6  VREXP=100.
7  VREXP=0.

```

```

8  READ 1,KE,KF
9  1  FORMAT(2I5)
10  DO 80 I=1,KE
11  READ 37,PT
12  37  FORMAT(F10.5)
13  DO 90 J=1,KF
14  IF(VREXP.GT.0.) GO TO 43
15  READ 2,D(I),R(J),I0,I1,TH1
16  2  FORMAT(SF10.5)
17  GO TO 44
18  43  READ 45,D(I),I2,VREXP,I0,I1,TH1
19  45  FORMAT(6F10.5)
20  44  CONTINUE

```

```

21  IF(VRTT.GT.0.) GO TO 501
22  VDUP=0.
23  VINF=1.
24  IF(VDUP.GT.0.) GO TO 502
25  VDDOWN=11.
26  VD=VDDOWN
27  VRO=VINF+VD
28  GO TO 501

```

```

29  502  VRO=ABS(VDUP-VINF)
30  VD=VDUP

```

```

31  501  CONTINUE

```

```

32  TV=T1
33  THETU=0.
34  HAPPO=0.
35  HAPSTP=0.
36  HAPINT=0.
37  H0=0.
38  HSTEP=0.
39  HINT=0.
40  HAPCHO=0.
41  HAPCHT=0.

```

```

42      TIME=0.
43      TAVOLD=T0
44      NI=0
45      NM=0
46      NN=0
47      ZRK=0.
48      VRRK=0.
49      G=9.80665
50      PI=3.14159

      C
      C      DENSITY OF MIXTURE__BULK
      C
51      IF(VREXP.GT.0.) GO TO 46
52      PPP=R(J)*PI
53      CALL TEMP1(PPP,TZ)
54      GO TO 47
55  46      CONTINUE
56      CALL PZAS(TZ,PPP)
57      R(J)=PPP/PT
58  47      CONTINUE
59      RMB=8314.7/(R(J)*18.02+(1.-R(J))*28.96)
60      ROMB=100000.*PI/(RMB*(TZ+273.15))

      C
      C      VISCOSITY OF MIXTURE__BULK
      C
61      CALL SEKPV(TZ,PV)
62      ROP=PI/PV
63      VISP=80.4+0.407*TZ-ROP*(1858.-5.9*TZ)/1000.
64      VISV=173.0+0.454*TZ
65      FI12=0.3536/SQRT(1.+0.6222)*(1.+SQRT(VISP/VISV))*1.12593)**2
66      FI21=0.3536/SQRT(1.+1.6071)*(1.+SQRT(VISV/VISP))*0.88814)**2
67      VISM=R(J)*VISP/(R(J)+(1.-R(J))*FI12)+(1.-R(J))*VISV/(R(J)*FI21
1-R(J))

      C
      C      MASS OF A DROPLET
      C
68      CALL VVODE5(PT,T1,VVOD)
69      ROV=1./VVOD
70      DM=ROV*PI*D(I)**3/(6.*10.**9)
71      AREA=PI*D(I)**2*10.**(-6)
72      PRINT 11,D(I),R(J),PT,T1,VD,VINF
73  11      FORMAT(/,2X,5HD(I)=,F10.5,2X,5HR(J)=,F10.5,2X,3HPT=,F10.5,2X,3
1=,F10.5,2X,3HVD=,F10.5,2X,'VINF=',F10.5)

      C
      C      TERMINAL VELOCITY OF MIXTURE
      C
74      IF(VREXP.GT.0.) GO TO 17
75      IF(D(I)-1.0)3,3,5
76  3      FK1=8.625*SQRT(VISM*RMB/10.**7)/(D(I)/1000.)*1.5/ROV
77      FK2=1.3913*FK1
78      VRT=(9.80665/FK1)**(2./3.)
79      REMB=VRT*D(I)*ROMB*10000./VISM
80      IF(REMB-10.)6,6,4
81  4      VRT1=(9.80665/FK2)**(2./3.)
82      REMB=REMB*VRT1/VRT
83      VRT=VRT1
84      GO TO 6
85  5      VRT=9.43*(1.-EXP(-(D(I)/1.77)**1.147))
86      GO TO 18
87  17      CONTINUE
88      VRT=VREXP
89  18      CONTINUE
90      REMB=VRT*D(I)*10000./VISM

```

```

92      IF(VRTT.GT.0.) GO TO 15
93      GO TO 16
94      15  CONTINUE
95      VR=VRT
96      VR0=VRT
97      Z=0.
98      16  CONTINUE
99      KI=30
100     DT=(TZ-11)/KI
101     DT1=DT
102     KJ=KI+10
103     BDT=0.99
      C
      C
104     *****
      DU 100 K=1,KJ
      C
      C
105     IF(K.GT.(KJ-11)) GO TO 12
106     GO TO 13
107     12  CONTINUE
108     IF(K.GT.(KJ-7)) GO TO 14
109     DT=DT1/5.
110     GO TO 13
111     14  RDT=BDT+9./10.** (K-31)
112     TVN=BDT*TZ
113     DI=TVN-1V
114     13  CONTINUE
115     TV=1V+DT
116     TVM=TV-DT/2.
117     IF(1V.GT.0.9999*TZ) GO TO 34
118     TF=(TZ+1V-DI/2.)/2.
119     TFM=(TZ+TVN-DI/2.)/2.
120     CALL PZAS(TF,PZF)
121     CALL PZAS(TFM,PZFM)
122     RF=PZF/PT
123     RFM=PZFM/PT
124     CALL SEKPV(TF,PV)
125     CALL SEKPV(TFM,PVM)
126     ROPF=PT/PV
127     ROPFM=PT/PVM
      C
      C  VISCOSITY OF MIXTURE--FILM
      C
128     CALL VISASM(TF,RF,ROPF,VISMF)
129     CALL VISASM(TFM,RFM,ROPFM,VISMFM)
      C
      C  THERMAL CONDUCTIVITY OF MIXTURE -- FILM
      C
130     CALL AMBASM(TF,RF,CPN2,CP02,CPAR,AMBMF)
131     CALL AMBASM(TFM,RFM,CPN2M,CP02M,CPARM,AMBMM)
      C
      C  DIFFUSIVITY-OF MIXTURE -- FILM
      C
132     CALL DIFASM(TF,RF,DIFMF)
133     CALL DIFASM(TFM,RFM,DIFMM)
      C
      C  DENSITY OF MIXTURE--FILM
      C
134     RMF=8314.7/(RF*18.02+(1.-RF)*28.96)
135     RMFM=8314.7/(RFM*18.02+(1.-RFM)*28.96)
136     ROMF=100000.*PT/(RMF*(TF+273.15))
137     ROMFM=100000.*PT/(RMFM*(TFM+273.15))

```

```

136 CALL CPPAR(PZF,TF,CPP)
139 CALL CPPAR(FZFM,TFM,CPPM)
140 CPA=0.7H*CPN2+0.21*CPD2+0.01*CPAR
141 CPAM=0.7H*CPN2M+0.21*CPD2M+0.01*CPARM
142 CPMF=RF*CPP*1000.+(1.-RF)*CPA/28.96
143 CPMFM=RFM*CPPM*1000.+(1.-RFM)*CPAM/28.96

```

PRANDTL NUMBER

```

144 PRN=CPMF*VISMF/AMBMF/10.**7
145 PRNM=CPMFM*VISMFM/AMBMFM/10.**7

```

REYNOLDS NUMBER

```

146 REN=VRT*D(1)*ROMF*10000./VISMF
147 RENM=VRT*D(1)*ROMFM*10000./VISMFM
148 WMMF=RF*18.02+(1.-RF)*28.96
149 WMMFM=RFM*18.02+(1.-RFM)*28.96
150 WMMB=P(J)*18.02+(1.-P(J))*28.96
151 K=VRT*ROMB/WMMB
152 NE=1
153 IF(VRT.GT.0.) GO TO 600
154 IF(K-1)404,404,405
155 405 REN=VR*D(1)*ROMF*10000./VISMF
156 RENM=VR*D(1)*ROMFM*10000./VISMFM
157 K=VR*ROMH/WMMH
158 TOLD=THE1U+THETA
159 600 CONTINUE

```

SCHMIDT NUMBER

```

160 404 SCN=VISMF/ROMF/DIFMF/10.**7
161 SCNM=VISMFM/ROMFM/DIFMFM/10.**7

```

PECLET NUMBER

```

162 PEN=REN*SCN
163 PENM=RENM*SCNM

```

NUSSELT NUMBER

```

164 IF(REN=450.)7,7,8
165 7 USN=2.+0.6*(REN**0.5)*(PRN**(1./3.))
166 USNM=2.+0.6*(RENM**0.5)*(PRNM**(1./3.))

```

SHERWOOD NUMBER

```

167 SHN=2.+0.6*(REN**0.5)*(SCN**(1./3.))
168 SHNM=2.+0.6*(RENM**0.5)*(SCNM**(1./3.))
169 GO TO 9
170 8 USN=2.+0.27*(REN**0.62)*(PRN**(1./3.))
171 USNM=2.+0.27*(RENM**0.62)*(PRNM**(1./3.))
172 SHN=2.+0.27*(REN**0.62)*(SCN**(1./3.))
173 SHNM=2.+0.27*(RENM**0.62)*(SCNM**(1./3.))

```

HEAT TRANSFER COEFFICIENT

```

174 9 H=1000.*AMBMF*USN/D(1)
175 HM=1000.*AMBMFM*USNM/D(1)

```

```

176      KMMH=R(J)*18.02+(1.-R(J))*28.96
177      F=SHN*W/PEM
178      FM=SHNM*W/PEM

      C
      C
      C      MASS TRANSFER RATE

179      CALL PZAS(TV,PZV)
180      TNA=F*(ALOG((1.-PZV/PT)/(1.-PPP/PT)))
181      CALL PZAS(TVM,PZVM)
182      TNAM=FM*(ALOG((1.-PZVM/PT)/(1.-PPP/PT)))

      C
      C
      C      HEAT OF VAPORIZATION

183      CALL SEKI(TF,HSEK)
184      CALL PRIM11(TF,HPRIM)
185      HVAP=HSEK-HPRIM
186      CALL SEKI(TFM,HSEK)
187      CALL PRIM11(TFM,HPRIM)
188      HVAPM=HSEK-HPRIM

      C
      C
      C      SENSIBLE HEAT TRANSFER

189      ACC=TNA*18020.*CPP/H
190      ACN=ACC/(1.-EXP(-ACC))
191      QS=ACN*H*(TZ-TV+DT/2.)
192      ACCM=TNAM*18020.*CPP/HM
193      ACNM=ACCM/(1.-EXP(-ACCM))
194      QSM=ACNM*HM*(TZ-TV+DT/4.)

      C
      C
      C      LATENT HEAT TRANSFER

195      QL=HVAP*TNA*18020.
196      QLM=HVAPM*TNAM*18020.

      C
      C
      C      TOTAL HEAT TRANSFER

197      QT=QL+QS
198      QTM=QLM+QSM

      C
      C
      C      APPARENT HEAT TRANSFER COEFFICIENT

199      HAPP=QT/(TZ-TV+DT/2.)
200      HAPPM=QTM/(TZ-TVM+DT/4.)

      C
      C
      C      BIOT NUMBER

201      CALL AMDA(PT,TV,VLAMB)
202      BI=HAPP*D(I)/VLAMB/2000.

      C
      C
      C      THE ROOTS OF TRANSCENDENTAL EQUATION TAN(X)+X/(BI-1.)=0.

203      CALL TRANEQ(BI,Y)
      C      *****
      C      TIME TAKEN FOR DROPLET TEMPERATURE INCREASE DT--HALF INTERVAL
      C      SEARCH METHOD
      C      *****

204      EPS=0.0001
205      THA=0.00001
206      THH=TH1
207      IF(K.GT.1) GO TO 371
208      TEMPR=(TZ-TV)/(TZ-T0)

```



```

209      GO TO 372
210      371      CONTINUE
211      TEMPR=TZ-TV
212      372      CONTINUE
C
C      THERMAL DIFFUSIVITY OF WATER DROPLET
C
213      CALL CPVUD2(PT,TV,CPV)
214      CALL VVODE5(PT,TV,VVUD)
215      RUV=1./VVUD
216      ALFA=VLAMB/CPV/ROV/1000.
C
C      FOURIER NUMBER
C
217      FONA=4.*ALFA*THA*(10**6)/(D(I)**2)
218      FONB=4.*ALFA*THB*(10**6)/(D(I)**2)
219      SUMA=0.
220      SUMB=0.
221      DO 110 L=1,200
222      IF(L.GT.20) GO TO 109
223      X(L)=SNGL(Y(L))
224      GO TO 108
225      109      X(L)=X(L-1)+PI
226      108      CONTINUE
227      IF(K.GT.1) GO TO 310
228      AISA=(SIN(X(L))-X(L)*COS(X(L)))/(X(L)-SIN(X(L))*COS(X(L)))*(SIN
1(L))/X(L))
229      GO TO 311
230      310      CONTINUE
231      AIS=SIN(X(L))/(X(L)-SIN(X(L))*COS(X(L)))/X(L)
232      S1A=(12-A0)*(SIN(X(L))-X(L)*COS(X(L)))
233      S2A=A1*(1/(1*(2.*X(L)*SIN(X(L))-(X(L)**2-2.)*COS(X(L))-2.)/
1(2.*X(L)))
234      S3A=A2*(1/(1**2*(3.*(X(L)**2-2.)*SIN(X(L))-X(L)*(X(L)**2-6.)*
1COS(X(L)))/(4.*X(L)**2)
235      S4A=A3*(1/(1**3*(4.*X(L)*(X(L)**2-6.)*SIN(X(L))-(X(L)**4-12.*X(L)
1**2+24.)*COS(X(L))+24.)/(8.*X(L)**3)
236      S5A=A4*(1/(1**4*(5.*X(L)**4-60.*X(L)**2+120.)*SIN(X(L))-X(L)*(
1)**4-20.*X(L)**2+120.)*COS(X(L)))/(16.*X(L)**4)
237      S6A=A5*(1/(1**5*(X(L)*(6.*X(L)**4-120.*X(L)**2+720.)*SIN(X(L))-
1(L)**6-30.*X(L)**4+360.*X(L)**2-720.)*COS(X(L))-720.)/(32.*X(L)**5)
238      S7A=A6*(1/(1**6*(7.*X(L)**6-210.*X(L)**4+2520.*X(L)**2-5040.)*
1SIN(X(L))-X(L)*(X(L)**6-42.*X(L)**4+840.*X(L)**2-5040.)*COS(X(L)
2/(64.*X(L)**6)
239      S8A=A7*(1/(1**7*(X(L)*(8.*X(L)**6-336.*X(L)**4+6720.*X(L)**2-
140320.)*SIN(X(L))-(X(L)**8-56.*X(L)**6+1680.*X(L)**4-20160.*X(L)
2**2+40320.)*COS(X(L))+40320.)/(128.*X(L)**7)
240      SUSA=S1A-S2A-S3A-S4A-S5A-S6A-S7A-S8A
241      AISA=AIS*SUSA
242      311      CONTINUE
243      STEPA=(X(L)**2)*FONA
244      IF(STEPA.GT.175.) GO TO 107
245      SA=2.*AISA*EXP(-STEPA)
246      SUMA=SUMA+SA
247      IF(ABS(SUMA/10.**6).GT.ABS(SA)) GO TO 107
248      110      CONTINUE
249      107      FTHA=TEMPR-SUMA
250      DO 111 L=1,200
251      IF(L.GT.20) GO TO 112
252      X(L)=SNGL(Y(L))
253      GO TO 113
254      112      X(L)=X(L-1)+PI
255      113      CONTINUE

```

```

257      AISB=(SIN(X(L))-X(L)*COS(X(L)))/(X(L)-SIN(X(L))*COS(X(L)))*(SIN(X(L))/X(L))
258      GO TO 313
259 312    CONTINUE
260      AIS=SIN(X(L))/(X(L)-SIN(X(L))*COS(X(L)))/X(L)
261      S1B=(12-40)*(SIN(X(L))-X(L)*COS(X(L)))
262      S2B=A1*D(I)*(2.*X(L)*SIN(X(L))-(X(L)**2-2.)*COS(X(L))-2.)/
263      1(2.*X(L))
264      S3B=A2*D(I)**2*(3.*(X(L)**2-2.)*SIN(X(L))-X(L)*(X(L)**2-6.)*
265      1COS(X(L)))/(4.*X(L)**2)
266      S4B=A3*D(I)**3*(4.*X(L)*(X(L)**2-6.)*SIN(X(L))-(X(L)**4-12.*X(L)
267      1**2+24.)*COS(X(L))+24.)/(8.*X(L)**3)
268      S5B=A4*D(I)**4*(5.*X(L)**4-60.*X(L)**2+120.)*SIN(X(L))-X(L)*(X(L)
269      1)**4-20.*X(L)**2+120.)*COS(X(L))/(16.*X(L)**4)
270      S6B=A5*D(I)**5*(X(L)*(6.*X(L)**4-120.*X(L)**2+720.)*SIN(X(L))-(X(L)
271      1)**6-30.*X(L)**4+360.*X(L)**2-720.)*COS(X(L))-720.)/(32.*X(L)**5)
272      S7B=A6*D(I)**6*(7.*X(L)**6-210.*X(L)**4+2520.*X(L)**2-5040.)*
273      1SIN(X(L))-X(L)*(X(L)**6-42.*X(L)**4+840.*X(L)**2-5040.)*COS(X(L)):
274      2/(64.*X(L)**6)
275      S8B=A7*D(I)**7*(X(L)*(8.*X(L)**6-336.0*X(L)**4+6720.*X(L)**2-
276      140320.)*SIN(X(L))-(X(L)**8-56.*X(L)**6+1680.*X(L)**4-20160.*X(L)
277      2**2+40320.)*COS(X(L))+40320.)/(128.*X(L)**7)
278      SUSB=S1B-S2B-S3B-S4B-S5B-S6B-S7B-S8B
279      AISB=AIS*SUSB
280 313    CONTINUE
281      STEPB=(X(L)**2)*FONB
282      IF(STEPB.GT.175.) GO TO 114
283      SB=2.*AISB*EXP(-STEPB)
284      SUMB=SUMB+SB
285      IF(ABS(SUMB/10.**6).GT.ABS(SB)) GO TO 114
286 111    CONTINUE
287 114    FTHB=TEMPR-SUMB
288      N=0
289 207    N=N+1
290      XTH=(THA+THB)/2.
291      IF(XTH.GT.0.9995*TH1)GO TO 91
292      TEMP=TEMPR
293      FONX=4.*ALFA*XTH*(10.**6)/(D(I)**2)
294      SUMX=0.
295      DO 120 L=1,200
296      IF(L.GT.20) GO TO 115
297      X(L)=SNGL(Y(L))
298      GO TO 116
299 115    X(L)=X(L-1)+PI
300 116    CONTINUE
301      IF(K.GT.1) GO TO 314
302      AISX=(SIN(X(L))-X(L)*COS(X(L)))/(X(L)-SIN(X(L))*COS(X(L)))*(SIN(X(L))/X(L))
303      GO TO 315
304 314    CONTINUE
305      AIS=SIN(X(L))/(X(L)-SIN(X(L))*COS(X(L)))/X(L)
306      S1X=(12-40)*(SIN(X(L))-X(L)*COS(X(L)))
307      S2X=A1*D(I)*(2.*X(L)*SIN(X(L))-(X(L)**2-2.)*COS(X(L))-2.)/
308      1(2.*X(L))
309      S3X=A2*D(I)**2*(3.*(X(L)**2-2.)*SIN(X(L))-X(L)*(X(L)**2-6.)*
310      1COS(X(L)))/(4.*X(L)**2)
311      S4X=A3*D(I)**3*(4.*X(L)*(X(L)**2-6.)*SIN(X(L))-(X(L)**4-12.*X(L)
312      1**2+24.)*COS(X(L))+24.)/(8.*X(L)**3)
313      S5X=A4*D(I)**4*(5.*X(L)**4-60.*X(L)**2+120.)*SIN(X(L))-X(L)*(X(L)
314      1)**4-20.*X(L)**2+120.)*COS(X(L))/(16.*X(L)**4)
315      S6X=A5*D(I)**5*(X(L)*(6.*X(L)**4-120.*X(L)**2+720.)*SIN(X(L))-(X(L)
316      1)**6-30.*X(L)**4+360.*X(L)**2-720.)*COS(X(L))-720.)/(32.*X(L)**5)

```

```

303      S7X=A6*(I)**6*((7.*X(L)**6-210.*X(L)**4+2520.*X(L)**2-5040.)*
1SIN(X(L))-X(L)*(X(L)**6-42.*X(L)**4+840.*X(L)**2-5040.)*COS(X(L)
2/(64.*X(L)**6)
304      S8X=A7*(I)**7*(X(L)*(8.*X(L)**6-336.0*X(L)**4+6720.*X(L)**2-
140320.)*SIN(X(L))-(X(L)**8-56.*X(L)**6+1680.*X(L)**4-20160.*X(L)
2**2+40320.)*COS(X(L))+40320.)/(128.*X(L)**7)
305      SUSX=S1X-S2X-S3X-S4X-S5X-S6X-S7X-S8X
306      AISX=AIS*SUSX
307      315  CONTINUE
308      STEPX=(X(L)**2)*F0NX
309      IF(STEPX.GT.175.) GO TO 117
310      SX=2.*AISX*EXP(-STEPX)
311      SUMX=SUMX+SX
312      IF(ABS(SUMX/10.**6).GT.ABS(SX)) GO TO 117
313      120  CONTINUE
314      117  FTHX=TEMP-SUMX
315      IF(FTHX)212,210,211
316      212  IF(FTHX+EPS)203,210,210
317      211  IF(FTHX-EPS)210,210,203
318      203  IF(FTHX*FTHA)205,208,206
319      205  THB=XIH
320      FTHB=FTHX
321      GO TO 207
322      206  THA=XIH
323      FTHA=FTHX
324      GO TO 207
325      208  PRINT 209
326      209  FORMAT(14HA IS TRUE ROOT)
327      GO TO 198
328      210  CONTINUE
329      GO TO 197
330      198  XTH=A
331      197  THETA=XTH
332      IF(VRTI.GI.0.) GO TO 407
333      NE=NE+1
334      IF(NE.LE.3) GO TO 406
335      T=THETU+THETA
336      IF(NE.GE.8) GO TO 413
337      IF(ABS(T/TOLD-1.).LT.0.001) GO TO 407
338      GO TO 406
339      413  CONTINUE
340      IF(NE.GE.20) GO TO 414
341      IF(ABS(T/TOLD-1.).LT.0.02 ) GO TO 407
342      GO TO 406
343      414  CONTINUE
344      IF(NE.GE.30) GO TO 415
345      IF(ABS(T/TOLD-1.).LT.0.03 ) GO TO 407
346      GO TO 406
347      415  CONTINUE
348      IF(NE.GE.40) GO TO 407
349      IF(ABS(T/TOLD-1.).LT.0.04 ) GO TO 407
C
C      SURFACE TENSION OF WATER IN AIR
C
350      406  SURFT=(75.6-0.145*TV-0.25*10.**(-3)*TV**2)/1000.
C
C      SURFACE TENSION GROUP
C
351      IF(VDUP.GT.0.) GO TO 505
352      CALL VELDDU
353      GO TO 405
354      505  CONTINUE
355      CALL VELDUP

```

```

356      GU TO 405
357      407      CONTINUE
          C
          C
          C      AVERAGE TEMPERATURE OF DROPLET
          C
358      FONAV=4.*ALFA*THETA*(10.**6)/(D(I)**2)
359      SUMAV=0.
360      DO 151 L=1,200
361      IF(L.GT.20) GO TO 152
362      X(L)=SNGL(Y(L))
363      GO TO 153
364      152      X(L)=X(L-1)+PI
365      153      CONTINUE
366      IF(K.GT.1) GO TO 320
367      AISAV=((SIN(X(L))-X(L)*COS(X(L))**2)/(X(L)-SIN(X(L))*COS(X(L)))
368      GO TO 321
369      320      CONTINUE
370      AIS=(SIN(X(L))-X(L)*COS(X(L)))/(X(L)-SIN(X(L))*COS(X(L)))
371      S1AV=(TZ-A0)*(SIN(X(L))-X(L)*COS(X(L)))
372      S2AV=A1*D(I)*(2.*X(L)*SIN(X(L))-(X(L)**2-2.)*COS(X(L))-2.)/
373      1(2.*X(L))
374      S3AV=A2*D(I)**2*(3.*(X(L)**2-2.)*SIN(X(L))-X(L)*(X(L)**2-6.)*
375      1COS(X(L)))/(4.*X(L)**2)
376      S4AV=A3*D(I)**3*(4.*X(L)*(X(L)**2-6.)*SIN(X(L))-(X(L)**4-12.*X(L)
377      1**2+24.)*COS(X(L))+24.)/(8.*X(L)**3)
378      S5AV=A4*D(I)**4*(5.*X(L)**4-60.*X(L)**2+120.)*SIN(X(L))-X(L)*(X(L)
379      1**4-20.*X(L)**2+120.)*COS(X(L))/(16.*X(L)**4)
380      S6AV=A5*D(I)**5*(X(L)*(6.*X(L)**4-120.*X(L)**2+720.)*SIN(X(L))-(X
381      1L)**6-30.*X(L)**4+360.*X(L)**2-720.)*COS(X(L))-720.)/(32.*X(L)**5)
382      S7AV=A6*D(I)**6*(7.*X(L)**6-210.*X(L)**4+2520.*X(L)**2-5040.)*
383      1SIN(X(L))-X(L)*(X(L)**6-42.*X(L)**4+840.*X(L)**2-5040.)*COS(X(L)).
384      2/(64.*X(L)**6)
385      S8AV=A7*D(I)**7*(X(L)*(8.*X(L)**6-336.*X(L)**4+6720.*X(L)**2-
386      140320.)*SIN(X(L))-(X(L)**8-56.*X(L)**6+1680.*X(L)**4-20160.*X(L)
387      2**2+40320.)*COS(X(L))+40320.)/(128.*X(L)**7)
388      SUSAV=S1AV-S2AV-S3AV-S4AV-S5AV-S6AV-S7AV-S8AV
389      AISAV=AIS*SUSAV
390      321      CONTINUE
391      STEPAV=(X(L)**2)*FONAV
392      IF(STEPAV.GT.175.) GO TO 154
393      SAV=6.*AISAV*EXP(-STEPAV)/X(L)**3
394      SUMAV=SUMAV+SAV
395      IF(ABS(SUMAV/10.**6).GT.ABS(SAV)) GO TO 154
396      151      CONTINUE
397      154      CONTINUE
398      IF(K.GT.1) GO TO 381
399      TAV=TZ-(TZ-T0)*SUMAV
400      GO TO 382
401      381      TAV=TZ-SUMAV
402      382      CONTINUE
403      FONN=4.*ALFA*THETA*(10.**6)/(D(I)**2)
404      DO 301 M=1,20
405      RD(M)=M*D(I)/40.
406      RN(M)=SNGL(RD(M))
407      SUMN=0.
408      DO 302 L=1,200
409      IF(L.GT.20) GO TO 303
410      X(L)=SNGL(Y(L))
411      GO TO 304
412      303      X(L)=X(L-1)+PI
413      304      CONTINUE
414      IF(K.GT.1) GO TO 300
415      AISN=(SIN(X(L))-X(L)*COS(X(L)))*(D(I)/2.)*SIN(X(L)+2.*RN(M)/D(I)).

```

```

1(X(L)-SIN(X(L))*COS(X(L)))/RN(M)/X(L)
407 GO TO 305
408 300 CONTINUE
409 AIS=SIN(X(L)*2.*RN(M)/D(I))*(D(I)/2.)/(X(L)-SIN(X(L))*COS(X(L))
1RN(M)/X(L)
410 SIN=(I2-A0)*(SIN(X(L))-X(L)*COS(X(L)))
411 S2N=A1*D(I)*(2.*X(L)*SIN(X(L))-(X(L)**2-2.)*COS(X(L))-2.)/
1(2.*X(L))
412 S3N=A2*D(I)**2*(3.*(X(L)**2-2.)*SIN(X(L))-X(L)*(X(L)**2-6.)*
1COS(X(L)))/(4.*X(L)**2)
413 S4N=A3*D(I)**3*(4.*X(L)*(X(L)**2-6.)*SIN(X(L))-(X(L)**4-12.*X(
1**2+24.)*COS(X(L))+24.)/(8.*X(L)**3)
414 S5N=A4*D(I)**4*(5.*X(L)**4-60.*X(L)**2+120.)*SIN(X(L))-X(L)*(
1)**4-20.*X(L)**2+120.)*COS(X(L))/(16.*X(L)**4)
415 S6N=A5*D(I)**5*(X(L)*(6.*X(L)**4-120.*X(L)**2+720.)*SIN(X(L))-
1L)**6-30.*X(L)**4+360.*X(L)**2-720.)*COS(X(L))-720.)/(32.*X(L)
416 S7N=A6*D(I)**6*(7.*X(L)**6-210.*X(L)**4+2520.*X(L)**2-5040.)*
1SIN(X(L))-X(L)*(X(L)**6-42.*X(L)**4+840.*X(L)**2-5040.)*COS(X(L)
2/(64.*X(L)**6)
417 S8N=A7*D(I)**7*(X(L)*(8.*X(L)**6-336.0*X(L)**4+6720.*X(L)**2-
140320.)*SIN(X(L))-(X(L)**8-56.*X(L)**6+1680.*X(L)**4-20160.*X(L)
2**2+40320.)*COS(X(L))+40320.)/(128.*X(L)**7)
418 SUSN=S1N-S2N-S3N-S4N-S5N-S6N-S7N-S8N
419 AISN=AIS*SUSN
420 305 CONTINUE
421 STEPN=(X(L)**2)*FOMN
422 IF(STEPN.GT.175.) GO TO 306
423 SN=2.*AISN*EXP(-STEPN)
424 SUMN=SUMN+SN
425 IF(ABS(SUMN/10.**6).GT.ABS(SN)) GO TO 306
426 302 CONTINUE
427 306 CONTINUE
428 IF(K.GT.1) GO TO 330
429 TN(M)=I2-(I2-I0)*SUMN
430 GO TO 331
431 330 TN(M)=I2-SUMN
432 331 CONTINUE
433 301 CONTINUE
434 CALL TSQFIT(RD,TN,A0,A1,A2,A3,A4,A5,A6,A7)
435 A0=SNGL(A0)
436 A1=SNGL(A1)
437 A2=SNGL(A2)
438 A3=SNGL(A3)
439 A4=SNGL(A4)
440 A5=SNGL(A5)
441 A6=SNGL(A6)
442 A7=SNGL(A7)
443 DO 390 M=1,10
444 TNP(M)=A0+A1*RN(M)+A2*RN(M)**2+A3*RN(M)**3+A4*RN(M)**4+A5*RN(M)
1+A6*RN(M)**6+A7*RN(M)**7
445 390 CONTINUE
446 THETU=THETU+THETA
447 IF(VRTT.GT.0.) GO TO 408
448 IF(VDUP.EQ.0.) GO TO 408
449 IF(VRRS.GT.0.) GO TO 408
450 NI=1
451 408 CONTINUE
452 IF(VRTT.GT.0.) GO TO 409
453 GO TO 410
454 409 CONTINUE
455 Z=Z+VRT*THETA
456 410 CONTINUE
C

```

```

C
457 DD=(2.*TNA*18.02/ROV)*THETA*1000. 232
458 D(I)=D(I)+DD
C
C C
C THERMAL UTILIZATION
C
459 THUT=(TAV-T0)/(TZ-T0)
C
C C
C RATIO OF THERMAL DIFFUSIVITY AND DIFFUSION COEFFICIENT
C
460 A=AMBHF/(ROMF*CPMF)
461 RTMD=A/DIFMF
C
C C
C AVERAGE APPARENT HEAT TRANSFER COEFFICIENT
C
462 HAPSTP=HAPSTP+HAPP
463 HAPAVS=HAPSTP/K
464 HAPINT=HAPINT+(HAPP0+4.*HAPP+HAPP)*THETA/6.
465 HAPAVI=HAPINT/THETU
466 HAPPO=HAPP
C
C C
C AVERAGE APPARENT HEAT TRANSFER COEFFICIENT--CHECK UP
C
467 HAPCH=DM*CPV*(TAV-TAVOLD)*1000./AREA/(TZ-TV+DT/2.)/THETA
468 HAPCHI=HAPCHI+(HAPCH0+HAPCH)*THETA/2.
469 HAPCH0=HAPCH
470 HAPCTR=HAPCHI/THETU
471 TAVOLD=TAV
C
C C
C AVERAGE SENSIBLE HEAT TRANSFER COEFFICIENT
C
472 HSTEP=HSTEP+H
473 HAVSTP=HSTEP/K
474 HINT=HINT+(H0+4.*H+H)*THETA/6.
475 HAVINT=HINT/THETU
476 H0=H
C
C C
C ENHANCEMENT FACTOR
C
477 EFSTEP=HAPAVS/HAUSTP
478 EFINT=HAPAVI/HAUINT
C
479 DLSSTP=(TZ-TAV)/(TZ-T0)
480 DLSRHS=(VR*PPP*THETU**3)/(D(I)**3)
481 PRINT 25,TV,TAV,D(I),RTMD,THUT,THETU
482 25 FORMAT(2X,3HTV=,E14.7,1X,4HTAV=,E14.7,1X,5HD(I)=,E14.7,1X,5HRTMD=,
1E14.7,1X,5HTHUT=,F14.7,1X,6HTHETU=,E14.7)
483 PRINT 26,TNA,F,F1,HAPP,HAPAVS,HAPAVI
484 26 FORMAT(2X,'TNA=',E14.7,1X,'F=',E14.7,1X,'B1=',E14.7,1X,'HAPP=',
1E14.7,1X,'HAPAVS=',E14.7,1X,'HAPAVI=',E14.7)
485 PRINT 24,H,HAUSTP,HAUINT,EFSTEP,EFINT,FONAV
486 24 FORMAT(2X,'H=',E14.7,1X,'HAUSTP=',E14.7,1X,'HAUINT=',E14.7,1X,
1'EFSTEP=',E14.7,1X,'EFINT=',E14.7,1X,'FONAV=',E14.7)
487 PRINT 23,TOLD,VR,Z,REN,NE,DI,HAPCTR
488 23 FORMAT(2X,5HTOLD=,E14.7,1X,'VR=',E14.7,1X,'Z=',E14.7,1X,'REN=',
1E14.7,1X,'NE=',I3,1X,'DI=',F10.5,1X,'HAPCTR=',F10.1)
489 WRITE(7,22)THUT,PT,VR0,DM,THETU
490 22 FORMAT(5E14.6)
491 PRINT 29,PRN,SCN,SHN,USN,NS,QL,ACN,HAPCH
492 29 FORMAT(2X,'PRN=',F10.5,1X,'SCN=',F10.5,1X,'SHN=',F10.5,1X,'USN=
1',F10.5,1X,'NS=',F10.2,1X,'QL=',F10.2,1X,'ACN=',F10.5,1X,'HAPCH=
2,F10.1)

```

```

493 100 CONTINUE
494 GU TO 33
495 91 PRINT 55
496 55 FORMAT('0','ITERATION CANT BE ACCOMPLISHED BETWEEN THE LIMITS
1THAXIHH','0')
497 GU TO 33.
498 34 CONTINUE
499 PRINT 35
500 35 FORMAT('0','WATER SURFACE TEMPERATURE IS GREATER THAN 99.99% OF
1THE SURROUNDING TEMPERATURE',/)
501 33 CONTINUE
502 PRINT 27,PPP,TZ,RGP,VISP,VISV,VISMB
503 27 FORMAT(2X,4HPPP=,E14.7,1X,3HTZ=,E14.7,1X,4HROP=,E14.7,1X,5HVISP=
114.7,1X,5HVISV=,E14.7,1X,6HVISM=,E14.7/)
504 90 PRINT 28,VRT,REMB,DT,EFINT,HAPAVI,HAVINT
505 28 FORMAT(2X,4HVRT=,E14.7,1X,5HREMB=,E14.7,1X,3HDT=,E14.7,1X,'EFIN
1,E14.7,1X,'HAPAVI=,E14.7,1X,'HAVINT=,E14.7///)
C
506 80 CONTINUE
507 STOP
508 END
C
C *****
509 SUBROUTINE PZAS(T,PS)
C *****
C
510 X=1/100.
511 PS((((((((((1.55318/10000.*X-2.6934527/1000.)*X+2.0153393/100.)
18.659025/100.)*X+2.4775634/10.)*X-5.6080594/10.)*X+1.2567591)*X
2033727)*X+7.2704899)*X-5.07871)
512 PS=EXP(PS)/1.01972
513 RETURN
514 END
C
C *****
515 SUBROUTINE TEMP1(PPP,TZ)
C *****
C
516 X=ALOG(1.01972*PPP)
517 TZ((((((((((-4.2924603/10000./10000.*X-4.2685685/10000000.)*X+
1343731/1000000.)*X+2.2071712/100000.)*X-1.7417752/100000.)*X-3.
23484/10000.)*X+1.3283773/1000.)*X+2.129082/100.)*X+2.1077805/10
3X+2.3753577)*X+27.854242)*X+99.092712
518 RETURN
519 END
C
C *****
520 SUBROUTINE VVODES(PT,TV,VVOD)
C *****
C
521 A=(TV+273.15)/647.3
522 S=PT/221.286
523 U=100.*(3700000.-3122199.*A*A-1999.85/A**6)
524 W=(U+SQRT(1.72*U*U+1302926.*10.**10*(S-1.500705*A)))*0.2941177
525 B=1.052356*(62.5+S*(13.10268+S))/10.*11/(1.5108/100000.+A**11)
526 C=(0.6537/154-A)**2
527 C=C*(7.241165/100000.+0.7676621*C**4)
528 VVOD=0.417/W+C-B-(11.39706-9.949927*A)/100000.
529 RETURN

```

C
C

531

SUBROUTINE SEKPV(TZ,PV)

C
C

532

X=TZ/100.

533

$$PV = (((((-2.469006/10000.*X+3.156533/1000.)*X-1.5067829/100.)*X+1.3488546/100.)*X-3.8647549/100.)*X+1.1476149/10000.)*X-7.0419435/2000.)*X+4.5905064/10.)*X+1.2602044$$

534

RETURN

535

END

C
C

** ***** ** * * * * *

536

SUBROUTINE CPVOD2(PT,TV,CPV)

C
C

537

X=TV/100.

538

Y=PT/100.

539

Z=X**5

540

CPV=1./(Y+2.)+0.021*Y-0.24927

541

$$CPV=CPV*(0.032+Z*(0.003264+0.026412*Z+7/100000.))$$

542

$$Z=((-1.100455*X+4.837206)*X-24.208803)*X+33.444712)*X+30.72526$$

543

CPV=Z*Y/1000.+CPV

544

$$Z=(((2.259965*X-7.403256)*X+19.097088)*X-13.04363)*X+419.82594$$

545

CPV=Z/100.+CPV

546

RETURN

547

END

C
C

548

SUBROUTINE CPPAR(PT,TF,CPP)

C
C

549

X=(TF+273.15)/647.3

550

S=PT/221.246

551

$$B=1.6283287*(1.55106-S/2.)*X**1.82/10000.-5.0986846/100./X**3.82$$

552

$$C=(2.010378*S*(17.722/4*S-11.*X**3)/1000.-0.2057615)/X**15$$

553

$$D=22128.703*(6*S+(C-1.5329846/X**33/1000.)*S**3)$$

554

$$CPP=(1169.8648-D*X*(-16.110723+X*(221.29742-X*52.106736)))/647.3$$

555

RETURN

556

END

C
C

557

SUBROUTINE SEKI(T,ENTA)

C
C

558

X=T/100.

559

$$ENTA=(((1.0265952*X-9.4307509)*X+27.974559)*X-43.077814)*X+15.719571)*X+181.50666)*X+2500.6256$$

560

RETURN

561

END

C
C

562

SUBROUTINE PRIM11(T,ENTA)

C
C

563

X=T/100.

564

$$ENTA=(((2.7663765/10.*X-3.9629482)*X+23.865162)*X-78.226638)$$

1X+151.59421)*X-175.79053)*X+120.80923)*X-44.519838)*X+425.1734
2-7.4554093/100.

235

565 IF(T-350.)2,2,1
566 1 ENTA=ENTA+0.388739*EXP(0.225556*(T-350.))
567 2 RETURN
568 END

C
C *****

569 SUBROUTINE AMDA(P,T,VLAMB)

C
C *****

570 X=1.+T/273.15
571 CALL PZAS(T,PS)
572 VLAMB=((0.29323-0.071693*X)*X-0.38929)*X+0.1656)*(P-PS)/100000
573 VLAMB=(VLAMB+((5.1536*X-20.012)*X+25.186)*X-9.473)/100000.)*(P-
574 VLAMB=VLAMB+((0.52577-0.07344*X)*X-1.8007)*X+2.8395)*X-0.92247
575 RETURN
576 END

C
C *****

577 SUBROUTINE TRANEN(BI,X1)

C TRANSCENDENTAL EQUATION SOLUTION -- TAN(X)+X/(BI-1.)=0.--HALF
C INTERVAL SEARCH METHOD
C *****

578 IMPLICIT REAL*8(A-H,O-Z)
579 DIMENSION X1(20)
580 C=BI-1.
581 PI=3.1415926535
582 IF(DABS(C).LT.0.005) GO TO 79
583 79 CONTINUE
584 DO 13 I=1,20
585 IF(DABS(C).LT.0.005) GO TO 21
586 IF(BI-1.)20,21,22
587 20 A=(I-1)*PI+0.000001
588 B=(2*I-1)*PI/2.
589 EPS=0.00001*(A+B)/2./(1.-BI)
590 GO TO 23
591 21 Y=(2*I-1)*PI/2.
592 GO TO 25
593 22 PI=3.1415926537
594 A=(2*I-1)*PI/2.
595 B=I*PI-0.00001
596 EPS=0.0001*(A+B)/2./(BI-1.)
597 23 FA=DTAN(A)-A/(1.-BI)
598 FB=DTAN(B)-B/(1.-BI)
599 K=0
600 7 K=K+1
601 Y=(A+B)/2.
602 TA=DTAN(Y)
603 CX=Y/C
604 F=1A+CX
605 IF(F)12,10,11
606 12 IF(F+EPS)3,10,10
607 11 IF(F-EPS)10,10,3
608 3 IF(F*FA)5,8,6
609 5 B=Y
610 FB=F
611 GO TO 7
612 6 A=Y
613 FA=F

```

614      GO TO 7
615      PRINT 9
616      9      FORMAT(1JHA IS TRUE ROUT)
617      GO TO 13
618      25      PRINT 9H,Y
619      9H      FORMAT(10X,5HX(L)=,F15.8)
620      GO TO 13
621      10      CONTINUE
622      13      X1(I)=Y
623      RETURN
624      END

```

236

C
C
C

625 SUBROUTINE VEL000

C
C
C
C
C

NUMERICAL SOLUTION OF THE EQUATION OF MOTION FOR A DROPLET MOVING
DOWNWARDS RUNGE--KUTIA TECHNIQUE

```

626      COMMON K,VET,NE,VRK,ZRK,ROMB,VISMB,G,NI,NM,NN,THETA,VINF,VDUP,
1SURET,ROV,D,VR0,I,VR,Z,THETU,VRRS
627      DIMENSION D(20)
628      IF(K-1)408,408,409
629      408      VR=VR0
630      Z=0.
631      GO TO 410
632      409      IF(NE.LE.2) GO TO 415
633      VR=VRRK
634      Z=ZRK
635      GO TO 410
636      415      VPRK=VR
637      ZRK=Z
638      410      IF(VR0-VRT)451,452,453
639      451      IF(VR-VRT)454,452,452
640      453      IF(VR-VRT)452,452,454
641      454      CONTINUE
642      RE0=VR*D(1)*ROMB*10000./VISMB
643      CALL COREIN(RE0,CDCDR)
644      PROD=3000.*ROMB*VR**2/(4.*D(1)*ROV)
645      CK0=G-PROD*CDCDR
646      RE1=(VR+CK0*THETA/2.)*D(1)*ROMB*10000./VISMB
647      REM1=(VR+CK0*THETA/4.)*D(1)*ROMB*10000./VISMB
648      CALL COREIN(RE1,CDCDR)
649      PROD=3000.*ROMB*(VR+CK0*THETA/2.)*2/(4.*D(1)*ROV)
650      CK1=G-PROD*CDCDR
651      CALL COREIN(REM1,CDCDR)
652      PROD=3000.*ROMB*(VR+CK0*THETA/4.)*2/(4.*D(1)*ROV)
653      RE2=(VR+CK1*THETA/2.)*D(1)*ROMB*10000./VISMB
654      REM2=(VR+CK1*THETA/4.)*D(1)*ROMB*10000./VISMB
655      CKM1=G-PROD*CDCDR
656      CALL COREIN(RE2,CDCDR)
657      PROD=3000.*ROMB*(VR+CK1*THETA/2.)*2/(4.*D(1)*ROV)
658      CK2=G-PROD*CDCDR
659      CALL COREIN(REM2,CDCDR)
660      PROD=3000.*ROMB*(VR+CKM1*THETA/4.)*2/(4.*D(1)*ROV)
661      CKM2=G-PROD*CDCDR
662      RE3=(VR+CK2*THETA)*D(1)*ROMB*10000./VISMB
663      REM3=(VR+CKM2*THETA/2.)*D(1)*ROMB*10000./VISMB
664      CALL COREIN(RE3,CDCDR)
665      PROD=3000.*ROMB*(VR+CK2*THETA)*2/(4.*D(1)*ROV)
666      CK3=G-PROD*CDCDR

```

```

667      CALL CDREIN(CKM3,CDCDR)
668      PROD=3000.*ROMB*(VR+CKM2*THETA/2.)*2/(4.*D(1)*ROV)      237
669      CKM3=G-PROD*CDCDR
670      Z1=VR-VINF
671      VRM=VR+(CK0+2.*CKM1+2.*CKM2+CKM3)*THETA/12.
672      Z2=VRM-VINF
673      VR=VR+(CK0+2.*CK1+2.*CK2+CK3)*THETA/6.
674      Z3=VR-VINF
675      Z=Z+(Z1+4.*Z2+Z3)*THETA/6.
676      GO TO 405
677      452  VR=VRT
678          IF(K-1)468,468,469
679      468  TIME=0.
680          Z=0.
681          GO TO 470
682      469  IF(NE.LE.2) GO TO 475
683          TIME=TIMEC
684          Z=ZC
685          GO TO 470
686      475  TIMEC=TIME
687          ZC=Z
688      470  TIME=TIME+THETA
689          Z=Z+(VR-VINF)*TIME
690      405  CONTINUE
691          RETURN
692          END

```

C
C
C
C

693 SUBROUTINE VELDUP

C
C
C
C
C

NUMERICAL SOLUTION OF THE EQUATION OF MOTION FOR A DROPLET MOVING
UPWARDS RUNGE--KUTTA TECHNIQUE

```

694      COMMON K,VRT,NF,VRK,ZRK,ROMB,VISMB,G,N,NM,NN,DT,VAIR,VDO,SURFT,
1ROV,D,VR0,I,VR,Z,THEIU,VRRS
695      DIMENSION D(20)
696      IF(K-1)408,408,409
697      408  VR=VR0
698          Z=0.
699          GO TO 410
700      409  IF(NE.LE.2) GO TO 415
701          VR=VRK
702          Z=ZRK
703          GO TO 410
704      415  VRRK=VR
705          ZRK=Z
706      410  CONTINUE
707          REO=VR*D(1)*ROMB*10000./VISMB
708          CALL CDREIN(REO,CDCDR)
709          PROD=3000.*ROMB*VR**2/(4.*D(1)*ROV)
710          IF(VAIR-VRT)60,61,60
711      61  VAIR=VAIR-0.001
712      60  IF(VDO.LT.VAIR) GO TO 210
713          IF(N.LT.1) GO TO 116
714          GO TO 16
715      116  CONTINUE
716          IF(NH.GT.1) GO TO 201
717          GO TO 151
718      210  NM=NM+1
719      201  CONTINUE

```

```

720      GO TO 16
721 151  CONTINUE
722      CK0 = -(G+PROD*CDCDR)
723      GO TO 17
724 16   CK0 = G-PROD*CDCDR
725 17   RE1 = (VR+CK0*DT/2.)*D(1)*RUMB*10000./VISM8
726      REM1 = (VR+CK0*DT/4.)*D(1)*RUMB*10000./VISM8
727      CALL COREIN(RE1,CDCDR)
728      PROD = 3000.*(VR+CK0*DT/2.)*2/(4.*D(1)*ROV)
729      IF(N.LI.1) GO TO 118
730      GO TO 18
731 118  CONTINUE
732      IF(NM.GT.0) GO TO 18
733      CK1 = -(G+PROD*CDCDR)
734      GO TO 19
735 18   CK1 = G-PROD*CDCDR
736 19   CALL COREIN(REM1,CDCDR)
737      PROD = 3000.*(VR+CK0*DT/4.)*2/(4.*D(1)*ROV)
738      IF(N.LI.1) GO TO 120
739      GO TO 20
740 120  CONTINUE
741      IF(NM.GT.0) GO TO 20
742      CKM1 = -(G+PROD*CDCDR)
743      GO TO 21
744 20   CKM1 = G-PROD*CDCDR
745 21   RE2 = (VR+CK1*DT/2.)*D(1)*RUMB*10000./VISM8
746      REM2 = (VR+CK1*DT/4.)*D(1)*RUMB*10000./VISM8
747      CALL COREIN(RE2,CDCDR)
748      PROD = 3000.*(VR+CK1*DT/2.)*2/(4.*D(1)*ROV)
749      IF(N.LI.1) GO TO 122
750      GO TO 22
751 122  CONTINUE
752      IF(NM.GT.0) GO TO 22
753      CK2 = -(G+PROD*CDCDR)
754      GO TO 23
755 22   CK2 = G-PROD*CDCDR
756 23   CALL COREIN(REM2,CDCDR)
757      PROD = 3000.*RUMB*(VR+CKM1*DT/4.)*2/(4.*D(1)*ROV)
758      IF(N.LI.1) GO TO 124
759      GO TO 24
760 124  CONTINUE
761      IF(NM.GT.0) GO TO 24
762      CKM2 = -(G+PROD*CDCDR)
763      GO TO 25
764 24   CKM2 = G-PROD*CDCDR
765 25   RE3 = (VR+CK2*DT)*D(1)*RUMB*10000./VISM8
766      REM3 = (VR+CKM2*DT/2.)*D(1)*RUMB*10000./VISM8
767      CALL COREIN(RE3,CDCDR)
768      PROD = 3000.*RUMB*(VR+CK2*DT)*2/(4.*D(1)*ROV)
769      IF(N.LI.1) GO TO 126
770      GO TO 26
771 126  CONTINUE
772      IF(NM.GT.0) GO TO 26
773      CK3 = -(G+PROD*CDCDR)
774      GO TO 27
775 26   CK3 = G-PROD*CDCDR
776 27   CALL COREIN(REM3,CDCDR)
777      PROD = 3000.*RUMB*(VR+CKM2*DT/2.)*2/(4.*D(1)*ROV)
778      IF(N.LI.1) GO TO 128
779      GO TO 28
780 128  CONTINUE
781      IF(NM.GT.0) GO TO 28
782      CKM3 = -(G+PROD*CDCDR)

```

```

783      GO TO 29
784      28      CKM3= G-PROD*CDCCR
785      29      CONTINUE
786      IF(N.LT.1) GO TO 130
787      GO TO 7
788      130     CONTINUE
789      IF(NM.GT.0) GO TO 7
790      Z1=VR+VAIR
791      GO TO 51
792      7       Z1=VAIR-VR
793      GO TO 51
794      51      VRM=VR+(CK0+2.*CKM1+2.*CKM2+CKM3)*DT/12.
795      IF(N.LT.1) GO TO 132
796      GO TO 71
797      132     CONTINUE
798      IF(NM.GT.0) GO TO 71
799      Z2=VRM+VAIR
800      GO TO 53
801      71      Z2=VAIR-VRM
802      GO TO 53
803      53      CONTINUE
804      VR=VR+(CK0+2.*CK1+2.*CK2+CK3)*DT/6.
805      VRHS=VR
806      IF(VR.LT.0.) GO TO 112
807      GO TO 111
808      112     CONTINUE
809      VR=ABS(VR)
810      111     CONTINUE
811      IF(N.LT.1) GO TO 134
812      GO TO 72
813      134     CONTINUE
814      IF(NM.GT.0) GO TO 72
815      Z3=VR+VAIR
816      GO TO 35
817      72      Z3=VAIR-VR
818      GO TO 35
819      35      CONTINUE
820      Z=Z+(Z1+4.*Z2+Z3)*DT/6.
821      56      CONTINUE
822      IF(N.LT.1) GO TO 145
823      GO TO 73
824      145     CONTINUE
825      IF(NM.GT.0) GO TO 73
826      VD=VR+VAIR
827      GO TO 41
828      73      VD=VAIR-VR
829      41      CONTINUE
830      T=THEIU+DT
831      PRINT 102,CK0,CK1,CK2,CK3,RE0,RE1,RE2,RE3,M,N,NN
832      102     FORMAT(1X,4HCK0=,F10.5,1X,4HCK1=,F10.5,1X,4HCK2=,F10.5,1X,4HCK3=,
110.5,1X,4HRE0=,F5.1,1X,4HRE1=,F5.1,1X,4HRE2=,F5.1,1X,4HRE3=,F5.1,
21X,2HNM=,13,1X,2HNN=,13,1X,3HNN=,13)
833      PRINT 101,T,VR,Z,VD,VRHS,Z1,Z2,Z3,CDCCR,NM
834      101     FORMAT(10X,2HT=,F5.2,5X,3HVR=,F5.2,5X,2HZ1=,F5.2,5X,3HVD=,F5.2,2X,
15HVRHS=,F5.2,2X,3HZ2=,F5.2,2X,3HZ3=,F5.2,2X,3HCDCCR=,F5.2,1X,4HCDCCR=,
2,F5.1,1X,3HNM=,13)
835      RETURN
836      END

```

C
C

837 SUBROUTINE CDREIN(RE1,CD)

C

```

838      COMMON K,VRT,NE,VRK,ZRK,ROMB,VISM,G,NI,NM,NN,THETA,VINF,VDUP,
1SURFT,RUV,D,VR0,I,VK,Z,THETU,VRRS
839      DIMENSION D(20)
840      RE1=ABS(RE1)
841      S=ROMB*SURFT**3*10.**2K/G/VISM**4
842      DELRO=RUV-ROMB
843      DSTAR=10.*D(1)*((ROMB**2)*G*10.**2/VISM**2)**(1./3.)
844      DSTAR1=1.215/(DELRO/ROMB)**(1./3.)
845      DSTA2A=70.0*(DELRO/ROMB)**(-1./3.)*(S*10.**(-12))**(-0.111)
846      DSTA2B=50.5*(DELRO/ROMB)**(-1./3.)*(S*10.**(-12))**(-0.111)
847      DSTA3A=122.*(DELRO/ROMB)**(-0.535)*(S*10.**(-12))**(-0.275)
848      DSTA3B=500.*(DELRO/ROMB)**(-0.535)*(S*10.**(-12))**(-0.0367)
849      DSTAR4=160.*(DELRO/ROMB)**(-0.447)*(S*10.**(-12))**(-0.114)
850      RE2A=974.*(S*10.**(-12))**(-0.192)
851      RE2B=230.*(S*10.**(-12))**(-0.192)
852      RE3A=2240.*(DELRO/ROMB)**(-0.303)*(S*10.**(-12))**(-0.388)
853      RE3B=7160.*(DELRO/ROMB)**(-0.303)*(S*10.**(-12))**(-0.08)
854      RE4=3190.*(DELRO/ROMB)**(-0.173)*(S*10.**(-12))**(-0.18)
855      RE5=4470.*(DELRO/ROMB)**(-0.238)*(S*10.**(-12))**(-0.232)
856      DMAXS=224.*(DELRO/ROMB)**(-0.5)*(S*10.**(-12))**(-1./6.)
857      CDMAX=0.75*(DELRO/ROMB)**(-0.0232)*(S*10.**(-12))**(-0.036)
858      WSTAM=3.273*((DELRO/ROMB)*S**0.25)**0.262
859      WMAXS=RE5/DMAXS
860      WSTAR4=RE4/DSTAR4
861      WSTA3A=RE3A/DSTA3A
862      WSTA3B=RE3B/DSTA3B
863      WSTA2A=RE2A/DSTA2A
864      WSTA2B=RE2B/DSTA2B
865      WSTAR1=0.1/DSTAR1
866      DST=DMAXS
867      A=0.085-(1./29.54)*ALOG10(S**0.5/(DELRO/ROMB)*10.**(-3))
868      IF(RE1.LE.0.5) GO TO 10
869      IF(S.GT.44.*10**12) GO TO 20
870      IF(RE1.GT.RE2A) GO TO 25
871      CD=(24./RE1)*(1.+0.150*RE1**0.687)
872      DSTA=(3.*RE1**2*CD*ROMB/(4.*DELRO))**(-1./3.)
873      WSTA=(4.*RE1*DELRO/(3.*CD*ROMB))**(-1./3.)
874      GO TO 210
875 20      CONTINUE
876      IF(RE1.GT.RE2B) GO TO 26
877      CD=(24./RE1)*(1.+0.150*RE1**0.687)
878      DSTA=(3.*RE1**2*CD*ROMB/(4.*DELRO))**(-1./3.)
879      WSTA=(4.*RE1*DELRO/(3.*CD*ROMB))**(-1./3.)
880      GO TO 210
881 25      CONTINUE
882      IF(RE1.GT.RE3A) GO TO 50
883      CD=0.48*(S*10.**(-12))**0.05
884      DSTA=(3.*RE1**2*CD*ROMB/(4.*DELRO))**(-1./3.)
885      WSTA=(4.*RE1*DELRO/(3.*CD*ROMB))**(-1./3.)
886      GO TO 210
887 26      CONTINUE
888      IF(RE1.GT.RE3B) GO TO 50
889      CD=0.7*(S*10.**(-12))**(-0.05)
890      DSTA=(3.*RE1**2*CD*ROMB/(4.*DELRO))**(-1./3.)
891      WSTA=(4.*RE1*DELRO/(3.*CD*ROMB))**(-1./3.)
892      GO TO 210
893 10      CD=24./RE1
894      DSTA=(3.*RE1**2*CD*ROMB/(4.*DELRO))**(-1./3.)
895      WSTA=(4.*RE1*DELRO/(3.*CD*ROMB))**(-1./3.)
896      GO TO 210
897 50      CONTINUE
898      IF(RE1.GT.RE4) GO TO 60

```

```

899      DSTA=(RE1/(4.5*(DELRO/ROMH)**0.388*(S*10.**(-12))**0.0323))**0.241
900      WSTA=DSTA**0.24*4.5*(DELRO/ROMH)**0.388*(S*10.**(-12))**0.0323
901      CD=0.06570*DSTA**0.42*(DELRO/ROMH)**0.224*(S*10.**(-12))**(-0.0
902      GO TO 210
903      60 CONTINUE
904      IF(RE1.GT.RE5) GO TO 70
905      WSTA=19.96*(DELRO/ROMH)**0.262*(S*10.**(-12))**0.0654
906      DSTA=RE1/WSTA
907      CD=0.00335*(DELRO/ROMH)**0.477*(S*10.**(-12))**(-0.131)*DSTA
908      GO TO 210
909      70 CONTINUE
910      11 GR=4.*DELRO*DST**3-3.*RE1**2*ROMH*(A*(DST-DMAXS)+CDMAX)
911      GRPRIM=12.*DELRO*DST**2-3.*RE1**2*ROMH*A
912      DSTN=DST-GR/GRPRIM
913      IF(ABS((DSTN-DST)/DST).LT.0.001) GO TO 12
914      DST=DSTN
915      GO TO 11
916      12 CD=CDMAX+A*(DSTN-DMAXS)
917      WST=SQRT(4.*DELRO*DSTN/(3.*ROMH*(A*(DSTN-DMAXS)+CDMAX)))
918      DSTA=DSTN
919      WSTA=WST
920      210 CONTINUE
921      RETURN
922      END

```

```

C
C *****

```

```

923      SUBROUTINE ISNFIT(X1,Y1,A0,A1,A2,A3,A4,A5,A6,A7)
924      C *****
925      IMPLICIT REAL*8(A-H,U-Z)
926      DIMENSION A(10,20),B(20,10),Y(20,1),X1(20),Y1(20),W(10),IR(10),
927      1 IC(10),C(10,10),R(20)
928      N=20
929      M=R
930      DO 1 I=1,N
931      A(1,I)=1.
932      A(2,I)=X1(I)
933      A(3,I)=X1(I)**2
934      A(4,I)=X1(I)**3
935      A(5,I)=X1(I)**4
936      A(6,I)=X1(I)**5
937      A(7,I)=X1(I)**6
938      A(8,I)=X1(I)**7
939      DO 8 J=1,M
940      B(1,J)=A(J,1)
941      1 Y(1,1)=Y1(1)
942      CALL MAMP2D(A,10,20,B,20,10,M,N,M,W,10)
943      DO 6 I=1,M
944      DO 6 J=1,M
945      6 C(I,J)=B(I,J)
946      CALL MAMP2D(A,10,20,Y,20,1,M,N,1,W,10)
947      CALL MINVRD(C,10,M,DET,IER,IR,IC)
948      CALL MAMP2D(C,10,10,Y,20,1,M,M,1,W,10)
949      PRINT 3,(Y(1,1),I=1,M)
950      3 FORMAT(9E13.5)
951      A0=Y(1,1)
952      A1=Y(2,1)
953      A2=Y(3,1)
954      A3=Y(4,1)
955      A4=Y(5,1)
956      A5=Y(6,1)
957      A6=Y(7,1)

```

```

956      A7=Y(8,1)
957      RU=0.
958      SSR=0.
959      DO 4 J=1,N
960      YF=0.
961      DO 5 J=1,M
962  5      YF=YF+Y(J,1)*A(J,1)
963      R(I)=Y1(1)-YF
964      RU=RU+R(I)
965      SSR=SSR+R(I)*R(I)
966      PRINT 10,1,Y1(1),YF,R(I)
967  10      FORMAT(110,7E15.7)
968  4      CONTINUE
969      RETURN
970      END

C
C      *****

971      SUBROUTINE VISASM(TF,RF,RUPF,VISMF)
C      *****
972      VISPF=80.4+0.407*TF-RUPF*(1858.-5.9*TF)/1000.
973      VISVF=173.6+0.454*TF
974      FI12F=0.3536/SQRT(1.+0.6222)*(1.+SQRT(VISPF/VISVF))*1.12593)**2
975      FI21F=0.3536/SQRT(1.+1.6071)*(1.+SQRT(VISVF/VISPF))*0.88814)**2
976      VISMF=RF*VISPF/(RF+(1.-RF)*FI12F)+(1.-RF)*VISVF/(RF*FI21F+1.-RF)
977      RETURN
978      END

C
C      *****

979      SUBROUTINE AMBASM(TF,RF,CPN2,CPO2,CPAR,AMBPF)
C      *****
980      AMBPF=0.0176+5.97/100000.*TF+1.04/10.**7*TF*TF-0.451*TF*TF*TF/10.
1*11
981      WMN2=28.02
982      WMO2=32.
983      WMAK=39.94
984      TRN2=(TF+273.15)/126.1
985      TRU2=(TF+273.15)/154.4
986      TRAR=(TF+273.15)/151.2
987      SIN2=1.673/100000.
988      SIU2=1.343/100000.
989      SIAR=1.272/100000.
990      CPN2=27214.+4.187*(TF+273.15)
991      CPO2=34025.+1.0802*(TF+273.15)-78586.*10000./(TF+273.15)**2
992      CPAR=20808.
993      CVN2=(CPN2-8315.)/WMN2
994      CVO2=(CPO2-8315.)/WMO2
995      CVAR=(CPAR-8315.)/WMAK
996      VISN2=8.175*(4.58*TRN2-1.67)**(5./8.)/SIN2/10.**11
997      VISU2=8.175*(4.58*TRU2-1.67)**(5./8.)/SIU2/10.**11
998      VISAR=8.175*(4.58*TRAR-1.67)**(5./8.)/SIAR/10.**11
999      AMBN2=VISN2*(1.32*CVN2+508.-104.6/TRN2)
000      AMBU2=VISU2*(1.32*CVO2+444.8-91.59/TRU2)
001      AMBAR=2.5*VISAR*CVAR
002      AMBVF=((0.78*(AMB2**((1./3.)))*AMBN2+0.21*(WMO2**((1./3.)))*AMBU2+0.01*
1(WMAK**((1./3.)))*AMBAR)/(0.78*(WMN2**((1./3.)))+0.21*(WMO2**((1./3.)))+
20.01*(WMAK**((1./3.))))
003      FI12L=0.3536/SQRT(1.+0.6222)*(1.+SQRT(AMBPF/AMBVF))*1.12593)**2
004      FI21L=0.3536/SQRT(1.+1.6071)*(1.+SQRT(AMBVF/AMBPF))*0.88814)**2
005      AMBPF=RF*AMBPF/(RF+(1.-RF)*FI12L)+(1.-RF)*AMBVF/(RF*FI21L+1.-RF)
006      RETURN
007      END

```


C
C

1008

SUBROUTINE DIFASM(TF,RF,DIFMF)

C

1009

 $DIFMF = (1.-RF) * ((TF+273.15) * 1.81) / 10. ** 9 / ((1.-RF) * 0.78 / 0.7577 + (1$ $RF) * 0.21 / 0.7794 + (1.-RF) * 0.01 / 0.7503)$

1010

RETURN

1011

END

C

SENTRY

APPENDIX H

THE AIR ROTAMETER CALIBRATION CURVE

The linear least square fit of the third order gave the values of the coefficients

$$Y = - 0.49282 + 1.7852X - 0.28669X^2 + 0.0638X^3$$

where X - rotameter reading

Y - flow rate [l/s].

The error variance was less than 1%.

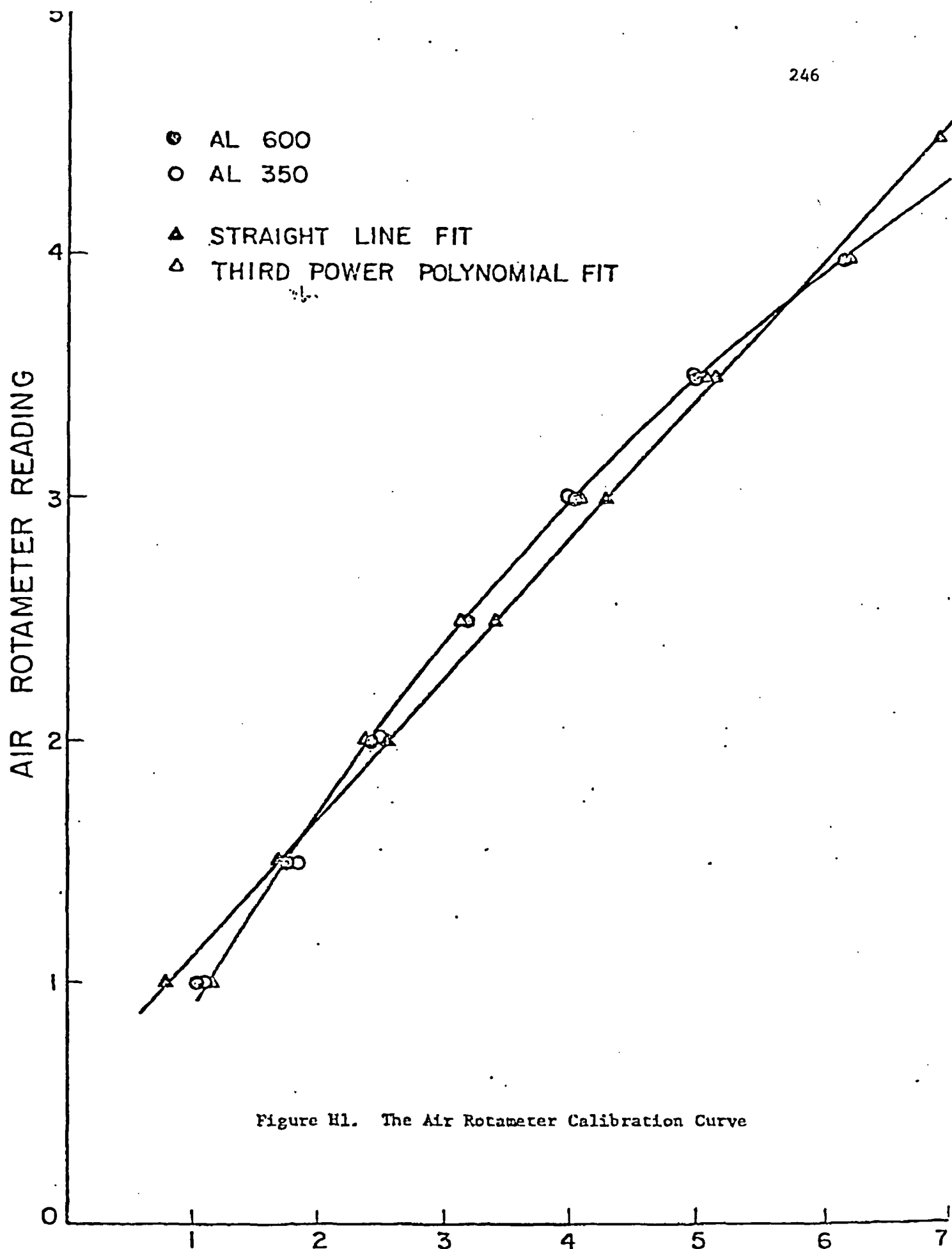


Figure H1. The Air Rotameter Calibration Curve

APPENDIX I

THE HUMIDITY CALIBRATION CURVE

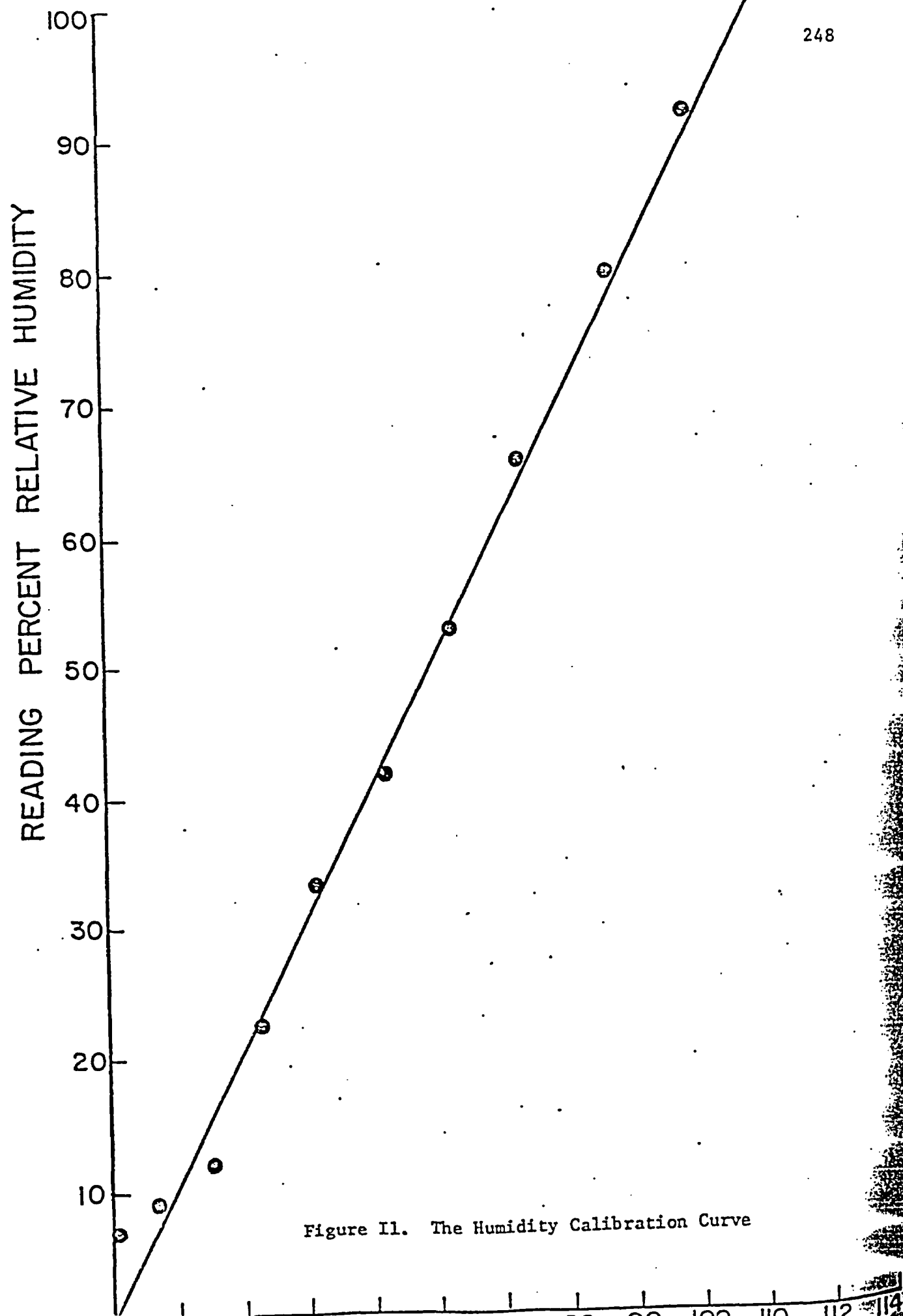
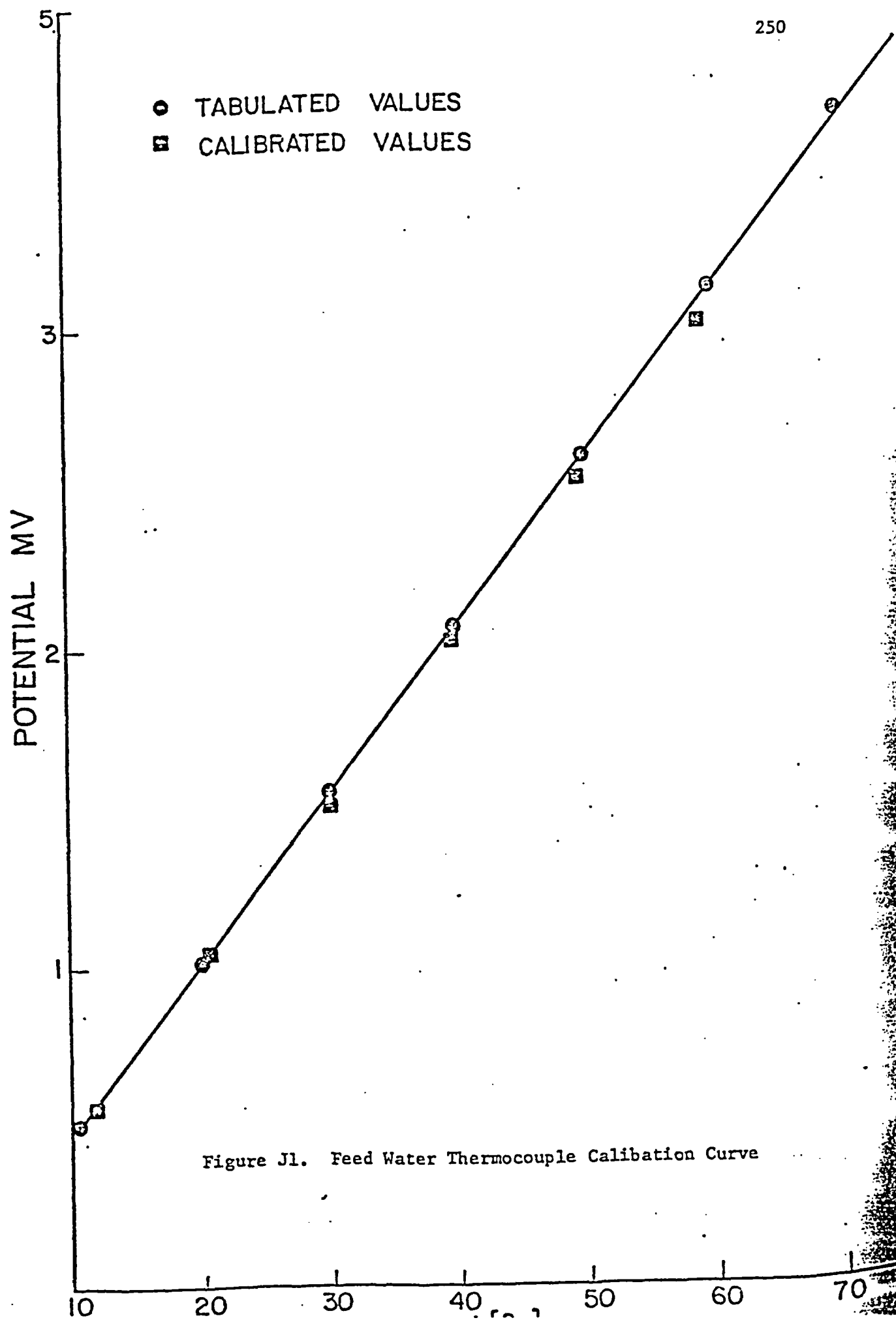


Figure 11. The Humidity Calibration Curve

APPENDIX J

FEED WATER THERMOCOUPLE CALIBRATION CURVE



APPENDIX K

THERMISTOR AND RECORDER CALIBRATION CURVES

The least square fit through the measured values gave the following values of coefficients:

a) Thermistor 1

$$T = 140.15 - 0.24765R + 2.4901(R/100)^2 - 0.11235(R/100)^3 + 0.0019093(R/100)^4, \quad [^{\circ}\text{C}]$$

where, R - thermistor resistance, [Ω].

The error variance is less than 1%.

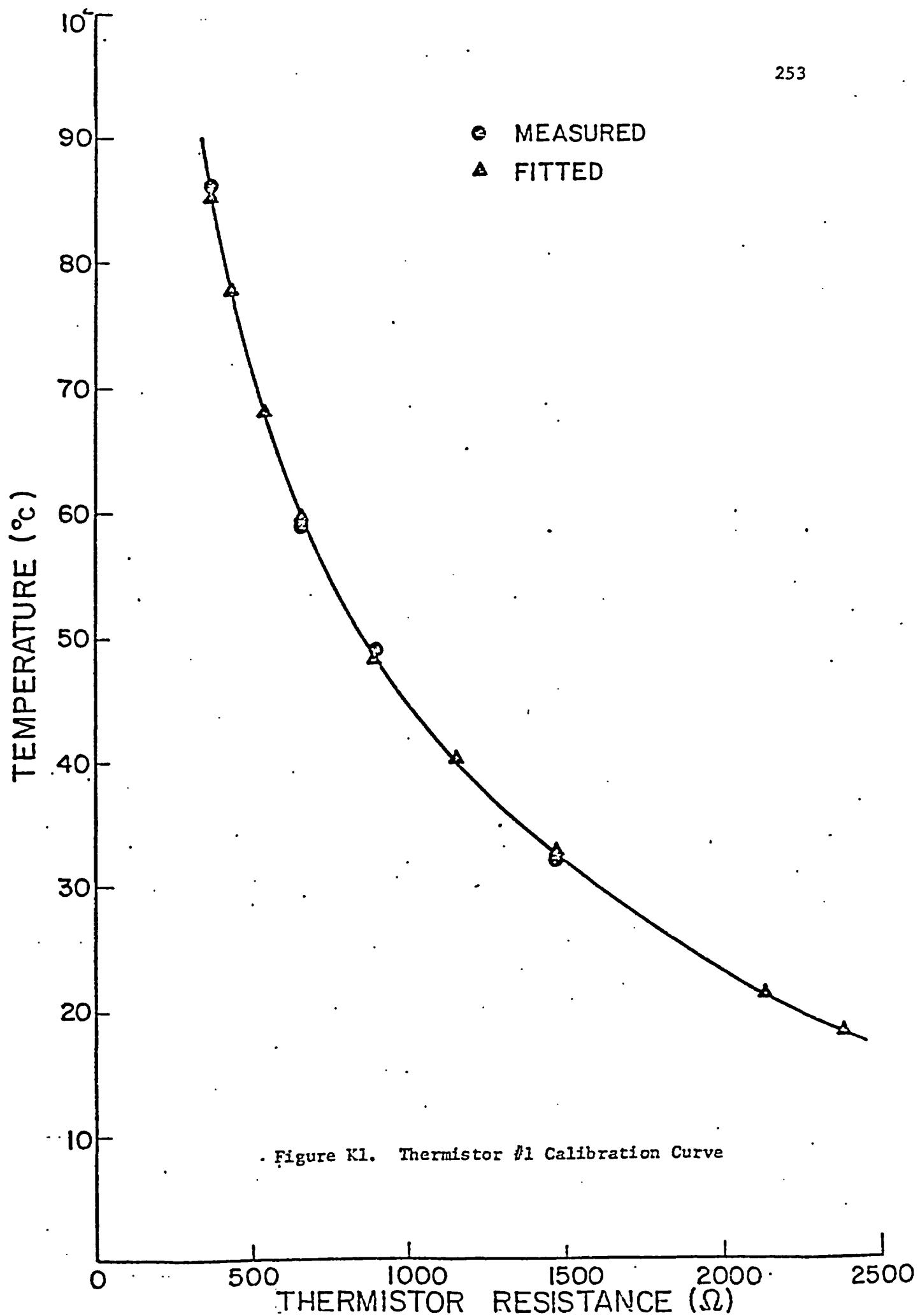
$$T = 0.12864 - 0.081275(\text{CHP}) + 0.022249(\text{CHP})^2 - 4.2562 \cdot 10^{-4}(\text{CHP})^3 + 2.9725 \cdot 10^{-6}(\text{CHP})^4, \quad [^{\circ}\text{C}]$$

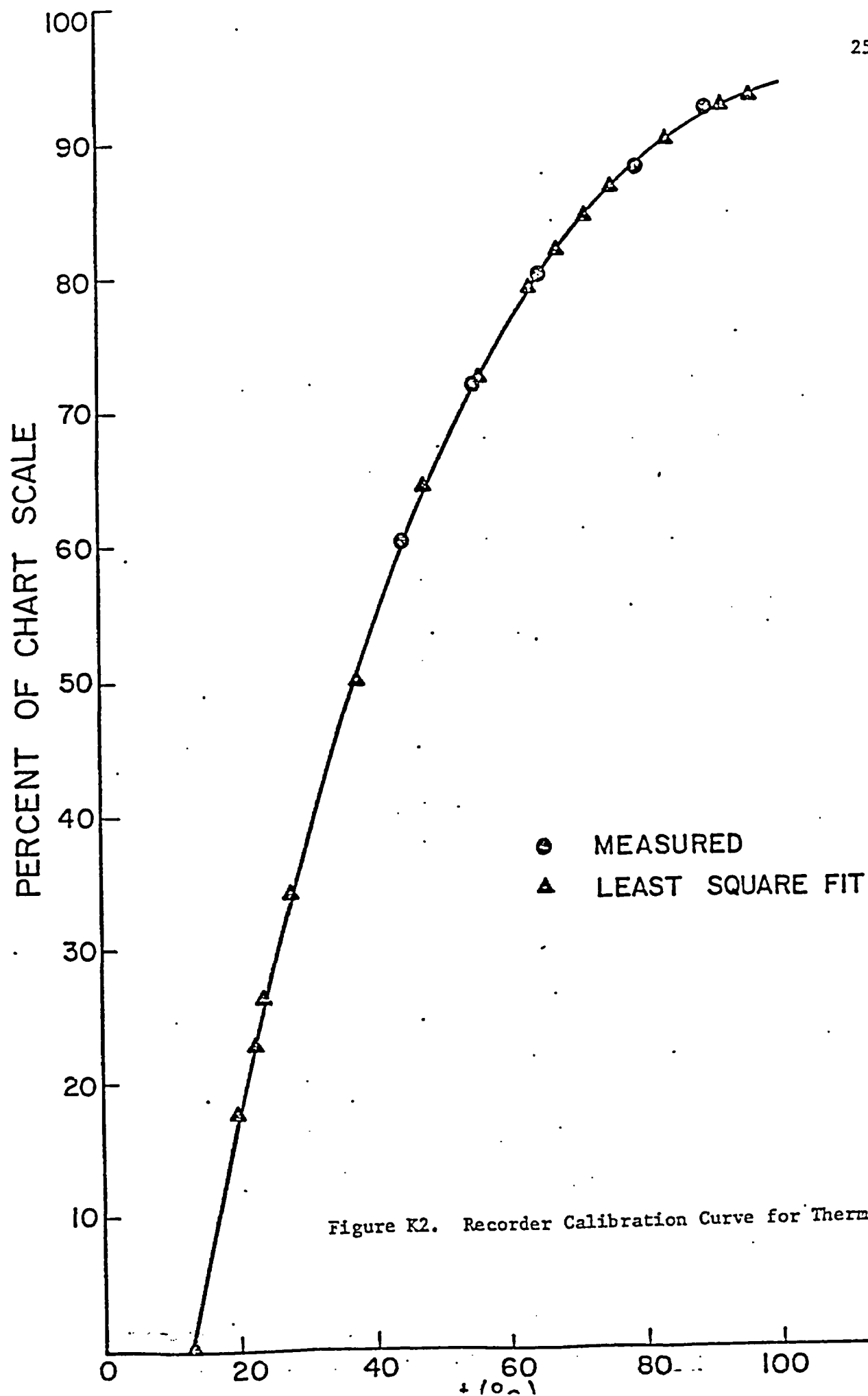
where, CHP - percent of chart reading, %.

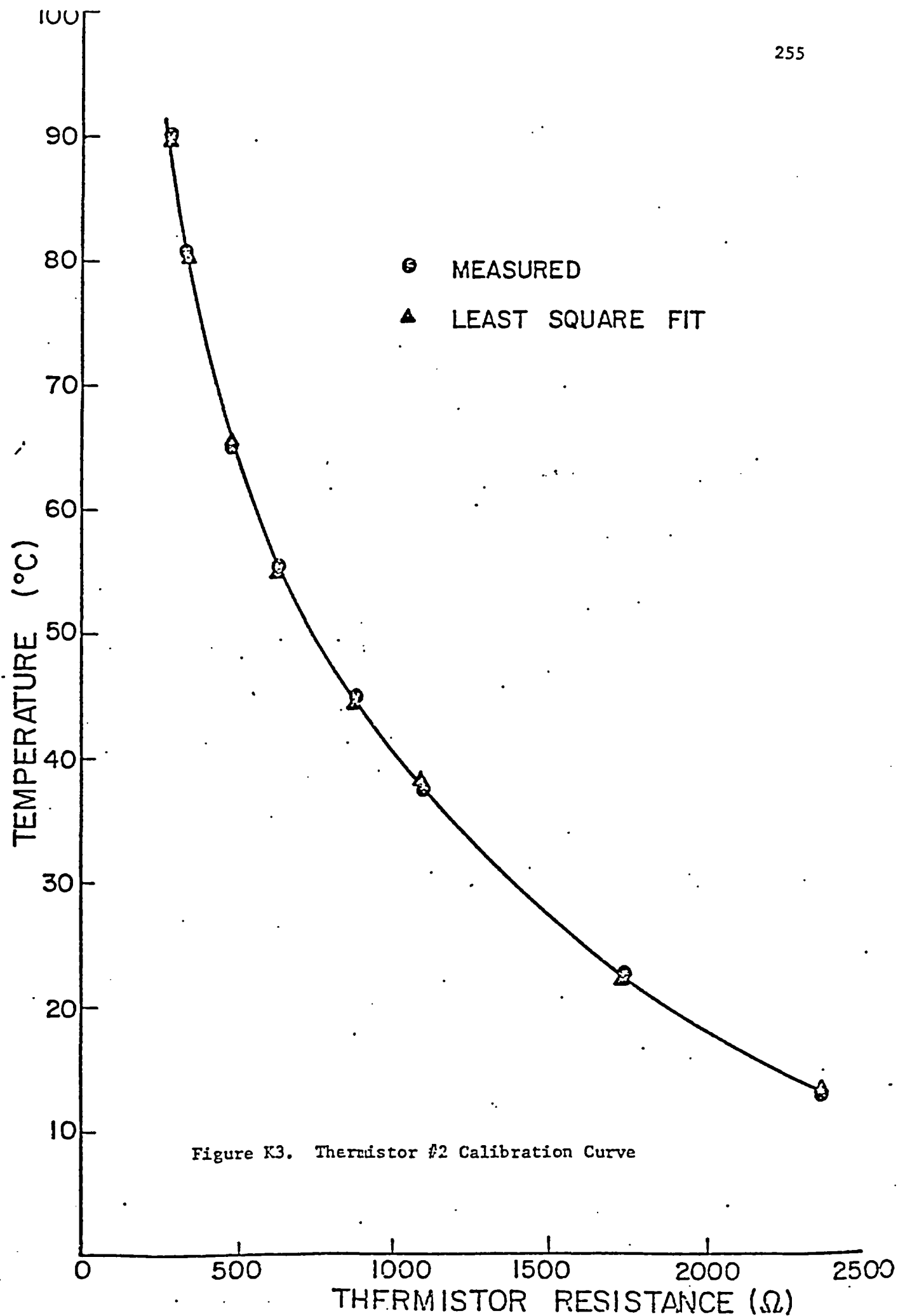
b) Thermistor 2

$$T = 143.77 - 0.21354 \cdot R + 1.7122(R/100)^2 - 0.067465(R/100)^3 + 0.0010052(R/100)^4, \quad [^{\circ}\text{C}]$$

$$T = 18.423 - 0.18619(\text{CHP}) + 0.22464 \cdot 10^{-1}(\text{CHP})^2 - 0.34394 \cdot 10^{-3}(\text{CHP})^3 + 0.21776 \cdot 10^{-5}(\text{CHP})^4$$







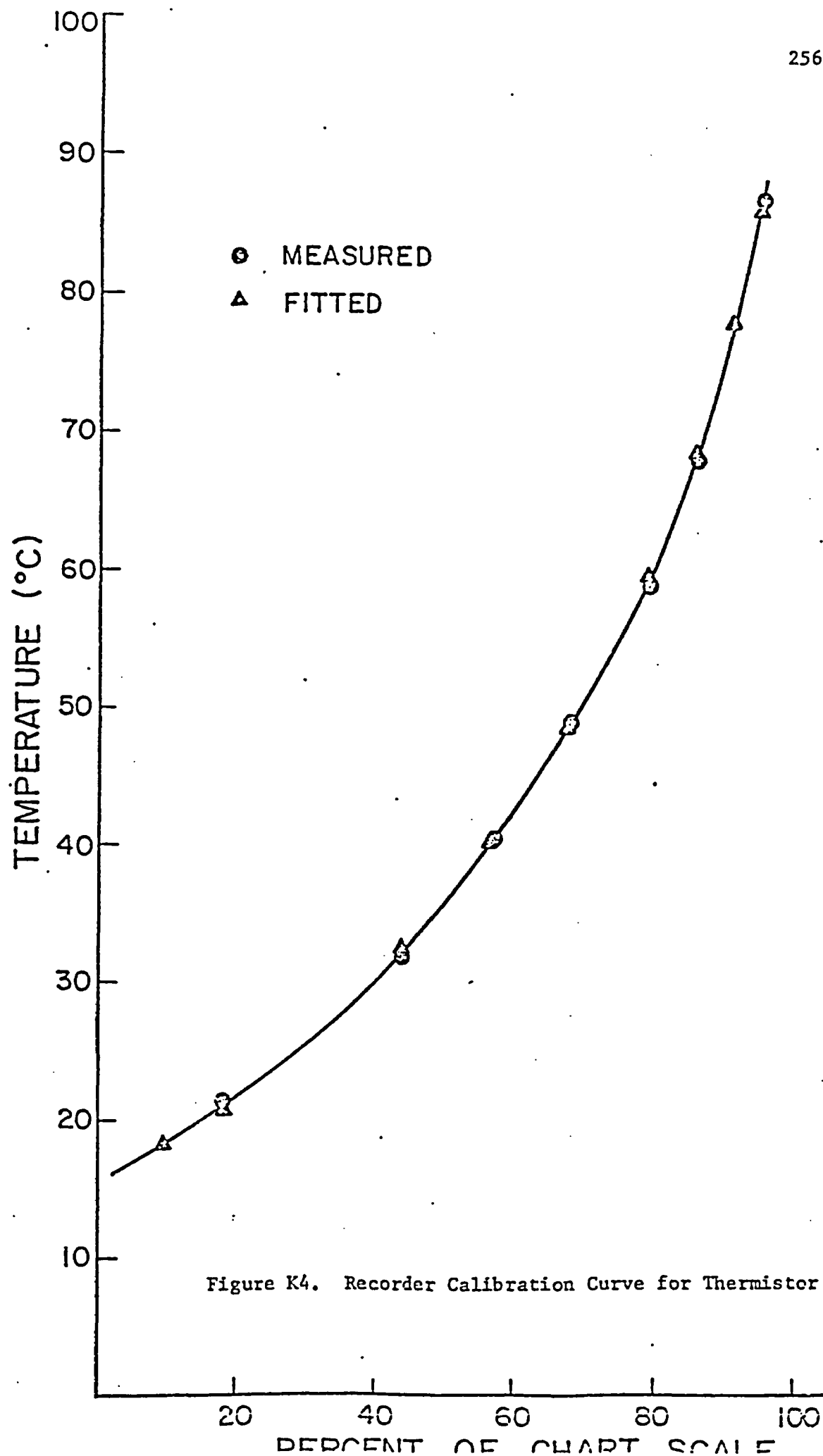


Figure K4. Recorder Calibration Curve for Thermistor #2

APPENDIX L

DATA OF EXPERIMENTAL RUNS FOR SINGLE DROPLETS

TABLE L.1

Run #	Diameter [mm]	Steam Con- centration, %	Droplet Init. Temp. °C	Relative Velo- city, cm/s	Thermal Utilization θ [%]												
					Predicted	10	20	30	40	50	60	70	75	80	90	95	
1	2.6	47	15.8	191	Experimental		5.5	13.5	23.5	33	43	52	66	70	74	89.5	96
2	2.9	47	16	191			6	17	33	57	57	67	75	78.5	83	93	98
3	2.9	47	16	191			6	12	25	51.5	51.5	63.5	73	77	81.5	91.5	-
4	1.9	47	16.2	191			8	21	34	55	55	64	71.5	75	79.5	91	96
5	2.5	65	17	140			6.5	18	28.5	48	48	67.5	73.5	78	80.5	89	94.5
6	1.4	66	17.5	140			5	18	30	57	57	66	74	78	81	92	97.5
7	2.5	31	16.9	258			7	20	34	50.5	50.5	57	64	68	72	81	87
8	2.1	24	16.7	360			3.5	13	26	49.5	59.5	58	67	73			
9	2.7	33	19.2	691			8	20	35	61	61	68.5	76	79	82.5	89	92
10	1.4	36	22.5	199			4	14	23	50.5	50.5	70	80	84	90	94	96
11	1.6	52	20	108			2	8	21	39	39	51	64	72	80	91.5	93.5

TABLE L.1 (Cont'd)

						10	20	30	40	50	60	70	75	80	90	95
12	1.9	52	18.7	108	Experimental	6.5	21.5	37	51.5	58.5	68	75.5	78	81	87	93
13	1.7	53	19.8	108		8.5	20	34	46.5	57	69	76.5	81	85.5	91.5	94
14	1.6	53	19.3	108		2	9	21	33	47	60	70.5	75	79.5	87.5	92
15	1.7	53	19.5	108		6.5	18	35	47.5	57.5	69	77	80	84.5	90	92.5
16	2.9	17	18.1	376		5.5	13	22	33	51.5	52.5	68	71	77	88	94
17	2.5	18	18	376		2	6	11	18	34	57	72	77.5	82	90	83.5
18	3.1	19	19	376		6	13.5	23	38	50	61.5	73	27.5	84.5	93.5	97
19	2.6	19	18.7	376		4	8.5	16	28	43	57.5	77	83	86.5	94.5	98.5
20	2.4	18	18.5	376		10	23	41	51	60	68	73	77	81.5	91.5	97
21	3	13	18.5	405		5.5	16	27	41	54	65	75	80.5	86.5	95	98
22	2.4	13	18	405		5	13	23	32.5	45	59	70.5	75	80.5	91.5	96.5
23	2.8	14	17.8	405		3.5	13.5	26	39	54.5	65	75	80	84	92.5	96.5
24	2.4	8	16.2	273		6.5	13.5	21.5	23	49	59	59	77	82.5	93.5	98.5
25	2.4	8	16.4	273		4.5	12	21.5	29.5	40.5	44	44	72	78.5	89.5	95
26	2.8	8	16.4	273		4.5	11.5	23	36	48.5	61.5	61.5	79	84.5	93.5	-

TABLE L.1 (Cont'd)

					10	20	30	40	50	60	70	75	80	90	95
27	1.3	8	16.9	273	5.5	16.5	27.5	39	49	59	69	74	78.5	87.5	94
28	3.0	8	16.8	273	5.5	14	22.5	41.5	53.5	65	75.5	79	84	-	-
29	1.5	8	17	273	7.5	20	30	42.5	53.5	63.5	73	77.5	82	91.5	26.5
30	1.3	7	17.2	349	6	17	17.5	36.5	46	55	65	70	74	86.5	92
31	1.3	6	16.8	349	5	17	26.5	36.5	47	57	68	73	78.5	89.5	95
32	1.3	6	16.8	349	5.5	16.5	27	39	48.5	58	68	72	77.5	87	92.5
33	2.3	6	16.2	349	5	14	22	32	43.5	56	67	73	80	89	94
34	2.9	6	17.8	349	5	14.5	25	36.5	46	58	78	73	78.5	-	-
35	1.8	6	16.5	349	9	20	31.5	43	53	62	71	77	81	91	95.5
36	3.1	38	18.3	168	7	18.5	36	48	57	62	69	73.5	79	89	94.5
37	3.0	38	17.6	168	8.5	21.5	32	39	46	53.5	64	69	76	89	94
38	2.5	38	18.5	168	7	18	32	43	55	64	74.5	80	84.5	91.5	94
39	3.3	38	16.7	168	6	15.5	28.5	39.5	47	58	70	76	82.5	92	96
40	3	38	17.6	168	4.5	13	27	40.5	50	57	67	72	78	90.5	95.5
41	2.9	36	17.3	168	4.5	13.5	24	37.5	47.5	57	67.5	72.5	79	91.5	97

Experimental

TABLE L.1 (Cont'd)

						10	20	30	40	50	60	70	75	80	90	95
42	3.4	36	17.5	168	Experimental	3.5	10	25	46	60	67.5	-	-	-	-	-
43	3.0	36	18.3	168		2.5	6.5	13	22	36	55	67	73	80	91	96
44	3.2	36	17.4	168		3.5	10	18.5	23	48	62	70.5	76.5	81.5	91.5	97
45	3.0	36	17.7	168		3.5	10	22	33	44	57.5	68.5	74	80	91.5	97.5
46	3.0	36	17.2	168		4	11.5	23	35	48.5	58.5	68.5	74.5	80	92.5	97.5
47	2.1	26	18.3	250		10	24	38	47	56	64.5	72.5	78	81.5	88.5	92.5
48	2.6	25	17.3	250		3.5	9	12.5	16.5	50	60	70	75	80.5	90.5	96
49	3.1	25	18.8	250		5	15	23.5	36	49.5	61	71.5	78.5	83.5	93	97
50	3.0	25	19.7	250		6	13	27	36.5	49	60.5	69.5	73.5	78	87	92
51	2.5	25	18.2	250		6.5	20	36	48	60	70	78	80	82	91.5	96.5
52	2.8	25	16.7	250		3.5	11	23	32	49	60	70.5	78	13	93.5	97
53	3.0	25	18.9	250		3.5	13	24	36.5	50	61.5	70.5	76.5	81.5	91.5	96.5
54	2.9	25	17.5	250		3.5	9	21	33	45.5	59	73.5	79	84.5	93.5	97
55	2.9	25	17.6	250		5	14	22	35	47	57	69.5	75	80	92	96.5
56	2.6	25	17.2	250		3.5	9	17.5	29	44	58	67	73.5	79.5	91	95.5

TABLE L.1 (Cont'd)

					10	20	30	40	50	60	70	75	80	90	95
57	2.6	25	16.6	250	5.5	12	24	36	48	59.5	72	78	83.5	94.5	98
58	3.2	14	20.1	341	3	75	17	28	43	58	70.5	77	81.5	88	-
59	3.7	14	18.7	341	5.5	14.5	28	41.5	53	66	77	82	85	90	-
60	3.2	14	19.3	341	2	6	14	27	40.5	53.5	67.5	73	78.5	88	-
61	3.2	14	17.7	341	4.5	11	22.5	36	49	63.5	77	80.5	84	90	-
62	3.4	14	19	341	6	16	27.5	40	54	67.5	77.5	84	87	91.5	-
63	3.0	14	17.7	341	5	10	23	36.5	47	61.5	73	78.5	84	90	94
64	3.0	14	17.5	341	7	17	29	42	53	67.5	78.5	83	87	91	-
65	3.1	14	20.2	341	6	17	20	42	52	6.1	70	74	78.5	87	91.5
66	3.9	14	20.6	341	4	11.5	24	39	53.5	-	-	-	-	-	-
67	3.5	6	19.7	351	7.5	18.5	27.5	38	49	60	60.5	75.5	81	-	-
68	3.8	6	18.9	351	5	17.5	28.5	41	53.5	65	75	80.5	-	-	-
69	2.8	6	19.3	351	6.5	16.5	27	38.5	50.5	61.5	72	77	81.5	88	-
70	2.5	6	18.8	351	7	17.5	29.5	41	52	62	71	76	80	86	-
71	2.4	6	18.6	351	6	17	29	41	51	63.5	73.5	78.5	82	88	-

Experimental

TABLE L.1 (Cont'd)

TABLE E.1 (CONT'D)					10	20	30	40	50	60	70	75	80	90	95	
72	3.4	6	18.4	351	Experimental	7	15	25	37.5	47	57.5	70	73.5	78	-	-
73	3.2	5	19.2	497		8.5	18.5	30	39.5	50.5	61.5	72	77	81	-	-
74	4.0	5	17.5	497		10	20.5	33	43	53	63.5	74.5	77	-	-	-
75	3.3	5	16.8	497		9.5	20.5	33	44	55.5	68	77	79.5	-	-	-
76	3.8	5	18.8	497		10	20.5	33	45	56	67	75.5	80	-	-	-
77	3.9	5	17.7	497		12	23	35	46	57	68	78.5	81.5	-	-	-
78	3.5	5	17	497		6	21.5	30.5	41.5	51	60	69	73	77	-	-
79	3.8	5	17.2	497		9	20.5	31	42.5	53	63	72	77	81	-	-
80	3.8	5	18.8	497		9	18.5	29.5	40	50	59	68.5	72	75.5	-	-
81	2.9	29	16.6	258		7	11.5	19	28.5	43	55	71	77	82	93.5	-
82	2.4	14	15.9	405		5	12	21	45.5	64	73	80	62.5	90.5	91.5	94
83	2.8	6.7	16.2	349		8.5	17	28.5	37	52.5	66	77.5	83	89	98	-
84	2.6	6.4	16.2	349		5.5	13	22	30.5	42.5	60.5	74	79	84.5	95.5	-
85	2.5	6.2	16.2	349		4.5	9.5	17	26	35	50	64	71	78	92.5	-
86	2.9	6.4	17.6	349		5	13	24	36	49	63	74	81	87	-	-

TABLE L.1 (Cont'd)

						10	20	30	40	50	60	70	75	80	90	95
87	1.5	5	19.2	1.76	Experimental	5	11	20	26.5	35	37.5	60	67	73.5	86	93
88	2.5	5	19.6	1.76		10.5	20.5	31.5	42	59	71	84	88	91	-	-
89	2.5	5	19	1.76		8.5	18	28	42	56.5	68	78.5	83	88	-	-
90	2.5	5	19.1	1.76		9	17	29	44	54	64	75	82	89	-	-

APPENDIX M

DIMENSIONAL ANALYSIS FOR THE RESPONSE TIME

CORRELATION

Let us assume that the response time will be a function of a steam saturation pressure P_{SM} , initial relative velocity of a droplet v_{Ro} , mass of a droplet m and time t . The dimensional matrix in the MLT system of units is [120]

	P	V	m	t	
M	1	0	1	0	
L	-1	1	0	0	
t	-2	-1	0	1	

(M.1)

We can construct square matrices from this dimensional matrix by deleting various rows or columns. The determinant formed from the last three columns in the dimensional matrix is:

$$\begin{vmatrix} 0 & 1 & 0 \\ 0 & 0 & 1 \\ 1 & 0 & -1 \end{vmatrix} = (0) \begin{vmatrix} 0 & 1 \\ 0 & 1 \end{vmatrix} - (1) \begin{vmatrix} 0 & 1 \\ 1 & 1 \end{vmatrix} + 0 \begin{vmatrix} 0 & 0 \\ 1 & 0 \end{vmatrix} = 0$$

$$- (1)(-1) + 0 = 1 \quad (M.2)$$

Since the largest-order determinant, we can construct, is a third-order determinant, and the above third-order determinant is different from zero the rank of the dimensional matrix is 3. Since the rank is 3, the number of dimensionless products in a complete set is $N = n - r = 4 - 3 = 1$.

Any product of the variables has the form

$$\pi = P^{k_1} V^{k_2} m^{k_3} t^{k_4} \quad (M.3)$$

or for the corresponding dimensions of π

$$\pi = [ML^{-1}t^{-2}]^{k_1} [Lt^{-1}]^{k_2} [M]^{k_3} [t]^{k_4} \quad (M.4)$$

or rewritten

$$\pi = M^{(k_1+k_3)} L^{(-k_1+k_2)} t^{(-2k_1-k_2+k_4)} \quad (M.5)$$

In order for π to be dimensionless the exponents of M, L, and t must all be zero

$$k_1 + k_3 = 0$$

$$-k_1 + k_2 = 0 \quad (M.6)$$

$$-2k_1 - k_2 + k_4 = 0$$

Any solution of these equations results in a set of exponents for the dimensionless product π . Notice that the coefficients in each equation are a row of numbers in the dimensional matrix. Equations (M.6) are a system of three equations in four unknowns and are undetermined, therefore, since there is an infinite set of solutions. For our purposes we shall assign a value 1 for k_4 , and solving for remaining unknowns

$$k_1 = k_2 = 1/3 \quad k_3 = -1/3 \quad (M.7)$$

and

$$\pi = \frac{(PV)^{1/3} t}{m^{1/3}} = \left(\frac{PV}{m} \right)^{1/3} t \quad (M.8)$$

APPENDIX N

DOUSING CHAMBER SIMULATION ALGORITHM

\$JOB WATFIV ***** ,KP=29,P=50

THIS PROGRAM GENERATES PRESSURE DROPS IN NUCLEAR DOUSING SYSTEMS
BY SOLVING THE DISCRETIZED HEAT BALANCE EQUATION.

INPUT PARAMETERS ARE:

UPPER-LIMIT DISTRIBUTION PARAMETERS
NUMBER OF DROPLET DIAMETER DISCRETIZATIONS
CHAMBER VOLUME AND HEIGHT
INITIAL PARTIAL PRESSURES OF STEAM AND AIR
INLET WATER VELOCITY, FLOW RATE, AND TEMPERATURE
DRAG COEFFICIENT CORRELATION PARAMETERS
PRESSURE DROP TIME INCREMENT

LIST OF SYMBOLS AND ARRAYS

SYMBOL		UNITS
-----		-----
AMASS	MASS OF WATER DROPLET	KG
CPWF	HEAT CAPACITY OF WATER DROPS LEAVING CHAMBER	KJ/(KG*DEG.C)
CPWO	HEAT CAPACITY OF WATER DROPS ENTERING CHAMBER	KJ/(KG*DEG.C)
CPWT	HEAT CAPACITY OF WATER DROPS WITHIN CHAMBER	KJ/(KG*DEG.C)
DCT	TOTAL ENERGY CHANGE OF ALL DROPLETS IN A TIME INCREMENT	KJ
DELAY	TIME DELAY FACTOR	SEC
DLCONT	TOTAL ENERGY CHANGE OF ALL DROPLETS IN GIVEN TIME INCREMENT	KJ
DNWL	DENSITY OF WATER DROPS LEAVING CHAMBER	KG/M**3
DNWO	DENSITY OF WATER DROPS ENTERING CHAMBER	KG/M**3
DNWT	DENSITY OF WATER DROPS WITHIN CHAMBER	KG/M**3
DPINC	TOTAL NUMBER OF DROPLETS OF A SPEC- IFIC DIAMETER GENERATED IN A TIME INCREMENT	
ENAIR	ENTHALPY OF AIR	KJ/KG
ENST	ENTHALPY OF STEAM	KJ/KG
ENMIX	ENERGY OF AIR-STEAM MIXTURE	KJ
ENINA	INTERNAL ENERGY OF AIR	KJ/KG
ENINM	INTERNAL ENERGY OF AIR-STEAM MIXTURE	KJ/KG
ENINST	INTERNAL ENERGY OF STEAM	KJ/KG
FREQ	FREQUENCY DISTRIBUTION CORRELATION	
FRNEW		
FROLD		
HEIGHT	HEIGHT OF CHAMBER	M
HTINC	HEIGHT INCREMENT	
N	TIME COUNTER	
NHI	NUMBER OF HEIGHT INCREMENTS	
NINC	NUMBER OF DIAMETER DISCRETIZATIONS	
NSS		
PAIR	PARTIAL PRESSURE OF AIR	BAR
PAIR0	INITIAL PARTIAL PRESSURE OF AIR	BAR
PAIR1	INITIAL PARTIAL PRESSURE OF AIR	PSIA
PPP	PARTIAL PRESSURE OF STEAM	BAR
PPPO	INITIAL PARTIAL PRESSURE OF STEAM	BAR


```

2      DIMENSION TIME(2000),DIST(2000),VDROP(2000),TIM(5,650),VEL(5,650)
3      DIMENSION CONT(5,2),FOOT(10),FIN(10),OUT(10),S(500),VRTSA(2000)
4      DIMENSION ITRANS(5,200),VELTR(5,200),N55(10)
5      DIMENSION DRPHT(5,650),ISE(10),TPES(10),FRULD(10),IFLAG(10)
6      DIMENSION WTPA(5,650),C(10),NH(100)
7      COMMON TZ,PI/AREA1/ G,AREA,DMASS,ROMB,VISMB,A,SS,DIAM,DELRO,
1      1DSTAR1,DSTA2A,DSTA2B,DSTA3A,DSTA3B,DSTAR4,RE2A,RE2B,RE3A,RE3B,RE
2      2RES,DMAXS,CDMAX,WSTAM,WMAXS,WSTAR4,WSTA3A,WSTA3B,WSTA2A,WSTA2B,
3      3WSTAR1,DST,SURFT/AREA2/TKVOL,PPP,ENINM,WAIR,PAIRU,TZO,T
8      100  FORMAT('1',9X,'SIMULATION OF PRESSURE DROP IN NUCLEAR DOUSING '
9      101  FORMAT(' ',9X,'*****')
1     102  FORMAT('0',9X,'INITIAL DROPSIZE DISTRIBUTION')
11    103  FORMAT(' ',9X,'*****',//)
12    104  FORMAT('0',11X,'UPPER-LIMIT PARAMETERS')
13    105  FORMAT(' ',11X,'-----')
14    106  FORMAT('0',14X,'XMAX =',F6.3,' MM')
15    107  FORMAT(' ',14X,'DELTA=',F6.4)
16    108  FORMAT(' ',14X,'A      =',F6.3,//)
17    109  FORMAT(' ',11X,'DISCRETIZED INITIAL DROPSIZE DISTRIBUTION')
18    110  FORMAT(' ',11X,'-----')
19    111  FORMAT('0',12X,'DROPSIZE VOLUME FRACTION  NUMBER IN')
20    112  FORMAT(' ',12X,' (MM)                      UNIT VOLUME')
21    113  FORMAT(' ',9X,F10.3,F13.4,F16.4)
22    114  FORMAT(' ',//,9X,' SYSTEM PARAMETERS')
23    115  FORMAT(' ',9X,'*****')
24    116  FORMAT('0',11X,'TANK VOLUME                      =',F10.3,' M**3')
25    117  FORMAT(' ',11X,'TANK HEIGHT                      =',F10.3,' M')
26    118  FORMAT(' ',11X,'INITIAL STEAM PRESSURE           =',F10.4,' BAR')
27    119  FORMAT(' ',11X,'INITIAL AIR PRESSURE             =',F10.4,' BAR')
28    120  FORMAT(' ',11X,'INITIAL SYSTEM PRESSURE          =',F10.4,' BAR')
29    121  FORMAT(' ',11X,'INITIAL SYSTEM TEMPERATURE= ',F10.2,' DEG. C')
30    122  FORMAT(' ',11X,'INLET WATER TEMPERATURE        =',F10.2,' DEG. C')
31    123  FORMAT(' ',11X,'INLET WATER VELOCITY             =',F10.2,' M/SEC')
32    124  FORMAT(' ',11X,'INLET WATER FLOWRATE            =',F10.4,' M**3/SEC')
33    125  FORMAT('1',9X,'DYNAMIC RESPONSE OF SYSTEM')
34    126  FORMAT(' ',9X,'*****')
35    127  FORMAT('0',9X,'      TIME      SYSTEM      STEAM      AIR      TOTAL
1      1 TOTAL      TOTAL ')
36    128  FORMAT(' ',9X,'      TEMP.      PRESS.      PRESS.      PRESS.
1      1 PRESS.      PRESS.')
37    129  FORMAT(' ',9X,'      (SEC)      (DEG C)      (BAR)      (BAR)      (BAR)
1      1 (PSIA)      (PSIG)')
38    130  FORMAT('0',9X,'-----')
39    131  FORMAT('0')
40    132  FORMAT(' ',9X,F7.2,F11.3,F10.4,F10.4,F10.4,F10.3,F10.3)
41    133  FORMAT(' ',11X,'INITIAL WATER DENSITY           =',F10.3,' KG/M**3')
42    134  FORMAT(' ',11X,'INITIAL SYSTEM DENSITY           =',F10.3,' KG/M**3')
43    135  FORMAT(' ',11X,'INITIAL SYSTEM VISCOSITY          =',F10.3,' 10**7*N*S/M'
44    136  FORMAT(' ',11X,'INITIAL SYSTEM SURF TENSIN= ',F10.5,' N/M',//)
45    137  FORMAT(' ',11X,'ENTERING WATER DELAY TIME = ',F10.3,' SEC',//)
46    138  FORMAT('1',8X,'D= ',F7.3,5X,'D= ',F7.3,5X,'D= ',F7.3,5X,'D= ',F7.3,
15    15X,'D= ',F7.3,5X,'D= ',F7.3,5X,'D= ',F7.3,5X,'D= ',F7.3)
47    139  FORMAT('0',5X,'VELOCITY OF DROPLET OF DIAMETER D(I) IN THE JTH HE
1      1IGHT INCREMENT')
48    140  FORMAT(5X,'-----')
49    141  FORMAT(3X,13,5F14.5)
50    142  FORMAT('0',5X,'FALL TIME OF DROPLET OF DIAMETER D(I) TO THE JTH I
1      1IGHT INCREMENT')
51    143  FORMAT('0',5X,'NUMBER OF DROPLETS OF DIAMETER D(I) OCCUPYING THE

```

```

1JTH HEIGHT INCREMENT')
52 145 FORMAT('0',SX,'AVERAGE TEMPERATURE OF DROPLET OF DIAMETER D(I)
1THE JTH HEIGHT INCREMENT')
53 144 FORMAT(3X,13,5F14.2)
54 146 FORMAT(' ',11X,'RUNGE-KUTTA TIME INCREMENT=',F10.4,' SEC')
55 147 FORMAT(' ',9X,'DYNAMIC RESPONSE OF SYSTEM')
C
C
56 G=9.81
57 ICH=1
58 KK=1
59 RAIR=8314.7/28.96
60 RMWA=28.96
61 SUM=0.
62 TOTAL=0.
63 DELTIM=0.05
C
C
C UPPER LIMIT PARAMETERS AND NUMBER OF DIAMETER DISCRETIZATIONS
C ARE INPUTTED
C
64 READ,SDEV,AA,UM,NINC
65 DINC=UM/NINC
66 DCHECK(1)=DINC
67 SINC=UM/500.
68 R=DCHECK(ICH)-SINC
69 DO 1 I=1,500
70 S(I)=(2*I-1)*SINC/2.
C
C
C DROPLET VOLUME DISTRIBUTION IS CALCULATED
C
71 FREQ=((UM*SDEV)/((S(I)*(UM-S(I))*SQRT(3.14159)))*EXP(-(SDEV*(
1ALOG((AA*S(I))/(UM-S(I)))))*2)
72 FRDROP=FREQ*SINC
73 TOTAL=TOTAL+FRDROP
C
C
C DROPLET SIZE AND VOLUME DISTRIBUTIONS ARE DISCRETIZED
C
74 IF(S(I).LT.R) GO TO 1
75 DISN(ICH)=TOTAL-SUM
76 IF(ICH.EQ.NINC) GO TO 1
77 ICH=ICH+1
78 DCHECK(ICH)=DCHECK(ICH-1)+DINC
79 R=DCHECK(ICH)-SINC
80 SUM=TOTAL
81 1 CONTINUE
82 DO 4 I=1,ICH
83 D(I)=(2*I-1)*DINC/2.
84 DISN(I)=DISN(I)/TOTAL
C
C
C DROPLET SIZE DISTRIBUTION IS CALCULATED
C
85 4 DROPS(I)=DISN(I)/(1.3333*3.14159*(D(I)/2.))**3)
C SYSTEM PARAMETERS ARE INPUTTED
86 READ,TKVOL,HEIGHT
87 READ,TPRESS
88 T=0.0
89 READ,PT1,PPP1,PAIR1
90 READ,WTFLOW,V0,TWATO
91 READ,DELAY
92 PTO=PT1/14.504
93 PPP0=PPP1/14.504
94 PAIR0=PAIR1/14.504
95 CALL TEMP1(PPP0,TZ0)

```

```

96      PT=PT0
      C
      C      INITIAL PHYSICAL PROPERTIES OF WATER DROPLETS ARE CALCULATED
      C
97      CALL PPWAT(TWATO,PT,CPWO,DNWO)
98      WTFOW1=WTFLOW/DNWO
99      WTFLOW=WTFOW1*10.**9
100     PRINT100
101     PRINT101
102     PRINT102
103     PRINT103
104     PRINT104
105     PRINT105
      C
      C      UPPER-LIMIT PARAMETERS ARE OUTPUTTED
      C
106     PRINT106,UM
107     PRINT107,SDEV
108     PRINT108,AA
      C
      C      DISCRETIZED DISTRIBUTIONS ARE OUTPUTTED
      C
109     PRINT109
110     PRINT110
111     PRINT111
112     PRINT112
113     PRINT113,(D(J),DISN(J),DROPS(J),J=1,ICH)
114     PRINT114
115     PRINT115
      C
      C      CHAMBER VOLUME AND HEIGHT ARE OUTPUTTED
      C
116     PRINT116,TKVOL
117     PRINT117,HEIGHT
      C
      C      INITIAL CHAMBER PRESSURES ARE OUTPUTTED
      C
118     PRINT118,PPP0
119     PRINT119,PAIRO
120     PRINT120,PT0
      C
      C      INITIAL SYSTEM TEMPERATURE IS OUTPUTTED
      C      C      INLET INLET WATER VELOCITY,FLOWRATE,AND TEMPERATURE ARE OUTPUTTED
      C
121     PRINT121,TZ0
122     PRINT122,TWATO
123     PRINT123,V0
124     PRINT124,WTFOW1
125     PSIG=P11-14,690
126     PPP=PPP0
127     XS=PPP/PT
128     HIN=HEIGHT/0.05
129     NH1=IF1X(HIN+0.5)
130     HTINC=HEIGHT/NH1
      C
      C      VELOCITY PROFILES ARE CALCULATED USING RUNGE-KUTTA TECHNIQUE
      C
      C      DENSITY OF AIR/STEAM MIXTURE
131     RMF=8314.7/(XS*18.02+(1.-XS)*28.96)
132     RUMF=100000.*PT0/(RMF*(TZ0+273.15))
      C
      C      VISCOSITY OF AIR/STEAM MIXTURE
      C

```

```

133 CALL SEKPV(TZ0,PV)
134 ROP=PT0/PV
135 VISP=80.4+0.407*TZ0-ROP*(1858.-5.9*TZ0)/1000.
136 VISV=173.6+0.454*TZ0
137 FI12=0.3536/SQRT(1.+0.6222)*(1.+SQRT(VISP/VISV))*1.12593)**2
138 FI21=0.3536/SQRT(1.+1.6071)*(1.+SQRT(VISV/VISP))*0.88814)**2
139 VISMF=XS*VISP/(XS+(1.-XS)*FI12)+(1.-XS)*VISV/(XS*FI21+1.-XS)

```

C
C
C

SURFACE TENSION OF WATER IN AN AIR/STEAM MIXTURE

```

140 SURFT=(75.6-0.145*TWAT0-0.25*10.**(-3.)*TWAT0**2)/1000.
141 VISMB=VISMF
142 ROV=DNWD
143 ROMB=ROMF
144 PRINT 133, DNWD
145 PRINT 134, ROMH
146 PRINT 135, VISMB
147 PRINT 136, SURFT
148 PRINT 137, DELAY
149 PRINT 146, DELTIM

```

C
C
C

PARAMETERS OF REINHARTIS DRAG COEFFICIENTS CORRELATIONS

```

150 SS=ROMB*SURFT**3*10.**28/G/VISMB**4
151 DELRO=ROV-ROMB
152 DSTAR1=1.216/(DELRO/ROMB)**(1./3.)
153 DSTA2A=70.0*(DELRO/ROMB)**(-1./3.)*(SS*10.**(-12))**(-0.111)
154 DSTA2B=30.8*(DELRO/ROMB)**(-1./3.)*(SS*10.**(-12))**(0.111)
155 DSTA3A=122.*(DELRO/ROMB)**(-0.535)*(SS*10.**(-12))**(0.275)
156 DSTA3B=300.*(DELRO/ROMB)**(-0.535)*(SS*10.**(-12))**(0.0367)
157 DSTAR4=160.*(DELRO/ROMB)**(-0.447)*(SS*10.**(-12))**(0.114)
158 RE2A=974.*(SS*10.**(-12))**(-0.192)
159 RE2B=236.*(SS*10.**(-12))**0.192
160 RE3A=2240.*(DELRO/ROMB)**(-0.303)*(SS*10.**(-12))**0.388
161 RE3B=7160.*(DELRO/ROMB)**(-0.303)*(SS*10.**(-12))**0.08
162 RE4=3190.*(DELRO/ROMB)**(-0.173)*(SS*10.**(-12))**0.18
163 RE5=4470.*(DELRO/ROMB)**(-0.236)*(SS*10.**(-12))**0.232
164 DMAXS=224.*(DELRO/ROMB)**(-0.5)*(SS*10.**(-12))**(1./6.)
165 CDMAX=0.75*(DELRO/ROMB)**(-0.0232)*(SS*10.**(-12))**0.036
166 WSTAM=3.273*((DELRO/ROMB)*SS**0.25)**0.262
167 WMAXS=RE5/DMAXS
168 WSTAR4=RE4/DSTAR4
169 WSTA3A=RE3A/DSTA3A
170 WSTA3B=RE3B/DSTA3B
171 WSTA2A=RE2A/DSTA2A
172 WSTA2B=RE2B/DSTA2B
173 WSTAR1=0.1/DSTAR1
174 DST=DMAXS
175 A=0.085-(1./29.54)*ALOG10(SS**0.5/(DELRO/ROMB)*10.**(-3))

```

C

```

176 DIST(1)=0.
177 TIME(1)=0.
178 VDROP(1)=V0

```

C

```

179 DO 15 ID=1, ICH
180 VELDRP=VDROP(1)
181 LL=2000
182 IF(D(ID).GT..5) GO TO 37
183 DO 38 IT=2, LL
184 TIME(IT)=(IT-1)*DELTIM

```

C

C

VELOCITY OF DROPLETS SMALLER THAN 0.5 MM, TAKEN AS THE TERMINAL

C

```

185      RSA=RAIR
186      ROSA=101300./RSA/293.15
187      IF(ROMF.GT.ROSA) GO TO 37
188      VRTSA(IT)=((((1.6486/1000.*D(ID)-2.8781/100.)*D(ID)+2.3612/10.)*
1      (ID)-1.3806)*D(ID)+5.4506)*D(ID)-3.1682/10.)
189      YSA=0.43*ALOG10(ROSA/ROMF)-0.4*(ALOG10(ROSA/ROMF))*2.5
190      VDROP(IT)=VRTSA(IT)*10.**YSA*(1.+0.0023*(1.1-ROMF/ROSA))*(20.-TZ0)
191      DIST(IT)=DIST(IT-1)+((VDROP(IT)+VDROP(IT-1))/2.)*DELTIM
192      IF(DIST(IT).GT.HEIGHT) GO TO 17
193      38 CONTINUE
194      IT=IT-1
195      GO TO 17
196      37 CONTINUE
197      DELTIM=.05
198      DMASS=(1.333*3.14159*(D(ID)/2000.))**3)*985.1
199      DO 16 IT=2,LL
200      TIME(IT)=(IT-1)*DELTIM
201      REN=(VELDRP*D(ID)*ROMF*10000.)/VISMF
202      DIAM=D(ID)
203      RKV0=DV(VELDRP)
204      RKV1=DV(VELDRP+(RKV0/2.)*DELTIM)
205      RKV2=DV(VELDRP+(RKV1/2.)*DELTIM)
206      RKV3=DV(VELDRP+RKV2*DELTIM)
207      VDROP(IT)=VELDRP+(DELTIM/6.)*(RKV0+2.*RKV1+2.*RKV2+RKV3)
208      VELDRP=VDROP(IT)
209      RKZ0=DZ(VELDRP)
210      RKZ1=DZ(VELDRP+(RKZ0/2.)*DELTIM)
211      RKZ2=DZ(VELDRP+(RKZ1/2.)*DELTIM)
212      RKZ3=DZ(VELDRP+RKZ2*DELTIM)
213      DIST(IT)=DIST(IT-1)+(DELTIM/6.)*(RKZ0+2.*RKZ1+2.*RKZ2+RKZ3)
214      IF(DIST(IT).GT.HEIGHT) GO TO 17
215      16 CONTINUE
216      IT=IT-1
217      17 CONTINUE
218      ISTART=1
219      DO 18 IH=1,NHI
220      Z=(IH*HTINC)-(HTINC/2.)
221      DO 20 IS=1START,IT
222      IF(DIST(IS).GT.Z) GO TO 21
223      20 CONTINUE
224      IS=IS-1
225      21 ISTART=IS-1
226      FACTOR=(Z-DIST(IS-1))/(DIST(IS)-DIST(IS-1))

```

C

C

LOCAL VELOCITIES AND FALL TIMES ARE STORED

C

```

227      VEL(ID,IH)=VDROP(IS-1)+FACTOR*(VDROP(IS)-VDROP(IS-1))
228      TIM(ID,IH)=TIME(IS-1)+FACTOR*(TIME(IS)-TIME(IS-1))
229      18 CONTINUE
230      15 CONTINUE

```

C

```

231      DO 200 K=1,NHI
232      NH(K)=K
233      200 CONTINUE
234      PRINT 138,(D(J),J=1,ICH)
235      PRINT 139
236      PRINT 140
237      PRINT 141,(NH(J),(VEL(I,J),I=1,ICH),J=1,NHI)
238      PRINT 138,(D(J),J=1,ICH)
239      PRINT 142
240      PRINT 140
241      PRINT 141,(NH(J),(TIM(I,J),I=1,ICH),J=1,NHI)

```

```

242      IF(DELAY.LE.0.0) GO TO 210
243      PRINT 125
244      PRINT 126
245      PRINT 127
246      PRINT 128
247      PRINT 129
248      PRINT 130
249      PRINT 131
250      210 CONTINUE
      C
      C      VARIABLES ARE INITIALIZED
      C
251      DO 40 I=1,ICH
252      DO 40 J=1,NHI
253      WTPA(I,J)=0.
254      40  DRPHT(I,J)=0.
255      TTEST=0.
256      TZ=TZ0
257      N=1
258      DO 24 ID=1,ICH
259      IFLAG(ID)=0
260      ISE(ID)=1
      C
      C      CONTRIBUTION OF ENERGY OF WATER ENTERING SYSTEM TO SYSTEM PRESSU
      C      DROP IS CALCULATED
      C
261      FIN(ID)=(TPRESS*WTFLOW*CPWO*DNWO*DISN(ID)*TWATO)/10.**9
262      NSS(ID)=NHI+1
263      CONT(ID,1)=0.0
264      24  TRES(ID)=TIM(ID,NHI)
265      WAIR=PAIR0*10.**5*TKVOL/(RAIR*(TZ0+273.15))
      C
      C      INITIAL ENERGY CONTENT OF MIXTURE IS CALCULATED
      C
266      CALL COEF
      C
      C      TIME IS INCREMENTED
      C
267      YPR=DELAY+10.*TPRESS
268      41  T=TPRESS+T
269      IF(T.LE.DELAY) GO TO 62
270      TTEST=TTEST+TPRESS
271      N=N+1
272      DO 94 IG=1,ICH
273      94  CONT(IG,2)=0.0
      C
      C      MAXIMUM TIME IS SET
274      IF(T.GT.90.) GO TO 42
      C
      C      LOCAL DROPSIZE DISTRIBUTIONS ARE CALCULATED
      C
      C-----
275      DO 22 ID=1,ICH
276      DPINC=TPRESS*WTFLOW*DROPS(ID)
277      IF(IFLAG(ID).EQ.1) GO TO 56
278      K1=ISE(ID)
279      MM=0
280      DO 23 ITEST=K1,NHI
281      IF(TIM(ID,ITEST).GT.ITEST) GO TO 39
282      IF(ITEST.EQ.NHI) GO TO 27
283      23  CONTINUE
284      39  CONTINUE
285      TIMD=(TIM(ID,ITEST-1)+TIM(ID,ITEST))/2.

```

```

287      MM=1
288      IF(ISE(ID).NE.1) GO TO 29
289      FROLD(ID)=1.0-((TMID-TTEST)/(TIM(ID,ITEST)-TIM(ID,ITEST-1)))
290      ZINC=FROLD(ID)+FLOAT(ITEST-2)
291      GO TO 31
292      29  FRNEW1=1.-FROLD(ID)
293      FRNEW2=1.0-((TMID-TTEST)/(TIM(ID,ITEST)-TIM(ID,ITEST-1)))
294      ZINC=FRNEW1+FRNEW2+FLOAT(ITEST-ISE(ID)-1)
295      GO TO 28
296      25  IF(ISE(ID).NE.1) GO TO 33
297      FROLD(ID)=(TTEST-TMID)/(TIM(ID,ITEST)-TIM(ID,ITEST-1))
298      ZINC=FROLD(ID)+FLOAT(ITEST-1)
299      GO TO 31
300      33  FRNEW1=1.-FROLD(ID)
301      FRNEW2=(TTEST-TMID)/(TIM(ID,ITEST)-TIM(ID,ITEST-1))
302      ZINC=FRNEW1+FRNEW2+FLOAT(ITEST-ISE(ID))
303      28  DRPHT(ID,ISE(ID)-1)=DRPHT(ID,ISE(ID)-1)+DPINC*(FRNEW1/ZINC)
304      FROLD(ID)=FRNEW2
305      31  CONTINUE
306      J4=ITEST-1-MM
307      DRPHT(ID,ITEST-MM)=DPINC*(FROLD(ID)/ZINC)
308      VELTR(ID,N-1)=VEL(ID,ITEST-MM)
309      GO TO 30
310      27  FRNEW2=(TTEST-(TIM(ID,NHI)+.5*(TIM(ID,NHI)-TIM(ID,NHI-1))))/(TIM(
311      2D,NHI)-TIM(ID,NHI-1))
312      FRNEW1=0.0
313      IF(ISE(ID).NE.1) FRNEW1=1.-FROLD(ID)
314      ZINC=FRNEW1+FRNEW2+FLOAT(NHI-ISE(ID)+1)
315      IF(ISE(ID).EQ.1) GO TO 34
316      34  DRPHT(ID,ISE(ID)-1)=DRPHT(ID,ISE(ID)-1)+DPINC*(FRNEW1/ZINC)
317      34  OUT(ID)=(TTEST-(TIM(ID,NHI)+.5*(TIM(ID,NHI)-TIM(ID,NHI-1))))/TPR
318      3S
319      IFLAG(ID)=1
320      J4=NHI
321      30  K3=ISE(ID)
322      DO 35 IC=K3,J4
323      35  DRPHT(ID,IC)=DPINC/ZINC
324      ITRANS(ID,N-1)=ITEST-MM
325      ISE(ID)=ITEST+1-MM
326      22  CONTINUE
327      C-----
328      56  CONTINUE
329      C-----
330      IF(T.GT.YPR) GO TO 201
331      PRINT 138,(D(J),J=1,ICH)
332      PRINT 143
333      PRINT 140
334      PRINT 144,(NH(J),(DRPHT(I,J),I=1,ICH),J=1,NHI)
335      201  CONTINUE
336      DO 47 ID1=1,ICH
337      C
338      C  LOCAL DROPLET TEMPERATURE DISTRIBUTIONS ARE CALCULATED
339      C
340      N2=1
341      TINIT(ID1,N2,1)=TINIT(ID1,N2,2)=TWATO
342      AMASS=(1.3333*3.14159*(D(ID1)/2.))**3.*DNWD)/10.**9.
343      V123=V0
344      NO=NHI+1
345      DO 45 IH1=1,NO
346      IF(IH1.LE.ITRANS(ID1,N2))GO TO 46
347      N2=N2+1
348      TINIT(ID1,N2,2)=TPA(ID1,IH1-1)

```

```

342      IF(N2.EQ.(N55(ID1)+1)) GO TO 6
343      TINIT(ID1,N2-1,1)=TINIT(ID1,N2-1,2)
344      6 CONTINUE
345      IF(IH1.EQ.N0) GO TO 44
346      IF(N2.GT.(N-1)) GO TO 44
347      IF(N2.GT.N55(ID1)) GO TO 48
348      V123=VELTR(ID1,N2-1)
349      IF(N2.NE.N55(ID1)) GO TO 50
350      IF(TINIT(ID1,N2,1).LT.TZ) N55(ID1)=N55(ID1)+1
351      50 CONTINUE
352      IF(TINIT(ID1,N2,1).LT.TZ) GO TO 46
353      N55(ID1)=N2
354      48 T123=TIM(ID1,IH1)-(TPRESS*(N55(ID1)-1))
355      TINIT(ID1,N2,1)=TINIT(ID1,N55(ID1),1)
356      GO TO 49
357      46 CONTINUE
358      IF(N2.GE.N55(ID1)) GO TO 48
359      T123=TIM(ID1,IH1)-(TPRESS*(N2-1))
360      49 CONTINUE
361      CALL DTEMP(PT,V123,T123,AMASS,XS,DLST)
362      WTPA(ID1,IH1)=TINIT(ID1,N2,1)+(TZ-TINIT(ID1,N2,1))*DLST
363      45 CONTINUE
364      44 CONTINUE
365      IF(N55(ID1).LT.N0) TINIT(ID1,N55(ID1),1)=TINIT(ID1,N55(ID1),2)
366      47 TINIT(ID1,N2,1)=WTPA(ID1,IH1-1)
C-----
367      98 OCT=0.
C-----
368      IF(T.GT.YPR) GO TO 202
369      PRINT 138,(O(J),J=1,ICH)
370      PRINT 145
371      PRINT 140
372      PRINT 144,(NH(J),(WTPA(I,J),I=1,ICH),J=1,NHI)
373      202 CONTINUE
374      DO 61 ID2=1,ICH
375      L1=NHI
376      IF(IFLAG(ID2).NE.1) L1=ITRANS(ID2,N-1)
377      FOUT(ID2)=0.
378      DO 60 IH2=1,L1
379      TV1=WTPA(ID2,IH2)
380      CALL PPWAT(TV1,PT,CPWT,DNWT)
381      CONT(ID2,2)=CONT(ID2,2)+(DNWT*CPWT*DRPHT(ID2,IH2)*((1.333*3.14159*
SD(ID2)/2.)*3)*TV1)/10.**9
382      IF(IH2.LT.NHI) GO TO 60
C
C      CONTRIBUTION OF ENERGY OF WATER LEAVING SYSTEM TO SYSTEM PRESSURE
C      DROP IS CALCULATED
C
383      TV4=WTPA(ID2,NHI)
384      CALL PPWAT(TV4,PT,CPWF,DNWF)
385      FOUT(ID2)=(OUT(ID2)*TV4*DISN(ID2)*CPWF*DNWF*TPRESS*WTFLOW)/10.**9
386      OUT(ID2)=1.0
387      60 CONTINUE
C
C      TOTAL ENERGY CHANGE OF WATER IS CALCULATED
C
388      DLCONT=CONT(ID2,2)+FOUT(ID2)-CONT(ID2,1)-FIN(ID2)
389      DCT=DCT+DLCONT
390      CONT(ID2,1)=CONT(ID2,2)
391      61 CONTINUE
C-----
C
C      A NEW ENERGY OF THE SYSTEM IS CALCULATED

```

```

C
C
392      ENINH=ENINH-DCT
C
C      A NEW PARTIAL PRESSURE OF STEAM IS CALCULATED
C
393      CALL COEF
394      62  CONTINUE
C
C      A NEW ENERGY OF THE SYSTEM IS CALCULATED
C
395      CALL WALLS(PSIG,TPRESS,WALEF)
396      PPP=PPP-WALEF
397      CALL TEMP1(PPP,TZ)
398      CALL SPVOL(TZ,PPP,VPRIM)
399      CALL ENTHAL(TZ,ENST)
400      ENINST=ENST-0.461415*(TZ+273.15)
401      ENINA=0.709*TZ
C
C      PARTIAL PRESSURE OF AIR IS CORRECTED FOR TEMPERATURE EFFECTS
C
402      PAIR=PAIRO*((TZ+273.15)/(TZ0+273.15))
C
C      A NEW TOTAL PRESSURE OF THE SYSTEM IS CALCULATED
C
403      PT=PPP+PAIR
404      XS=PPP/PT
405      ENINH=ENINA*WAIK+ENINST*TKVOL/VPRIM
- 406      PSIG=PT*14.504-14.696
-> 407      PTBAR=PSIG/14.504
408      P=PT*14.504
C
C      DYNAMIC VARIABLES ARE OUTPUTTED
C
409      IF(T.LE.DELAY) GO TO 203
410      IF(T.GT.YPR) GO TO 203
411      PRINT 147
412      PRINT126
413      PRINT127
414      PRINT128
415      PRINT129
416      PRINT130
417      PRINT131
418      203 CONTINUE
419      PRINT132,T,TZ,PPP,PAIR,PTBAR,P,PSIG
420      IF(TZ.LE.TWATO) GO TO 42
C
C      ENTIRE PROCESS IS REPEATED USING NEW VALUES OF DYNAMIC VARIABLES
C
421      GO TO 41
422      42  CONTINUE
423      STOP
424      END
C
C      *****
425      FUNCTION DV(VELDRP)
C      *****
426      COMMON /AREA1/ G,AREA,DMASS,ROMB,VISMB,A,SS,DIAM,DELRO,
1DSTAR1,DSTA2A,DSTA2B,DSTA3A,DSTA3B,DSTAR4,RE2A,RE2B,RF3A,FE3B,RE4
2RES,DMAXS,CDMAX,WSTAM,WMAXS,WSTAR4,WSTA3A,WSTA3B,WSTA2A,WSTA2B,
3WSTAR1,DST,SURFT
427      ROMF=ROMB

```

```

428 VISMF=VISM8
429 RENDR=(DIAM*VELDRP*ROMF*10000.)/VISMF
430 SIGN=1.
431 CALL COREIN(RENDR,C)
432 AREA=3.14159*(DIAM/2000.)**2
433 DV=G-((SIGN*C*AREA*ROMF*VELDRP**2)/(2.*DMASS))
434 RETURN
435 END

```

C
C

```

436 FUNCTION DZ(VELDRP)

```

C
C

```

437 DZ=VELDRP
438 RETURN
439 END

```

C
C

```

440 SUBROUTINE SEKPV(TZ,PV)

```

C
C

```

441 X=TZ/100.
442 PV=((((( (-2.489006/10000.*X+3.156533/1000.)*X-1.5087829/100.)*X
1.3488548/100.)*X-3.8647589/100.)*X+1.1476149/10000.)*X-7.0419435
2000.)*X+4.5905064/10.)*X+1.2602044
443 RETURN
444 END

```

C
C

```

445 SUBROUTINE PPWAT(TV,PT,CPV,DENS)

```

C
C

```

446 A=(TV+273.15)/647.3
447 S=PT/221.286
448 U=100.*(3700000.-3122199.*A*A-1999.85/A**6)
449 W=(U+SQRT(1.72*U*U+1362926.*10.**10*(S-1.500705*A)))*0.2941177
450 B=1.052356*(62.5+S*(13.10266+S))/10.**11/(1.5108/100000.+A**11)
451 C=(0.6537154-A)**2
452 C=C*(7.241165/100000.+0.7676621*C**4)
453 VVOD=0.417/W+C-B-(11.39706-9.949927*A)/100000.
454 DENS=1./VVOD
455 X=TV/100.
456 Y=PT/100.
457 Z=X**5
458 CPV=1./(Y+2.)+0.021*Y-0.24927
459 CPV=CPV*(0.032+Z*(0.003264+0.026912*Z*Z/100000.))
460 Z=(((-1.100455*X+4.837208)*X-24.208803)*X+33.444712)*X+30.72526
461 CPV=Z*Y/1000.+CPV
462 Z=((2.259985*X-7.403256)*X+19.097088)*X-13.04363)*X+419.82594
463 CPV=Z/100.+CPV
464 RETURN
465 END

```

C
C

```

466 SUBROUTINE DTEMP(PT,V,T,AM,XS,DLST)

```

C
C

```

467 P=PT*100000
468 D=- (2.317*10.**(-9))*P**1.225492*V**0.2628159*T**1.020822*(X/57)

```

```

469      4** (0.5199322)
470      IF (ABS(D).GT.170.) GO TO 6
471      DLST=1-EXP(D)
472      GO TO 8
473      6 DLST=1.0
474      8 CONTINUE
475      RETURN
476      END

C
C *****

476      SUBROUTINE WALLS(PSIG,T,W)
C
C *****

477      C=-0.00200
478      W=(PSIG/14.504)*(1-EXP(C*T))
479      RETURN
480      END

C
C *****

481      SUBROUTINE TEMP1(PPP,TZ)
C
C *****

482      X=ALOG(1.01972*PPP)
483      TZ=((((((-4.2924603/10000./10000.*X-4.2685685/100000000.)*X+1.
1343731/1000000.)*X+2.2071712/100000.)*X-1.7417752/100000.)*X-3.7.
23484/10000.)*X+1.3263773/1000.)*X+2.129682/100.)*X+2.1077605/10.
3X+2.3753577)*X+27.854242)*X+99.092712
484      RETURN
485      END

C
C *****

486      SUBROUTINE ENTHAL(T,ENTA)
C
C *****

487      X=T/100.
488      ENTA=((((((1.0285952*X-9.4307509)*X+27.974559)*X-43.077814)*X+15.
19571)*X+161.50666)*X+2500.6256
489      RETURN
490      END

C
C *****

191      SUBROUTINE SPVOL(TC,PPP,VPRIM)
C
C *****

192      DIMENSION A(9)
193      A(1)=1.26020437
194      A(2)=4.59050639/10.
195      A(3)=-7.04194353/1000.
196      A(4)=1.14761494/10000.
197      A(5)=-3.86475885/100.
198      A(6)=3.34885479/100.
199      A(7)=-1.50878287/100.
200      A(8)=3.15653300/1000.
201      A(9)=-2.48900598/10000.
202      PV=A(1)
203      X=TC/100.
204      DO 10 I=1,8
205      10 PV=PV+A(I+1)*X**I
206      VPRIM=PV/PPP
207      RETURN

```

C
C

509

SUBROUTINE CGEF

C
C

```

510 COMMON /AREA2/TKVOL,PPP,ENMIX,WAIR,PAIRO,TZ0,T
511 PPP=PPP+.001
512 DO 1 I=1,90
513 PPP=PPP-.001
514 CALL TEMP1(PPP,TZ)
515 CALL ENTHAL(TZ,ENTA)
516 ENINT=ENTA-0.461415*(TZ+273.15)
517 CALL SPVOL(TZ,PPP,VPRIM)
518 PAIR=PAIRO*((TZ+273.15)/(TZ0+273.15))
519 ENINS=ENINT*TKVOL/VPRIM
520 ENINA=0.709*TZ
521 TENINT=ENINS+ENINA*WAIR
522 IF(T.LE.0.1) ENMIX=TENINT
523 IF(TENINT.LE.ENMIX) GO TO 4
524 1 CONTINUE
525 4 CONTINUE
526 RETURN
527 END

```

C

528

SUBROUTINE CDREIN(RE1,CD)

C
C

529

```

COMMON /AREA1/ G,AREA,DMASS,ROMB,VISM8,A,SS,DIAM,DELRO,
1DSTAR1,DSTA2A,DSTA2B,DSTA3A,DSTA3B,DSTA4,RE2A,RE2B,RE3A,RE3B,RE
2RE5,DMAXS,CDMAX,WSTAM,WMAXS,WSTAR4,WSTA3A,WSTA3B,WSTA2A,WSTA2B,
3WSTAR1,DST,SURFT

```

```

530 DSTAR=10.*DIAM*((ROMB**2)*G*10.**2/VISM8**2)**(1./3.)
531 IF(RE1.LE.0.5) GO TO 10
532 IF(SS.GT.44.*10**12) GO TO 20
533 IF(RE1.GT.RE2A) GO TO 25
534 CD=(24./RE1)*(1.+0.150*RE1**0.687)
535 DSTA=(3.*RE1**2*CD*ROMB/(4.*DELRO))** (1./3.)
536 WSTA=(4.*RE1*DELRO/(3.*CD*ROMB))** (1./3.)
537 GO TO 210
538 20 CONTINUE
539 IF(RE1.GT.RE2B) GO TO 26
540 CD=(24./RE1)*(1.+0.150*RE1**0.687)
541 DSTA=(3.*RE1**2*CD*ROMB/(4.*DELRO))** (1./3.)
542 WSTA=(4.*RE1*DELRO/(3.*CD*ROMB))** (1./3.)
543 GO TO 210
544 25 CONTINUE
545 IF(RE1.GT.RE3A) GO TO 50
546 CD=0.48*(S*10.**(-12))**0.05
547 DSTA=(3.*RE1**2*CD*ROMB/(4.*DELRO))** (1./3.)
548 WSTA=(4.*RE1*DELRO/(3.*CD*ROMB))** (1./3.)
549 GO TO 210
550 26 CONTINUE
551 IF(RE1.GT.RE3B) GO TO 50
552 CD=0.7*(SS*10.**(-12))**(-0.05)
553 DSTA=(3.*RE1**2*CD*ROMB/(4.*DELRO))** (1./3.)
554 WSTA=(4.*RE1*DELRO/(3.*CD*ROMB))** (1./3.)
555 GO TO 210
556 10 CD=24./RE1
557 DSTA=(3.*RE1**2*CD*ROMB/(4.*DELRO))** (1./3.)
558 WSTA=(4.*RE1*DELRO/(3.*CD*ROMB))** (1./3.)

```



```

559      GO TO 210
560      50      CONTINUE
561      IF(RE1.GT.RE4) GO TO 60
562      DSTA=(RE1/(4.5*(DELRO/ROMB)**0.388*(SS*10.**(-12))**0.0323))**(1
11.29)
563      WSTA=DSTA**0.29*4.5*(DELRO/ROMB)**0.388*(SS*10.**(-12))**0.0323
564      CD=.06570*DSTA**0.42*(DELRO/ROMB)**0.224*(SS*10.**(-12))**(-0.06
565      GO TO 210
566      60      CONTINUE
567      IF(RE1.GT.RE5) GO TO 70
568      WSTA=19.96*(DELRO/ROMB)**0.262*(SS*10.**(-12))**0.0654
569      DSTA=RE1/WSTA
570      CD=0.00335*(DELRO/ROMB)**0.477*(SS*10.**(-12))**(-0.131)*DSTA
571      GO TO 210
572      70      CONTINUE
573      11      GR=4.*DELRO*DST**3-3.*RE1**2*ROMB*(A*(DST-DMAXS)+CDMAX)
574      GRPRIM=12.*DELRO*DST**2-3.*RE1**2*ROMB*A
575      DSTN=DST-GR/GRPRIM
576      IF(ABS((DSTN-DST)/DST).LT.0.001) GO TO 12
577      DST=DSTN
578      GO TO 11
579      12      CD=CDMAX+A*(DSTN-DMAXS)
580      WST=SQRT(4.*DELRO*DSTN/(3.*ROMB*(A*(DSTN-DMAXS)+CDMAX)))
581      DSTA=DSTN
582      WSTA=WST
583      210     CONTINUE
584      RETURN
585      END

```

3ENTRY

APPENDIX O

DROPLET SIZE DISTRIBUTION MEASUREMENTS

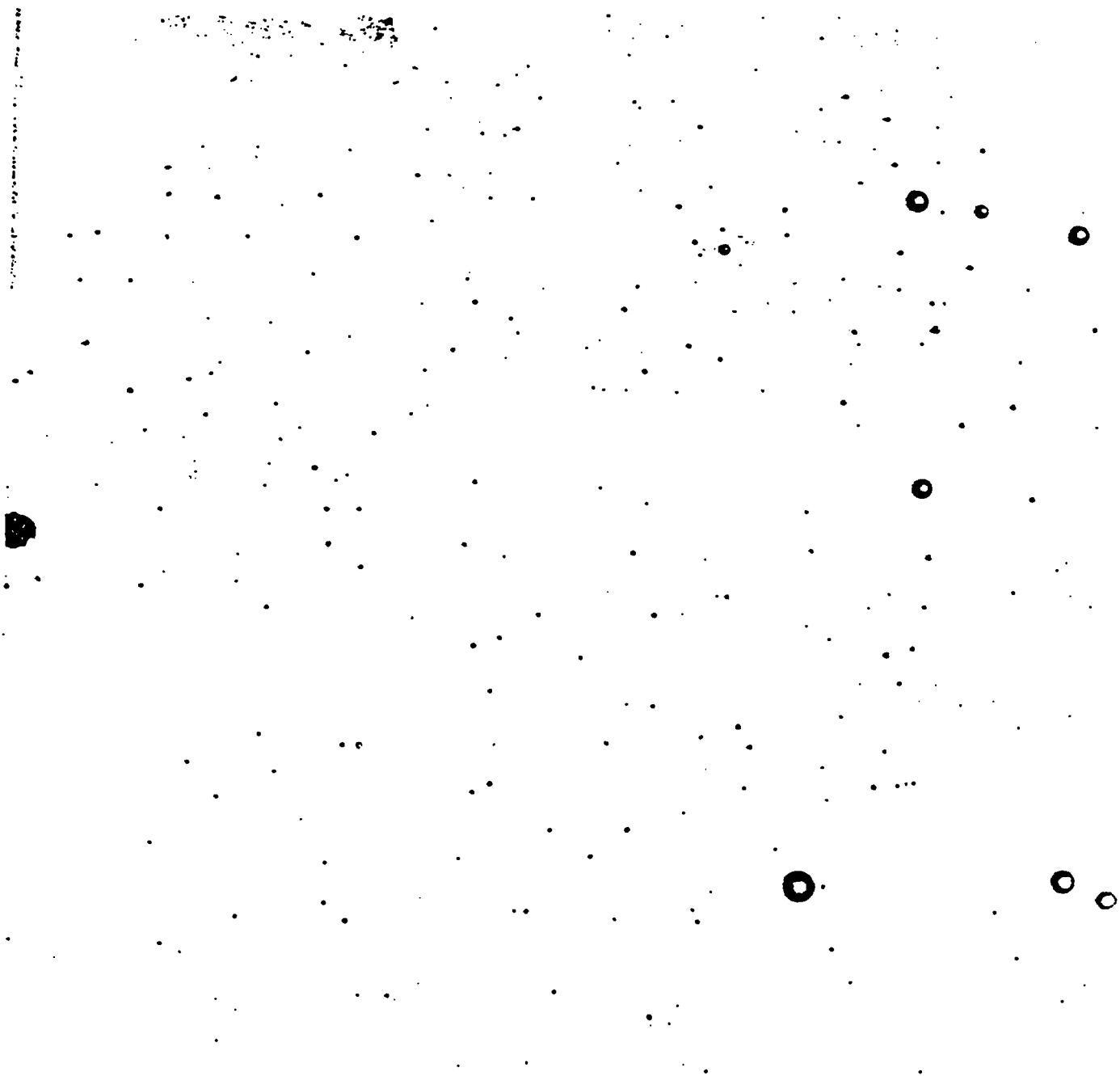


Figure 01. Photograph of droplets obtained using the catch in cell technique for 30 IGPM near the spray centre.

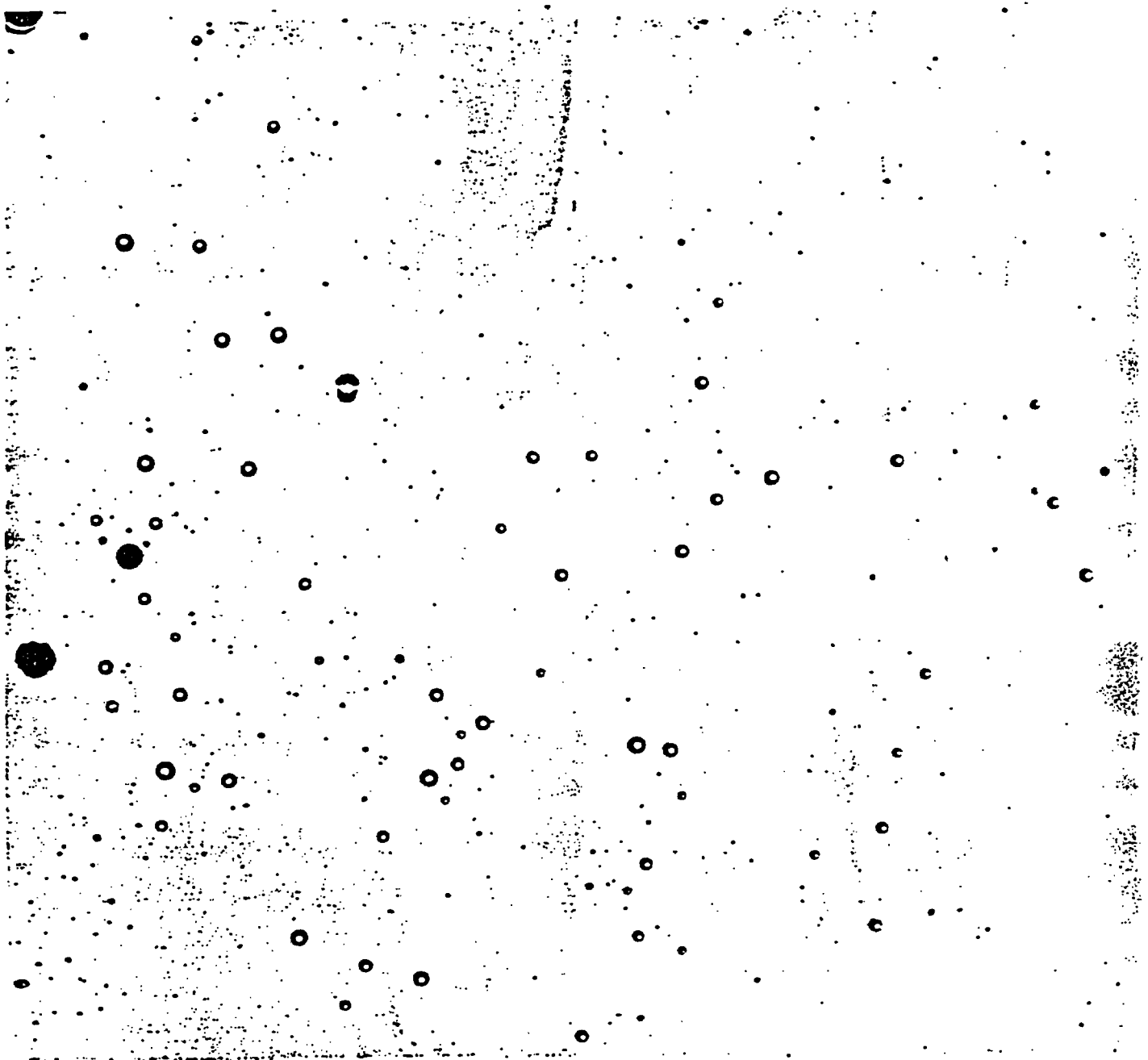


Figure 02. Photograph of droplets obtained using the catch in cell technique for 30 IGPM near to the edge of the spray.

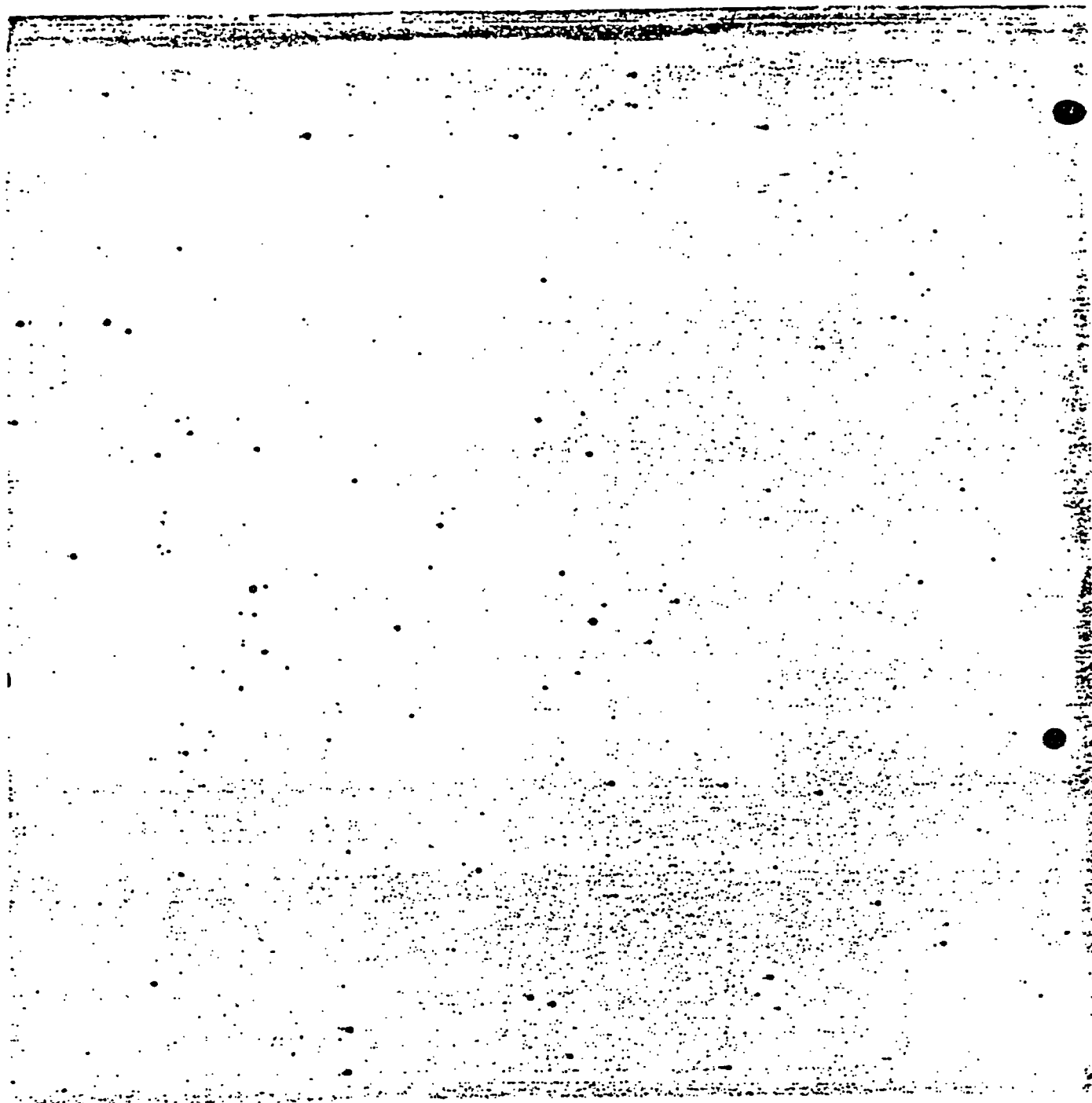


Figure 03. Photograph of droplets obtained using the catch in cell technique for 40 IGPM near the spray centre.

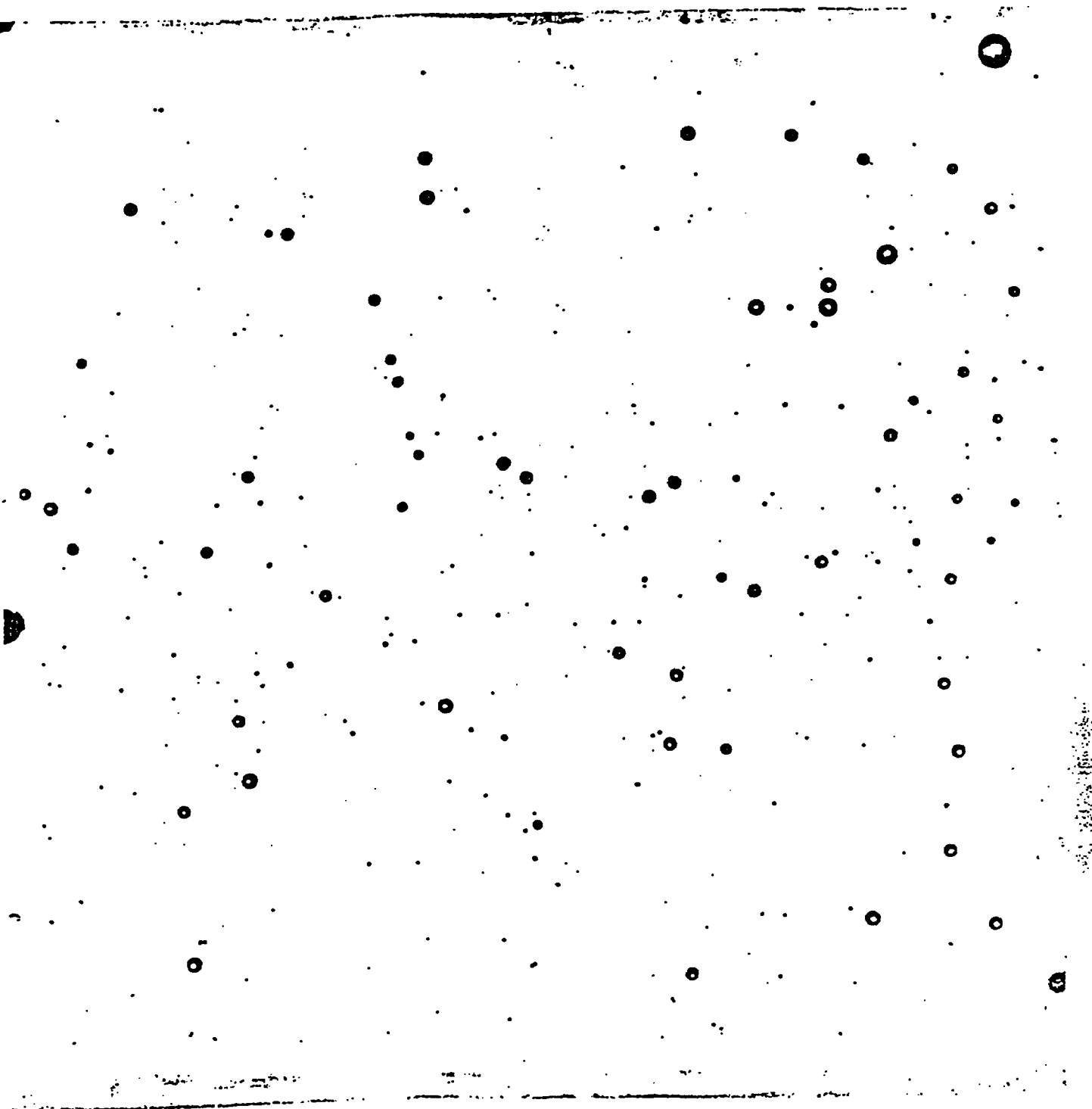


Figure 04. Photograph of droplets obtained using the catch in cell technique for 40 IGPM near to the edge of the spray.

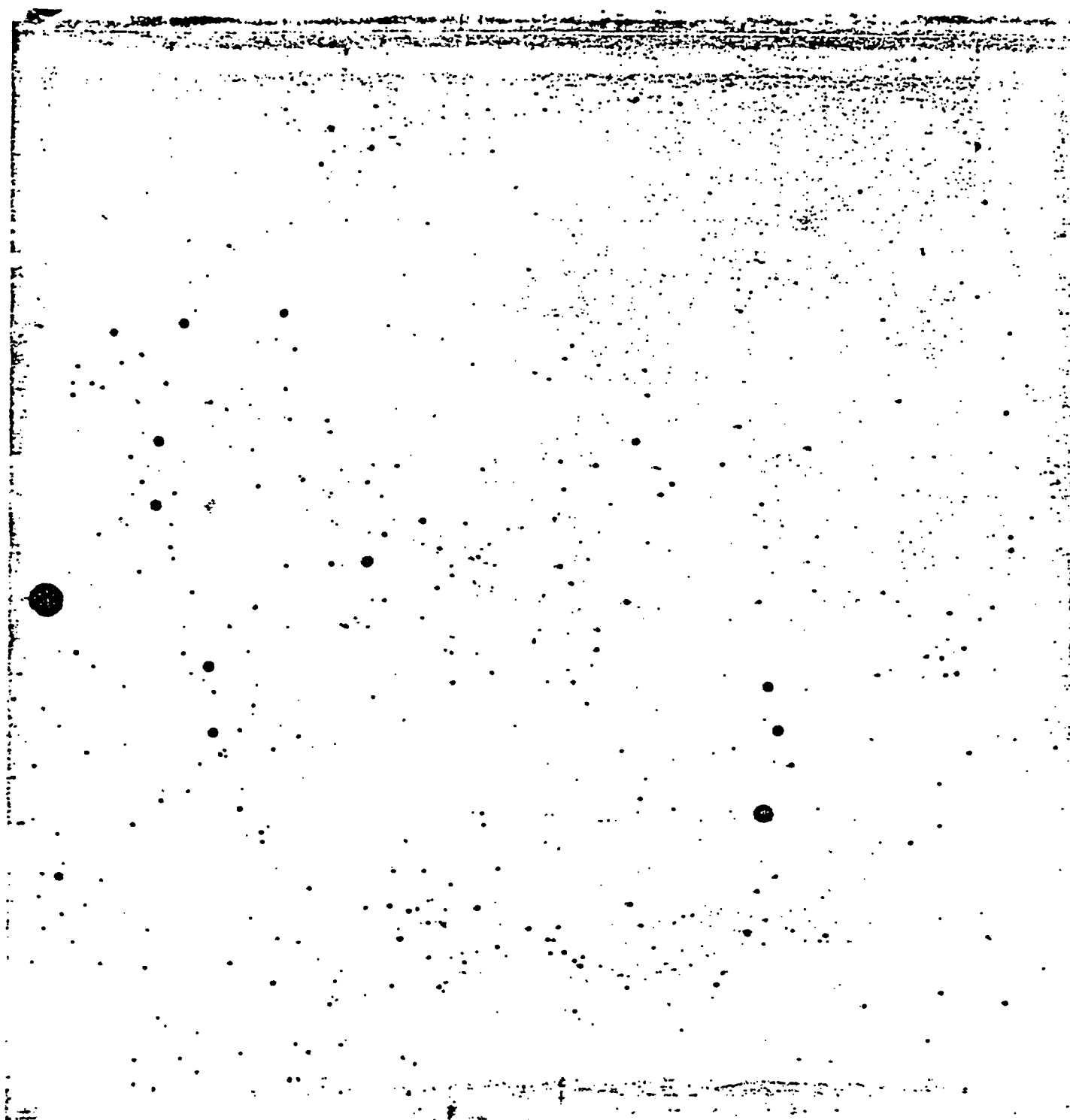


Figure 05. Photograph of droplets obtained using the catch in cell technique for 50 IGPM near the spray centre.

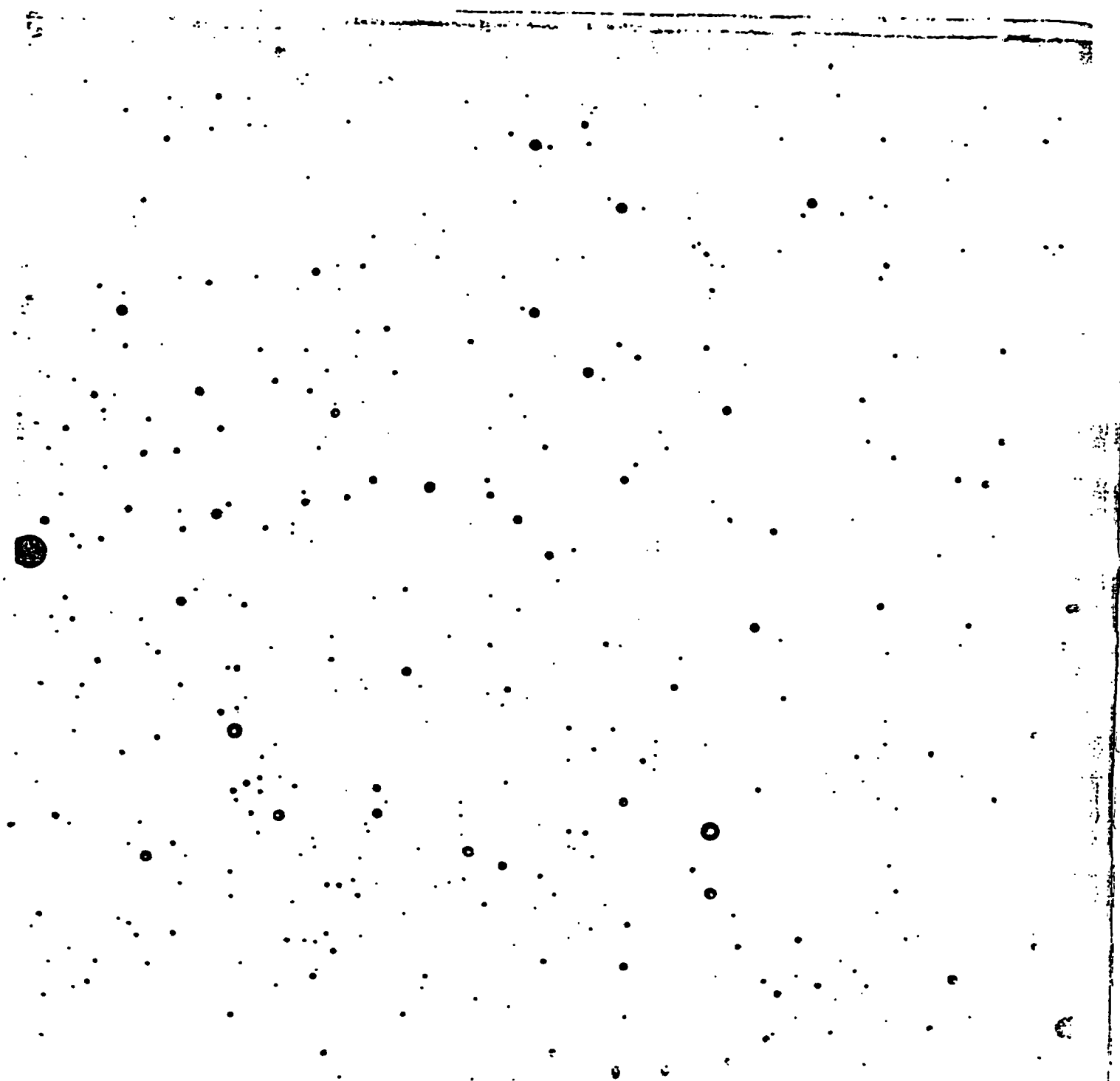


Figure 06. Photograph of droplets obtained using the catch in cell technique for 50 IGPM near to the edge of the spray.

Figure 07. Droplet Size Distribution for Droplets Shown
in Figure 01.

$$X_m = 5.252 \text{ mm}, \quad b = 0.292 \quad \delta = 1.265$$

FLOW RATE - 30 IGPM, NEAR THE CENTER OF THE SPRAY

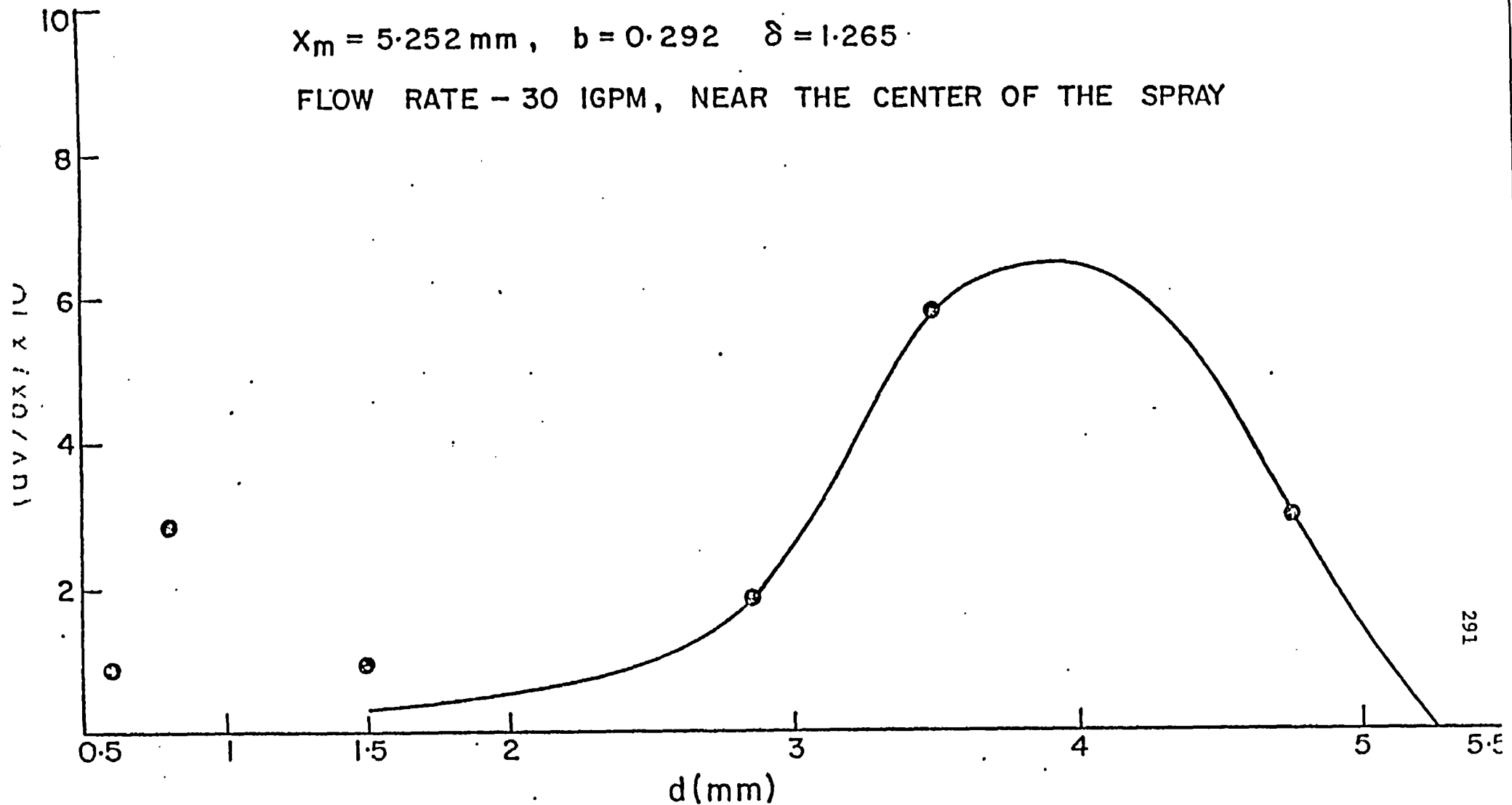
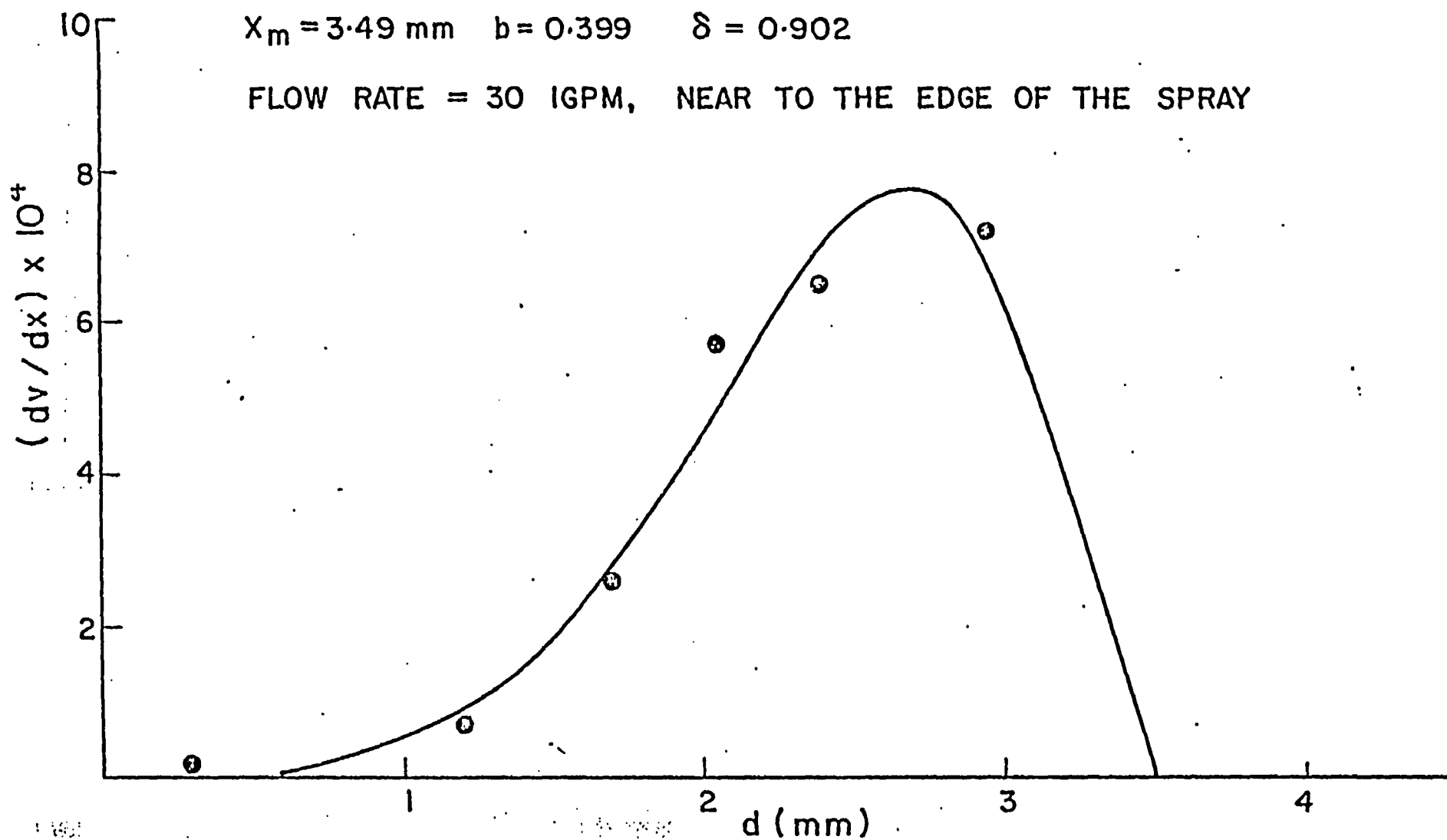


Figure 08. Droplet Size Distribution for Droplets Shown
in Figure 02.

$$X_m = 3.49 \text{ mm} \quad b = 0.399 \quad \delta = 0.902$$

FLOW RATE = 30 IGPM, NEAR TO THE EDGE OF THE SPRAY



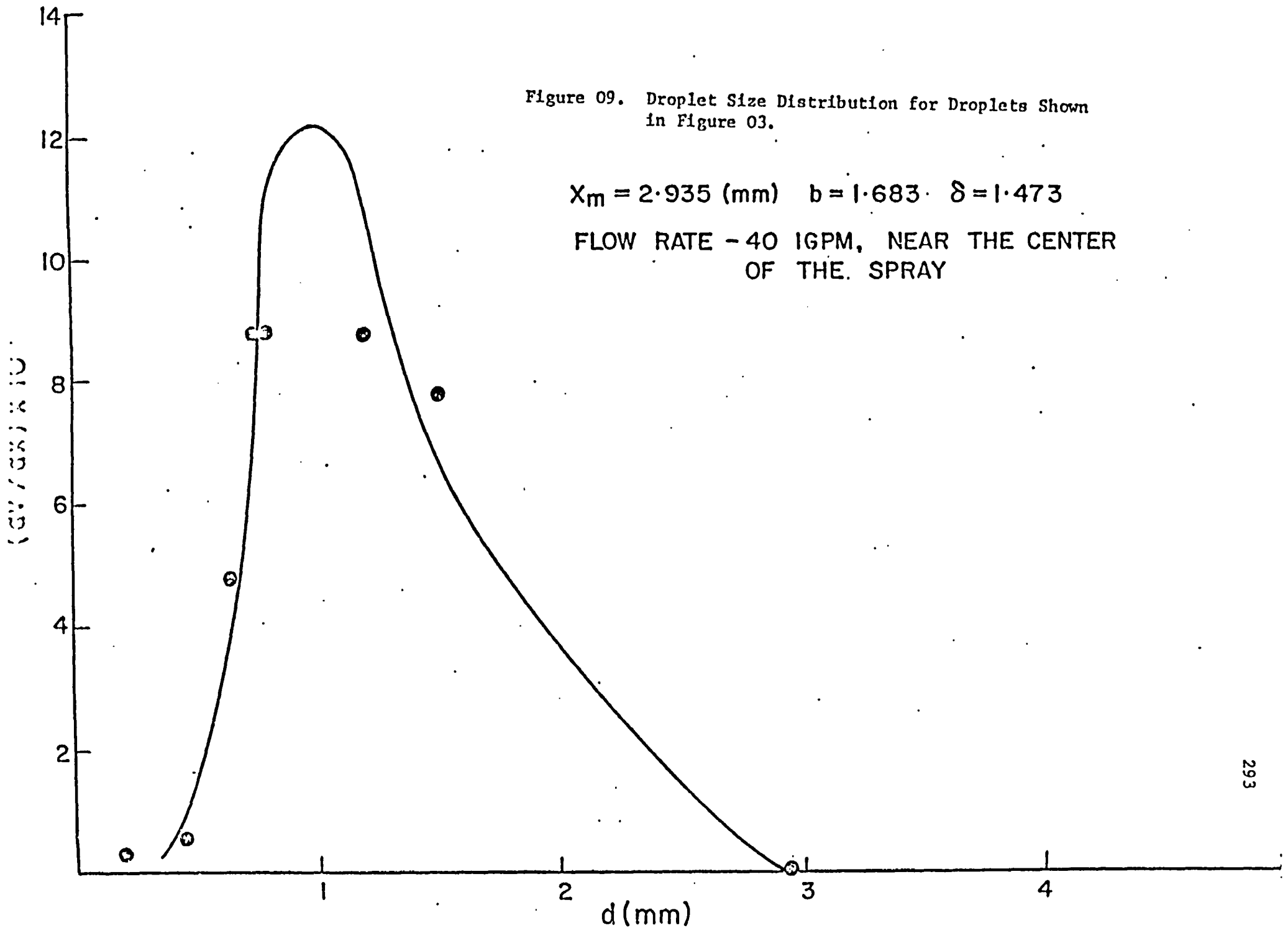


Figure 010. Droplet Size Distribution for Droplets Shown
in Figure 04.

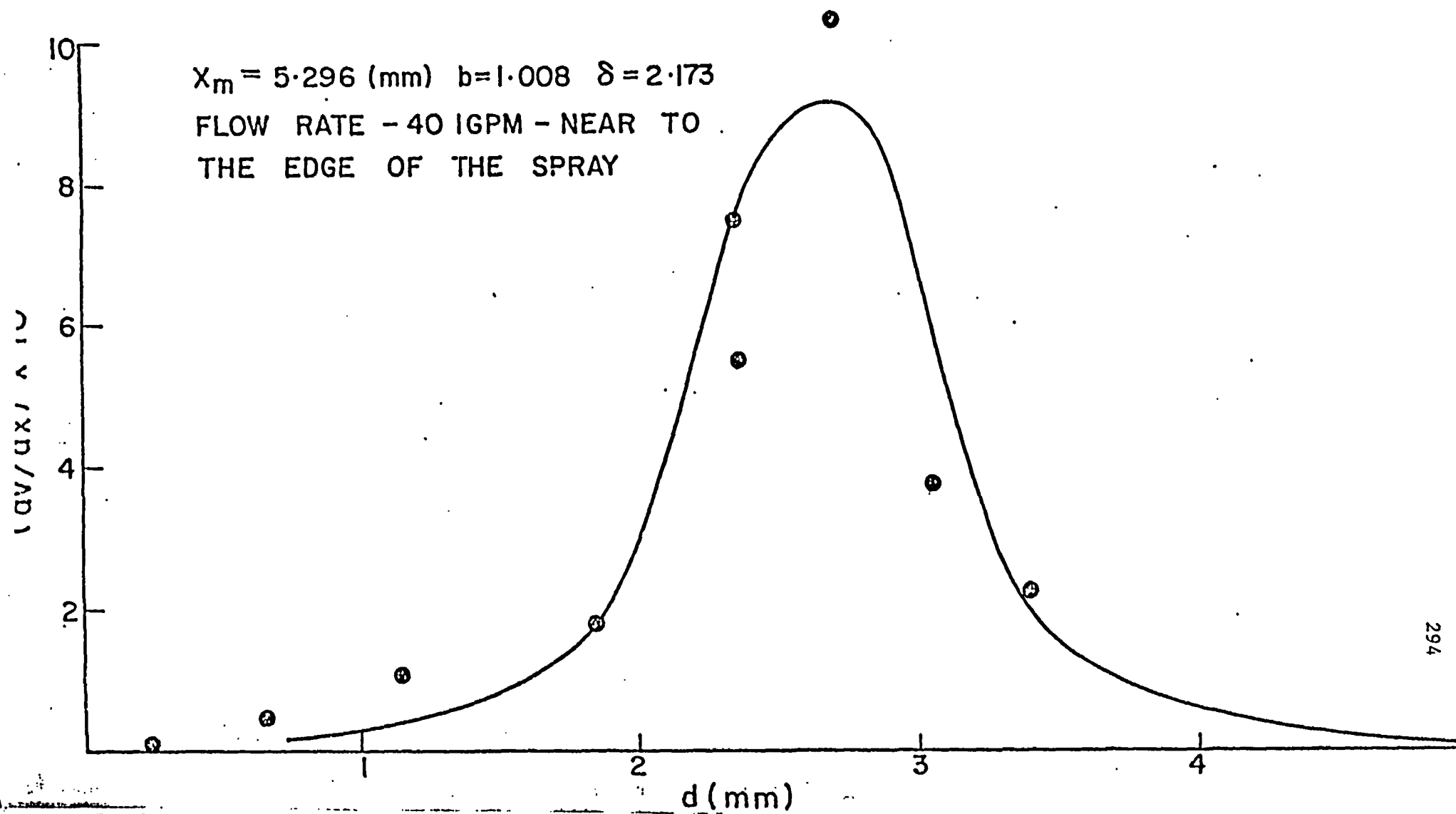


Figure 011. Droplet Size Distribution for Droplets Shown
in Figure 05.

$$X_m = 4.629 \text{ (mm)} \quad b = 1.569 \quad \delta = 0.677$$

FLOW RATE - 50 IGPM, NEAR THE CENTER OF THE SPRAY

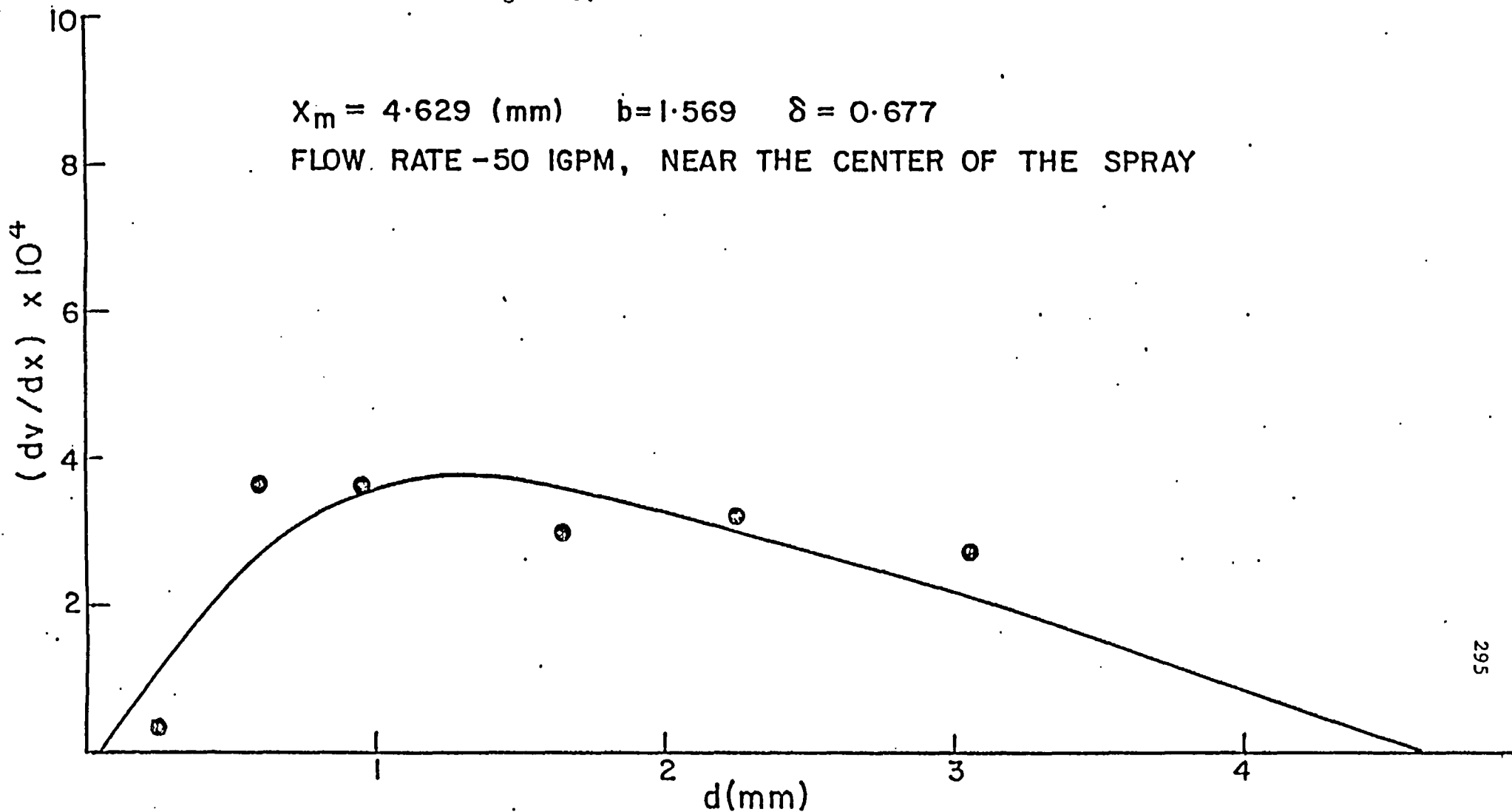
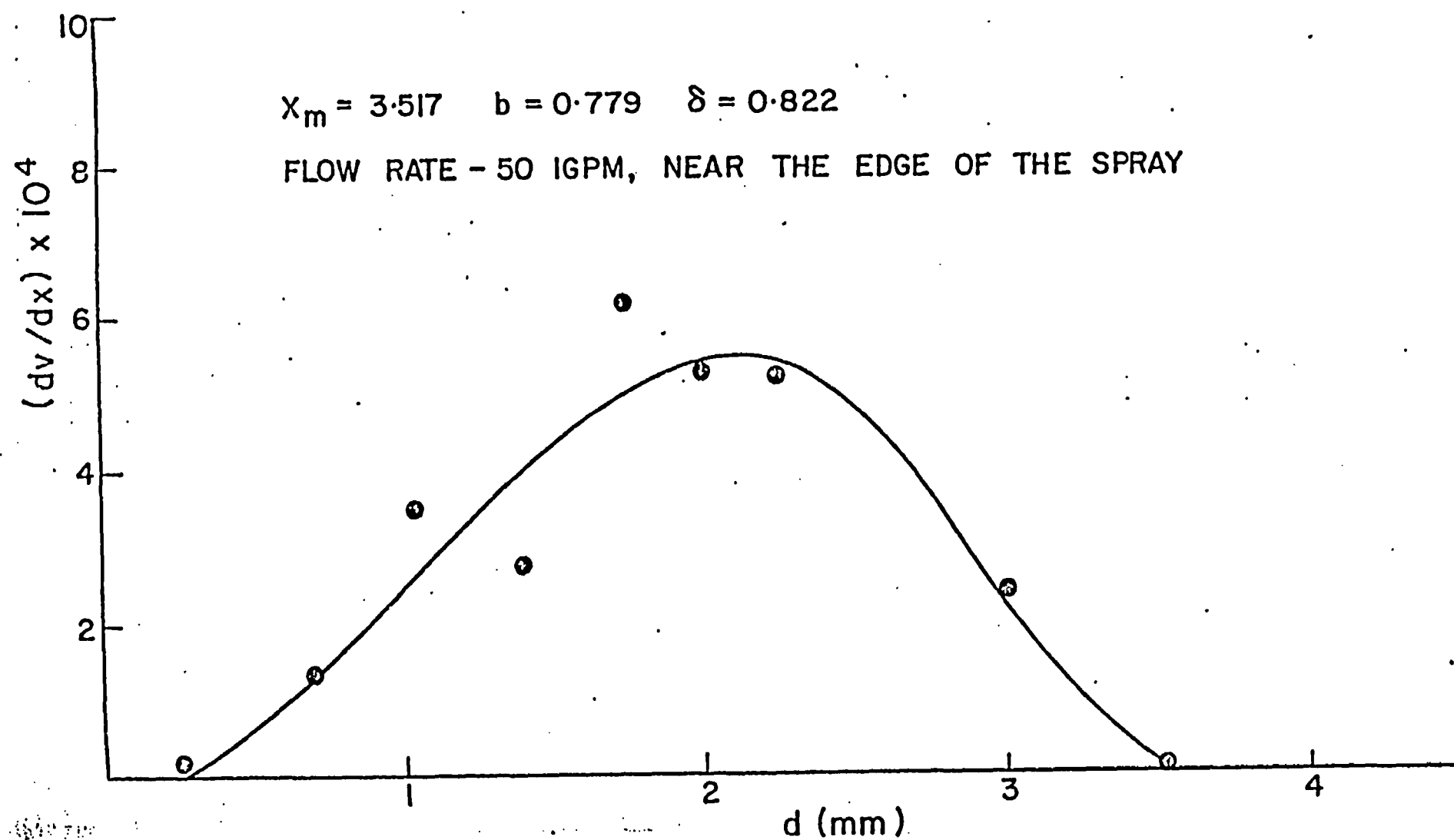


Figure 012. Droplet Size Distribution for Droplets Shown
in Figure 06.



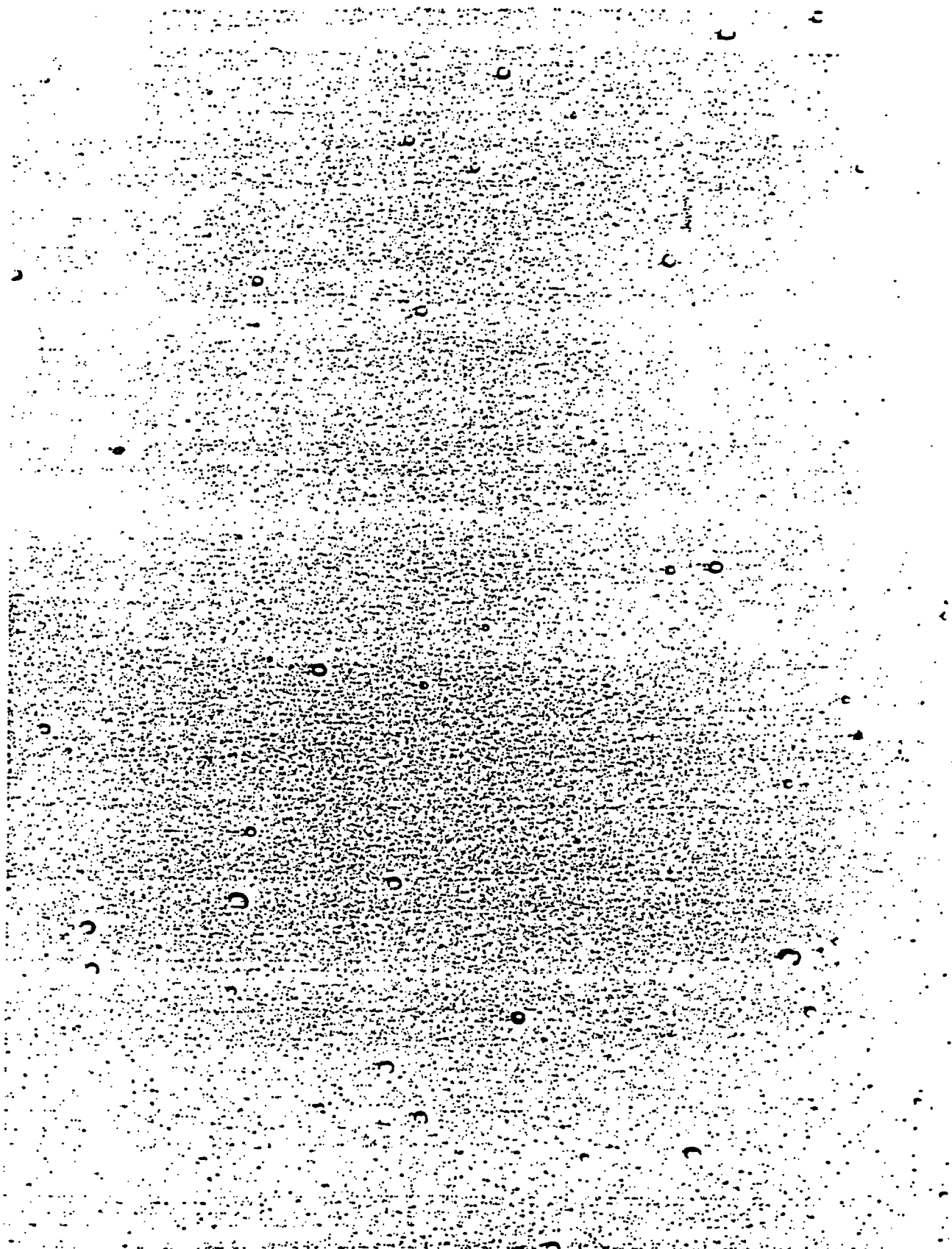


Figure 013. Photograph of droplets obtained using the direct photography technique for 30 IGPM near to the edge of the spray.

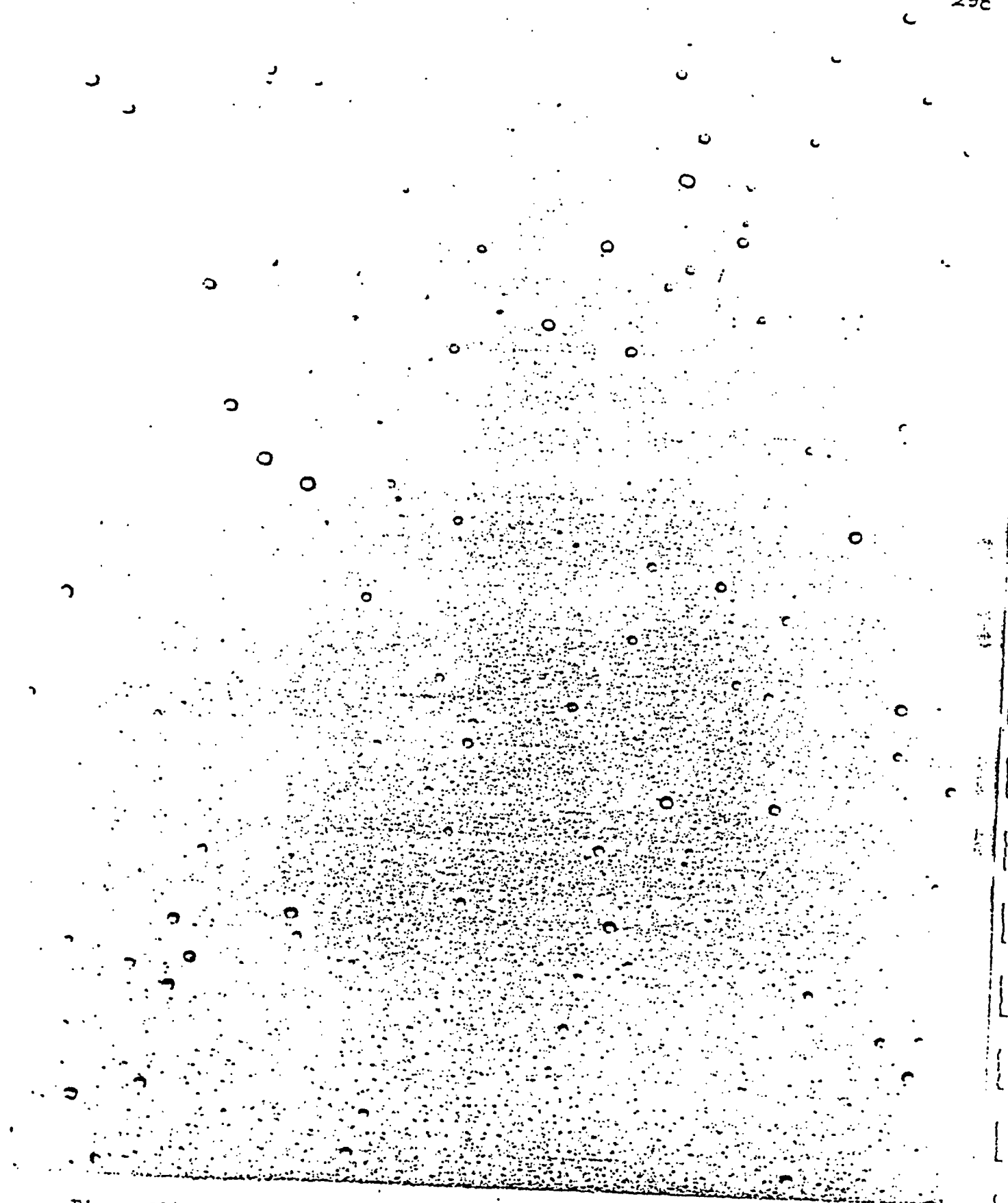


Figure 014. Photograph of droplets obtained using the direct photography technique for 40 IGPM near to the edge of the spray.

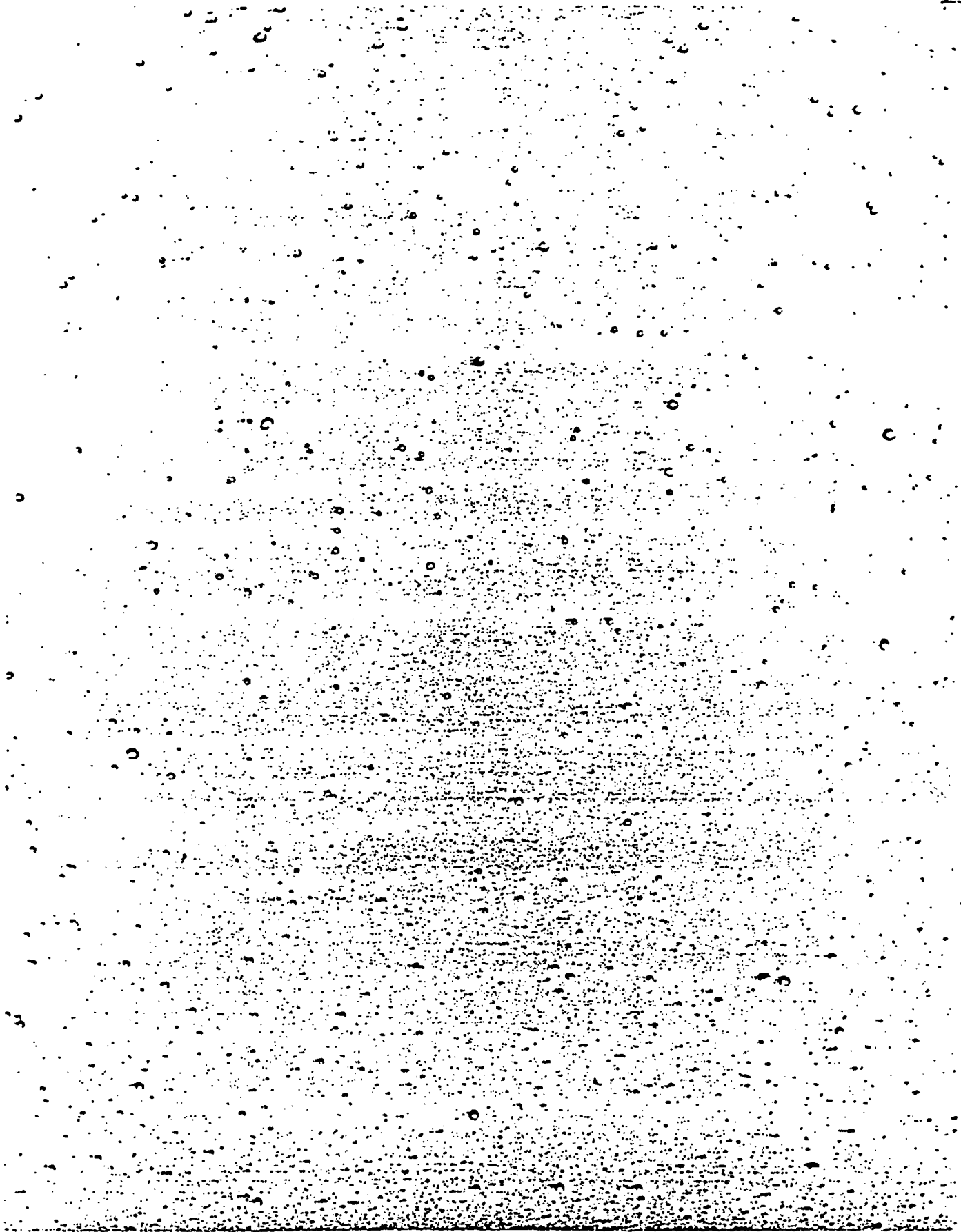


Figure 015. Photograph of droplets obtained using the direct photography technique for 50 IGPM near to the edge of the spray.

Figure 016. Droplet Size Distribution for Droplets Shown
in Figure 014.

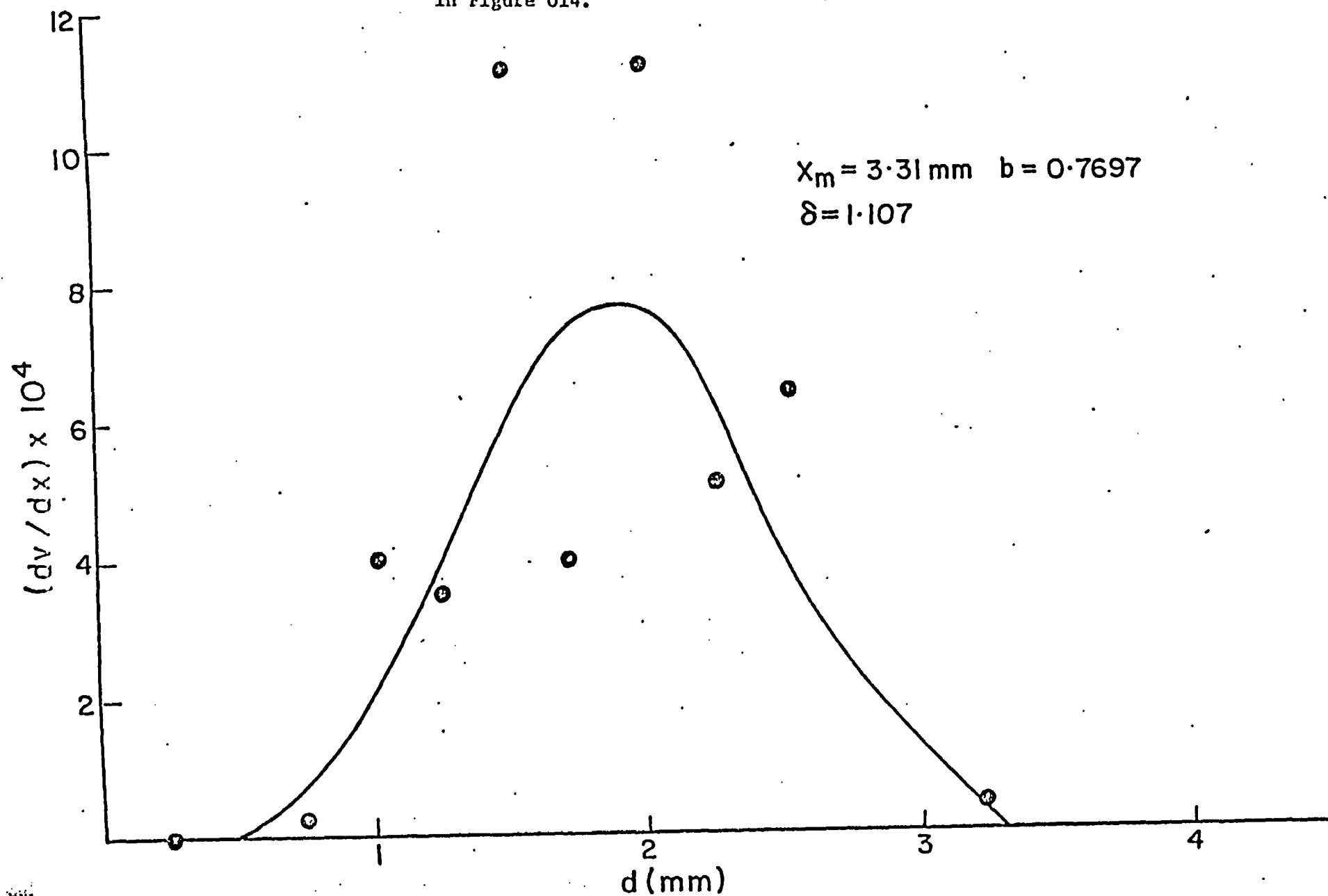


Figure 017. Droplet Size Distribution for Droplets Shown
in Figure 015.

